NUREG/CR-0912, Vol. 2
UCRL-52719, Vol. 2

Geoscience Data Base Handbook for Modeling a Nuclear Waste Repository

Volume 2

Manuscript Completed: February 1980
Date Published: January 1981

Prepared by
Dana Isherwood

Lawrence Livermore Laboratory
7000 East Avenue
Livermore, CA 94550

Prepared for
Office of Nuclear Material Safety and Safeguards
U.S. Nuclear Regulatory Commission
Washington, D.C. 20555
NRC FIN No. A0277

ABSTRACT

This handbook contains reference information on parameters that should be considered in analyzing or modeling a proposed nuclear waste repository site. Only those parameters and values that best represent the natural environment are included. Rare extremes are avoided. Where laboratory and field data are inadequate, theoretical treatments and informed engineering judgments are presented.

Volume 1 contains a data base on salt as a repository medium. Chapters on the geology of bedded and dome salt, the geomechanics of salt, hydrology, geochemistry, natural and man-made features, and seismology provide compiled data and related information useful for studying a proposed repository in salt. These and other data will be needed to derive generic deep geologic modeling parameters and will also serve as background for the verification of source data that may be presented in licensing applications for nuclear waste repositories. Volume 2 is the result of a scoping study for a data base on the geology, geomechanics, and hydrology of shale, granite, and basalt as alternative repository media. Except for the geomechanics of shale, most of the sections contain relatively complete compilations of the available data, as well as discussions of the properties that are unique to each rock type.

CONTENTS

LIST OF FIGURES

LIST OF FIGURES

LIST OF FIGURES

LIST OF FIGURES

LIST OF FIGURES

LIST OF FIGURES

LIST OF TABLES

LIST OF TABLES

LIST OF TABLES

LIST OF TABLES

FOREWORD

This document supports the Nuclear Regulatory Commission's efforts on nuclear waste management. It is the second volume of a study designed to provide the NRC staff with an objective and representative presentation of the data hat are available to the technical community and that should be considered in the derivation of generic deep geologic modeling parameters. These data will also aid in the evaluation of licensing applications for deep geologic repositories.

As principal author, I acknowledge with thanks the efforts and contributions of the many individuals who worked with me on this handbook. I also appreciate the input and guidance provided by the NRC staff. The people listed below were especially helpful in providing technical input and were responsible for writing all or major sections of the several chapters.

Lawrence Livermore Laboratory
- David Carpenter (Volume 1, Chapter 6)
- Willard Murray (Volume 1, Chapter 3)
- Abelardo Ramirez (Volume 1, Chapter 5)
- Donald Towse (Volume 1, Chapter 6)

Serata Geomechanics, Inc., Berkeley, California
- Shosei Serata (Volume 1, Chapters 2 and 3)
- Stefan Milnor (Volume 1, Chapters 2 and 3)

Geotechnical Engineers, Inc., Winchester, Massachusetts
- Bartlett Paulding (Volume 1, Chapter 5)

California State University, Hayward, California
- Alexis Moiseyev (Volume 2, Chapter 1)

Willard Owen Associates, Inc., Wheat Ridge, Colorado
- Scott Mefford (Volume 2, Chapters 2 and 3)

Colorado School of Mines, Golden, Colorado
- William Hustrulid (Volume 2, Chapters 2 and 3)

PREFACE TO VOLUME 2

The three chapters of Volume 2 are the results of a scoping study on the geology, geomechanics, and hydrology of basalt and granite, and on the geology and hydrology of shale. The chapters include relatively complete compilations of the data currently available, as well as discussions of the properties that are unique to each rock type. Most of the data are, however, undigested; many of the figures and tables were taken from the original sources without extensive review. The use of symbols, especially in the sections on geomechanics, has been made generally consistent with the chapters of Volume 1; nonetheless, owing to the inconsistencies that pervade the literature, some differences remain.

Volume 1 presented the available data on salt formations in the U.S. It also outlined general principles relevant to all geologic formations and rock types, especially in the chapters on hydrology, geochemistry, natural and man-made features, and seismology. The discussions of porous flow in the hydrology chapter and of nuclide retardation in the geochemistry chapter are especially important in understanding how the hydrologic data in Volume 2 might be used. The thorough discussion of the geomechanics of salt in Volume 1, though not an elementary introduction, also provides a context in which the geomechanical data on basalt and granite can be better understood.

The discussion of shales in the present volume presents brief geologic descriptions of shale formations in the U.S. and compiles extensive hydrologic data. The most thorough data are from the Great Basin, the Rocky Mountains, and the Colorado Plateau. The data on basalts are less copious. Nonetheless, geomechanical data are presented from a variety of places, notably Amchitka Island, the Great Lakes region (the Dresser Basalt), and the Columbia Plateau. The most useful hydrologic data have been collected at the Idaho National Engineering Laboratory and the Hanford reservation on the Columbia Plateau. The geological descriptions of basalt flows focus on the Pacific Northwest. Data on granites come from widely scattered sources, including dam sites, tunnel sites, and quarries around the world. The most systematic geomechanical data, including the results of thermal modeling experiments,

have been collected at the Stripa mine project currently underway in Sweden. The chapter on granites also includes descriptions of the major granite batholiths of the U.S. and a discussion of fracture flow that is equally applicable to other rock types.

CHAPTER 1

SHALE

This chapter is a compilation of available data on the hydraulic conductivity, porosity, and density of shales, and it provides a general outlook on the relationships between these parameters. More importantly, it outlines areas where more research is needed to allow better predictions to be made of the long-term behavior of waste repositories in shale. Notably missing from this scoping study is a discussion of the geomechanical properties of shale. Only a few values for geomechanical parameters, found during the compilation of the hydrologic data, have been included. Time constraints did not allow a thorough study of geomechanics.

Shale and related rocks (including siltstone, mudstone, and claystone) belong to a group of broadly represented, relatively impervious rocks which offer some potential for long-term storage of radioactive wastes. Hydrologically, they are characterized by the uncommon combination of high porosity and low permeability, a combination that is related in part to their very fine grain size. Their low permeability results in a scarcity of hydrologic data: neither oil companies nor hydrologists have been particularly eager to take measurements in rock of low economic importance. Furthermore, estimating shale permeabilities in the subsurface by producing fluids from wells is impractical, because shale normally produces no fluid.

GEOLOGIC PROPERTIES OF SHALE

Definitions

Shale is the generic name given to the widespread group of sedimentary rocks which is characterized by a predominance of silt- and clay-size fractions. Variations in textures and structures are used to define specific rock types--the most common being shale proper, mudstone, siltstone, and claystone.

The following definitions are quoted directly from the Glossary of Geologic Terms (AGI, 1972).

Shale. "A fine-grained, indurated, detrital sedimentary rock formed by the consolidation (as by compression or cementation) of clay, silt, or mud, and characterized by finely stratified (laminae 0.1-0.4 mm thick) structure and/or fissility that is approximately parallel to the bedding (along which the rock breaks readily into thin layers) and that is commonly most conspicuous on weathered surfaces, and by a composition with an appreciable content of clay minerals and with a high content of detrital quartz; a thinly laminated or fissile claystone, siltstone or mudstone. . . .The term 'shale' is regarded sometimes as a structural term with the significance of thin bedding or fissility and without implying a particular composition: it has been loosely applied to massive or blocky indurated silts and clays that are not laminated, to laminated silts and clays that are not indurated, to fine-grained and thinly laminated sandstones, and to slates."

Mudstone. "(a) An indurated mud having the texture and composition, but lacking the fine lamination or fissility, of shale; a mucky or massive, fine-grained sedimentary rock in which the proportions of clay and silt are approximately the same; a non-fissile mud shale. . . . (b) A general term that includes clay silt, claystone, siltstone, shale, and argillite, and that should be used only when the amounts of clay and silt are not known."

Siltstone. "An indurated or somewhat indurated silt having the texture and composition, but lacking the fine lamination or fissility, of shale: a massive mudstone in which the silt predominates over clay: a non-fissile shale. Pettijohn regards siltstone as a rock whose composition is intermediate between those of sandstone and shale and of which at least two-thirds is material of silt size."

Claystone. "An indurated clay having the texture and composition, but lacking the fine lamination or fissility, of shale: a massive mudstone in which the clay predominates over silt; a non-fissile clay shale."

Other Types of Shales. Just about any type of fine-grained sedimentary rock exhibiting laminations has been called shale by some field geologists. One example is the Monterey Shale, a Miocene formation of coastal California. Locally this rock is a finely layered diatomite entirely composed of siliceous remains of diatoms with minimal amounts of clay. Another example is the Oil Shale, a hydrocarbon-rich member of the Green River Formation (Middle Eocene) of Utah and Wyoming. This rock is unusually rich in calcium carbonate and should be referred to as marl or marlstone, a European term sometimes used for rocks containing clay and calcite with minor amounts of other constituents.

In summary, the term shale has been applied indiscriminately to very diverse rocks: massive or finely layered, indurated or soft, rich or devoid of clay minerals, fissile or not. This abusive labeling practice has led to the inclusion of sedimentary rocks of widely different origins in a single category. Unfortunately, by looking through a list of references, it is not always possible to determine the actual meanings intended by the various authors. This explains in part the wide variations in the hydrologic properties of shale; for example, the hydraulic conductivity, which spans more than ten orders of magnitude.

Mineralogy

Geologists have used the term clay to designate both a family of layered silicate minerals and a very fine grain size (less than 4 μm). Most clay minerals are, in fact, in the clay size range, but other minerals, particularly quartz, are also sometimes found in the clay fraction. In the Monterey Shale (Miocene) of California, for example, some sections are made up entirely of clay-size siliceous fragments. Another classic example is glacial "clay," a rock flour generally composed of nearly unaltered clay-size rock fragments. With this confusion between the mineral clay and the use of the word to denote a fragment size, there can be little doubt that the wide spectrum of hydrologic properties observed in shale is partly due to semantics. In this chapter, clay will be restricted to mean clay minerals, and clay-size to mean a grain size smaller than 4 μm.

Clays. A complete mineralogic description of the most important constituents of shale is beyond the scope of this report. Only the general types of clays

are outlined here, with the emphasis on the major characteristics which affect their physical and chemical properties. Clay mineral sorption characteristics, as measured by the cation exchange capacity, is shown in Table 1-1. The interested reader can find additional information in Grim (1968), Weaver (1959), and Weaver and Pollard (1975). The clay minerals found in shale include the following:

- Kaolinite, which has a simple two-layer structure comprising one layer of silica tetrahedrons and one layer of alumina octahedrons. It has little capacity for ionic exchange and sorption. This clay somewhat lacks plasticity.*
- Illite, which has a three-layer structure characterized by some replacement of Si^{+4} by Al^{+3}, together with an addition of K^{+} on the outside of the structure. Illite is sometimes called hydromuscovite, has moderate ion exchange properties, moderate sorption affinities, and a variable plasticity.
- Smectite, also a three-layer clay characterized by the replacement of Si^{+4} by Al^{+3}. In this case, however, electronic imbalance is compensated for by the addition of various ions (magnesium, iron, zinc, etc.) in the

TABLE 1-1. Cation-exchange capacity of clay minerals, in milliequivalents per 100 g (from Grim, 1968).

Kaolinite	3-15
Halloysite $2H_2O$	5-10
Halloysite $4H_2O$	40-50
Smectite	80-150
Illite	10-40
Vermiculite	100-150
Chlorite	10-40
Sepiolite-attapulgite-palygorskite	3-15

*Plasticity is the property of the moistened material to be deformed under pressure, with the deformed shape being retained when the deforming pressure is removed (Grim, 1968, p. 1).

vacant octahedral sites inside the structure. Smectites have extreme variations in plasticity and ion exchange capabilities (swelling clays can sorb enormous amounts of fluids), and their physical properties are greatly affected by the nature of the ions sorbed. Sodium ions make them sticky and plastic when wet; calcium ions make them less sticky and less prone to sorb water. Other names used for minerals of this type are montmorillonite (when used in a generic sense) and bentonite.

- Chlorites, which have composite structures that can be regarded as derivatives of kaolinite structure or as two illite structures tied by Mg^{+2} instead of K^{+}. Rich in iron and magnesium, they lack the swelling properties of smectite.

- Mixer-layer clays, which are combinations of two types of clays in a large structure. In some instances the layers follow an orderly pattern, in others they are random. The illite/smectite mixed-layer clay is an important constituent of shale. Its properties are depend greatly on the smectite content, but as a whole, they are intermediate between those of smectite and illite.

Other types. Among the less important clay constituents of shale are sepiolite and attapulgite, consisting of hornblendelike chains of silica tetrahedrons, linked together by octahedral groups of oxygens and hydroxyls containing aluminum and magnesium ions. Many clay minerals are very sensitive to prevailing physical and chemical conditions. Their relative abundances change during burial in response to changes in pressure or temperature, and perhaps in response to the duration of burial.

Nonclay Constituents. Among nonclay constituents are the following:

- Feldspars. These are common clastic constituents of shale, particularly in the silt-size fractions. Calcic plagioclase, albite, and potassium feldspars are all present in shale, and like clays, their relative abundances change during burial: potassium feldspar and calcic plagioclase progressively disappear (Hower et al., 1976).

- Quartz. Together with amorphous silica varieties, quartz is found in all size fractions. These minerals are derived from terrestrial and biological sources (weathering, volcanism, sponges, diatoms), or are formed during diagenesis. All are mobilized by solution and deposition, and may radically change the hydrologic properties of a rock by filling pore space and/or making the rock brittle.

• Carbonates, which are primarily found as calcite and aragonite of biogenic origin. Their tendency to mobilize is greater than that of silica and results in concentrations in the form of concretions or pore space fillings. Typical shale contains less carbonate than silica.

In summary, the physical properties of shale depend mainly upon the abundance of clay minerals and the relative proportions of clay types. When kaolinite and illite predominate, rock properties are likely to remain fairly constant and predictable. When smectites and smectite-rich mixed-layer clays are the most common, rock properties can be unpredictable and are subject to change by reaction with pore fluids. Other minerals that are present are less likely to have a widespread effect on shale properties.

Environments of Deposition of Shale

Shale and related rocks are found in sedimentary units of both continental and marine origin. The accumulation of fine-grained sediment requires an abundant source of clay size fragments generally derived from the chemical weathering of landmasses and a substantial reduction in the coarser fractions through either sorting by a turbulent current (streams, surf, wind, etc.) or rapid "dumping" of clays. Since such conditions can be realized in a multitude of different ways, beds or lenses of shales can be expected in terrestrial environments (flood plains, lakes), near shorelines (lagoons, sheltered coves), on the continental shelf (the "normal" setting for shales), or in abyssal plains (turbidites, clays, oozes). Few shales are found without other clastic sediments. When shales predominate, they usually give their name to a stratigraphic unit: for example, Chinle Shale is a term sometimes used to describe a Triassic unit of the Colorado Plateau which also contains lenses of sandstones and conglomerates.

Large accumulations of shales are found in terrestrial environments (a classic example is the Green River Shale (Middle Eocene), which has a thickness of 2100 m), but marine shales are usually thicker, especially in areas of high subsidence rates and minimal deformation, such as miogeoclines and stable continental margins.

Diagenesis of Shale

Shale undergoes profound changes between the time it settles as a soft sediment and the time it acquires the appearance of a rock. This "curing" process, or diagenesis, is quite complex: water is expelled by compaction, new minerals form, grain-size changes, the composition of pore fluids is modified, and occasionally, pores are filled with silica or calcite. The following discussion deals mainly with the diagenetic effects which may affect the hydrologic properties of shale.

Compaction. The effect of compaction on the hydrologic properties of shale has been well investigated (Smith, 1971, 1973; Magara, 1973). Because of the low permeabilities of clays, rapid burial of clay-rich sediments may result in a build-up of fluid pressure, leading to abnormal porosity/depth relationships. Smith and Magara, using similar approaches, showed that these abnormally high pore pressures can persist for tens of millions of years, a fact also observed by Magara in the Upper Cretaceous shale of Canada. Smith (1971) has presented tables listing calculated variations in porosity, permeability, pressure, water velocity, etc. These calculated figures suggest that during compaction permeability increases in general (up to tenfold) while porosity decreases. However, Smith's assumptions about initial porosity/permeability relationships disagree with the seemingly more accurate estimates of Magara (1973). There seems to be a consensus that compaction overpressures are unlikely to extend into the Paleozoic strata.

Mineralogic Changes. Under the conditions of pressure and temperature likely to prevail in a depositional basin (less than 10 km deep, less than 200°C), the changes in mineralogy affect mainly the smectites and illite/smectite mixed-layer clays. According to Powers (1967), smectite undergoes dehydration and begins to change into illite at a depth of 2000 m; he found that the reaction is complete at about 3500 m. More recently, this transitional process was thoroughly investigated by Hower et al. (1976), Aronson and Hower (1976), and Yeh and Savin (1977). Results show that, between 1400 and 3800 m and at temperatures between 44 and 100°C shales from the Gulf Coast area exhibit a progressive enrichment of illite (from 20% to 80%) in the illite/smectite mixed-layer clays. No further change occurs until about

7500 m (about 200°C), where both the remaining smectite and the illite disappear, and shales evolve into an assemblage of dioctahedral mica (muscovite), chlorite, albite, and quartz. The initial change follows the scheme

$$\text{smectite} + K^{+} + Al^{+3} \rightarrow \text{illite} + Si^{+4} + H_2O$$

and is not reversible. The potassium and aluminum are supplied by potassium feldspar, calcic plagioclase, and kaolinite, which show a conspicuous disappearance at depth. The reaction is further complicated by a loss of iron and magnesium.

Diagenetic changes that affect mineralogy have a tremendous impact on the hydrologic properties of shale. Decreases in the smectite content lower the variability in the plasticity, ion exchange characteristics, hydration-dehydration characteristics, semipermeable behavior, etc. Water release, increased compaction, silica release, and silicification may be equally important in some cases (Towe, 1962). The extreme conditions needed to eliminate completely the mixed-layer clays are not common, except perhaps in deeply buried (hence often the oldest) shale, such as the argillites of the Precambrian Belt Series of Montana and Idaho (Maxwell and Hower, 1967).

There is compelling evidence that a relationship, perhaps unrelated to burial, exists between clay mineralogy and the age of the shale. Kaolinite- and smectite-rich mixed-layer clays are more common in Cenozoic shale, whereas chlorite and illite predominate in pre-Mesozoic clays. This difference may reflect variations in the source material, differences in burial depth, or a dependence on the rate of reaction for diagenetic changes. The two latter possibilities cannot be easily distinguished, but Hower et al. (1976) have concluded that burial metamorphism is at least partly responsible for age-related differences. They found that recent clays (which underwent shallow burial) contain 30% illite, that Cenozoic and Mesozoic clays (buried to variable depths) contain between 30% and 65% randomly stratified illite, and that pre-Mesozoic clays contain 65% illite with ordered interstratification. Similar age-related changes are found among other minerals. Such changes include the progressive disappearance of carbonates, calcic plagioclase, and potassium feldspars and the progressive increase in quartz and albite.

Changes in Pore Fluids. The composition of pore fluids in the early stages of burial is the same as that of the environment of deposition: fresh water or lake brine for terrestrial sediments and seawater for marine deposits. Later, interactions with the surrounding rocks occur: the transformation of smectite into illite decreases the potassium/sodium ratio, and the Eh and pH undergo changes which affect the concentrations of SO_3^{-2}, H_2S, NH_4^+, and NO_3^-. As the ion exchange sites on the clays become saturated, the shale acts as a semipermeable membrane. The resultant osmotic pressures have been observed to modify predicted patterns of fluid flow by their effect on hydraulic gradients (Berry, 1959).

The permeability of shale is likely to be affected during reactions with pore fluids, but precise data are once again scanty. Samuels (1950) showed that the dissolved ions (notably their charges) affect permeabilities (the higher the charge, the greater the permeability). Smectites are more affected than kaolinite (Fig. 1-1); permeability ratios (Al/Na) are 0 and 3.5, respectively. It is important to note that, although permeabilities decrease with pressure, their ratios appear to remain constant. In terms of its sensitivity to dissolved ions, illite would presumably lie somewhere between smectite and kaolinite. A reasonable guess would be that the ionic substitution effect would be reduced during the illitization of smectite-rich sediments. Another guess would be that the permeability of shale can increase if different ions are introduced by ground water movements.

Cementation. Since the illitization of clay is a possible source of soluble silica (Towe, 1962), drastic drops in porosity and permeability can be expected during burial. If such changes were to take place, however, they would produce anomalous porosity/permeability relationships. Obviously, a silicified shale could also yield rocks of high fracture permeability, but such instances would be very difficult to predict.

Other Changes. A common diagenetic change is the growth of larger grains at the expense of smaller fragments of the same materials. In shale the process affects quartz and carbonates more often than clays, and it contributes to the filling of pores and the disappearance of plasticity. Locally, it may produce a dense, massive rock in which later deformations may induce fracture permeabilities much higher than those ordinarily found in shale.

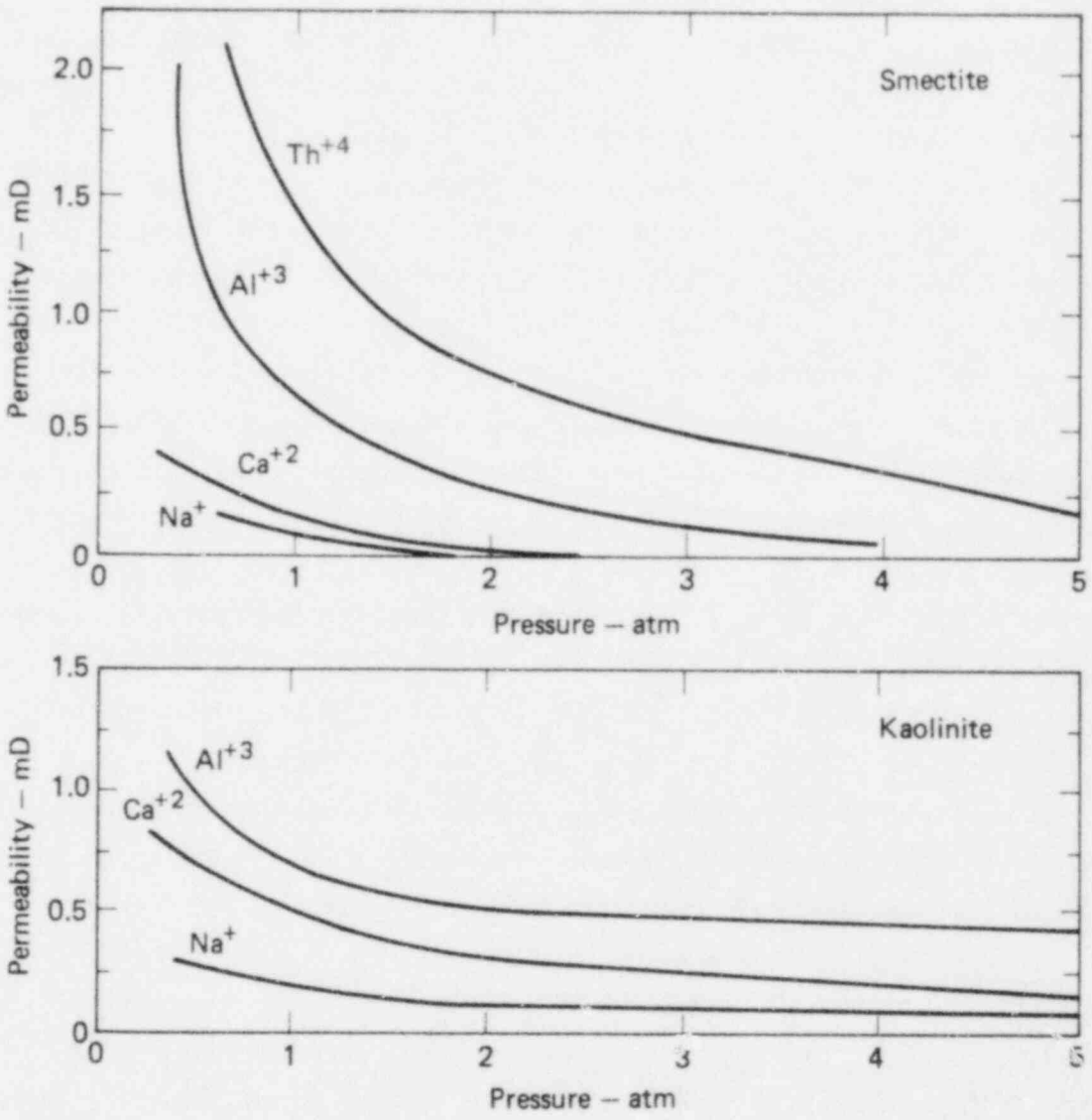

FIG. 1-1. Effect of ion adsorption on the permeability of two clay minerals: (a) smectite (montmorillonite) and (b) kaolinite (from Samuels, 1950). In all cases, clays are saturated with the indicated cations.

To sum up, during diagenesis the physical, chemical, and hydrologic properties of shale can be modified by predictable regional factors--depth of burial, age, initial composition, etc.--or by local conditions which are more difficult to evaluate--osmosis, loss of plasticity, etc.

Major Shale Occurrences in the United States

Shale appears on nearly all geologic maps of the United States. Many units are thin interbeds in clastic sequences and, as such, offer limited potential for repository sites. Others, more suitable for such use, occur in massive beds up to a thousand meters thick and have a wide areal extent.

The thickest and widest shale units are Cenozoic and Mesozoic in age and are found mainly west of the Mississippi Valley. Believed to be the source of many petroleum deposits, they have received more attention than the older shale. A few widespread Paleozoic shales are found, mainly east of the Rocky Mountains, and occasionally, thick Precambrian shales have been described in scattered parts of the continent. The following major shale units are listed in order of increasing age.

Tertiary Shale. Shale of marine origin is found in the thick clastic wedges of California (Great Valley, Coast and Transverse ranges) and the Gulf Coast. Its age ranges from Pliocene to Miocene in the Coast Range and to Eocene elsewhere. Shale of continental origin reaches considerable thickness in the northern Colorado Plateau (Green River Basin of Eocene age).

Cretaceous Shale. Shale of Cretaceous age occurs in several areas. Its greatest extent is a vast blanket spread from the Colorado Plateau to the edge of the Appalachians and from the Canadian Rockies to the Gulf Coast. This broad unit has received various names: it is best known as the Pierre Shale in the northern Great Plains and has been correlated elsewhere with such units as the Adaville, Mentor, Benton, etc. Also, the thick Mancos Shale from the Mesa Verde Wedge is partially contemporaneous with the Pierre Shale. Cretaceous shale is also found along the Atlantic Coast (Middendorf Shale) and in the Great Valley sequence of California.

Jurassic and Triassic Shale. In contrast with younger groups, Jurassic and Triassic shale is rather uncommon. Occurrences include the continental shale in the Colorado Plateau (Upper Jurassic Morrison Formation) and along the East Coast (Brunswick Shale in Triassic basins).

Paleozoic and Precambrian Shale. A particularly persistent shale unit occupies the Upper Paleozoic section between the Rocky Mountains and the East Coast. It is best known as the Chattanooga Shale with other names being approximate equivalents: Cherokee, Stanley, Hamilton, etc. However, this unit does not have the same age everywhere (Clark and Stearn, 1968). Beyond the limits of the Chattanooga Shale, a somewhat similar unit is found in the Great Basin (eastern Nevada and western Utah). It is the Eleana Formation (Devonian-Mississippian), which is part of a thick flysch sequence in the Antler Trough (Poole and Sandberg, 1977). Finally, a few instances of large shale units have been reported in the Upper Precambrian; an example is the Terrigenous Detrital sequence which occupies the same general area as the Eleana Formation in the Great Basin and the Nonesuch Formation in the northern Appalachians.

COMPILED HYDROLOGIC DATA

The following lists of hydrologic properties of shales are divided among six geologic regions (Fig. 1-2). Each list is preceded by a brief description of the geology of the region and a stratigraphic table designed to show the position of the shales with respect to other geologic units.

For each region, permeabilities, porosities, and densities are presented first. Other parameters, for which fewer data are available are listed separately. Bibliographic references for the hydrologic data are listed in alphabetical order at the end of each section.

In general, permeability values were changed into water conductivities at $15^{o}C$, assuming that 1 darcy is equivalent to 8.54×10^{-4} cm/s (Davis and DeWiest, 1966).

FIG. 1-2. Location of areas containing shales discussed in the table of hydrologic properties.

Region 1: Pacific Coast, Great Valley, and Great Basin

The western edge of the American continent has been the site of converging plate activity at least since mid-Paleozoic times. Activity occurred intermittently until the Late Cenozoic, when subduction was replaced by a combination of strike-slip movement along the San Andreas Fault system and tensional deformation in the Great Basin (Atwater, 1970). As plates were consumed under North America, shale-rich sediments were laid down in a series of linear basins more or less parallel to the present Pacific shoreline. The oldest zone of deposition developed during the Paleozoic in an area presently located in eastern Nevada and western Utah; younger zones appeared in the Great Valley of California and in the Coastal and Transverse ranges. The following shales are associated with these zones.

• The Great Basin shales, which belong to the Terrigenous Detrital sequence (Stewart and Suczek, 1977) and the Eleana Formation (of Eocambrian-Cambrian and Devonian-Mississippian ages, respectively). Stewart and Suczek believe that their Terrigeneous Detrital sequence evolved during the early stages of the opening of the ancestral Pacific Ocean. The location of this sequence is shown in Fig. 1-3. The Eleana Formation represents, according to Poole and Sandberg (1977), a forearc assemblage of the Antler geosyncline. Figure 1-4 shows its general location and thickness. The stratigraphic of both shales of the Great Basin are included in Table 1-2.

• The Great Valley shales. These shales developed within a Mesozoic, and perhaps Tertiary, forearc basin which has persisted nearly unchanged until the present. During that time alternations of shale and sandstone were accumulated to thicknesses which locally exceed 10,000 m, mainly as Cretaceous, flysch-type, Great Valley sequence. The Panoche Formation is an

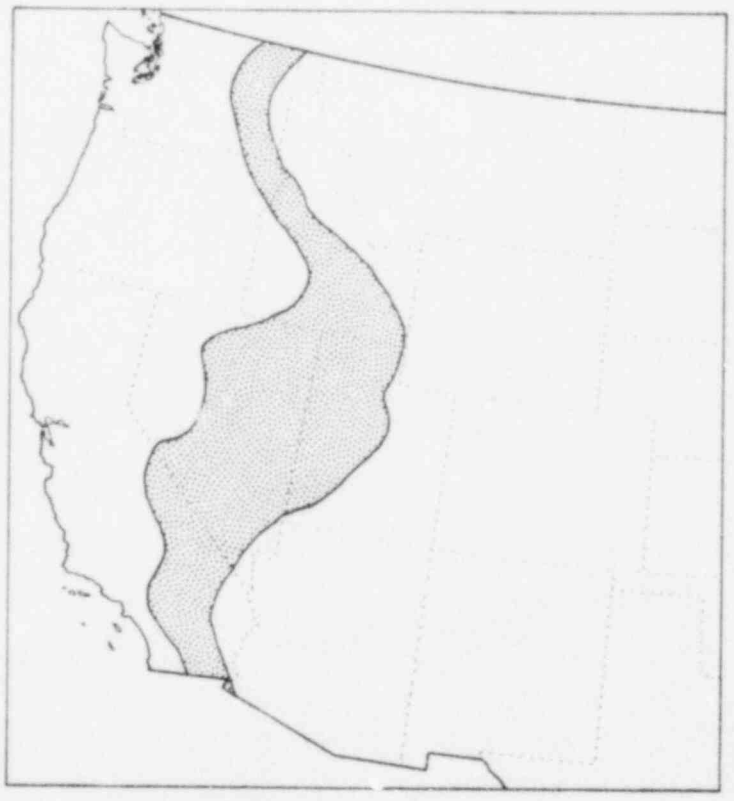

FIG. 1-3. Map showing the location of the Cambrian Terrigenous sequence in the Great Basin (from Stewart and Suczek, 1977). The stippled area shows the zone where the thickness of the sequence exceeds 300 m.

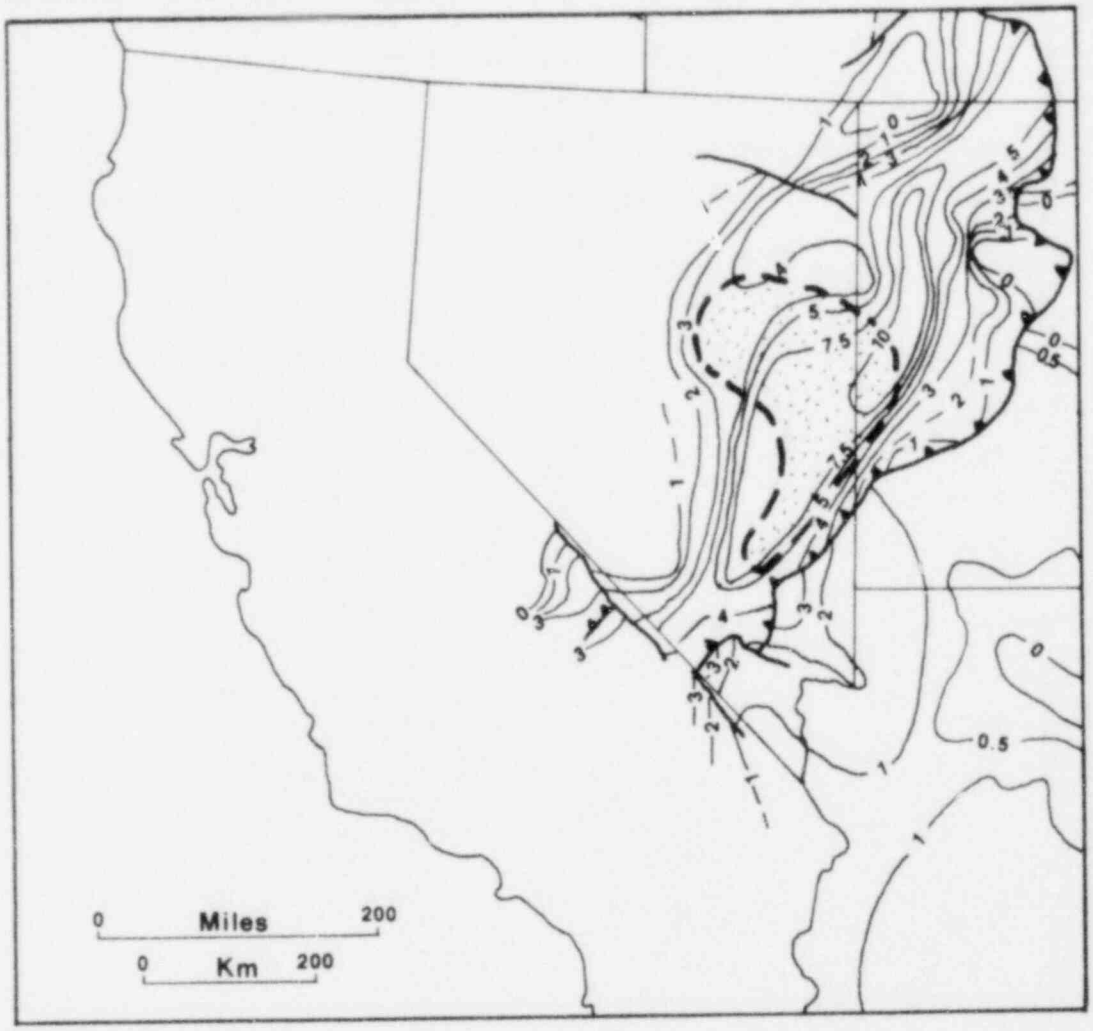

FIG. 1-4. Map showing the location of the Eleana Formation facies (dotted area) within the Upper Devonian-Mississippian of the Great Basin (after Poole and Sandberg, 1977). Isopacs are labeled in hundreds of meters.

example of a predominately shaly unit which locally reaches thicknesses of 6700 m. The bibliographic search undertaken for this chapter did not turn up parameter values for this formation. Further search would be useful. Cenozoic shale of the Great Valley is much thinner (less than 1000 m), but, being associated with oil and gas fields, the rock has undergone more scrutiny. The many names of the shale formations of that group (Eocene to Pliocene) are shown in Table 1-3.

- Coastal shale. This shale is Miocene and Pliocene in age and represents western extensions of similar units in the Great Valley. It is associated with hydrocarbon deposits. Examples of the structural style characterizing the Great Valley and the Coastal Range are given in Figs. 1-5 and 1-6. Detailed stratigraphy is shown in Table 1-4.

Hydrologic properties for region 1 are given in Tables 1-5 and 1-6.

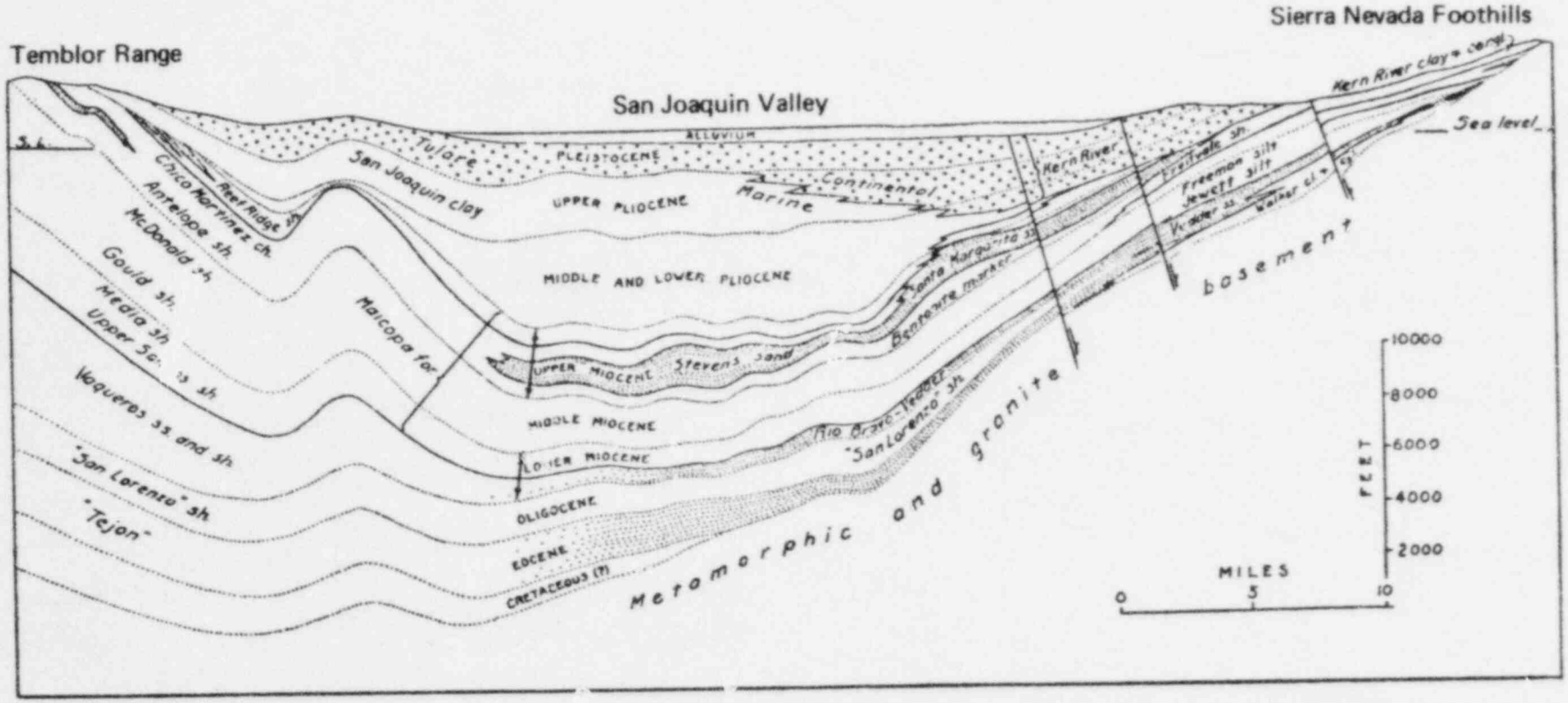

FIG. 1-5. Generalized section across the San Joaquin Valley (from Eardley, 1962).

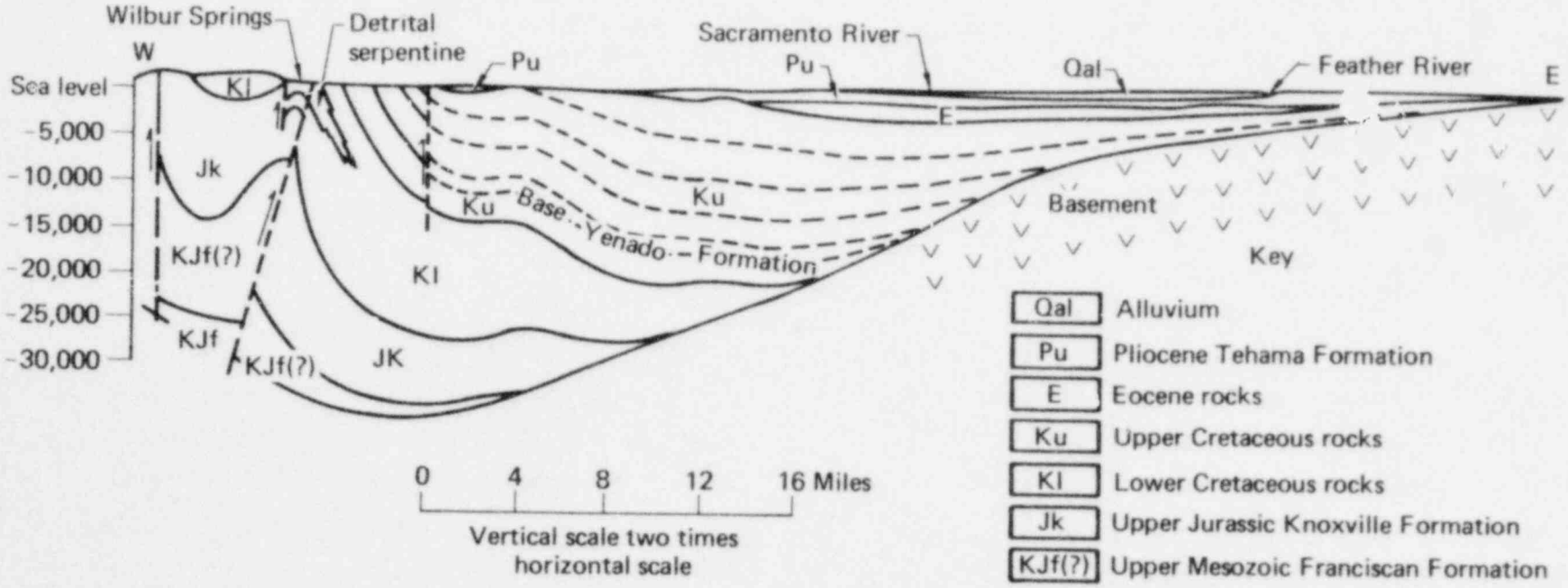

FIG. 1-6. Generalized section across the Sacramento Valley, showing the thicknesses of Mesozoic sediments (after Emerson and Rich, 1966).

TABLE 1-2. Summary of Paleozoic rocks in the Great Basin (Eastern Nevada, Western Utah) (from Stewart and Suczek, 1977). Shales described in Tables 1-5 and 1-6 are followed by an asterisk.

Age		Stratigraphic Unit	Thickness, m	Description
Permian		Antler sequence	1500	Miogeosynclinal limestones, dolomites, and minor mudstone
Pennsylvanian		Tippipah Limestone	approx 400	Massive limestone
Mississippian		Eleana formation	1500-3000	Shales, sandstones, mudstones, and minor limestones of the Antler Flysch Trough
Devonian	Upper			
		----------		Unconformity
	Middle	Nevada formation	450-1450	Silty dolomite
		----------		Unconformity
	Lower	Spotted Range Dolomite	50-500	Dolomite, dolomitic limestone, with minor chert beds
Silurian	Upper			
	Lower	Ely Springs Dolomite	40-360	Massive crystalline dolomite
Ordovician				
		----------		Unconformity
Cambrian	Upper	Eureka Quartzite	approx 1000	Massive quartzite
	Middle	Antelope Limestone	approx 1000	Limestone with a few interbeds of siltstone
	Lower	Terrigenous Detrital sequence*	6000+	Siltstone, carbonate rich siltstones, and fine-grained quartzite
Uppermost Precambrian				

TABLE 1-3. Summary of rock units in the San Joaquin Valley area, California (from Kirby, 1943; Hackel, 1966; Maher et al., 1975.) Shales described in Tables 1-5 and 1-6 are followed by an asterisk.

Age		Stratigraphic Unit	Thickness, m		Description
Recent		Alluvium	0-45		Poorly sorted, unconsolidated silts, clays, and sands and pebbles
Pleistocene		Tulare formation	0-915		Nonmarine: Contains Corcoran Clay member, interbedded nonmarine mudstones and pebbly sands
Pliocene		San Joaquin Formation*	0-549		Shale and interbedded clayey siltstone and silty sandstone
	Middle	Etchegoin Formation*			
		Carmen Sandstone member	394		Interbedded grayish green siltstone and feldspathic, glauconitic, fine- to medium-grained sandstone
	Lower	Tupman Shale member	406		Olive gray silty shale
Miocene	Upper	Reef Ridge Shale*	56-176		Soft blue clay shale, minor layers of sandy shale
		----------			----Unconformity
	Middle	Monterey Shale*			
		Elk Hills Shale	549-1000		Gray siliceous shale, siltstone, and minor claystone
		McDonald Shale*	95		Massive brown silty shale
		Gould and Devilwater Shale member*	59-235		Siliceous shale
	Lower	Temblor Formation*	457		Contains Media Shale member, alternating sandstone and shale sequence
		----------			----Unconformity
Oligocene		Wagonwheel Formation	0-152		Argillaceous sandy shale interbedded with sandy beds
Eocene		Kreyenhagen Formation*	274		Fissile shales and fine- to coarse-grained arkosic sandstones
		Lobo Formation			Shales, sandy shales, sandstones
Paleocene					

Marine

continued

TABLE 1-3 continued.

Age		Stratigraphic Unit	Thickness, m		Description
Cretaceous	Upper	Chico series			
		Moreno Formation	915	Miogeoclynal	Interbedded organic shale and fine-grained sandstone
		Panoche Formation	6708		Predominantly shale with sandstone and conglomerate
	Lower	Shasta series	6098		Mudstone, siltstone, graywacke, conglomerate, and minor limestone
Jurassic		Knoxville Formation	6098	Eugeoclynal facies	Black, hackly, fracturing shales or mudstones; massive lenticular conglomerates
		Franciscan	15,000+		Graywacke, dark shale, volcanics, chert, limestones, metamorphics
		----------			Unconformity
Pre-Jurassic and Paleozoic					

TABLE 1-4. Summary of rock units in the California Coast ranges (from Page, 1966; Cummings et al., 1962; Kirby, 1943.) Shales described in Tables 1-5 and 1-6 are followed by an asterisk.

Age	Stratigraphic Unit	Thickness, m	Description
Pleistocene	Terrace deposits	12	Interbedded coarse sand and gravels
Plio-Pleistocene	Santa Clara Formation*	549	Poorly consolidated, interbedded conglomerates, sandstone and mudstone
Pliocene and Mio-Pliocene	Purisima Formation	23	Sandstone, mudstone, siliceous mudstone and porcellanite, volcanic standstones, diatomite, vitritic tuffs
Miocene	Monterey Formation*	2744	Light-colored, diatomaceous and siliceous shale and sandstones
	Mindego Formation	610-1220	Complex interstratified basaltic volcanic rocks, mudstone, sandstone, and carbonates
Oligocene	Vaqueros Sandstone	732-1372	Fine- to medium-grained arkosic arenite with interbedded shale and mudstone
	San Lorenzo Formation	396-823	Mudstone and shale
	----------		Unconformity
Eocene	Butano Sandstone		Arkosic sandstone, including turbidite, with mudstone interbeds
Paleocene	Logatelli Formation	76-244	Dark gray, massive siltstone

continued

TABLE 1-4 continued.

Age			Stratigraphic Unit	Thickness, m	Description
Cretaceous	Upper		Great Valley sequence		
			Forbes Formation	640	Mudstone, interbedded siltstone and sandstone
			Guinda Formation	335	Arkosic sandstone (turbidite)
			Funks Formation	457	Mudstone, minor sandstone
			Sites Formation	762	Arkosic sandstone; mudstone and siltstone
			Yolo Formation	945	Mudstone, minor sandstone
			Venado Formation	915	Arkosic sandstone (turbidite); mudstone; local conglomerate
			Fiske Creek Formation	1220	Mudstone; minor interbedded siltstone; sandstone
	Lower		Brophy Canyon Formation	457	Sandstone, mudstone, local conglomerate
			Dav's Canyon Formation	1951	Mudstone and feldspathic sandstone (turbidite); mudstone
			Little Valley Formation	1372	Mudstone and minor feldspathic sandstone (turbidite)
			Crack Canyon Formation	1098	Mudstone, minor arkose, conglomerate lenses
Jurassic	Upper		Knoxville formation	2165+	Mudstone, shale, graywacke, conglomerate lenses, basalt breccias and flows, detrital serpentine
		Dual-core complex	Franciscan Formation core	15,000+	Graywackes, shales, volcanics (pillow lavas), chert, limestone, metamorphics
Cretaceous			Granitic-metamorphic core		
			Granitic plutons		Quartz diorite, grandodiorite, adamellite, 69-110 m.y.
Paleozoic(?)			Sur series		Gneisses, schists, quartzites, marbles and granulites; metamorphic miogeoclynal equivalents

TABLE 1-5. Hydrologic data for region 1: Pacific Coast, Great Valley, and Great Basin.

Geologic setting	Age	Locality	Depth, m	Number of samples	Porosity Av.	Porosity Max.	Porosity Min.	Hydraulic conductivity, cm/s Av.	Hydraulic conductivity, cm/s Max.	Hydraulic conductivity, cm/s Min.	Ref.	Method
Silts and clays[a]	Recent	Santa Barbara basin off S. Calif.	1		79			6E-12			2	Graphical
			2		77			3.9E-12				
			3		75			1.7E-12				
			4		74			7.7E-13				
			5		73			6.0E-13				
Core-hole 75/1E-16C6	Recent-Pliocene	Santa Clara Valley, Calif.[b]									4	Porosity: (d) dry unit specific weight (s) measured, porosity, then calculated from equation r = (sd/s)(100%)
Clayey silt			70.1		42.1			2.8E-8				Permeability: measured using both a constant-head permeameter for samples with medium to high permeability and a variable-head permeameter for samples with low permeability
Clayey silt			78.7		40.9			9.4E-9(H)				
Clayey silt			84.0		41.8			3.3E-7(V) 1.9E-7(H)				
Clayey silt			101.9		40.7			9.4E-9(H)				
Silty clay			122.4		43.0			1.4E-8(V) 4.7E-8(H)				
Clayey silt			247.5		40.9			4.7E-7(H)				
Clayey silt			277.0		34.8			9.4E-9(V) 1.4E-8(H)				
Clayey silt			285.9		40.8			4.7E-9(V) 9.4E-8(H)				

continued

[a] Analysis of 100 cores.

[b] Bay sediments and Santa Clara Formation (boundary not located on cores). H = horizontal hydraulic conductivity; V = vertical hydraulic conductivity.

TABLE 1-5 continued.

Geologic setting	Age	Locality	Depth, m	Number of samples	Porosity Av.	Porosity Max.	Porosity Min.	Hydraulic conductivity, cm/s Av.	Hydraulic conductivity, cm/s Max.	Hydraulic conductivity, cm/s Min.	Ref.	Method
Core-hole 65/2W-24C7	Recent-Pliocene	Santa Clara Valley, Calif.[b]									4	Same as above
Clayey silt			15.3		40.8							
Clayey silt			21.9		39.3			4.8E-5(V) 4.8E-5(H)				
Silty clay			27.6		44.7			2.4E-5(V) 3.8E-5(H)				
Silty clay			43.1		40.5			1.9E-5(V) 3.3E-5(H)				
Silty clay			48.8		43.4			9.5E-5(V) 9.5E-5(H)				
Clayey silt			54.4		41.0			1.9E-4(V) 9.5E-5(H)				
Silty clay			58.4		36.8			2.8E-8(V) 3.3E-8(H)				
Silty clay			67.9		43.4			1.9E-7(V) 4.7E-8(H)				
Clayey silt			93.7		37.1			9.4E-[illegible](V) 1.9E-8(H)				
Clayey silt			100.7		37.6			3.8E-7(V) 4.2E-7(H)				
Clayey silt			124.5		36.4			4.9E-9(V) 1.4E-7(H)				
Clayey silt			139.8		39.3			4.7E-8(V) 2.4E-7(H)				

continued

[b]Bay sediments and Santa Clara Formation (boundary not located on cores). H = horizontal hydraulic conductivity; V = vertical hydraulic conductivity.

TABLE 1-5 continued.

Geologic setting	Age	Locality	Depth, m	Number of samples	Porosity Av.	Porosity Max.	Porosity Min.	Hydraulic conductivity, cm/s Av.	Hydraulic conductivity, cm/s Max.	Hydraulic conductivity, cm/s Min.	Ref.	Method
(Core-hole 65/2W-24C7)												
Clayey-silt			166.3		38.5			1.4E-8(H)				
Clayey-silt			171.8		39.9			9.4E-8(V) 9.4E-8(H)				
Silty-clay			218.3		37.8			3.3E-8(V) 2.4E-8(H)				
Silty-clay			227.2		44.9			2.4E-8(V) 4.7E-8(H)				
Clayey-silt			247.6		37.4			1.9E-8(V) 4.7E-8(H)				
Silty-clay			263.8		40.1			9.4E-9(V) 3.8E-8(H)				
Clayey-silt			266.0		31.4			9.4E-9(H)				
Silty-clay			274.5		39.4			1.9E-7(H)				
Clay			281.7		43.7			1.9E-7(V) 3.3E-7(H)				
Core-hole 24/26-36A2	Upper Pliocene to Pliocene(?)	Tulare-Wasco area, Calif.[c]									4	Same as above
Clayey-silt			257.2	N/A	48.9			1.4E-7(V)				
Silt			259.9	N/A	46.0			2.8E-7(V)				

continued

[c]Marine strata.

TABLE 1-5 continued.

Geologic setting	Age	Locality	Depth, m	Number of samples	Porosity Av.	Porosity Max.	Porosity Min.	Hydraulic conductivity, cm/s Av.	Hydraulic conductivity, cm/s Max.	Hydraulic conductivity, cm/s Min.	Ref.	Method
(Core-hole 24/26-36A2)												
Clayey-silt			279.5		46.9			2.8E-7(V)				
Silty-clay			316.1		50.2			1.9E-7(V)				
Core-hole 23/25-16N1	Pleistocene to Upper Pliocene	Tulare-Wasco[d] area, Calif.									4	Same as above
Clayey-silt			87.7		50.7			1.9E-8(V) 2.4E-8(H)				
Clayey-silt			89.9		61.0			1.9E-8(V) 1.9E-8(H)				
Clayey-silt			104.7		39.5			4.7E-7(V) 1.9E-7(H)				
Core-hole 14/13-11D1	Pleistocene to Upper Pliocene	Los Banos-Kettleman Hills[d] area, Calif.									4	Same as above
Silty-clay			131.8		42.8			3.3E-9(V)				
Silty-clay			155.7		47.3			9.4E-9(V)				
Core-hole 16/15-34N1	Pleistocene to Upper Pliocene	Los Banos-Kettleman Hills[d] area, Calif.									4	Same as above
Clayey-silt			154.8		42.9			9.4E-8(V)				
Clayey-silt			155.4		48.4			2.8E-7(V) 1.8E-7(H)				
Clayey-silt			160.4		47.9			9.4E-8(V) 1.8E-7(H)				

continued

[d]Corcoran Shale.

TABLE 1-5 continued.

Geologic setting	Age	Locality	Depth, m	Number of samples	Porosity Av.	Porosity Max.	Porosity Min.	Hydraulic conductivity, cm/s Av.	Hydraulic conductivity, cm/s Max.	Hydraulic conductivity, cm/s Min.	Ref.	Method
Core-hole 19/17-22J1,2	Pleistocene to Upper Pliocene	Los Banos-Kettleman Hills area, Calif.[d]									4	Same as above
Clayey-silt			237.5		42.9			1.9E-8(V)				
Clayey-silt			247.1		43.4			2.4E-7(V)				
Etchegoin Formation[e]	Pliocene	Naval Petroleum Reserve #1, Elk Hills, Calif.									6	Self-potential log and core analysis
Buliminella silt zone,			1225-1236	14	28	32	24	1E-2	6.8E-2	0		
well 324-19R			1238-1436	60				(all wells = 0)				
Reef Ridge Shale[f]	Middle to late Miocene	Naval Petroleum Reserve #1, Elk Hills, Calif.	1439-1482	13				(all wells = 0)			6	Same as above
Monterey Shale and Stevens oil zone	Middle to late Miocene	Naval Petroleum Reserve #1, Elk Hills, Calif.									6	Same as above
N-zone[g]												
358-22R			2220-2221	4	17	20	15	1.1E-2	2.3E-2	4E-3		
378-22R			2095	2	(all wells = 14)			3E-4		0		

continued

[d] Corcoran Shale.

[e] Tupman Shale member; olive gray silty shale beds.

[f] Brown clayey and silty shale beds.

[g] Brown to gray diatomaceous siltstones and lesser amounts of brown to gray, silty, partly siliceous shale, and very fine to medium-grained silty sandstone.

TABLE 1-5 continued.

Geologic setting	Age	Locality	Depth, m	Number of samples	Porosity			Hydraulic conductivity, cm/s			Ref.	Method
					Av.	Max.	Min.	Av.	Max.	Min.		
(Monterey Shale and Stevens oil zone)												
A-zone[h]												
342-3G			2139-2150	8	20	25	14	2.2E-2	7.3E-2	0		
362-3G			2125-2143		20	29	12	1.1E-2	3.6E-2	0		
382-3G			2140-2153	20	15	19	12	1E-3	6E-3	0		
343-4G			1984-2044	9	16	20	11	6E-4	4E-3	0		
382-4G			2055-2067	16	15	21	8	3E-3	1.1E-2	0		
378-22R			2099-2204	50	17	26	12	1.9E-2	3E-1	0		
322-25R			1647-1704	19	16	23	8	2E-3	1E-2	0		
312-26R			1962-1963	3	20	23	14	1.4E-1	3E-1	1E-3		
344-26R			1830-1876	10	19	26	13	5.2E-1	1.9E-1	0		
526-28R			1571-1576	5	23	25	18	2E-3	6E-3	0		

continued

[h]Brown to gray, diatomaceous, partly sandy dolomitic siltstone interbedded with brown to gray, silty, mostly siliceous shale; gray, silty, very fine-grained sandstone in beds 1-4 ft thick; and some thin layers of dolomite.

TABLE 1-5 continued.

Geologic setting	Age	Locality	Depth, m	Number of samples	Porosity			Hydraulic conductivity, cm/s			Ref.	Method
					Av.	Max.	Min.	Av.	Max.	Min.		
(Monterey Shale and Stevens oil zone)												
(A-zone)												
344-305			2241-2280	14	14	21	9	1E-3	5E-3	0		
542-315			1530-1537	5	23	30	7	2E-3	5E-3	0		
366-325			1706-1757	33	14	23	10	1.4E-2	7.1E-2	0		
388-325			1866-1890	7	18	19	16	4E-5	2E-3	0		
386-335			2076-2086	13	18	23	10	8E-3	2.2E-2	0		
337-345			2020-2021	2	16	19	13	3.5E-5	1E-3	0		
344-345			2137-2152	17	17	20	13	3E-3	1.5E-2	0		
326-355			2027-2043	19	17	22	11	4.6E-3	6E-3	0		
344-355			2090-2095	8	17	26	13	5.9E-2	2.5E-1	6E-3		
384-355			2166-2172	7	19	21	16	1.2E-2	4.5E-2	0		
17-14Z			1513-1518	8	24	29	19	2E-3	1.1E-2	0		

continued

TABLE 1-5 continued.

Geologic setting	Age	Locality	Depth, m	Number of samples	Porosity			Hydraulic conductivity, cm/s			Ref.	Method
					Av.	Max.	Min.	Av.	Max.	Min.		
(Monterey Shale and Stevens oil zone)												
B-zone[i]												
342-2G			2218-2420	415	22	32	9	7.5E-5	7.9E-4	0		
342-3G			2152-2326	413	23	33	8	1E-4	8.7E-4	0		
382-3G			2168-2346	402	22	29	12	1.8E-4	1.2E-3	0		
343-4G			2064-2221	247	22	29	14	9.8E-5	7.9E-4	0		
345-4G			2211-2334	121	17	26	6	3.6E-5	3E-4	0		
382-4G			2118-2284	355	22	30	11	9.8E-5	1.9E-3	0		
321-5G			1830-1940	178	22	29	13	1E-4	6.1E-4	0		
362-5G			1976-2063	145	23	29	14	6.5E-5	6.9E-4	0		
342-6G			2205-2206	2	15	16	14	3.4E-6	4.3E-6	2.6E-6		
342-6G			2236-2237	3	13	14	12	5.1E-6	1.1E-5	1.7E-6		
362-6G			2141-2145	3	19	21	18	9.4E-6	1.7E-5	8.6E-7		
322-23R			2709-2719	28	8	14	8	2.9E-7	6.6E-7	0		

continued

[i] Interbedded brown to gray diatomaceous siltstone; brown to gray, silty, mostly siliceous shale; and very fine grained silty sandstone.

TABLE 1-5 continued.

Geologic setting	Age	Locality	Depth, m	Number of samples	Porosity			Hydraulic conductivity, cm/s			Ref.	Method
					Av.	Max.	Min.	Av.	Max.	Min.		
(Monterey Shale and Stevens oil zone)												
(B-zone)												
388-23R			1876-1991	120	23	30	16	3.5E-5	5.5E-4	0		
322-25R			1711-1771	63	21	26	12	1.6E-5	1.8E-4	0		
335-25R			1641-1700	75	22	32	16	2.5E-5	1.8E-4	0		
348-25R			1679-1767	60	23	31	14	3.0E-5	1.2E-4	0		
362-25R			1842-1909	70	22	30	11	1.4E-5	9E-5	0		
368-25R			1589-1685	6	21	26	17	5.8E-5	1.5E-4	8.6E-6		
382-26R			1687-1777	115	21	29	6	2.1E-5	5.4E-4	0		
382-26R			1813-1912	56	21	27	13	3.3E-5	2.6E-4	0		
526-28R			1634	1	20			1.2E-5				
526-28R			1656	1	25			1.9E-4				
382-34R			2482-2529	18	13	19	7	3.6E-7	2.6E-6	0		
362-36R			1668-1771	65	23	32	17	5.9E-5	4.5E-4	8.6E-7		
326-30S			1740-1830	63	24	31	14	1.4E-5	7.6E-5	0		

continued

TABLE 1-5 continued.

Geologic setting	Age	Locality	Depth, m	Number of samples	Porosity			Hydraulic conductivity, cm/s			Ref.	Method
					Av.	Max.	Min.	Av.	Max.	Min.		
(Monterey Shale and Stevens oil zone)												
(S-zone)												
388-30S			1953-2025	4	17	20	14	1E-5	2.7E-5	2.6E-6		
322-31S			1588-1663	70	21	29	11	2.3E-5	1.1E-4	8.6E-7		
325-31S			1716-1769	50	22	29	17	1.1E-4	4.5E-4	0		
366-31S			1661-1740	103	25	36	15	8.6E-4	9.7E-4	0		
384-31S			1644-1753	46	21	27	15	1.8E-5	6.2E-5	8.6E-7		
388-31S			1860-1993	79	21	28	11	3.5E-5	5.4E-4	0		
542-31S			1586-1628	33	29	35	15	9.7E-5	1.6E-3	0		
322-32S			1842-1917	33	18	23	10	1.1E-5	9.9E-5	0		
326-32S			1680-1752	119	23	30	14	4.9E-5	7.1E-4	0		
366-32S			1757-1877	183	17	29	8	6E-5	3.6E-4	0		
384-32S			1940-2069	168	21	29	5	2.6E-5	1.6E-4	0		
388-32S			1902-2005	193	22	29	12	4.6E-5	5.8E-4	0		

continued

TABLE 1-5 continued.

Geologic setting	Age	Locality	Depth, m	Number of samples	Porosity			Hydraulic conductivity, cm/s			Ref.	Method
					Av.	Max.	Min.	Av.	Max.	Min.		
(Monterey Shale and Stevens oil zone)												
(B-zone)												
348-33S			2005-2122	212	22	29	9	1.2E-4	3.9E-3	0		
386-33S			2087-2230	274	21	28	10	6.1E-5	1.3E-3	0		
337-34S			2070-2071	1	15			5.1E-6				
337-34S			2092-2198	271	22	29	15	1.4E-4	4.1E-3	0		
344-34S			2153-2226	130	18	25	13	5.1E-6	8.5E-5	0		
366-34S			2036-2184	268	21	28	5	1E-4	7.3E-4	0		
384-34S			2091-2220	242	18	24	12	2.9E-5	2.1E-4	0		
326-35S			2046-2220	437	21	30	5	8.9E-5	9.8E-4	0		
344-35S			2104-2271	218	21	28	11	1.2E-4	1.8E-3	8.6E-7		
366-35S			2117-2297	398	21	30	6	5.1E-5	4.9E-4	0		
384-35S			2212-2341	206	18	29	8	7.7E-5	6.7E-4	0		
324-3[illegible]T			2588-2747	179	19	24	5	9.4E-6	2.4E-4	0		
343-31T			2637-2667	22	20	25	13	4.7E-5	4.8E-4	8.6E-6		

continued

TABLE 1-5 continued.

Geologic setting	Age	Locality	Depth, m	Number of samples	Porosity			Hydraulic conductivity, cm/s			Ref.	Method
					Av.	Max.	Min.	Av.	Max.	Min.		
(Monterey Shale and Stevens oil zone)												
C-zone[j]												
343-4G			2223-2250	27	18	22	14	4.3E-6	1.4E-4	0		
362-25R			1915-1922	12	21	26	18	3.6E-5	1E-4	1.7E-6		
382-26R			1788-1812	5	22	26	13	5.1E-6	1.6E-5	0		
386-26R			2046-2070	28	23	29	9	4.7E-5	1.7E-4	0		
322-36R			2019-2148	56	21	29	14	2.6E-5	1.6E-4	8.6E-7		
362-36R			1772-1785	10	16	24	11	5.1E-6	3.3E-5	0		
322-32S			1934	1	15			8.6E-7				
366-32S			1912-1918	9	20	24	14	1E-5	2.8E-5	0		
326-35S			2222-2295	9	15	21	10	1.7E-6	6E-6	0		
324-31T			2750-2885	252	16	24	5	1.2E-5	4.7E-4	0		

continued

[j]Gray, partly siliceous shale that includes some interbedded diatomaceous siltstone, some thin sandstone, and dolomite layers.

TABLE 1-5 continued.

Geologic setting	Age	Locality	Depth, m	Number of samples	Porosity			Hydraulic conductivity, cm/s			Ref.	Method
					Av.	Max.	Min.	Av.	Max.	Min.		
(Monterey Shale and Stevens oil zone)												
D-zone[k]												
368-25R			1794-1795	4	22	25	20	5.3E-5	1.4E-4	2.1E-5		
366-32S			1962-1977	5	14	19	11	4.3E-6	8.6E-6	0		
DD-zone[l]												
368-25R			1898-1934	53	21	31	15	3.3E-5	4.7E-5	0		
382-26R			2003-2059	115	20	27	8	2.9E-5	3.5E-5	0		
E-zone[m,n,o]												
343-4G			2486-2501	26	15	21	6	4.3E-6	1.5E-5	0		
343-4G			2636-2692	78	18	23	11	1.7E-6	1.1E-5	0		
343-4G			2736-2764	41	14	17	11	3.4E-6	9.4E-6	0		
382-26R			2060-2071	33	18	26	12	(all wells = 0)				
524-31S			1870-1973	5	18	22	16	4.3E-6	1.5E-5	0		

continued

[k]Not specified.

[l]Brown to dark silty shale, dark-gray siltstone, and in the lower half, some light gray silty sandstone.

[m]Medium to dark gray siliceous and cherty shale abundant in lower part.

[n]Medium to dark gray partly sandy siltstone abundant in middle and upper parts.

[o]Several thin beds of fine-grained sandstone present in upper part.

TABLE 1-5 continued.

Geologic setting	Age	Locality	Depth, m	Number of samples	Porosity			Hydraulic conductivity, cm/s			Ref.	Method
					Av.	Max.	Min.	Av.	Max.	Min.		
McDonald Shale of local usage[p]	Miocene	Naval Petroleum Reserve #1, Elk Hills, Calif.									6	
343-4G			2885-2927	98	18	24	12	8.6E-7	1.2E-5	0		
343-4G			2954-2976	24	11	16	3	5.1E-6	8.6E-6	0		
556-25R			2129-2154	18	10	12	8	1.7E-7	0			
Gould and Devilwater Shale member[q]	Middle to late Miocene	Naval Petroleum Reserve #1, Elk Hills, Calif.									6	
556-25R			2166	2	7.5	8	7	8.6E-8	0			
Temblor Formation, Media Shale member[r]	Oligocene to early Miocene	Naval Petroleum Reserve #1, Elk Hills, Calif.									6	
556-25R			2251-2263	8	19	22	17	6E-8	8.6E-7	0		

continued

[p]Massive brown silty shale.

[q]Siliceous shale sequence.

[r]Dark, silty, foraminiferal shale, cherty shale, fine-grained sandstone.

TABLE 1-5 continued.

Geologic setting	Age	Locality	Depth, m	Number of samples	Porosity			Hydraulic conductivity, cm/s			Ref.	Method
					Av.	Max.	Min.	Av.	Max.	Min.		
Temblor Formation, Santos Shale member[s]	Oligocene to early Miocene	Naval Petroleum Reserve #1, Elk Hills, Calif.									6	
556-25R			2154	2	20	20		1.6E-5	1.8E-5	1.4E-8		
555-30R			3140	1	4			0				
Fractured shale reservoirs (cherty shale)[t]	Miocene (Monterey)	Santa Maria district, Calif.			6			(8.6E-3 to 1.3E-3)	3E-2		10,11	Empirical determination from production rates history
Shale	Middle Miocene	San Luis Obispo County, Calif.						3.4E-10			3	Streaming potential and SP log[u]
Shale in Stevens sand	Miocene	South Coles Levee Field, Calif.	2876-2877	1	8.0			8.6E-8			7	Estimated from region 1 data[v]
Temblor formation	Middle Miocene	Kettleman Hills, Calif.	1905-2844	(many)	≤3						7	

continued

[s] Light gray to tan and dark brown shale and siltstone.

[t] Fracturing the result of shrinkage during chemical changes.

[u] Measured using a 0.2N NaCl solution.

[v] Bulk density.

TABLE 1-5 continued.

Geologic setting	Age	Locality	Depth, m	Number of samples	Porosity			Hydraulic conductivity, cm/s			Ref.	Method
					Av.	Max.	Min.	Av.	Max.	Min.		
Shale Sh-3	Upper Miocene	Kettleman North Dome oil field, Calif.	6833-6838	1				2.9E-11			5	Measurements made on disaggregated shale in lab[w]
Shale Sh-6	Upper Miocene	Kettleman North Dome oil field, Calif.	6833-6838	1				4.9E-12			5	Same as above, 6000 psi compaction pressure
Shale Sh-9	Upper Miocene	Kettleman North Dome oil field, Calif.	6833-6838	1				8.1E-3			5	Same as above, 9000 psi compaction pressure
Salinas shale[x]	Miocene	Goleta Landing, Calif.	outcrop[y]		33.3			8.7E-4			8	Estimated from region I data
Kreyenhagen shale[z]	Upper Eocene-Oligocene	North Belridge, Calif.			3.9-4.3						1	
Solid shale body with a few fingers of light qtz sand[aa]	Middle Eocene	Rio Vista field, Calif.			25						9	Laboratory estimate
Terrigenous Detrital sequence[bb]	Cambrian, uppermost Precambrian	Yucca Flat, Nev.		10	2.0	3.6	0.7	9.5E-11	3.3E-10	3.3E-11	13	Effective porosity: mercury injection or water saturation methods Permeability: lab test

[w]Measured at 3000 psi compaction pressure.

Density: 1.78 g/cm^3 dry; 2.11 g/cm^3 satd.

[x]Density: 2.56-2.63 g/cm^3 dry; 2.60-2.67 g/cm^3 sat.

[y]Dips 55 S, thin stratum.

[aa]An elongate dome trending NW-SE, with a very complicated fault pattern (Midland 5 zone).

[bb]Siltstone and argillite from well 89-68.

TABLE 1-6. Other properties for region 1.

Formation	Age	Locality	Flow rate, Ml/h-1000 psi	Ref	Notes
Shale	Upper Miocene	Kettleman North Dome oil field, Calif., Well #E5(29-21-17)		5	
Sh-3			6.4		Measured in lab at 3000 psi compaction pressure
Sh-6			12.1		Measured in lab at 6000 psi compaction pressure
Sh-9			2.25		Measured in lab at 9000 psi compaction pressure

References: Tables 1-5 and 1-6 (Region 1)

1. Birch, F., J. R. Schairer, and C. H. Spicer, 1942, Handbook of Physical Constants, Geol. Soc. Am. Special Paper 36.
2. Emery, K. O., and S. L. Rittenberg, 1952, "Early Diagenesis of California Basin Sediments in Relation to Origin of Oil," Bull. Am. Assoc. Petrol. Geol. 36, 735.
3. Gondouin, M., and Scala, C., 1958, "Streaming Potential and the SP Log," Trans. A.I.M.E. 213, 170.
4. Johnson, A. I., R. P. Moston, and D. A. Morris, 1968, Physical and Hydrologic Properties of Water Bearing Deposits in Subsiding Areas of Central California, U.S. Geol. Survey Professional Paper 497-A.
5. Kharaka, Y. K., and F. A. F. Berry, 1973, "Simultaneous Flow of Water and Solutes through Geological Membranes--I. Experimental Investigation," Geochim. Cosmochim. Acta 37, 2577.
6. Maher, J. C., R. D. Carter, and R. J. Lantz,1975, Petroleum Geology of Naval Petroleum Reserve No. 1, Elk Hills, Kern County, California, U.S. Geol. Survey Professional Paper 912.
7. Manger, E. G., 1963, Porosity and Bulk Density of Sedimentary Rocks, U.S. Geol. Survey Bulletin 1144-E.
8. Melcher, A. F., 1924, "Texture of Oil Sands with Relations to the Production of Oil," Bull. Am. Assoc. Petrol. Geol. 8, 716.
9. Railroad Commission of the State of California and Department of Natural Resources, Estimate of the Natural Gas Reserves of the State of California as of January 1, 1946, Case No. 4591, Spec. Study S-525.
10. Regan, L. J., Jr., 1953, "Fractured Shale Reservoirs of California," Bull. Am. Assoc. Petrol. Geol. 37, 201.
11. Regan, L. J., Jr., and A. W. Hughes, 1949, "Fractured Reservoirs of Santa Maria District, California," Bull. Am. Assoc. Petrol. Geol. 33, 32.
12. Rieke, H. H., III, and G. V. Chilingarian, 1974, "Compaction of Argillaceous Sediments," in Developments in Sedimentology, Vol. 16.
13. Winograd, I. J., W. Thomdarson, and R. A. Young, 1971, Hydrology of the Nevada Test Site and Vicinity, Southeastern Nevada," U.S. Geol. Survey Open File Report.

Region 2: Rocky Mountains and Colorado Plateau

The region occupied by the Rocky Mountains and the Colorado Plateau corresponds to the eastern edge of the North American cordillera. The area is part of a craton which felt the commotions of the continuous tectonic activity along the shores of the Pacific. The two zones responded rather differently: the Colorado Plateau by isostatic motion and the Rocky Mountains as an intracratonic folded mountain belt. During the Mesozoic, the Colorado Plateau became a landmass where thick continental units were piled up; at the same time the Rocky Mountains occupied a zone of subsidence (e.g., the Denver basin) where large amounts of marine sediments accumulated. With the close of the Cretaceous and folding of the Rockies the whole region emerged and became a zone of deposition of continental shales rich in organic material (oil shales) (Eardley, 1962).

Three shale units can be distinguished:

- Triassic (Ankareh) and Jurassic (Morrison) shales are part of the continental sequence preserved in the Colorado Plateau region.
- Cretaceous shales are of two types: continental in the Colorado Plateau (Thermopolis); marine in the Rocky Mountain basins, extending into adjacent regions. The most continuous of all is the Pierre Shale (Fig. 1-7).
- Cenozoic shales are continental and belong to the oil shale group, they are Eocene in age (Green River Formation).

Structural relationships involving these units are illustrated in Fig. 1-8. The stratigraphy is summarized Table 1-7.

Hydrologic properties for the shales of the Rocky Mountains and the Colorado Plateau are compiled in Tables 1-8 and 1-9.

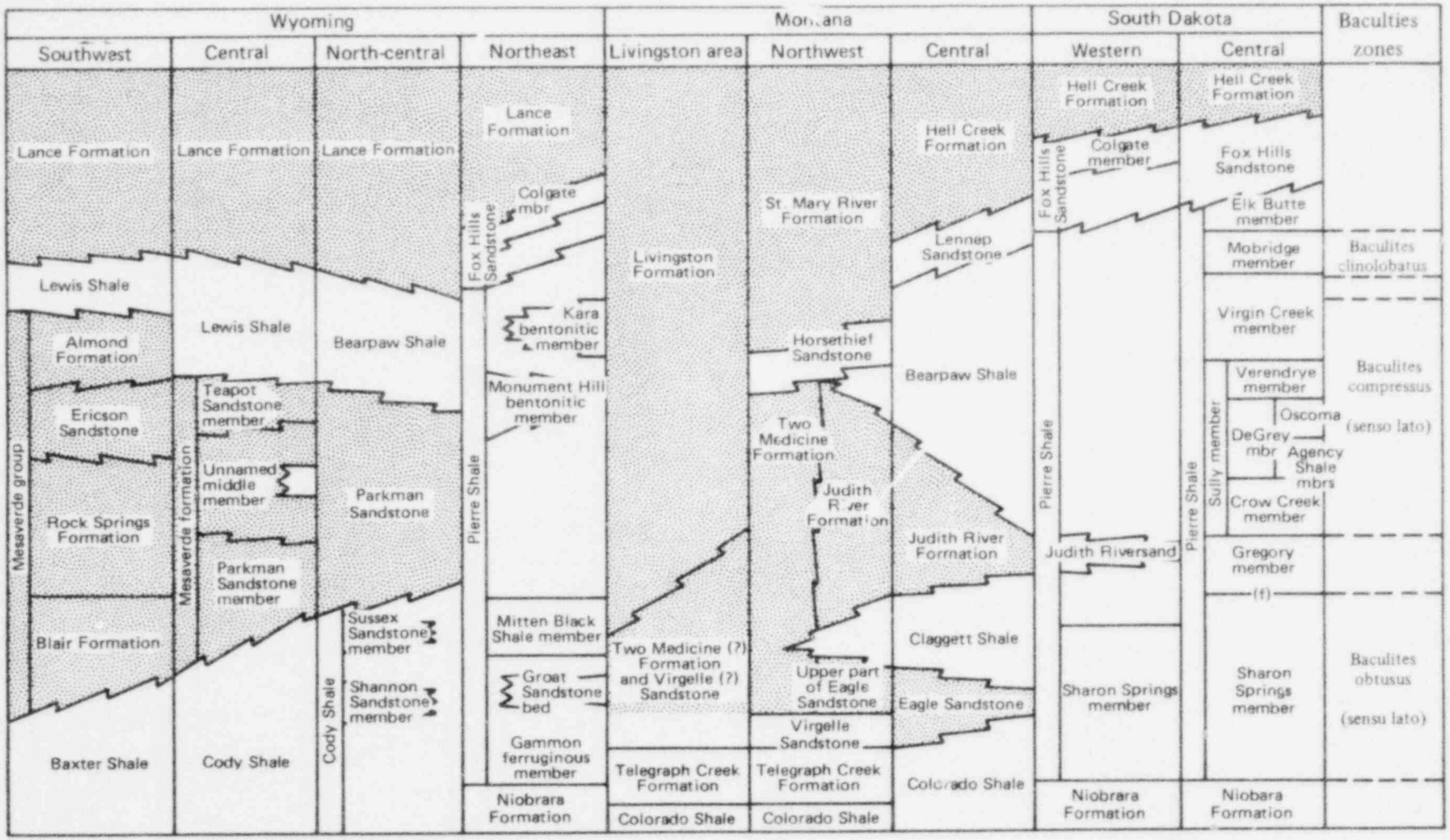

FIG. 1-7. Stratigraphic relations of the Pierre Shale and equivalent rocks (from Tourtelot, 1962).

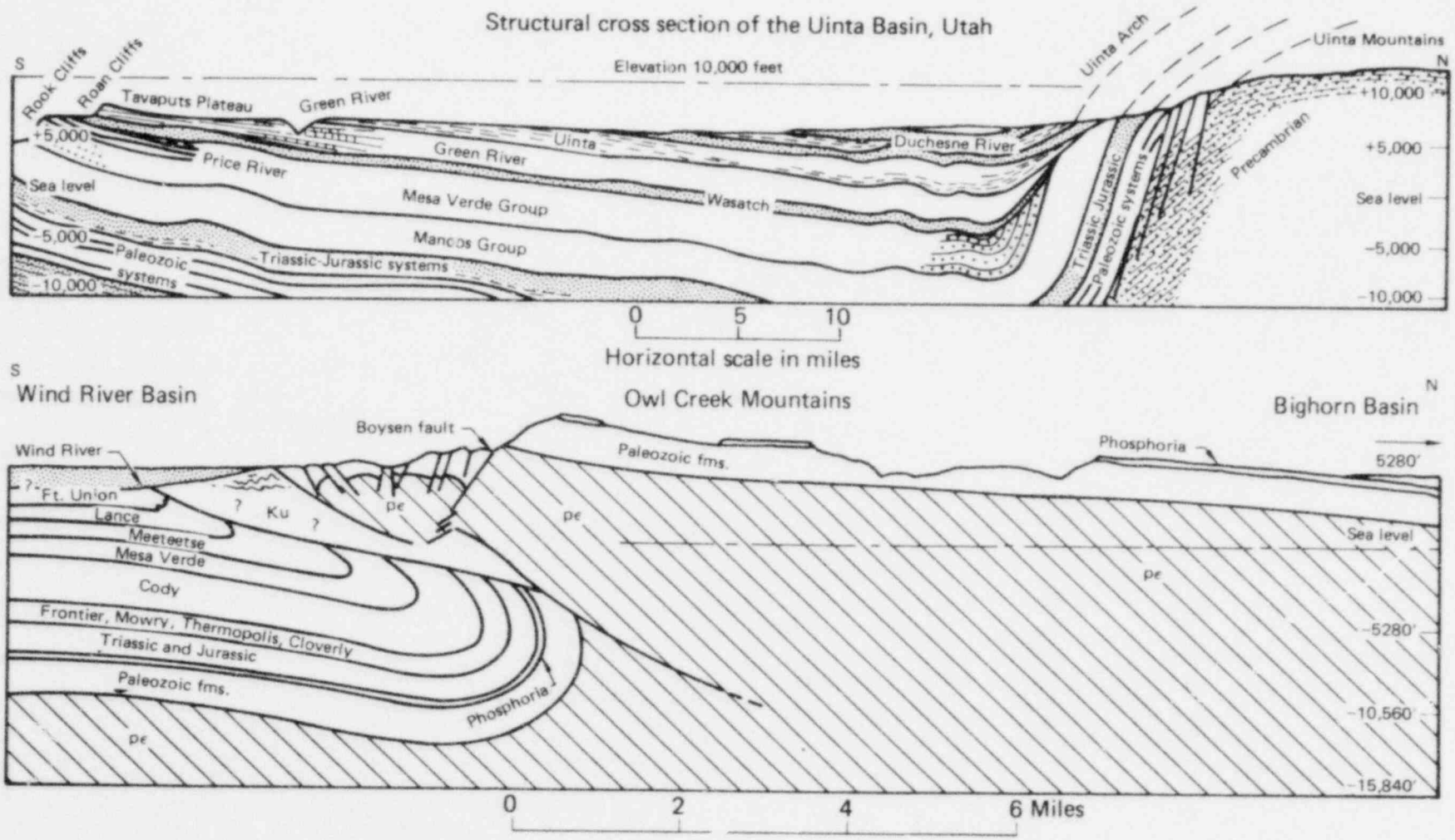

FIG. 1-8. Structural sections showing typical relationships in the Colorado Plateau (top) and the Rocky Mountains (bottom) (after Earley, 1962).

TABLE 1-7. Summary of rocky units in the Rocky Mountains, Colorado Plateau, and Great Plains (from Gill et al., 1970; Lee, 1927). Shales described in Tables 1-8 and 1-9 are followed by an asterisk.

Age		Stratigraphic Unit	Thickness, m		Description
Pliocene		Ogallala Formation	0-213		Interbedded sand, siltstone, clay, lenses of gravel, thin limestone, and caliche
		----------Unconformity----------			
Eocene	Upper	Uinta Formation	183		Mudstones, sandstones, marlstones, and tuffs
	Middle	Bridger Formation	762		Marlstones, mudstone, claystone, sandstones, tuffs
		Green River Formation*	976		Oil shale, marlstone, minor sandstone and limestone
	Lower	Wasatch Formation			Carbonaceous shale, sandstone, conglomerate, lenticular coal beds
Eocene to Paleocene		Fort Union Formation*	1220		Alternating shale and sandstone; basal conglomerate
Paleocene to Upper Cretaceous		Lance Formation*	230		Alternating shale and sandstone; lenticular sandstone beds
Cretaceous	Upper	Pierre Shale*	213	Many equivalent units	Massive gray shale, marine
		Niobrara Formation	61		Fossiliferous limestone
		Mancos Shale*	915		Marine shale
		Graneros Shale*	61		Massive, gray shale
	Lower	Mowry Shale*	46		Gray shales and thin-bedded sandstones
		Thermopolis Shale*	213		Dark colored, flakey shales and shaly sandstones
Jurassic		Morrison Formation*	61		Variegated shale, irregular masses of sandstones, and few thin layers of limestone
Triassic		Ankareh Shale*	?		Shale and sandy shale
		----------Unconformity----------			
Permian		Rustler Formation*	85-159		Anhydrite and rock salt with minor dolomite, sandstone, claystone and polyhyalite

TABLE 1-8. Hydrologic data for region 2: Rocky Mountains, Colorado Plateau, and Great Plains.

Geological setting	Age	Locality	Depth, m	No. samples	Density, (g/cm^3)	Porosity			Hydraulic conductivity, cm/s			Ref.	Method
						Av	Max	Min	Av	Max	Min		
Lazert Formation	Eocene	Southwest Wyo.										7	Single and multiple hole permeability pumping tests
Siltstone										6.8E-5	9.6E-6		
Mudstone									1.0E-8				
Green River Formation	Eocene	Uintah County, Utah	579.1-901.9						4.4E-7			23	Based on transmissibility data
Shale			579.1-985.7										
Shale			579.1-860.2						3.1E-7				
Parachute Creek member, Green River Formation[a]	Eocene	Piceance Creek basin, Colo.				20			1.9E-3	5.9E-3	6.1E-4	21, 22	Estimates of effective porosity based on geologic estimation of salt amount originally in place in leached zone. Permeability based on transmissivity pumping tests.

continued

[a]"Oil shale"; T_{min} = 7400 gpd/ft; T_{max} = 50,000 gpd/ft; T_{av} = 10,000 gpd/ft. Thickness: max = 511 m, min = 400 m. permeability High fracture porosity caused by leaching of salts, remaining voids weakened.

TABLE 1-8 continued.

Geological setting	Age	Locality	Depth, m	No. samples	Density, (g/cm^3)	Porosity			Hydraulic conductivity, cm/s			Ref.	Method
						Av	Max	Min	Av	Max	Min		
Uinta and Green River formations[b]	Eocene	Piceance Basin, Colo.										7	
Siltstone-shale									2.1E-4(H) 2.1E-5(V)				
Siltstone-shale									2.1E-5(H) 3E-6(V)				
Oil shale--Pentz zone						-			2E-8				Laboratory test
Upper Parachute Creek						8			1.5E-4				
Mahogany									1.2E-5				
Lower Parachute Creek						8			2.1E-5				
Leached zone						6			2.8E-5				
Garden Gulch									2.3E-5				
Silty carbonaceous shale	Eocene	Northwest Colo.							1.2E-7			7	Laboratory test
Uinta and Green River formations[b]	Eocene	Piceance Basin, Colorado										7	
Shale									2E-6(H) 1E-6(V)				Single and multiple hole permeability pumping tests
Siltstone-shale									1.5E-4(H) 3E-6(V)				
Shale									1.2E-5(H) 1E-7(V)				

continued

[b] ±20% accuracy; H = horizontal hydraulic conductivity, V = vertical hydraulic conductivity.

TABLE 1-8 continued.

Geological setting	Age	Locality	Depth, m	No. samples	Density, (g/cm^3)	Porosity Av	Porosity Max	Porosity Min	Hydraulic conductivity, cm/s Av	Hydraulic conductivity, cm/s Max	Hydraulic conductivity, cm/s Min	Ref.	Method
Shale	Cenozoic	Piceance Basin, Colo.		1[c]	1.86				1.5E-5			20	
				1[d]	2.10				7.6E-6				
Fort Union Formation	Eocene	Rosebud County, Mont.			dry 1.71 sat 2.08	36.6						3	
					dry 1.67-2.06 sat 2.04-2.29	23.5-36.9							
Fort Union Formation[e]	Eocene	Rosebud County, Mont.										12	
Lebo Shale member			outcrop?	1	2.07	21.2							
Tongue River member			outcrop	2	1.87	30.2	36.9	23.5					
Fort Union Formation	Eocene	Rosebud County, Mont.										17	
Tongue River member (arenaceous shale)				1	2.06	23.5							
Tongue River member (shale)			sub-surface	1	1.67	36.9							
Lebo Shale member (shale)				1	1.91	26.2							

continued

[c]In situ. Room permeability 1.3E-5 cm/s. [d]In situ. Room permeability 9.4E-6 cm/s.

[e]Values are for total porosity.

TABLE 1-8 continued.

Geological setting	Age	Locality	Depth, m	No. samples	Density, (g/cm^3)	Porosity Av	Porosity Max	Porosity Min	Hydraulic conductivity, cm/s Av	Hydraulic conductivity, cm/s Max	Hydraulic conductivity, cm/s Min	Ref.	Method
Fort Union Formation, Lebo Shale member	Eocene	Rosebud County, Mont.			dry 2.07 sat 2.28	21.2						3	
Knight Formation	Eocene	Afton quad, Wyo.										3	
Sand clay					dry 1.99 sat 2.22	23.1							
Siltstone					dry 2.32 sat 2.48	11.1-15.4							
Lance Formation	Tertiary?	Rosebud County, Mont.										17	
Shale				1	1.65	40.1			2.3E-2				
Tullock member (shale)				1	1.92	29.8			7.2E-3				
Graneros Shale (slightly weathered)	Upper Cretaceous	Hamilton County, Kan.	outcrop	2	1.98	24.9	25.2	24.6	1E-8			11	Melcher method
Graneros Shale[f,g,h]	Upper Cretaceous	Hamilton County, Kan.	923-926	1	2.39	11.6			4.5E-11			11	Melcher method
			1202-1204	2	2.35	10.1	11.0	9.2	2.2E-11				
			1367-1370	1	2.41	8.9			1.4E-11				
			1462-1465	1	2.52	9.6			1.9E-11				

continued

[f]Ransom well. [g]Vertical succession. [h]Well cuttings.

TABLE 1-8 continued.

Geological setting	Age	Locality	Depth, m	No. samples	Density, (g/cm^3)	Porosity			Hydraulic conductivity, cm/s			Ref.	Method
						Av	Max	Min	Av	Max	Min		
(Graneros Shale)			1522-1526	1	2.45	8.7			1.7E-11				
			1626-1634	2	2.52	8.2	8.4	7.9	8.6E-12				
			1657-1658	1	2.52	8.1			8.6E-12				
Shale		Phillips County, Kan.[i]	427	2	2.15	22.0						11	
			453	2	2.15	22.7	22.1	23.3					
			785	2	2.31	17.1	16.5	17.8					
Green Horn Formation[j]	Upper Cretaceous	Black Hills, Wyo.	approx 1524			37.6						16	
Niobrara Formation (Beaver Creek chalky member)[k]	Upper Cretaceous	Black Hills, Wyo.	1631			25.4							
Colorado Shale[l]	Upper Cretaceous	Bowdoin Dome, Mont.				10			1.3E-11			1	Measured
Upper Skull Creek member[m]	Lower Cretaceous	Third Creek area, Denver Basin, Colo.		3		1.4	1.8	0.5	3.4E-13			15	Petrographic techniques

continued

[i]Phillips well. [j]Marl, 1° dip. [k]Marl, 10° dip, close to a fault.

[l]Sometimes referred to as a very fine grained, tight sand. Drillers log--producing Zone A shale.

[m]Highly variable, fine-grained units.

TABLE 1-8 continued.

Geological setting	Age	Locality	Depth, m	No. samples	Density, (g/cm^3)	Porosity			Hydraulic conductivity, cm/s			Ref.	Method
						Av	Max	Min	Av	Max	Min		
Cody Shale[n]	Upper Cretaceous	Powder River Basin, Wyo.				13			1E-5			13	
Shale		Neves, Mont.	2155			9.5			5.1E-10			8	Streaming potential and SP log[o]
		Hovenweep, Utah	1793			4.6				6E-12			
	Cretaceous	Sydney, Neb.				12.7			3.4E-9				
Bentonite		Wyo.		1		34			4E-12 ?			4	Lab[p]
Shale		N.M.							1.7E-12			16	Lab[q]
Shale		Fallon County, Mont.			dry 1.79 sat 2.08	28.8			1.4E-8 ?			3	
Bentonite		Utah							4.5E-8			15	Lab[r,s]
		Wyoming				34			3.4E-12				
		Wyoming				41			4.3E-12				
Shale and siltstone	Cretaceous	Lane, Neb.	1415				7.0	2.5		5.3E-12	5.3E-13	9	Gamma ray attenuation

continued

[n]Thick, rippled, very fine grained sandstone and shale, enveloped entirely in gray shale.

[o]Conductivity values under "Av" were obtained with 0.02N NaCl; that under "Max" with 0.2N NaCl.

[p]2.5N NaCl solution as permeant; compaction load 2.76E10 dynes/cm^2.

[q]0.2N NaCl solution as permeant. [r]Sodium-water permeant, 7 psi. [s]40,000 psi load.

TABLE 1-8 continued.

Geological setting	Age	Locality	Depth, m	No. samples	Density, (g/cm³)	Porosity Av	Porosity Max	Porosity Min	Hydraulic conductivity, cm/s Av	Hydraulic conductivity, cm/s Max	Hydraulic conductivity, cm/s Min	Ref.	Method
Carlile Shale, Turner Sandy member[t]	Upper Cretaceous	Weston County, Wyo.	approx 1768	1	2.00	23.8						16	
Niobrara Formation, Sage Breaks Shale member[u]	Upper Cretaceous	Weston County, Wyo.	approx 1692	1	1.99	7.3						16	
Hilliard Formation (shale)	Cretaceous	Afton quad, Wyo.	outcrop?		1.98-2.28		26.3	13.8				12	Total porosity measured
Wayan Formation	Cretaceous	Afton quad Wyo.										12	Total porosity measured.
Clay					1.8	25.3							
Mudstone					1.9	28.6							
Bear River Formation	Upper Cretaceous	Afton quad Wyo.										3	
Siltstone					dry 2.47 sat 2.54	7.4							
Shale					dry 2.64 sat 2.65	1.3							
Frontier Formation	Upper Cretaceous	Afton quad Wyo.			dry 1.89 sat 2.11	22.1						3	

continued

[t]Gray shale; dip 33° SW. [u]Gray shale; dip 50° S.

TABLE 1-8 continued.

Geological setting	Age	Locality	Depth m	No. samples	Density, (g/cm^3)	Porosity			Hydraulic conductivity, cm/s			Ref.	Method
						Av	Max	Min	Av	Max	Min		
Bearpaw Shale	Upper Cretaceous	Rosebud County, Mont.		1	1.57	41.1						17	
Judith River Formation (sandy shale)	Upper Cretaceous	Rosebud County, Mont.		1	1.54	44.8						17	
Mancos Shale	Upper Cretaceous	Black Mesa, Ariz.								4.6E-6	4.6E-10	5	Hydrologic laboratory studies[V]
Clagget Shale	Upper Cretaceous	Rosebud County, Mont.		1	1.81	36.3						17	
Cody Shale[W]	Upper Cretaceous	Gebo oil field, Hot Springs County, Wyo.	220-404		2.53	9.1±1.7						2	
Mowry Shale[W]	Lower Cretaceous	Gebo oil field, Hot Springs County, Wyo.	569-678		2.44	14.4±1.6						2	
Thermopolis Shale[W];	Lower Cretaceous	Gebo oil field, Hot	740-781		2.52	9.7±1.8						2	
Shell Creek member		Springs County, Wyo.	678-733		2.44	14.6±1.7							

continued

[V]Vertical measurements only. Travel time for contaminants, 126-1,260,000 y.

[W]Porosity and density calculated from borehole gravity survey.

TABLE 1-8 continued.

Geological setting	Age	Locality	Depth, m	No. samples	Density, (g/cm^3)	Porosity			Hydraulic conductivity, cm/s			Ref.	Method
						Av	Max	Min	Av	Max	Min		
Graneros Shale	Upper Cretaceous	Crook County, Wyo.										16	
Skull Creek member[x]			approx 2164	1	1.87	32.5							
Belle Fourche member[y]			approx 1615	1	1.78	33.3							
Pierre Shale	Upper Cretaceous											16	
Gammon Ferruginous member[z]		Crook County, Wyo.	approx 1509	1	2.04	26.0							
Mitten Black Shale member[aa]		Weston County, Wyo.	approx 1311	1	1.56	35.8							
Upper part[bb]			approx 1113	1	1.96	25.4							
Pierre Shale	Cretaceous	Cimarron, N.M							2.5E-11			19	
		N.D., S.D., and Colo.							1E-10[cc]			18	
Pierre Shale	Cretaceous					21			9.4E-11			15	Lab
Muddy Shale	Cretaceous					4.7			<4.3E-8			15	Lab
Colorado Shale	Upper Cretaceous	Fergus County, Mont.			dry 2.07 sat 2.30	22.6			5.8E-9			8	

continued

[x]Black shale; dip 5° SW. [y]Black shale; dip 4° NE. [z]Dip 5° SW. [aa]Dip 45° SW. [bb]Gray shale; dip 33° SW.
[cc]Regional permeability value; repository for cool (400°F) waste.

TABLE 1-8 continued.

Geological setting	Age	Locality	Depth, m	No. samples	Density, (g/cm^3)	Porosity Av	Porosity Max	Porosity Min	Hydraulic conductivity, cm/s Av	Hydraulic conductivity, cm/s Max	Hydraulic conductivity, cm/s Min	Ref.	Method
Muddy shale	Cretaceous	Logan County, Colo.	1490	13		Before deformation: 4.1-5.1 After deformation: 4.4-10.9				2.49E-7	8.58E-9	9	Lab
Adaville Formation	Cretaceous											12	
Mudstone		Afton quad, Wyo.	outcrop	2	2.07	23.0[dd]							
Shale			outcrop		2.34	11.9[ee]							
Shale		Sublette County, Wyo.	4151	1		7.8[ff]							Lab
Shale			1474	1		5.7[ee]			<8.58E-8				Lab
Cloverly Formation	Lower Cretaceous	Gebo oil field, Hot Springs County, Wyo.	781-794		2.44	14.2±2.1[gg]						2	
Morrison Formation (claystone)	Jurassic	Long Park, Colo.	62-75	6		16.5	20.3	8.8				12	
Ankareh Shale	Triassic	Afton quad, Wyo.	outcrop		2.40	9.2[dd]						12	
Woodside Formation (shale)	Triassic	Afton quad, Wyo.	outcrop		2.24	16.1[dd]						12	

continued

[dd] Total porosity. [ee] Total or effective porosity not specified. [ff] Effective porosity.

[gg] From borehole gravity survey.

TABLE 1-8 continued.

Geological setting	Age	Locality	Depth, m	No. samples	Density, (g/cm^3)	Porosity			Hydraulic conductivity, cm/s			Ref.	Method
						Av	Max	Min	Av	Max	Min		
Crow Mountain Sandstone (upper siltstone)	Upper Triassic	Gebo oil field, Hot Springs County, Wyo.	1107-1111		2.59	5.4±2.6						2	Borehole gravity survey
			1111-1115		2.46	11.7±2.2							
			1115-1128		2.55	7.0±2.1							
Red Peak Formation (calcareous red siltstone and claystone)	Lower Triassic	Gebo oil field, Hot Springs County, Wyo.	1134-1247		2.67	1.6±1.2						2	Borehole gravity survey
			1247-1347		2.63	3.9±1.8							
			1347-1371		2.74	1.9±2.0							
Rustler Formation	Permian	Eddy County, N.M.										6	
Tamarisk member (claystone)			147		2.08	22.1							
Forty-Niner member (siltstone)			101		2.00	24.9							
Lower member (claystone)			160		1.91	29.6							
			168		2.01	25.1							
Lower member (siltstone)			180		2.13	21.3							
			189		2.17	19.3							
Bentonite		Wyo.							2.8E-9			15	Lab[hh]
		Utah							7.2E-7				

continued

[hh]Calcium-water solution used as permeant at 7 psi.

TABLE 1-8 continued.

Geological setting	Age	Locality	Depth, m	No. samples	Density, (g/cm^3)	Porosity			Hydraulic conductivity, cm/s			Ref.	Method
						Av	Max	Min	Av	Max	Min		
Gros Ventre Formation	Cambrian	Afton quad, Wyo.	Outcrop		2.38	11.1[ii]						12	
Ophir Formation	Cambrian	Ophir, Utah										12	
Shale			sub-surface	1	2.81	0.9[jj]							
Silicified shale			sub-surface	1	2.8	0.6[jj]							

[ii] Total porosity.

[jj] Effective porosity.

TABLE 1-9 Other properties for region 2.

Geologic Setting	Age	Locality	Depth, m	No. of samples	Compressive strength, lbs/in.^{2}	Ultimate strength, bars	Resistivity, ohm m^2/m)	Ref.
Ophir Formation	Cambrian	Ophir, Utah						12
Shale			subsurface	2	31,300			
Silicified shale			subsurface	1	33,500			
Muddy Shale	Cretaceous	Logan County, Colo.	1490	13		400-4170		9
Cody Shale	Upper Cretaceous	Gebo oil field, Hot Springs County, Wyo.	220-404				range: 4-9 av: 5	2
Mowry Shale	Lower Cretaceous	Gebo oil field, Hot Springs County, Wyo.	569-678				range: 3-22 av: 8	2
Thermopolis Shale, Shell Creek member	Lower Cretaceous	Gebo oil field, Hot Springs County, Wyo.	678-733				range: 2-6 av: 4	2
Thermopolis Shale	Lower Cretaceous	Gebo oil field, Hot Springs County, Wyo.	740-794				range: 3-14 av: 5	2
Cloverly Formation	Lower Cretaceous	Gebo oil field, Hot Springs County, Wyo.	781-794				range: 3-6 av: 4	2
Crow Mountain Sandstone, upper siltstone	Upper Triassic	Gebo oil field, Hot Springs County, Wyo.	1107-1111				range: 20-25 av: 23	2
			1111-1115				range: 19-30 av: 25	
			1115-1128				range: 30-36 av: 33	
Moencopi Shale		Meteor Crater, Ariz.					2E-4 ohm-cm	3

References for Tables 1-8 and 1-9 (Region 2)

1. Bartram, J. G., and C. E. Erdmann, 1935, "Natural Gas in Montana," in Geology of Natural Gas, H. A. Ley, Ed., (Am. Assoc. Petrol. Geol., Tulsa,), pp. 245-276.
2. Beyer, L. A., and F. G. Clutsom, 1978, Density and Porosity of Oil Reservoirs and Overlying Formations from Borehole Gravity Measurements, Gebo Oil Field, Hot Springs County, Wyoming: Oil and Gas Investigations, U.S. Geol. Survey Chart OC-88.
3. Birch, F., J. R. Schairer, and C. H. Spicer, 1942, Handbook of Physical Constants, Geol. Survey Am. Special Paper 36.
4. Bredehoeft, J. D., and B. B. Hanshaw, 1968, "On the Maintenance of Anomalous Fluid Pressures--I. Thick Sedimentary Sequences," Bull. Geol. Soc. Am. 79(9), 1097.
5. Dove, A. H., and T. G. Roefs, 1973, "Competitive Groundwater Usage from the Navajo Sandstone," Hydrol. Water Resources Ariz. Southwest 3, 124.
6. Gard, L. M., Jr., 1968, Geologic Studies, Project Gnome, Eddy County, New Mexico, U.S. Geol. Survey Professional Paper 589.
7. Golder Associates, 1977, Second Study, Development of Site Suitability Criteria for a High Level Waste Repository, Lawrence Livermore Laboratory, Livermore, Calif., UCRL-13793.
8. Gondouin, M., and C. Scala, 1958, "Streaming Potential and the SP Log," Trans. A.I.M.E. 213, 170.
9. Handin, J., R. V. Hager, Jr., M. Friedman, and J. N. Feather, 1963, "Experimental Deformation of Sedimentary Rocks under Confining Pressure: Pore Pressure Tests," Bull. Am. Assoc. Petrol. Geol 47(5), 717.
10. Harms, J. C., 1966, "Stratigraphic Traps in a Valley Fill, Western Nebraska," Bull. Am. Assoc. Petrol. Geol. 50, 2119.
11. Hedberg, H. D., 1926, "The Effect of Gravitational Compaction on the Structure of Sedimentary Rocks," Bull. Am. Assoc. Petrol. Geol. 10, 1035.
12. Manger, E. G., 1963, Porosity and Bulk Density of Sedimentary Rocks, U.S. Geol. Survey Bulletin 1144-E.
13. Martinsen, R. S., and R. W. Tillmal, 1978, "Hartzog Draw, New Giant Oil Field," Bull. Am. Assoc. Petrol Geol. 62, 540.
14. Reinert, S. L., and D. K. Davies, 1976, "Third Creek Field, Colorado: A Study of Sandstone Environments and Diagenesis," Mountain Geol. 13, 47.

15. Rieke, H. H., III, and G. V. Chilingarion, 1974, "Compaction of Argillaceous Sediments," in Developments in Sedimentology, Vol. 16.
16. Rubey, W. W., 1930, Lithologic Studies of Fine-Grained Upper Cretaceous Sedimentary Rocks of the Black Hills Region, U.S. Geol. Survey Professional Paper 165-A.
17. Stearns, N. D., 1927, Laboratory Tests on Physical Properties of Water-Bearing Materials, U.S. Geol. Survey Water Supply Paper 596., pp. 121-176.
18. Shurp, G. W., and J. D. Bredehogdal, 1977, "The Pierre Shale as a Possible Waste Repository" abstract in Geol. Soc. Am. Abstr. Programs 9(7), 1174.
19. Summers, W. K., R. E. Balgstrom, C. W. Walker, and G. Hammock, 1977, "Hydrogeologic Investigation for Low-Level Radwaste Disposal Near Cimarron, New Mexico," Geol. Soc. Am. Abstr. Programs 9(7), 1193.
20. Thomas, C. W., 1966, "Some Effects of Overburden Pressure on Oil Shale during Underground Retorting," J. Soc. of Petrol. Engin. 6(1), 1.
21. Weichman, B. E., 1974, "Some Effects of the Rio Blanco Nuclear Detonation on the Leached Zone in the Parachute Creek Member of the Green River Formation," in Guidebook to the Energy Resources of the Piceance Creek Basin, Colorado, Rocky Mt. Assoc. Geol. Field Conf. Guide, No. 25, pp. 205-215.
22. Weichman, B. E., 1975, "Depositional History and Hydrology of the Green River Oil Shale, Piceance Creek Basin, Rio Blanco County, Colorado," Trans. A.I.M.E. 256, 272.
23. Weir, J. E., 1970, Geohydrology of the Area Near Wosco, Exploratory Hole Number 1, Unitah County, Utah, U.S. Geol. Survey Open File Report.

Region 3: The Mid-Continent

The Mid-Continent region is broadly spread between the Rocky Mountains and the Appalachians, and between the Canadian Shield and the Gulf Coast. It is a craton whose southern portion underwent some deformation at the end of the Paleozoic (Eardley, 1962), forming numerous domes and basins (Fig. 1-9). This is the common setting for the Chattanooga Shale (Fig. 1-10). During the Mesozoic the region was invaded by epicontinental seas where extensions of Rocky Mountain units (e.g., equivalents of the Pierre Shale) were deposited.

Examples of the simple structural relationships characterizing the Mid-Continent are shown in Fig. 1-11. The stratigraphy is described in Table 1-10. Hydrologic data are collected in Table 1-11.

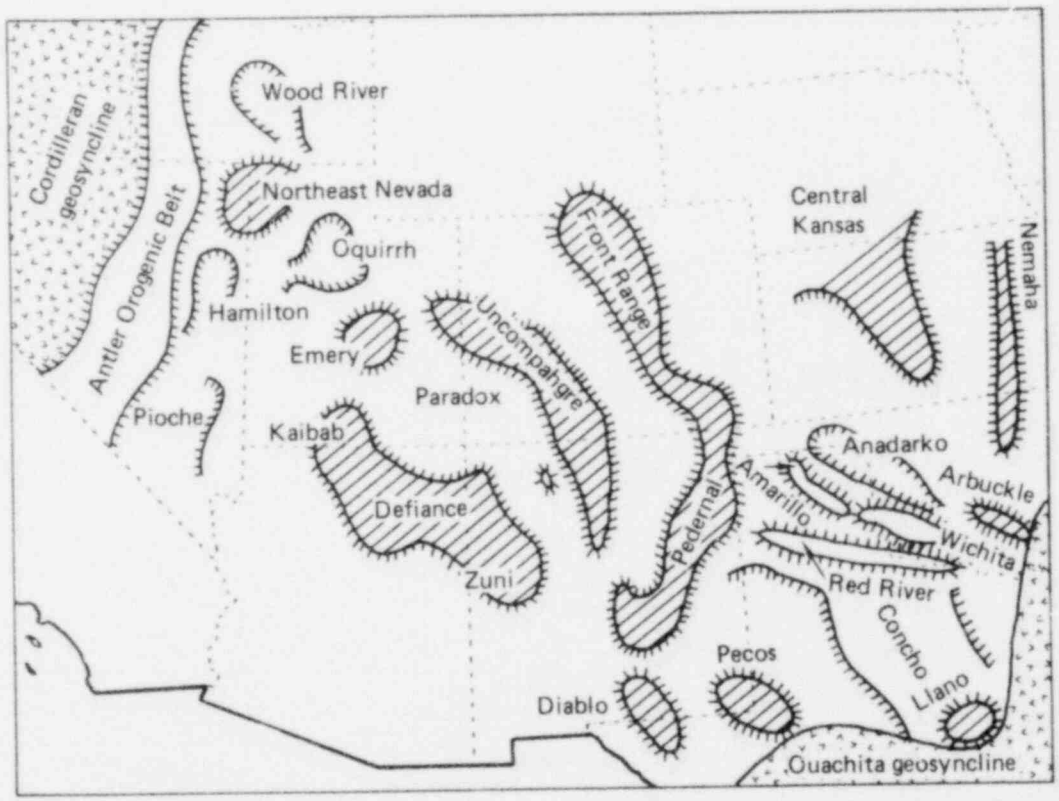

FIG. 1-9. Distribution of Paleozoic structures in the Mid-Continent and Great Plains regions (from Mintz, 1977).

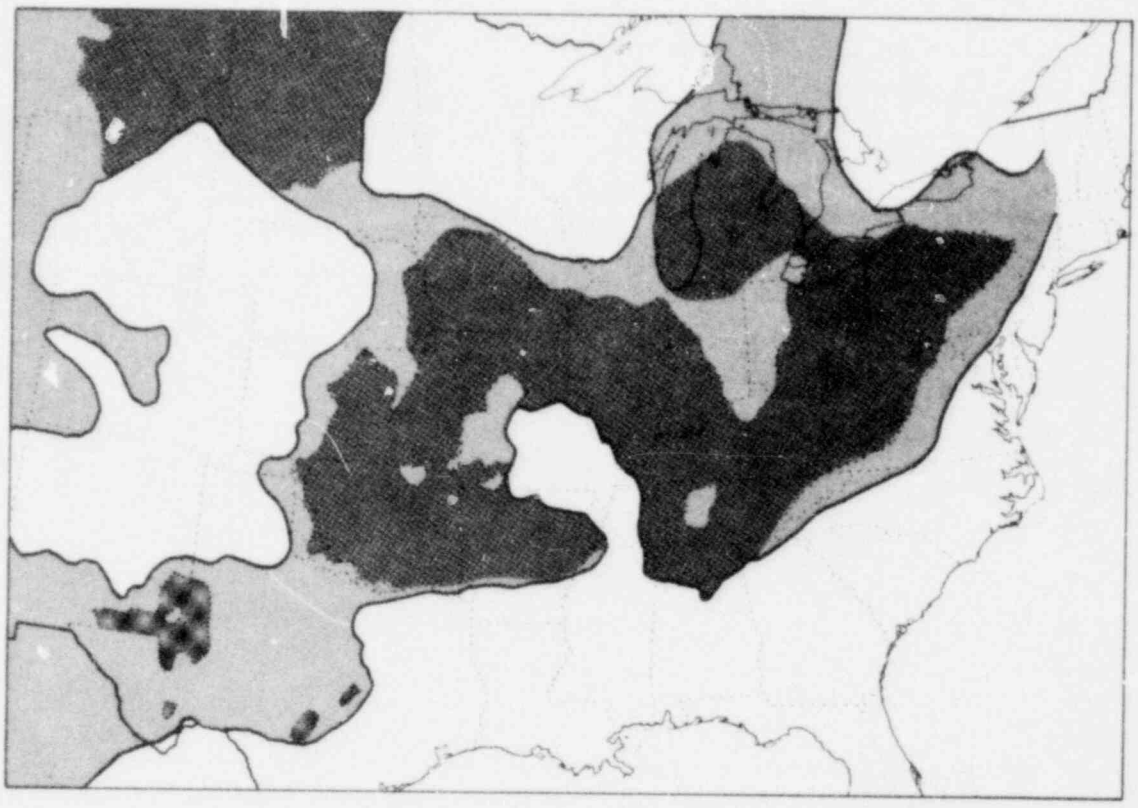

FIG. 1-10. Map showing the distribution of the Chattanooga Shale (Devonian-Mississippian) in the United States (from Mintz, 1977). Darker shades show the present extent of the unit.

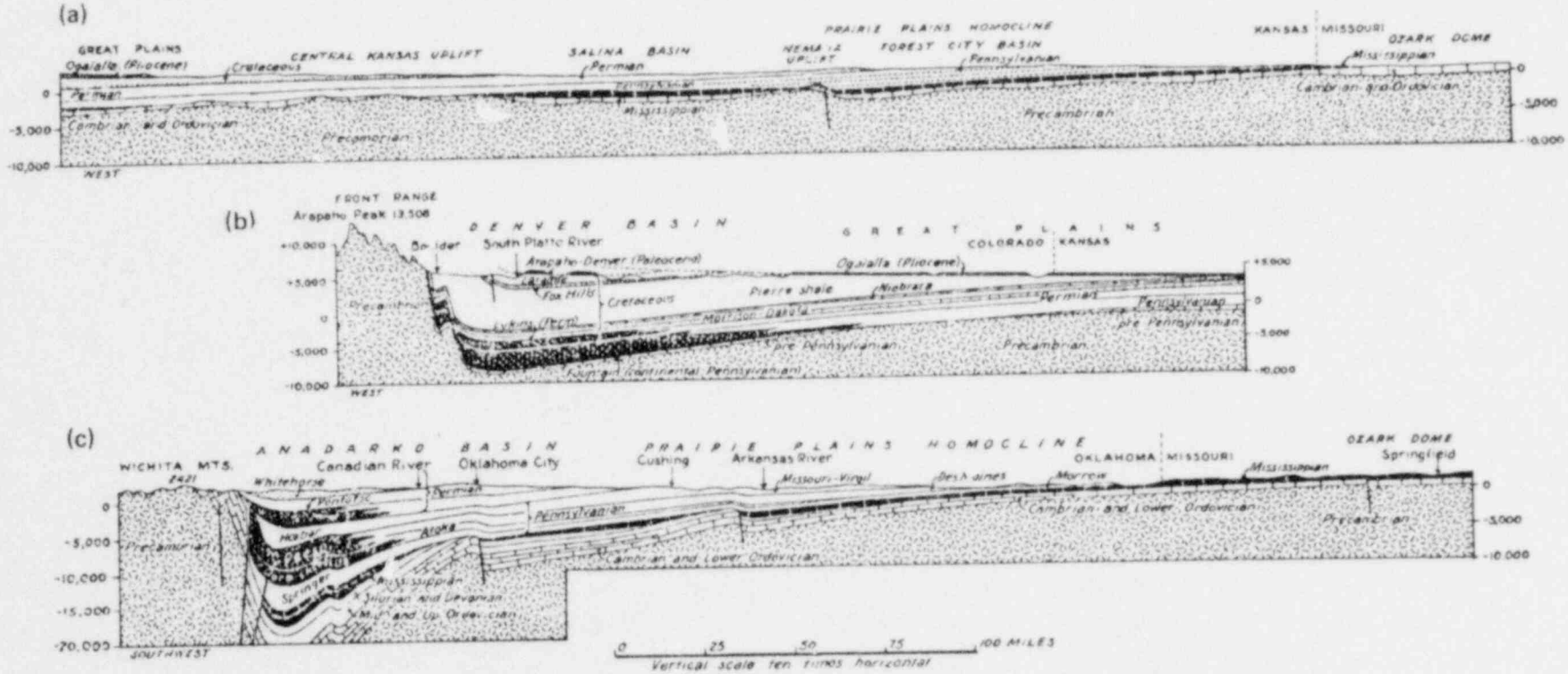

FIG. 1-11. Sections illustrating structural relationships in the Mid-Continent and Great Plains regions (from King, 1951). (a) Great Plains, (b) Denver Basin, and (c) Paleozoic basins and domes.

TABLE 1-10. Summary of rock units from the Mid-Continent region (from Ruedeman, 1939). Shales described in Table 1-11 are followed by an asterisk.

Age	Stratigraphic Unit	Thickness, m	Description
Tertiary			
Mesozoic			
Permian	Permian Red Beds		
	Quartermaster, Big Basin formations	91-152	Soft, red sandstone, sandy clays and shales
	Cloud Chief Hackberry Group	0-35	Massive white-pink gypsum, irregularly bedded with red clay shales
	Woodward Group	91-129	Red clay shales, dolomite, red sandstones, conglomeritic sandstones
	Blaine Gypsum	23	Massive white gypsum separated by beds of red clay shale and dolomite
	Enid Group	366-457	Red clays and shales with occasional sandstone beds; gypsiferous
	Asher Formation	76	Coarse red-gray sandstones and red-clay shale
	Sumner Group		
	Wellington Formation*	183-207	Bluish gray, greenish and red shales, thin sandstone beds, important salt beds in lower section
	Marion Formation	122-152	Buff, thin-bedded limestones and thick shale beds
	Chase Group	73-91	Interbedded limestones and shales with minor flint
	Council Grove Group	46	Massive shales, shaly limestones, yellow shales and thin limestones
	Eskridge Shale	12-23	Green, brown, or yellow shales
	Neva limestones	3-6	Massive gray limestone, one thin shale parting
Pennsylvanian	Wabaunsee Group	152	Eight members, shales, sandstones, and limestones
	Shawnee Group	111-152	Nine members, cherty-argillaceous shales, limestones, sandstones, some coal beds
	Douglas Group	107-167	Four members including Weston Shale. Sandstones, argillaceous shales and limestones
	Lansing Group	38-76	Four members. Clayey to sandy shales and massive limestones
	Chanute Shale*	8-31	Clay shale to sandy shale
	Cherokee Formation*	137-305	Variable colored shales with considerable lithologic variation
	Atoka Formation	60-2,134	Shales with lenses and thin ledges of brown sandstone
	Wapanucka Limestone	0-244	Limestone, chert, sandstone, and shale

continued

TABLE 1-10 continued.

Age	Stratigraphic Unit	Thickness, m	Description
Mississippian	Barnett Shale	0-15	Black shales and slates with a basal limestone member
	Jack Fork Formation	0-2012	Gray sandstones with dark shales at wide intervals
	Stanley Shale*	244-762	Irregularly bedded sandstones, shales, and slates
	Caney Shale	0-488	Black shales and slates with limestone lentils; blue shales with sandy members
	Pitkin Limestone	0-43	Rusty brown shaly strata to fine-textured, massive, bluish beds
	Mayes Formation	0-40	Contains Fayetteville Shale. Bituminous shale, limestone, sandstone
	Boone Limestone	18-168	Interstratified chert and cherty limestone
	Chattanooga Shale*	2-70	Black, slaty, bituminous shale; basal sandstone unit
Devonian-Mississippian	Sycamore Limestone	0-152	Hard slaty, blue limestone
	Woodford Chert*	61-213	Limey chert with shales
	Arkansas Novaculite	76-183	White to black novaculite thin to massive; slates
Devonian	Hunton Formation		
	Bois d'Arc Limestone	0-27	White to gray crystalline limestone with thin beds of chert
	Haragan Shale	0-51	Soft marly shaly, gray to drab color with interbedded marly limestone
Silurian	Henryhouse Shale	0-68	Gray to drab-colored shales and soft marly limestone
	Chimney Hill Limestone	0-16	Pink, crinoidal, and oolitic limestone
	St. Clair Marble	0-61	Pinkish white, coarsely crystalline marble
	Blaylock Sandstone	244-457	Gray, hard sandstone and interbedded shaly sandstone
	Talihina Chert	366	

continued

TABLE 1-10 continued.

Age		Stratigraphic Unit	Thickness, m	Description
Ordovician	Upper	Cason Shale	?	
		Fernvale Limestone	?	Gray, crystalline, fossiliferous limestone
		Sylvan Shale*	18-91	Green to green blue
		Polk Creek Shale	30	Black graphitic shales
		Tyner Formation	18-79	Sandstone, shale, calcereous cherty limestones
	Upper to Middle	Viola Limestone	0-288	Massive, heavy-bedded homogeneous limestone
		Jasper Limestone	0-15	Noncrystalline limestone with considerable sandstone
		Joachim Limestone	29	Fine crystalline Mg-limestone with quartz sandstone
		Big Fork Chert	152-244	Gray to black chert and ledges of cherty fossiliferous limestones
		Womble Schistose Sandstone	76-305	Micaceous, fine-grained sandstone interbedded with shales
		Blakely Sandstone	0-15	Gray sandstone and black and green shale
	Lower	Simpson Group	61-976	Sandstones, thin limestones interbedded with greenish clay, shales, and marls
		St. Peter Sandstone	0-61	Fine-grained, poorly cemented sandstone
		Yelville Formation		
		Everton Limestone	0-30	Fine-grained limestone, basal sandstone
		Powell Limestone	0-61	Mg-limestone, shale, basal conglomerate
		Cotter Dolomite	152	Fine-grained, argillaceous dolomite; massive medium-grained with shale and sandstone
		Jefferson City Dolomite	183	
		Mazarn Shale	305	Dark, carbonaceous hard clay shales and slates
		Crystal Mt. Sandstone	259	Uniform, medium-grained, massive sandstone. Basal conglomerate
		Arbuckle Limestone	1525-1829	Thin-bedded to massive Mg-limestone

continued

TABLE 1-10 continued.

Age	Stratigraphic Unit	Thickness, m	Description
Cambrian	Reagan Sandstone	0-152	Coarse, granitic sandstone to limey shale
	Ellenburger Limestone	610	Crystalline dolomite
	Wilberns Formation	61	Sandy, thin-bedded limestones; shale
	Cap Mountain Formation	27	Glauconite limestone and sandstone
	Hickory Sandstone	0-107	Conglomerate
	Collier Shale	61	Metamorphosed, graphitic, black shales capped by thin-bedded limestones
Precambrian	Basement Complex		Gneiss, schists, crystalline limestone and other metamorphic sedimentaries and plutonic rocks.

TABLE 1-11. Hydrologic data for region 3: the Mid-Continent.

Geological setting	Age	Locality	Depth, m	No. samples	Density, (g/cm^3)	Porosity			Hydraulic conductivity, cm/s			Ref.	Method
						Av	Max	Min	Av	Max	Min		
Wellington Shale (calcereous)	Permian	Salina, Kan.		2	2.39	15.4	15.5	15.3				5	Jolby balance[a]
Mentor beds (black shale)	(Cretaceous) Comanchean	Falun, Kan.		2	2.06	23.1	23.3	22.9				5	Same as above
Chanute Shale	Pensylvanian	Lynn well, Montgomery County, Kansas	152-154	2	2.47	10.4	10.6	10.2				5	Same as above
			297	2	2.54	7.8	8.2	7.3					
			396-398	3	2.53	7.8	8.5	7.1					
Fractured black, carbonaceous shales and silty shales[b]	Middle Permian	Dawson County, Tex.				8			4.3E-7			12	Micrometer gauge measured
Shales	Permian	Thomas Pool, Okla.	surface			20						1	
Shales	Pennsylvanian	Ponca City and Garber pools, Okla.	150		2.13	38						1	Graphical[c]
			300		2.24	31							
			1220		2.57	8							
			1830			4							
Chanute Shale	Pennsylvanian	Independence, Kan.	outcrops (mines, quarries, shale pits)[d]	2	2.31	14.9	15.0	14.8				5	Jolly balance

continued

[a]Averages from vertical sequences. [b]Induced fracturation to conduct oil to well bore. [c]Extrapolated from depth vs porosity plot.
[d]From areas of little or no deformation.

TABLE 1-11 continued.

Geological setting	Age	Locality	Depth, m	No. samples	Density, (g/cm^3)	Porosity			Hydraulic conductivity, cm/s			Ref.	Method
						Av	Max	Min	Av	Max	Min		
Weston Shale	Pennsylvanian	Bonner Springs, Kan.		2	2.28	15.8	16.0	15.5				5	% porosity = 100 × (1 - dry rock dens / dry mineral dens)
Cherokee Shale	Pennsylvanian	Oklahoma City, Okla.										7	Core analysis
Phillips well 1			1606	3		17	19	15					
Phillips well 2			1604-1612	5		21	23	19					
Phillips well 1			1611-1614	8		19	22	15					
Phillips well 7			1620	5		18	23	10					
Phillips well 2			1589-1604	21		18	23	11					
Well E[e]				5		12.7			1.2E-4				
Shales	Pennsylvanian	Kan.-Okla. region								9.5E-5	1.0E-5	11	Streaming potential and SP log
Shale	Pennsylvanian	Stockholm, Okla.	1267			13.6			6.9E-10			4	Same as above[f]
Shale	Pennsylvanian	Williams, N.M.	3426			3.8			1.7E-12			4	Same as above[f]

continued

[e] Newly constructed well.

[f] 0.2N NaCl.

TABLE 1-11 continued.

Geological setting	Age	Locality	Depth, m	No. samples	Density, (g/cm^3)	Porosity			Hydraulic conductivity, cm/s			Ref.	Method
						Av	Max	Min	Av	Max	Min		
Shale	Pennsylvanian	Hobbs wildcat, N.M.	2623			7.0						4	Direct measurement with a gas porosimeter
Shale	Pennsylvanian	Reagan County, Tex.				6.2						4	
Shales and siltstones[g]	Permian	Paduca, N.M.	1412			20					4.3E-6	2	
Stanley sandstone[h]	Pennsylvanian	Ouachita Mountains, Ark. and Okla.					26	0.5		2E-5	4.3E-8	9	
Shale	Pennsylvanian and Permian	Ponca City and Garber areas, Okla.	305		2.25	17						p	Direct measurement with a gas porosimeter
			610		2.42	11							
			914		2.52	7							
			1219		2.57	5							
			1524		2.62	4							
Burgess Sandstone (shale)	Pennsylvanian	South Moore pool, Okla.	2381-2384				4	3				8	
Shale, weathered		near Ponca City, Okla.					48	37				8	

continued

[g]Gentle homocline, dips to east. Turbidite sequence.

[h]Interbedded shales and sandstones.

TABLE 1-11 continued.

Geological setting	Age	Locality	Depth, m	No. samples	Density, (g/cm^3)	Porosity			Hydraulic conductivity, cm/s			Ref.	Method
						Av	Max	Min	Av	Max	Min		
Clay		near Ponca City, Okla.				53[i]						8	
Shale		Oklahoma							6.9E-10			10	Lab[j]
Shale		N. Okla.			dry 2.15 sat <2.35	<20						3	
Shale		N. Okla.			dry >2.55 sat 2.59	<4						3	
Stanley Shale	Pennsylvanian	Ouachita Mountains, Okla.			dry 2.45-2.60 sat 2.52-2.62		6.8	2.5				3	
Fayetteville Shale	Mississippian	Ozark Plateau, Okla.			dry 2.27-2.44 sat 2.41-2.53		14.1	8.6				3	
Sylvan Shale[k]	Ordovician	Murray County, Okla.	outcrop	8		39.94-43.30						6	Lab
Shale		Phillips Well, Russel County, Kan.	42.-453	4	2.15	22.5[i]	23.3	22.0				8	
Chanute Shale	Pennsylvanian	Montgomery County, Kan.	152-297	4	2.51	9.1	10.6	7.3				8	

[i]Effective porosity. [j]0.2N NaCl solution used as permeant. [k]Distribution coefficients available in Ref. 6. [l]Total porosity.

References for Table 1-11 (Region 3)

1. Athy, F. L., 1930, "Density, Porosity, and Compaction of Sedimentary Rocks," Bull. Am. Assoc. Petrol. Geol. 14, 1.
2. Berg, R. R., 1975, "Capillary Pressure in Stratigraphic Traps," Bull. Am. Assoc. Petrol Geol. 59, 939.
3. Birch, F., J. F. Schairer, C. H. and Spicer, 1942, Handbook of Physical Constants, Geol. Soc. Am. Special Paper 36.
4. Gondouin, M., and C. Scala, 1958, "Streaming Potential and the SP Log," Trans. A.I.M.E. 213, 170.
5. Hedberg, H. D., 1926, "The Effect of Gravitational Compaction on the Structure of Sedimentary Rocks," Bull. Am. Assoc. Petrol. Geol. 10, 1035.
6. Jennings, A. R., and M. C. Schroeder, 1968, "Laboratory Evaluation of Selected Radioisotopes as Ground-Water Tracers," Water Resources Res. 4(4), 829.
7. Katz, D. L., 1942, "Possibilities of Secondary Recovery for the Oklahoma City Wilcox Sand," Trans. A.I.M.E. 146, 28.
8. Manger, E. G., 1963, Porosity and Bulk Density of Sedimentary Rocks, U.S. Geol. Survey Bulletin 1144-E.
9. Morris, R. C., K. E. Proctor, and M. R. Koch, 1977, "Petrology and Diagenesis of Deep-Water Sandstones, Ouachita Mountains, Arkansas and Oklahoma," abstract in Bull. Am Assoc. Petrol. Geol. 61, 1384.
10. Rieke, H. H., III, and G. V. Chilingarion, 1974, "Compaction of Argillaceous Sediments," in Developments in Sedimentology, Vol. 16.
11. Schenck, K. D., 1955, An Investigation of the Streaming Potential Developed in Formations of Low Permeability, University of Oklahoma, M.S. Thesis.
12. Wilkinson, W. M., 1953, "Fracturing in Sprayberry Reservoir, West Texas," Bull. Am. Assoc. Petrol. Geol. 37, 250.

Region 4: Gulf Coast and Mississippi Embayment

The geologic history of the southeastern coast of the United States is characterized by a Paleozoic episode of plate convergence, followed by a period of diverging plates that began with the Triassic and is continuing today.

With the end of the Paleozoic, ancestral North America and Europe collided with Gondwanaland (Seyfert and Sirkin, 1973) after the closing of the Theic Ocean. This collision resulted in the formation of the Appalachian belt and its southern extension into the Gulf Coast area, the Marathon-Ouachita Mountains. After a brief continental episode (Permian), during which evaporites were formed, subsidence and deposition of a clastic wedge began to take place in response to the opening of the Atlantic Ocean. Most clastic sediments are Mesozoic and Cenozoic, and the shales are regarded as the likely source of the Gulf Coast oil and gas fields (many were formed by salt dome tectonics). Although most shales are Tertiary and Cretaceous, Paleozoic units, more representative of Appalachian and Mid-Continent regions, occasionally crop out around the periphery of the basin or in domal uplifts. Figure 1-12 shows typical relationships of this region. Table 1-12 summarizes the stratigraphy. Data on these regions are compiled in Tables 1-13 and 1-14.

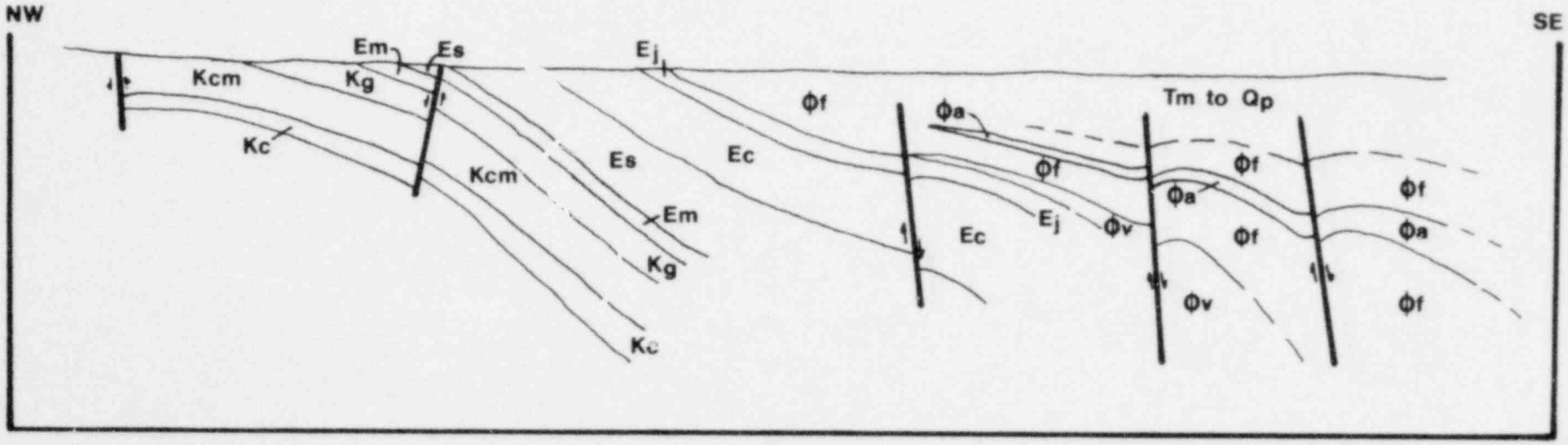

FIG. 1-12. Section across the Gulf Coast clastic wedge (after Murray, 1961). Abbreviations are: Kc, Coahuila series; Kcm, Comanche series; Kg, Gulf series; Em, Midway stage; Es, Sabine stage; Ec, Claiborne stage; Ej, Jackson stage; ϕv, Vicksburg stage; ϕf, Frio Formation; ϕa, Anahvac Formation; Tm to Qp, Mio-Plio-Pleistocene.

TABLE 1-12. Summary of rock units in the Gulf Coast and Mississippi embayment regions (from Murray, 1961). Units described in Tables 1-13 and 1-14 are followed by an asterisk.

Age		Stratigraphic Unit	Thickness, m	Description
Mio-Pliocene			600-1000	Marine clastics
Oligocene		Anahuac Formation*	300	Dark green shales and sandstones
		Hackberry-Frio formations*	1000-2500	Sandstones interbedded with subordinate shale
		Vicksburg stage	200	Limestone grading into clastics
Eocene		Jackson stage	300-1000	Shale sequence with minor limestone
		Claiborne stage	1000	Limestone with minor chert, gypsum, shale and sandstone
		Yegua Formation		
		Cook Mtn. Formation		
		Mt. Selman Formation		
		Sabine stage	1500	Sandstone, shale, with minor coal
		Wilcox Group		
		Midway stage	400	Calcareous sandstone, siltstone, claystone, minor chalk
Cretaceous	Upper	Gulf series	570-1830	Sandstone, glauconitic sandstone, shale, chalk, marl, limestone, coal
		Navarra stage		
		Taylor stage		
		Austin stage		
		Eagle Ford stage		
	Middle	Comanche series	400-200	Limestone, shale, sandstone, minor annydrite
	and	Washita stage		
	Lower	Fredericksburg stage		
		Trinity stage		
Cretaceous	Lower	Coahuila series	300-1000	Limestone and shale, with sandstone

continued

TABLE 1-12 continued.

Age		Stratigraphic Unit	Thickness, m	Description
Jurassic	Upper	Sabinas series	800	Red conglomerate and sandstone, limestone, shale, anhydrite
		----------Unconformity----------		
Paleozoic	Basement	(includes:) Cherokee Shale (Pennsylvanian)* Flint Clay (Pennsylvanian)* Hamilton Shale (Devonian)*		

TABLE 1-13. Hydrologic data for region 4: Gulf Coast and Mississippi embayment.

Geological setting	Age	Locality	Depth, m	No. samples	Density, (g/cm^3)	Porosity			Hydraulic conductivity, cm/s			Ref.	Method
						Av	Max	Min	Av	Max	Min		
Anahuac and Frio formations	Oligocene	Pan American #5, farm and land-canal well, Manchester Field, La.	1006			20			1.8E-7			17	Graphical: from porosity vs bulk rock density plots
			1524			18			2.6E-7				
			1981			16			4.1E-9				
			2438			14			7E-10				
			2896			12			1E-10				
			3048			12			1E-10				
			2079			14			7E-10				
			3139			16			4.1E-9				
			3566			16			4.1E-9				
Shales	Cenozoic?	Gulf Coast, Tex. and La.	surface		1.35	50						4,5	Laboratory measurement[a]
			610		2.03	25			2E-5				
	Cenozoic and Cretaceous		1220		2.11	22							
			1830		2.19	19							
			2440		2.27	16							
			3049		2.35	13							
			3659		2.43	10							
			4269		2.43	10							
			4878		2.46	9							
			5488		2.46	9							
			6098		2.48	8							
Shale	Upper Cretaceous	Houston County, Tex.				10.1						8	Direct measurement with a gas porosimeter and measurement of grain volume

continued

[a]Typical well parameters.

TABLE 1-13 continued.

Geological setting	Age	Locality	Depth, m	No. samples	Density, (g/cm^3)	Porosity			Hydraulic conductivity, cm/s			Ref.	Method
						Av	Max	Min	Av	Max	Min		
Shales	Upper Cretaceous?	E. Tex.	1128		2.48	14.5						18	Same as above[b]
			3336		2.30	27.5							
Anomilina Bilaterata zone	Upper Cretaceous?	Martin Ranch, Tex.					15	10	8.6E-6			2	
Upper Black Underclay	Pennsylvanian	New Brazil, Ind.	trench	1		19.1[c]						13	
Consolidated sandy shale[d]		S. Tex.	2513-2514	3		23			5.1E-5			1	Electrical resistivity data
Shale	Pennsylvanian	Centralia Field, Ill.	425			14.2				1.7E-12	8.6E-12	8	Streaming potential and SP log[e]
		Colorado County, Tex.	2761			7.4			2.6E-10	3.4E-12			
		Houston County, Tex.	?						8.6E-13	6E-12			
Cherokee Shale	Pennsylvanian	Fulton, Mo.	outcrop	2	2.29	17.1	17.2	17.0				9	Melcher method

continued

[b]Shale resistivities for these samples at 25°C and an effective stress of 1000 psi were 10.6 ohm-m (upper stratum) and 1.22 ohm-m (lower stratum).

[c]Total porosity.

[d]Formation resistivity = 14.

[e]Conductivity values under "Av" were obtained with 0.02N NaCl; those under "Max" with 0.2N NaCl; that under "Min" with 1N NaCl.

TABLE 1-13 continued.

Geological setting	Age	Locality	Depth, m	No. samples	Density, (g/cm^3)	Porosity			Hydraulic conductivity, cm/s			Ref.	Method
						Av	Max	Min	Av	Max	Min		
Flint Clay	Pennsylvanian	Fulton, Mo.	outcrop	2	2.37	10.1[f]			1.7E-11			13	
Shale[g]	Pennsylvanian	Union County, Ky.										7	
Core 3807													
#1			9.6	1		8							
#2			52.3	1		3.7							
#3			64.6	1		15.2							
Core 3733													
#1			27.0	1		8.9							
#2			29.8	1		6.4							
#3			52.7	1		6.0							
#4			76.3	1		5.8							
#5			76.4	1		5.4							
#6			76.6	1		5.8							
#7			77.0	1		7.1							
#8			77.3	1		5.0							
#9			77.3	1		5.4							
#10			77.5	1		4.0							
#11			88.2	1		3.6							
#12			110.7	1		4.3							
#13			113.8	1		5.3							
#14			155.9	1		6.0							

continued

[f] Total porosity.

[g] Samples taken from two wire test holes drilled by the Peabody Coal Company. Core 3807 starts 300 ft stratigraphically higher than Core 3733. Porosity decreases with increasing depth of burial; negative correlation strongly influenced by illite content and clay mineral orientation. Porosity decreases with an increase in preferred clay mineral orientation and an increase in illite content.

TABLE 1-13 continued.

Geological setting	Age	Locality	Depth, m	No. samples	Density, (g/cm^3)	Porosity Av	Porosity Max	Porosity Min	Hydraulic conductivity, cm/s Av	Hydraulic conductivity, cm/s Max	Hydraulic conductivity, cm/s Min	Ref.	Method
(Shale)													
(Core 3733)													
#15			164.3	1		6.1							
#16			213.1	1		6.1							
#17			236.7	1		5.8							
#20			343.4	1		10.1							
#21			349.3	1		5.8							
#22			386.3	1		4.5							
#23			402.3	1		7.1							
#24			429.5	1		3.3							
#25			?.2	1		3.6							
Shale		South Pass, La.	13?. 4270	many		15-20						15	
Shale		Pan American Farmers A-1 well, Manchester Field, La.	2460-3345	17	1.85-2.04		17.8	13.1				15	
			3345-3960	11	2.07-2.16		19.5	17.6					
Shale		Gulf Coast	3350-5490				20[h]	18[h]				15	
Shale		Tex. Gulf Coast	3510			20						15	

continued

[h]Porosity measured in lab using shale chips.

TABLE 1-13 continued.

Geological setting	Age	Locality	Depth, m	No. samples	Density, (g/cm^3)	Porosity			Hydraulic conductivity, cm/s			Ref.	Method
						Av	Max	Min	Av	Max	Min		
Shale		La. Gulf Coast	3190-5400	71			22.5	10.8				15	
Shale		Gulf Coast	121-3688	55			45	7.5				11	
			579-4267	23			34	11					
Shale		Tex.							6E-12			16	Lab[i]
Shale		Gulf Coast				3			7.7E-14			10	Lab
						3			1.3E-14			10	Lab
									9.58E-15			16	Lab
									2.1E-15			16	Lab[j]
						3			3.9E-9			12	Lab
			1216-4257				20	14		1.8E-8	1.7E-10	12	Lab[k]
Greenish shale[l]		Shreveport, La.			dry 2.10 sat 2.33	22.6						3,14	
Reddish shale[l]		Shreveport, La.			dry 2.22 sat 2.42	20.0						3,14	
Shale[m]		Shreveport, La.			dry 2.29 sat 2.46	16.9						3,14	
Shale		Batesville, Ark.			dry 2.85 sat 2.86	1.5						3	

[i] 0.2N NaCl solution used as permeant. [j] 10,000-psi load. [k] Estimates from graph for under-compacted shale.
[m] Just above pay sand of Curtis 1. [n] Deep gas sand of Horges Ward 1.

TABLE 1-14. Shale resistivity data for region 4. Values are from Ref. 6 for southwest Louisiana.

Well location	Shale zone	Depth, m	Resistivity, ohm-m
73-105-04E	Bolivina-Mex	4660-4664	0.77
21-105-03E	U. Camerina	3643-3645	0.59
20-105-03E	L. Camerina	3625-3627	0.62
17-105-03E	Bolivina-Mex	4060-4063	0.38
08-105-03E	Discorbis	3047-3049	1.10
31-075-04E	U. Nodosaria	3045-3048	1.02
20-075-03E	Daigle	2949-2954	0.83
76-075-03E	U. Nodosaria	3064-3069	0.97
01-085-02E	Struma	3318-3321	0.90
09-095-03E	Klumpp-D	3661-3665	0.60
04-095-03E	Frio	2927-2929	0.84
09-095-03E	Frio	4037-4040	0.94
11-105-02E	U. Texana	3529-3531	0.35
83-085-03E	Frio	4389-4392	0.50
14-115-02E	Marg Nowei	3765-3767	0.38
47-095-02E	Klumpp-E	3496-3501	0.83
36-085-02E	Nodosaria	3886-3891	0.95
02-115-02E	Marg Tex	3734-3737	0.65
01-115-02E	Marginulina	3744-3746	0.57

References for Tables 1-13 and 1-14 (Region 4)

1. Archie, C. E., 1947, "Electrical Resistivity, An Aid in Core-Analysis Interpretation," Bull. Am. Assoc. Petrol. Geol. 31, 350.
2. Bedoubt, D. G., and A. R. Gregory, 1977, "Texas Geothermal Project Slated to Begin Operations at Martin Ranch," Oil & Gas J. 75(41), 184.
3. Birch, F., J. F. Schairer, and C. H. Spicer, 1942, Handbook of Physical Constants, Geol. Soc. Am. Special Paper 36.
4. Bradley, J. S., 1975, "Abnormal Formation Pressure," Bull. Am. Assoc. Petrol. Geol. 59, 957.
5. Dickey, P. A., 1976, "Abnormal Formation Pressure: Discussion," Bull. Am. Assoc. Petrol. Geol. 60, 1124.
6. Dickey, P. A., A. G. Collins, and I. Fajarado, 1972, "Chemical Composition of Deep Formation Waters in Southwestern Louisiana," Bull. Am. Assoc Petrol. Geol. 56, 1530.
7. Gipson, M., Jr., 1966, "A Study of the Relations of Depth, Porosity, and Clay Mineral Orientation in Pennsylvanian Shales," J. Sedimentary Petrol. 36(4), 888.
8. Gondouin, M., and C. Scala, 1958, "Streaming Potential and the SP Log," Trans. A.I.M.E. 213, 170.
9. Hedberg, H. D., 1926, "The Effect of Gravitational Compaction on the Structure of Sedimentary Rocks," Bull. Am. Assoc. Petrol. Geol. 10, 1035.
10. Hubbert, M. K., and W. W. Rubey, 1959, "Role of Fluid Pressure in Mechanics of Overthrust Faulting, II. Overthrust Belt in Geosynclinal Area of Western Wyoming in Light of Fluid-Pressure Hypothesis," Bull. Geol. Soc. Am. 70(2), 167.
11. Magara, K., 1971, "Permeability Considerations in Generation of Abnormal Pressures," J. Soc. Petrol. Engin. 11, 236.
12. Magara, K., 1974, "Compaction, Ion Filtration, and Osmosis in Shale and their Significance in Primary Migration," Bull. Am. Assoc. of Petrol. Geol. 58(2), 283.
13. Manger, E. G., 1963, Porosity and Bulk Density of Sedimentary Rocks, U.S. Geol. Survey Bulletin 1144-E.
14. Melcher, A. F., 1921, "Determination of Pore Space of Oil and Gas Sands," Trans. Am. Inst. Min. Eng. 65, 480.

15. Price, L. C., 1976, "Aqueous Solubility of Petroleum as Applied to Its Origin and Primary Migration," Bull. Am. Assoc. Petrol. Geol. 60(2), 213.
16. Rieke, H., III, and G. V. Chilingarion, 1974, "Compaction of Argillaceous Sediments," in Developments in Sedimentology, Vol. 16.
17. Schmidt, G. W., 1973, "Interstitial Water Composition and Geochemistry of Deep Gulf Coast Shales and Sandstones," Bull. Am. Assoc. Petrol. Geol. 57, 321.
18. Waxman, M. H., and E. C. Thomas, 1975, "Electrical Conductivities of Shaly Sands--I. The Relation Between Hydrocarbon Saturation and Resistivity Index, II. The Temperature Coefficient of Electrical Conductivity," Trans. A.I.M.E. 257, 213.

Region 5: Appalachian Mountains and Great Lakes

The northern and eastern portions of the United States have evolved, much like the Gulf Coast--along two opposing trends. During the Paleozoic, the geologic history was characterized by collisions of plates, the disappearance of proto-oceans, and the building of one supercontinent (Pangea). In late Devonian time, the northern Appalachians (New England) were formed as the Iapetus Ocean disappeared (Mintz, 1977). In late Carboniferous time, the southern Appalachian-Ouachita range formed a weld between Laurasia and Gondwanaland, closing the Theic Ocean, but this union was short-lived: with the advent of the Triassic, the two continents began to part as the Atlantic Ocean started to grow.

Record of these geologic events has been preserved as Upper Precambrian and Paleozoic remnants of oceanic basins folded into Appalachian structures and as Triassic red beds (Newark series) occupying grabenlike basins. The following shales are found within this geologic record.

- Late Precambrian (Nonesuch Shale), Late Ordovician (Martinsburg Shale), and Devonian-Mississippian (Chattanooga shales) deposits characterize the early compressive tectonic style. Their relationship is illustrated in Fig. 1-13.
- Triassic (Brunswick Shale) is more representative of a setting found in the Atlantic Plains, which are discussed as part of region 6.

The stratigraphy is described in Table 1-15; hydrologic and resistivity data appear in Tables 1-16 and 1-17.

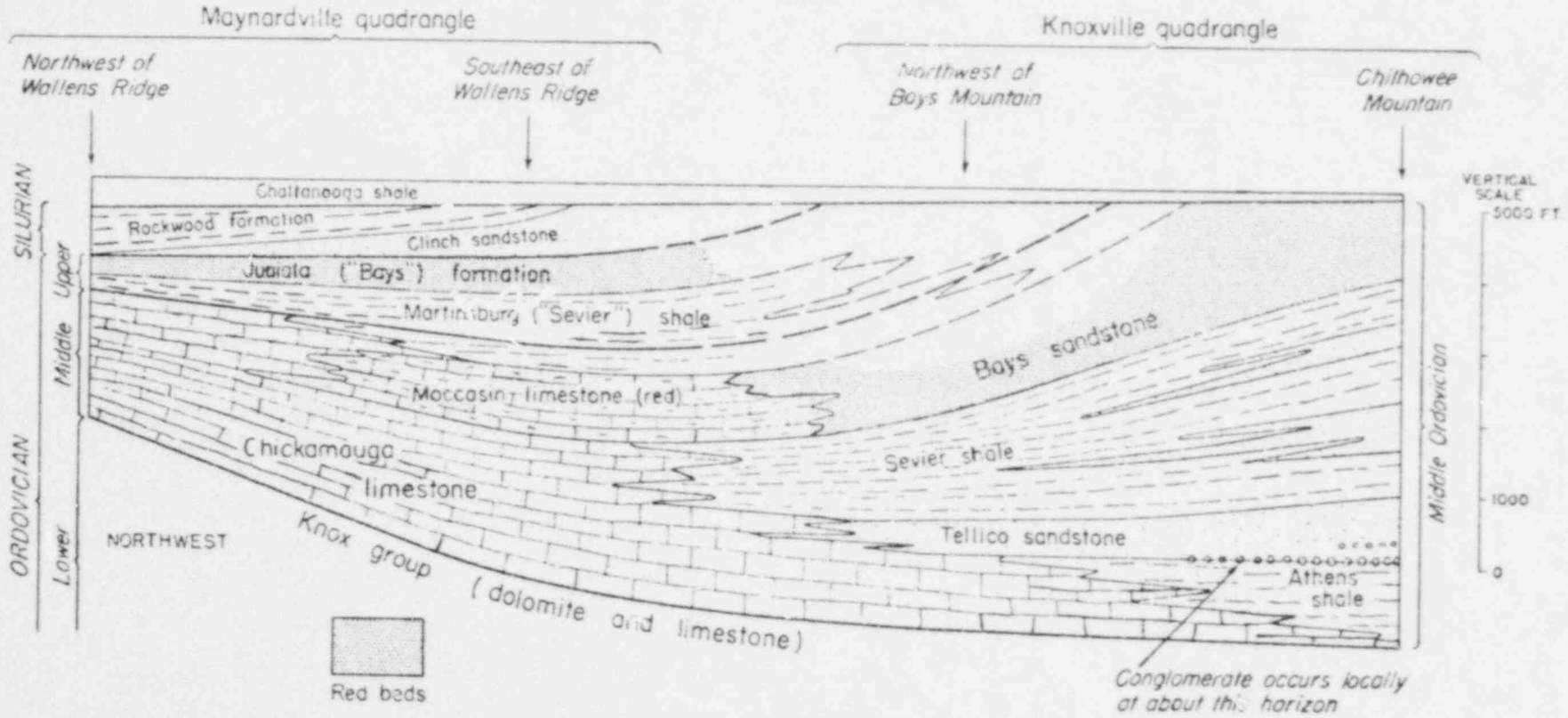

FIG. 1-13. Stratigraphic diagram showing the relationships between the Martinsburg and Chattanooga shales in the Appalachian and Great Lakes regions (after Eardley, 1962).

TABLE 1-15. Summary of rock units of the Appalachian and Great Lakes regions (from Schucher (1943). Units described in Tables 1-16 and 1-17 are followed by an asterisk.

Age		Stratigraphic Unit	Thickness, m	Description
Lower Permian and Upper Pennsylvanian		Cassaville and Washington formations	0-366	Brown and red sandstone, shale, thin limestone and unimportant coals
Pennsylvanian	Upper	Monongahela Formation*	79-91	Shale, limestone, sandstone, and coals
	Middle	Conemaugh Formation	122-244	Red shale, massive pebbly sandstone, with coals and fire clays
		Allegheny Formation (Flint Clay?)*	85-122	Sandstone, shale, limestone, coals, fire clays
	Lower	Pottsville Group	91-1265	Sandstone, shale, coals
		----------		Disconformity
Mississippian	Upper	Mauch Chunk Formation	91-1052	Green sandstone, interbedded with red and green shale
		----------		Disconformity
		Greenbrier Formation	247-549	Fossiliferous limestone, with red and green shale
		----------		Disconformity
	Middle	Maccrady Group	7-107	Red, purple and yellow shale, earthy limestone, and calcereous sandstone
	Lower	Pocono Formation	213-668	Gray or red sandstone, sandy shale, unimportant coal
Devonian	Upper	Hampshire Formation (partly correlative with the Chagrin Shale* and Chattanooga Shale*)	945-1143	Red and green shale, sandstone
		Chemung Formation	518-1067	Shale, sandstone, thin coals and underclay
		Portauge formation	518-610	Shale and sandstone
		Gensee formation	15-91	Shale
		----------		Disconformity

continued

TABLE 1-15 continued.

Age		Stratigraphic Unit	Thickness, m	Description
(Devonian)	Middle	Hamilton and Marcellus formations*	488(max)	Shale
	Lower	Ridgeley Formation	15-84	Sandstone
		Shriver Formation	0-56	Cherty limestone
		----------		Disconformity
		New Scotland Formation	4-20	Limestone and calcereous sandstone
		Coeymans Limestone	3-30	Massive crinoidal limestone
		----------		Disconformity
Silurian	Upper	Keyser Limestone	56	Limestone with local shale, and sandstone
		----------		Disconformity
		Tonoloway Formation	168	Argillaceous limestone, calcareous shale, sandstone at base
		Wills Creek Formation	0-183	Calcareous shale, argillaceous limestone, some sandstone
		----------		Disconformity
	Middle	McKenzie Formation	15-122	Shale, argillaceous limestone, some sandstone
		Clinton Formation	122-183	Shale, sandstone, and limestone
	Lower	Tuscorora Formation	15-94	Massive sandstone
		----------		Disconformity
Ordovician	Upper	Juanita Formation	122-335	Sandstone
	Upper to Middle	Martinsburg Formation*	610-1067	Shale, sandstone, and limestone
	Middle	Chambersburg Formation	146-175	Limestone with shale partings
		----------		Disconformity
		Stones River Group	113-223	Limestone
		----------		Disconformity

continued

TABLE 1-15 continued.

Age		Stratigraphic Unit	Thickness, m	Description
(Ordovician)	Lower	Beekmantown Formation	610-762	Dolomite
		----------		Disconformity
Cambrian	Upper	Conococheague Formation	488-549	Magnesian limestone
		----------		Disconformity
	Middle	Elbrook Limestone	427-762	Limestone, shaly limestone, shale
	Lower	Waynesboro Formation	488	Magnesian limestone, calcareous sandstone, red or purple siliceous shale
		----------		Unconformity
		Tomstown Formation	111-319	Dolomite, marble, limestone and shale
		Antietam Formation	152	Quartzite, sandstone
		Harpers Formation	366	Slate, quartzite
		Weverton Formation	152-183	Quartzite, conglomerate
		----------		Unconformity
Precambrian	Upper-most	Keweenawan (includes:)	15,500-12,200	Lava flows, red sandstone and shales
		Nonesuch Formation	100	Black shale
		----------		Unconformity
Proterozoic and earlier				

TABLE 1-16. Hydrologic data for region 5: Great Lakes and Appalachians.

Geological setting	Age	Locality	Depth, m	No. samples	Density, (g/cm^3)	Porosity			Hydraulic conductivity, cm/s			Ref.	Method
						Av	Max	Min	Av	Max	Min		
Blue gray shale overlying Keener sand	Mississippian	Jerusalem, Ohio	440		dry 2.46 sat 2.56	9.7						1,3	
		Miltonburg, Ohio	450		dry 2.41 sat 2.52	11.0						1,3	
Black shale	Devonian	Floyd County, Ky.	669		dry 2.41 sat 2.41	0.0						1	
West Falls Formation, Chagrin Shale	Upper Devonian	Lincoln County, W.Va.				2.5						4	From 230 matrix and bulk density measurements[a]
Chattanooga Shale	Devonian and Mississippian	Irvine Field, Ky.	subsurface	2	2.38	7.5[b]	7.6	7.4				2	
		near Smithville, Tenn.	mine	2	2.53	1.7[c]	1.7	1.7				2	
Allegheny Formation (shale and slate)	Pennsylvanian	Bakerton, Pa.	approx 152	2	2.72	1.7[c]						2	
Monongahela Formation	Pennsylvanian	Scotts Run, W.Va.	mine	5	2.5	6.1[d]						2	
Martinsburg Shale (slate)	Ordovician	Bangor, Pa.	quarry		2.74	1.0[c]						2	
Nonesuch Shale (siliceous)	Precambrian	White Pine, Mich.	mine	6	2.76	1.6[c]	1.7	1.5				2	

[a] 1250-ft core, overall average. [b] Total porosity. [c] Effective porosity. [d] Effective porosity. Compressive strength 11,600 lb/in.^{2}

TABLE 1-17. Resistivity data for region 5.

Formation	Age	Locality	Resistivity, ohm-cm	Reference
Nonesuch Shale (siliceous)	Precambrian	White Pine, Mich.	10^4	1
Shale	?	Shamokin, Pa.	10^5	1

References for Tables 1-16 and 1-17 (Region 5)

1. Birch, F., J. R. Schairer, and C. H. Spicer, 1942, Handbook of Physical Constants, Geol. Soc. Am. Special Paper 36.
2. Manger, E. G., 1963, Porosity and Bulk Density of Sedimentary Rocks, U.S. Geol. Survey Bulletin 1144-E.
3. Melcher, A. F., 1921, "Determination of Pore Space of Oil and Gas Sands," Trans. Am. Inst. Min. Engin. 65, 480.
4. Nuhfer, E. G., and R. J. Vinopal, 1978, "Nature of Porosity in Upper Devonian Shales of Lincoln County, West Virginia," Geol. Soc. Am. Abst. Programs 10(7), 464.

Region 6: Atlantic Coastal Plain and Triassic Basin

The east coast of the United States is a transitional zone between the Appalachian region and the Atlantic Ocean. Its geology contains a record of Mesozoic seafloor spreading and also presents some analogies with the Gulf Coast. Early stages of spreading are indicated by the Triassic basins of the Appalachians (which contain Brunswick Shale), and later stages are found along the Coastal plains to the east. A Cretaceous shale (Middendorf) is found in this second zone.

Structural relationships between the various units are shown in Figs. 1-14 and 1-15. The stratigraphy is summarized in Table 1-18. Available hydrologic data are gathered in Tables 1-19 and 1-20.

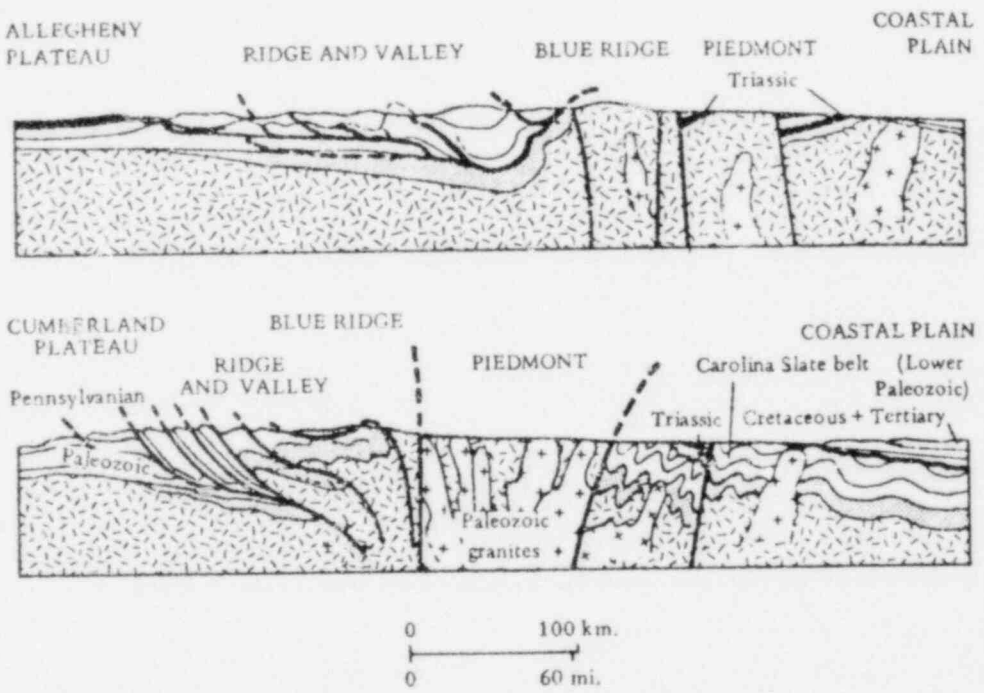

FIG. 1-14. Generalized structural sections across the Appalachians and the Atlantic Coastal Plain (from Mintz, 1977).

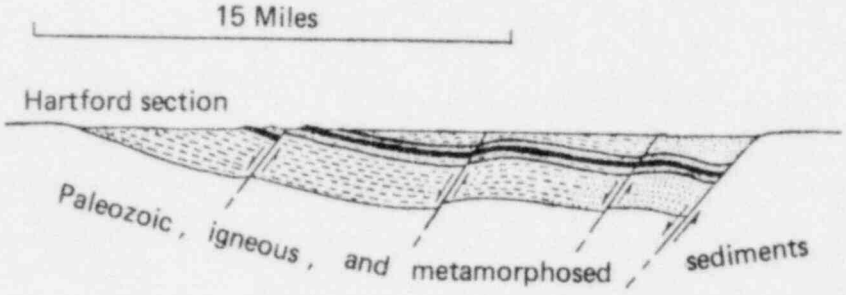

FIG. 1-15. Section showing detailed structure of a Triassic basin (from Eardley, 1962).

TABLE 1-18. Generalized stratigraphic column for New Jersey (Atlantic Coastal Plain) (from Schuchert, 1943). Units described in Tables 1-19 and 1-20 are followed by an asterisk.

Age		Stratigraphic Unit	Thickness, m	Description
Pliocene? to Pleistocene		Beacon Hill Formation	0-15	Gravel--occurs as isolated remnants (terrace gravels) (Archie, 1947)
		----------	----------	Disconformity
Miocene	Upper?	Cohansey Sand*	15-137	Quartz sand and lenses of clay and gravel
		----------	----------	Disconformity
	Middle	Kirkwood Formation*	2-30	Banded micaceous quartz sands, lignitic clays and clay at base
		----------	----------	Disconformity
Eocene	Middle	Shark River Formation	3	Glauconitic sand and clay
	Lower	Manasquan Formation	9-27	Nearly pure greensand marl
		Vincentown Formation	30	Yellow quartz sand facies grading into lime-sand to the southwest
		Hornerstorn Formation	0-9	Dark, sparsely fossiliferous, nearly pure greensand marl
		----------	----------	Disconformity
Cretaceous	Upper	Tinton and Redbank formations	4-37	Tinton: glauconitic red sand Redbank: very ferruginous red sand
		Mount Laurel and Navesink formations	3-21	Mount Laurel: fossiliferous quartz sand with some glauconite Navesink: nearly pure greensand marl
		Wenonah, Marshalltown formations	15-43	Wenonah: black to reddish brown sand sometimes strongly micaceous with small amounts of glauconite Marshalltown: sandy clay to clayey greensand and marl, or laminated micaceous clay or pure greensand marl
		Englishtown Sand	0-30	Quartz sand
		Woodbury Clay	15	Black, somewhat micaceous and slightly sandy clay
		Merchantville Clay Marl	11-18	Black, glauconitic, somewhat sandy clay marl
		Magothy Formation* (Middendorf Formation in S.C.)	3-53 (30-60)	Magothy: clay, white sand, with seams of black lignite and thin beds of black clay Middendorf: partly correlative with Magothy in New Jersey. Dark laminated clay and micaceous sand (Archie, 1947).

continued

TABLE 1-18 continued.

Age		Stratigraphic Unit	Thickness, m	Description
		Raritan Formation	46-152	Variable and variegated sands and plastic clays
		----------Unconformity----------		
Triassic	Upper	Newark Group		
		Brunswick Shale*	1524-3658	Red shale and sandstone
		Watchung Basalt	91-366	Basalt flows
		Lockatong Formation	518-1097	Black shale, dark argillite, flagstone, and rare thin limestone
		Stockton Formation	701-945	Arkosic sandstone, conglomerate and red shale (lies on Precambrian)
		----------Unconformity----------		
Paleozoic basement				

TABLE 1-19. Hydrologic data for region 6: Atlantic Coastal Plain and Triassic basins.

Geological setting	Age	Locality	Depth, m	No. samples	Density, (g/cm^3)	Porosity			Hydraulic conductivity, cm/s			Ref.	Method
						Av	Max	Min	Av	Max	Min		
Blue clay	Miocene	Salisbury, Md.							From consolidation		Constant flow	3	Lab. For each sample, lower conductivity value was measured at consolidation load of 8 kg/cm^2, higher value at 4 kg/cm^2
			23.7	1[a]					5.3E-7		5.8E-7		
									1.5E-7		8.7E-8		
			23.6	1[b]					4.2E-7		1.3E-7		
									2.7E-7		5.5E-8		
			24.4	1[c]					6.4E-7		2.2E-6		
									3.5E-7		5E-7		
			24.1	1[d]					1.9E-7		9.1E-7		
									1.5E-7		5.5E-7		
			23.1	1[e]					2.5E-7		1.5E-8		
									6E-8		1E-8		
			24.7	1[f]					1.8E-7		1.1E-7		
									1.4E-7		4.2E-8		
			25	1[g]					1.4E-7		4.2E-8		
									3.8E-8		1.8E-8		
Kirkwood Formation	Miocene	Yorktown, N.J.										1	Transmissibility computed from Theis nonequilibrium equation. Permeability computed using the relation T = Kb, where b is thickness. (T_{min} = 6000 ft; T_{max} = 16,000 ft.)
Yellowish clay			1.2	1	1.3	51.9[h]							
Yellowish clay			3	1	1.62	40.3[h]							
Blue clay			4	1	1.70	38.6[h]							

continued

[a]Sample C-2. [b]Sample C-11. [c]Sample C-7. [d]Sample C-12. [e]Sample C-8. [f]Sample C-14. [g]Sample C-9. [h]Total porosity.

TABLE 1-19 continued.

Geological setting	Age	Locality	Depth, m	No. samples	Density, (g/cm^3)	Porosity			Hydraulic conductivity, cm/s			Ref.	Method
						Av	Max	Min	Av	Max	Min		
Cohansey Sand (clay)	Miocene-Pliocene?	Crossley, N.J.	outcrop	2	1.67	37.0[h]	37.4	36.6				2	
Brunswick Formation (shale)[f]	Late Triassic to early Jurassic	Flemington, N.J.										4	
Observation well #1									3.7E-4	6.9E-4	2.6E-4		
Observation well #2									3.2E-4	5.9E-4	2.2E-4		
Observation well #3									2.5E-4	4.5E-4	1.7E-4		
Observation well #4									2.5E-4	4.5E-4	1.7E-4		
Middendorf Formation (white clay)	Cretaceous	Aiken and Richland counties, S.C.	outcrop	2	1.55	40.7[h]	42.3	39				1	
Claystone	Triassic	Savannah River Plant, S.C.	400[j] 388[k]						2.9E-10 3.9E-12			2	Calculated from well yield data
Mudstone[l]	Triassic	Savannah River Plant, S..C	1282	several		3.3			1.16E-10 to 1.16E-11			2	
Mudstone[m] (massive)	Triassic	Savannah River Plant, S.C.	1010	several					1.7E-9			2	

[h]Total porosity.

[f]Soft, hematite-stained red shales with some interbedded sandstone. Strike N53^{o}E, dip 25^{o}NW. Alignment of major fracture system is parallel strike. Sedimentation basin block faulted and rotated to present position. Fracture porosity measured. Wells perpendicular to strike.

[j]Well P5R. [k]Well P12R. [l]Well DRB-10. Effective porosity 0.53%. [m]Well DRB-11.

TABLE 1-20. Other properties for region 5 (laboratory results from Ref. 3).

	Consolidation load, kg/cm^2	Diffusivity, cm^2/s
Blue clay(Miocene) Salisbury, Md.		
Sample C-2	4	2.3E-2
	8	1.7E-2
Sample C-7	4	1.3E-2
	8	1.9E-2
Sample C-8	4	2.9E-2
	8	2.5E-2
Sample C-9	4	2.3E-2
	8	2.0E-2
Sample C-11	4	1.4E-2
	8	5.3E-3
Sample C-12	4	2.0E-2
	8	1.8E-2
Sample C-14	4	5.0E-3
	8	1.8E-3

References for Tables 1-19 and 1-20 (Region 6)

1. Manger, E. G., 1963, Porosity and Bulk Density of Sedimentary Rocks, U.S. Geol. Survey Bulletin 1144-E.
2. Marine, I. W., 1963, "Geohydrology of Buried Triassic Basin at Savannah River Plant, South Carolina," in Underground Waste Management and Artificial Recharge, 2nd International Symposium, New Orleans, La. (Am. Assoc. Petrol. Geol.), Vol. 1, pp. 481-504.
3. Wolf, R. G., 1970, "Field and Laboratory Determination of the Hydraulic Diffusivity of a Confining Bed," Water Resources Res. 6(1), 194.
4. Vecchiolli, J., 1967, "Directional Hydrolic Behavior of a Fractured Shale Aquifer in New Jersey," in Hydrology of Fractured Rocks (Assoc. Intern. D'Hyd. Sci.), pp. 318-326.

REFERENCES: CHAPTER 1

American Geological Institute (AGI), 1972, Glossary of Geology, M. Gary, R. McAfee, and C. L. Wolf, Eds. (Washington, D.C).

Archie, G. E., 1950, "Introduction to Petrophysics of Reservoir Rocks," Bull. Am. Assoc. Petrol. Geol. 34(5), 943.

Aronson, J. L., and J. Hower, 1976, "Mechanism of Burial Metamorphism of Argillaceous Sediments: 2. Radiogenic Argon Evidence," Bull. Geol. Soc. Am. 87, 738.

Atwater, J., 1970, "Implication of Plate Tectonics for the Cenozoic Tectonic Evolution of Western North America," Bull. Geol. Soc. Am. 81, 3513.

Berry, F. A. F., 1959, Hydrodynamics and Geochemistry of the Jurassic Cretaceous Systems in the San Juan Basin, Northwestern New Mexico and Southwest Colorado, Stanford University, Ph.D. dissertation.

Clark, T. H., and C. W. Stearn, 1968, Geological Evolution of North America (Ronald Press, New York), 2nd ed.

Cummings, J. C., R. M. Touring, and E. E. Brabb, 1962, Geology of the Northern Santa Cruz Mountains, Calif. Div. of Mines and Geol. Bulletin 181, pp. 179-220.

Davis, S., and R. DeWiest, 1966, Hydrogeology (John Wiley and Sons, Inc., New York), p. 165.

Eardley, A. J., 1962, Structural Geology of North America (Harper and Row Publishers, New York).

Emerson, D. O., and E. I. Rich, 1966, Calif. Div. of Mines and Geol. Bulletin 190, p. 476.

Gill, J. R., E. A. Merriwether, and W. A. Cobban, 1970, Stratigraphy and Nomenclature of Some Upper Cretaceous and Lower Tertiary Rocks in South Central Wyoming, U.S. Geol. Surv. Professional Paper 667.

Grim, R. E., 1968, Clay Mineralogy (McGraw-Hill Book Co., New York). 2nd Ed.

Hackel, O., 1966, Summary of the Geology of the Great Valley, Calif. Div. of Mines and Geol. Bulletin 190, pp. 217-238.

Hower, J., E. V. Eslinger, M. E. Hower, and E. A. Perry, 1976, "Mechanism of Burial Metamorphism of Argillaceous Sediments: 1. Mineralogical and Chemical evidence," Bull. Geol. Soc. Am. 87, 725.

King, P. B., 1951, The Tectonics of Middle North America, East of the Cordilleran System (Princeton Univ. Press, New Jersey).

Kirby, J. M., 1943, "Upper Cretaceous Stratigraphy of the West Side of the Sacramento Valley, South of Willows, Glenn County, California, Bull. Am. Assoc. Petrol. Geol. 27, 270.

Lee, W. T., 1927, Correlation of Geologic Formations between East Central Colorado, Central Wyoming, and Southern Montana, U.S. Geol. Surv. Professional Paper 149.

Magara, K., 1973, Compaction and Fluid Migration in Cretaceous Shales of Western Canada, Geol. Surv. of Canada Paper 72.

Maher, J. C., R. D. Carter, and R. J. Gantz, 1975, Petroleum Geology of Naval Petroleum Reserve No. 1, Elk Hills, Kern County, California, U.S. Geol. Surv. Professional Paper 912.

Maxwell, D. T., and Hower, 1967, "High Grade Diagenesis and Low Grade Metamorphism of Illite in the Precambrian Belt Series," Am. Mineralogist 52, 843.

Mintz, L. W., 1977, Historical Geology: The Science of a Dynamic Earth (Merrill Publ. Co., Columbus, Ohio).

Murray, G. E., 1961, Geology of the Atlantic and Gulf Coastal Provinces of North America (Harper Bros., New York).

Page, B. M., 1966, Geology of the Coast Ranges of California, Calif. Div. of Mines and Geol. Bulletin 190, pp. 255-276.

Poole, F. G., and C. A. Sandberg, 1977, "Silurian and Devonian paleography," in Paleozoic Paleogeography, J. H. Stewart, C. H. Stevens, and M. E. Fritsche, Eds., Pacific Coast Paleogeography Symposium 1 (Soc. Econ. Paleontol. and Mines), pp. 39-85.

Powers, M. C., 1967, "Fluid Release Mechanisms in Compacting Marine Mud Rocks and Their Importance in Oil Exploration," Bull. Am. Assoc. Petrol. Geol. 51, 1240.

Ruedemann, P., 1939, "Geology of the South Central Lowlands and Ouachita Province," in Geology of North America, P. Ruedemann, and E. Belk, Eds. (Verlag von Gebruder Borntraegen, Berlin), pp. 463-518.

Samuels, S. G., 1955, "The Effect of Base Exchange on the Engineering Properties of Soils," figure in R. C. Mielenz and M. E. King, Calif. Div. of Mines and Geol. Bulletin 169.

Schuchert, C., 1943, Stratigraphy of the Eastern and Central United States, (John Wiley and Sons, Inc., New York).

Seyfert, C. K., and L. A. Sirkin, 1973, Earth History and Plate Tectonics (Harper and Row Publishers, New York)

Smith, J. E., 1971, "The Dynamics of Shale Compaction and Evolution of Fore Fluid Pressures," Mathemat. Geol. 3(3), 239.

_____, 1973, "Shale Compaction," Soc. of Econ. Petrol. Engin. 255, 11.

Stewart, J. H., and C. A. Suczek, 1977, "Cambrian and Latest Precambrian Paleogeography," in Paleozoic Paleogeography, J. H. Stewart, C. H. Stevens, and H. E. Fritsche, Eds., Pacific Coast Paleogeography Symposium, No. 7 (Soc. Econ. Paleontol. and Mines), pp. 1-19.

Tourtelot, M. A., 1962, Preliminary Investigation of the Geologic Setting of the Pierre Shales, Great Plains Region, U.S. Geol. Surv. Professional Paper 390.

Towe, K. M., 1962, "Diagenesis of Clay Minerals as a Possible Source of Cement in Sedimentary Rocks," J. Sed. Petrol. 32, 26.

Weaver, C. E., 1959, "The Clay Petrology of Sediments," in Clay and Clay Minerals, Vol. 6, pp. 154-187.

Weaver, C. E., and E. Pollard, 1975, The Chemistry of Clay Minerals (Elsevier Scientific Publ. Co., New York).

Yeh, H. W., and S. M. Savin, 1977, "Mechanism of Burial Metamorphism of Argillaceous Sediments: 3. Isotop Evidence," Bull. Geol. Soc. Am. 88, 1321.

CHAPTER 2

BASALT

GEOLOGY

Basalt is a dark-colored, mafic, igneous rock composed of calcium plagioclase and clinopyroxene. It is generally extrusive or volcanic in origin, with a glassy or fine-grained texture. Most basalts occur in flows. There are small near-surface intrusions of basalt, but their volume is relatively small. Most of the great flow sequences underlie the oceans, but major continental flow deposits also occur. The continental flow sequences, known as flood or plateau basalts, spread to great thicknesses over various areas of all the continents during the Permian, Triassic, and mid-Tertiary periods. Because of their accessibility, these continental flood basalts have, until recently, received more attention than the oceanic basalts. For the purposes of studying deep geologic disposal of nuclear waste, we will consider only the characteristics of the largest flood basalts in the United States, which are located in the Columbia Plateau region of the Pacific Northwest.

Classification and Composition

All igneous rocks, including basalts, are classified on the basis of texture and mineralogy. By definition, basalts are all fine-grained, calcium plagioclase-clinopyroxene rocks. Within this framework, several textures and mineral subclasses specify different genetic types of basalt.

Basalts are divided into two main mineralogical subgroups (Fig. 2-1). Each of these is derived from a distinct type of parent magma. The tholeiitic magma is saturated with SiO_2 and produces basalts consisting of calcium-poor augite, $(Ca,Na)(Mg,Fe,Al,Ti)(Si,Al)_2O_6$, labradorite plagioclase, $(Ca,Na)Al(Si,Al)Si_2O_8$; and iron oxides. Olivine, $(Mg,Fe)_2SiO_4$, may be absent or, as in olivine tholeiite, present in accessory amounts.

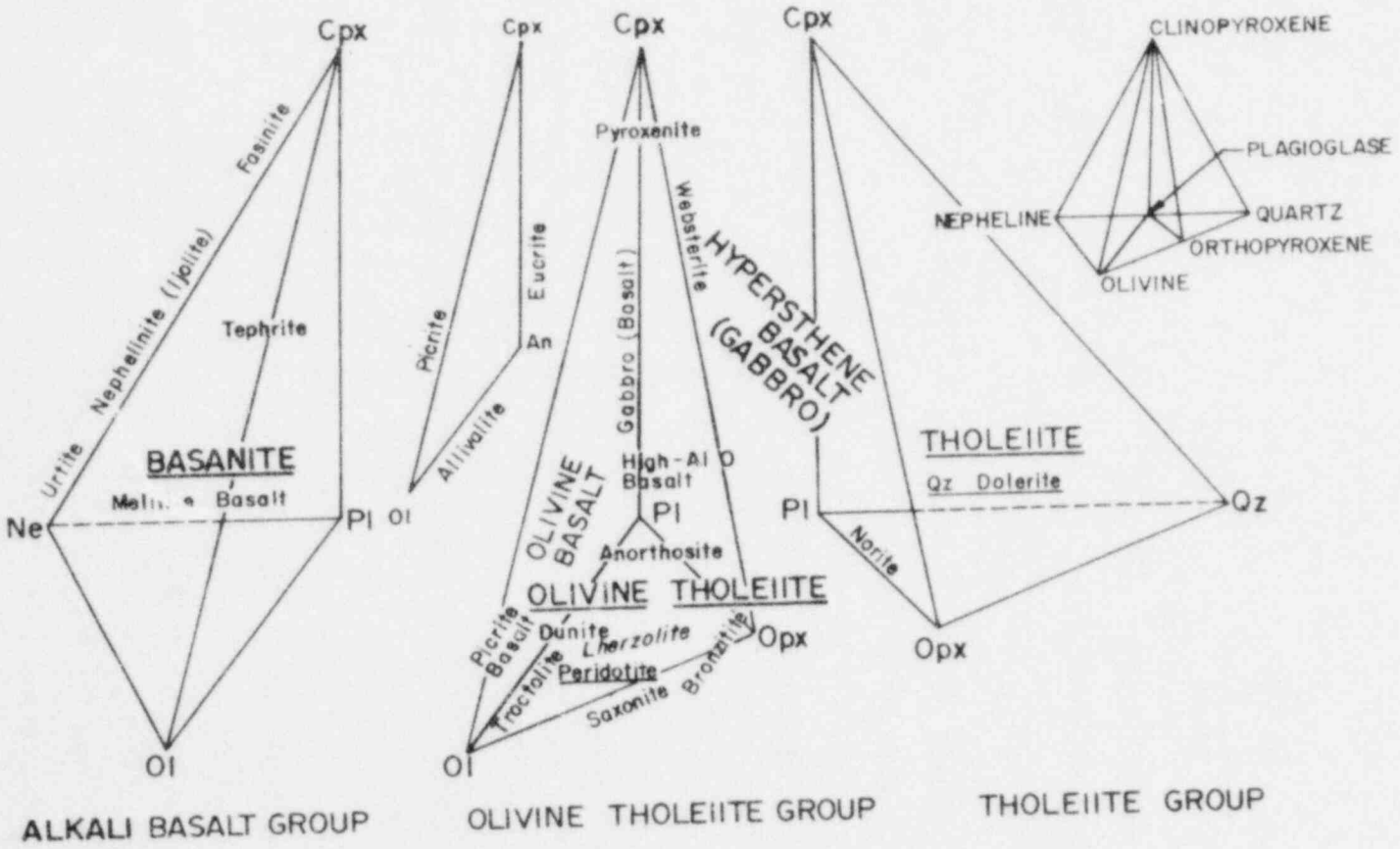

FIG. 2-1. Mineralogical subgroups of basalt (after Yoder and Tilley, 1962). The figure shows an exploded view of a generalized simple basalt system, illustrated in upper-right inset. Entered are names of rocks whose major normative phases are contained in the tetrahedron. Names underlined are within the tetrahedron. Names in the faces are written parallel to the base. Lherzolite is in the Ol-Cpx-Opx face. An additional inset, Ol-Cpx-An, gives alternative nomenclature when plagioclase is rich in anorthite.

The alkali basaltic magma is undersaturated with respect to SiO_2 and produces nepheline, $(Na,K)AlSiO_4$, bearing calcium-rich augite. In the resulting rocks, alkali feldspars often occur with the calcium plagioclases, and in general, alkali basalts contain much more complex assemblages of feldspars. As with the tholeiites, olivine may be absent or occur as an accessory; however, it is more common in the alkalis. Also, alkali-basaltic olivine occurs in the groundmass, and it tends to be zoned from magnesium-rich to iron-rich. This is unusual for tholeiite olivine.

Two lesser suites of basalts are the calc-alkali series and the high-alumina series. The genesis of both are controversial. The calc-alkalis are thought to be high alkali differentiates of the tholeiitic magmas. The high-alumina basalts contain more than 17% Al_2O_3 and are also thought to be derivatives of the tholeiites. Mineral and chemical analyses of three typical basalts are summarized in Table 2-1.

Basaltic textures and their causes are almost as numerous as the various basalt rock names. For practical purposes, particularly if the physical properties of the rock are of concern, only a few textures are important. Basalts tend to be porphyritic (having larger crystals set in a fine-grained groundmass). The large crystals, or phenocrysts, are often aligned, creating anisotropy. The groundmass may be vitreous or glassy. Although basalt glasses, or obsidians, are rare, matrices can contain high proportions of glass.

Genesis

Genetic theory for the basaltic rocks is extremely detailed and complicated. Basaltic magmas develop directly from the earth's mantle material (Carmichael et al., 1974; Hess and Poldervaart, 1967), but controversies continue over where in the mantle the magmas develop, what materials are involved, and how many primary basaltic magmas are developed.

The major type of basalt in both oceanic and continental occurrences is tholeiitic. The magma producing this basalt is thought to be a primary magma generated form a garnet-peridotite, or eclogit, in the upper mantle. Continental and oceanic tholeiites are slightly different in some respects, particularly in their trace element suites. However, these differences are believed to be due to contamination as the magmas pass up through either the

TABLE 2-1. Chemical composition and mineralogy of some basaltic rocks (from Hess and Poldervaart, 1967).

	Composition, wt%		
	Olivine Tholeiite[a]	High-Alumina Basalt[b]	Olivine Alkali Basalt[c]
Chemical constituents:			
SiO_2	49.18	48.27	41.60
TiO_2	2.29	0.89	2.64
Al_2O_3	13.33	18.28	10.38
Fe_2O_3	1.31	1.04	3.58
FeO	9.71	8.31	9.07
MnO	0.16	0.17	0.20
MgO	10.41	8.96	14.38
CaO	10.93	11.32	10.90
Na_2O	2.15	2.80	4.32
K_2O	0.51	0.14	1.02
H_2O	0.09	0.22	1.46
P_2O_5	0.16	0.07	0.38
Mineral constituents:			
Quartz, SiO_2	--	--	--
Orthoclase, $KAlSi_3O_8$	2.78	0.56	0.56
Albite, $NaAlSi_3O_8$	17.82	23.58	--
Anorthite, $CaAl_2Si_2O_8$	25.30	39.97	5.84
Diopside, $CaMgSi_2O_6$	22.93	15.23	36.54
Hypersthene, $(Mg,Fe)_2Si_2O_6$	15.35	--	--
Olivine, $(Mg,Fe)SiO_4$	9.14	20.55	20.37
Magnetite, Fe_3O_4	2.09	1.39	5.10
Ilmenite, $FeTiO_3$	4.41	1.67	5.02
Apatite, $Ca_5(PO_4)_3(F,OH,Cl)$	0.34	0.17	1.01
Nepheline, $(Na,K)AlSiO_4$	--	--	19.88
Leucite, $KAlSi_2O_6$	--	--	4.36

[a]From Kilawea Caldera, Hawaii.

[b]From Medicine Lake highlands, Calif.

[c]From Ponape Island.

continental or oceanic crusts (Carmichael et al., 1974; Hess and Poldervaart, 1967).

Alkali, calc-alkali, and high-alumina basaltic magmas hypothetically develop from tholeiite magma. For calc-alkali and high-alumina magmas, this hypothesis is very tentative, because the data are insufficient and inconclusive. Alkali magma can be differentiated from tholeiitic magma, but an enormous volume of tholeiitic magma is requred. Proponents of the tholeiitic origin of alkali magma postulate a partial melting of tholeiites, followed by filter pressing of alkali magma, to explain the differentiation. Opponents invoke a separate primary alkalic magma (Hess and Poldervaart, 1967), which would imply that the concept of a relatively homogenous mantle is suspect. The problem of the alkali basaltic magma source still awaits solution.

Physical Characteristics of Basalt Flows

Lava Forms. Lava flows issuing from fissure eruptions in the Pacific Northwest are predominantly of two types, pahoehoe and aa. These two forms of lava are distinguished by various flow features controlled by the viscosity and degree of agitation in the extruded lava mass. Most flows issue as pahoehoe, and as viscosity declines downslope, the pahoehoe flows change into aa.

Pahoehoe flows are characterized by a rolling, billowy, or "ropy" surface, which is produced by the deformation and folding of the thin, cooled lava surface by deeper flowing lavas. Vesicles, resulting from the release of gas by the lava, are abundant in pahoehoe flows. Spherical or nearly spherical vesicles may fully permeate thin flows, whereas in thicker flows vesicles are concentrated near the top of the flow. In some cases, vesicles may also be found in a chilled layer near the base of a flow.

In contrast to the relatively smooth, undulating surface of a pahoehoe flow, aa flows are rough, spiny, fragmented, and blocky. The surface is scoriaceous, the top and margins of the flow being covered with clinker. Occasionally, a layer of clinker may also be found on the lower surface of the flow; however, in the Columbia River and Cascade regions, flows generally lack this feature. Aa flows are generally much less vesicular than pahoehoe flows. Vesicularity may reach 50% in some aa flows, but is normally less than

30% (MacDonald, 1966). Those vesicles present are generally less than 2 cm in diameter and nonspherical.

A third type of subareal flow, block lavas, is rarely found in the Northwest. Block flows are generally characteristic of siliceous lavas rather than lavas of basaltic composition such as those of the Columbia Plateau region.

Since lavas were extruded in some areas of the Northwest into shallow seas or freshwater lakes, subaqueous flows are also of some interest. The predominant subaqueous form is pillow lava. These flows consist of stacked ellipsoidal bodies of lava, generally ranging from 10 cm to 7 m in diameter. Pillows may be compactly molded together or separated partly or wholly by detrital materials. Most have glassy skins and are radially fractured.

Joints and Cooling Features. As a basalt flow cools, shrinkage of the lava causes vertical tension fractures or joints to develop. In a massive flow, these joints form in regular patterns. Thin flows are normally characterized by rectangular or irregular polygonal joint configurations in the horizontal plane. Thicker flows exhibit more uniform hexagonal systems of joints in the x-y plane, producing hexagonal columns. Holmes (1965) explains the formation of "columnar" joints:

> When a hot homogenous rock cools uniformly against a plane surface, the contraction is equally developed in all directions throughout the surface. This is mechanically the same as if the contraction acted towards each of a series of equally spaced centres. Such centres [C, 1,2,3, etc., in Fig. 2-2a] form the corners of equilateral triangles, and theoretically, this is the only possible arrangement. At the moment of rupture the distance between any given centre C and those nearest to it is such that the contraction along lines such as C-1 is just sufficient to overcome the tensile strength of the rock. A tension crack then forms halfway between C and 1 and at right angles to the line C-1. As each centre is surrounded by six others [1-6 in Fig. 2-2a], the resultant system of cracks is hexagonal. Once a crack occurs somewhere in the cooling layer the centres are definitely localized, and a repeated pattern of hexagonal cracks spreads almost simultaneously throughout the layer [Fig. 2-2b]. As cooling proceeds into the sheet of rock the cracks grow inward at right angles to the cooling surface and so divide the body into a system of hexagonal columns.

This description, although generally accepted in principle, is somewhat oversimplified. A diagramatic cross section of the Pomona flow of the Columbia River Basalt (Fig. 2-3) shows jointing to be more complex. Ryan

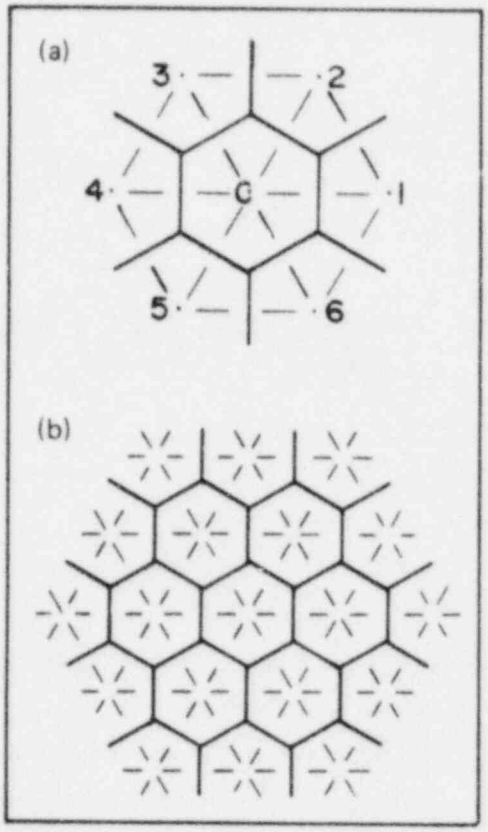

FIG. 2 2. Ideal hexagonal fracture pattern, formed by uniform contraction toward evenly spaced centers (from Ryan, 1974).

(1974) suggested that the Pomona flow consists of seven relatively distinct, vertically distributed zones. The uppermost zone, Zone I, which he identified as the flow top, consists of a 20- to 30-cm layer of weathered scoriaceous lava and rubble, underlain by a 2- to 3-m-thick zone of high vesicularity. Vesicles in this zone range form 5 to 25 mm in diameter.

Zone II is termed the upper colonnade. This region contains vertically standing hexagonal columns 2 to 3 m in diameter, with face widths of 1 to 2 m and heights of 4 to 8 m. These columns, the largest in the flow unit, often bear faces that are nonplanar and that appear warped or twisted. Some cross-fracturing is evident in this zone, and it often coincides with elliptical vesicles having horizontal major axes.

Underlying the upper colonnade is an upper transition zone, Zone III, wherein both the diameters of the columns and the sizes of column faces diminish rapidly. Within this 3- to 5-m-thick zone, the large columns of the

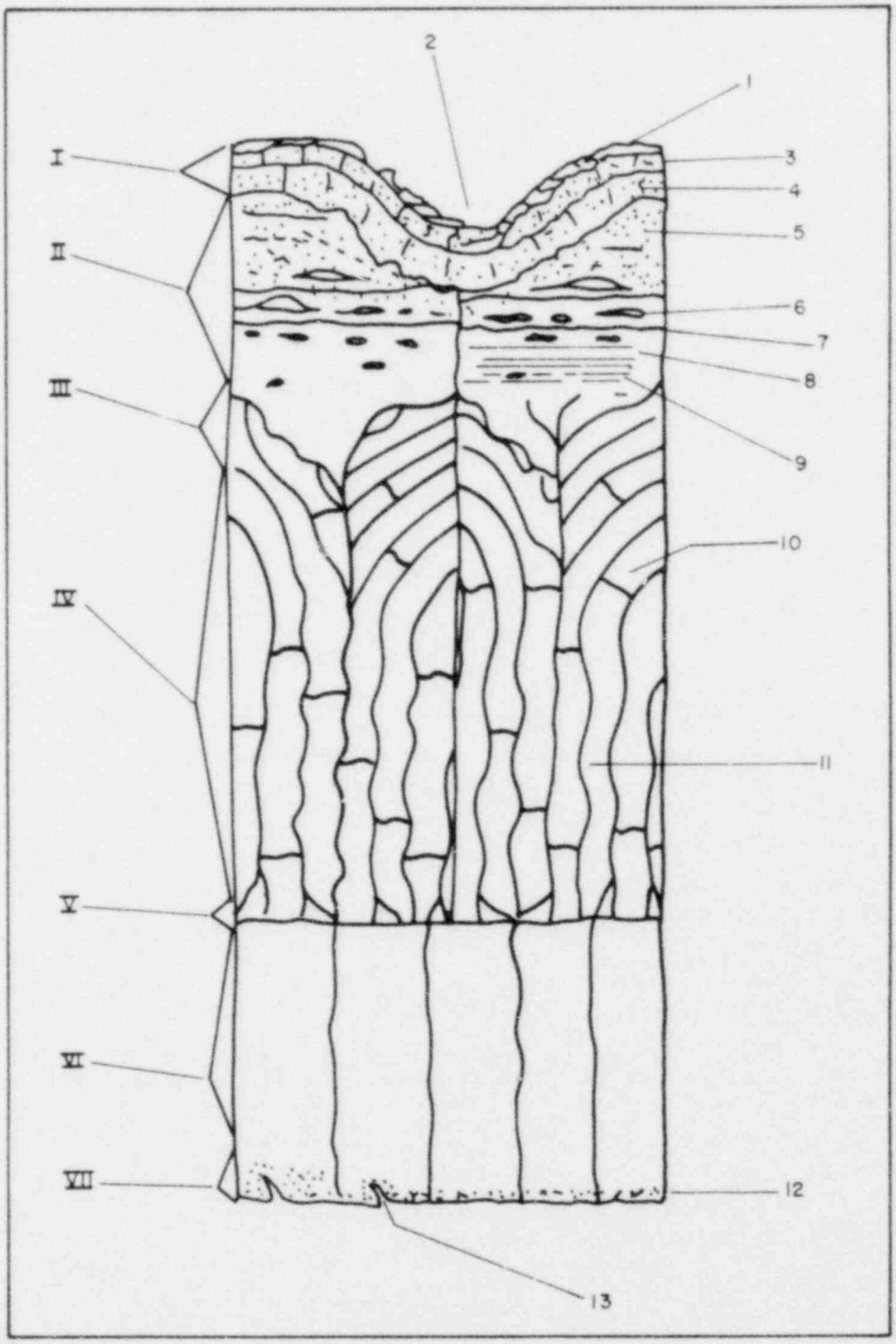

FIG. 2-3. Simplified cross section of the Pomona flow unit (from Ryan, 1974): (I) flow top, (II) upper colonnade, (III) upper transition zone, (IV) entablature, (V) lower transition zone, (VI) lower colonnade, (VII) flow base. Smaller structures are: (1) pahoehoe or ropy lava, (2) localized sags in the flow top (not to scale), (3) blocky scoria, (4) small subvertical jointing confined to flow top, (5) transition form spherical vesicles to elongate ones, (6) large elliptical vesicles, (7) cross-fractures, (8) upper colonnade column, (9) horizontal ridges, (10) cross-fractures, (11) undulating fracture surfaces, (12) vesicular zone, (13) spiracles.

upper colonnade are subdivided into smaller and smaller polygons. The large columns of the upper colonnade are thus transformed into bundles of smaller columns which blend to form the next lower zone, known as the entablature.

The entablature, Zone IV, is characterized by slender, subparallel columns 15 to 20 m in height. The joints bounding the columns of Zone II often extend into the entablature, grouping columns in this unit into "megacolumns." Individual columns within each megacolumn are often cross-fractured, although fractures among columns are not generally coincident.

Below the entablature is a lower transition zone, Zone V, about 1 m thick. This zone marks the abrupt boundary between the entablature and the lower colonnade. The lower colonnade, Zone VI, consists of columns 6 to 7 m high and 1 to 1.5 m in diameter. Symmetry among hexagonal columns is generally most evident in the lower colonnade.

Ryan identified the lowermost zone in the Pomona flow, Zone VII, as the flow base. This region consists of small vesicles and spiracles which result from gases formed along the lower contact and which migrate upward into the lava. The flow base, where present, is 20 to 30 cm thick.

Not all lava flows exhibit all the classical features described by Ryan in the Pomona flow. However, the configurations of most are similar.

Flow Geometry. Individual flows are topographically controlled. In regions of low relief, viscous lavas generally fill valleys or flow onto plains, then solidify, leaving a basalt mass with a roughly convex cross section perpendicular to the direction of flow. Lavas of lower viscosity or those flowing in areas with greater topographic relief often produce basaltic masses with a concave cross section. This feature results when cooling begins along the margins of a flow while the core remains mobile. In many of the larger flows of the Columbia Plateau, the convex or concave shape is apparent only in terminating tongues of the flow. Because of the large quantity of lava extruded and the great areas covered, the central portions of the flow may appear nearly horizontal.

Interbeds. In the deeper parts of the Columbia Plateau, more than 50 Miocene lava flows have been identified, many more than 10 m thick. Between flow events, the surfaces of the exposed flows were exposed to weathering and erosion. Fluvial silts, sands, and gravels, as well as lacustrine silts and

clays, were deposited in some regions, forming interbeds between the flows. Strata consisting of tuff and volcanic ash can also be found interspersed in the flows.

Tectonic Features. As volcanism proceeded, tectonic activity caused faulting and folding of previously deposited sequences. Faults and structural axes often control groundwater flow through basaltic aquifers. Also of some importance are regional joint systems. These systems may be mapped throughout most of the area of deposition of the northwest basalts; however, their relation to lava emplacement and later tectonic activity is not well understood.

Description of Basalt Occurrences in the United States

Extensive areas of flood basalts occur in the northwestern United States. This region, known as the Columbia Plateau, is the largest area of basalt in the United States. All of the flows in this region are of the continental tholeiitic type.

The Columbia Plateau flood basalt region consists of three distinct, smaller areas of basalt flows (Fig. 2-4): the Columbia River Basalt, covering a large area in central and southern Washington; the Modoc Plateau, extending south to California; and the Snake River Plain, extending across most of southern Idaho. The basalts of each area differ slightly in their stratigraphic and water-bearing properties.

The following discussions of these three areas will concentrate on general features that are consistent with the entire area. We will not present geologic and hydrologic data (for example, data on small-scale fracturing or jointing) that are applicable only to specific locales. Trends, intensities, and depths for such small-scale features can only be measured, and their importance to rock properties judged, for specific sites.

Columbia River Basalts.

Description and Geologic History. The Columbia River flows cover an area of more than 150,000 km^2 in southeast Washington, northeast Oregon, and adjacent Idaho. Their volume exceeds 300,000 km^3. The flows comprise a

FIG. 2-4. Principal basalt flows in the Columbia Plateau region.

thick sequence of layered lava flows and interbedded sediments (Newcomb, 1969). The thickness of individual basalt flows generally ranges from 1.5 to about 61 m, averaging 24 m (Newcomb, 1969). The average thickness of the entire sequence underlying the Columbia Plateau is greater than 500 m, and the greatest known thickness in 3200 m (Deju et al., 1977).

During the middle and late Miocene, repeated eruptions of enormous volumes of basaltic lava filled a slowly subsiding planoconvex basin. Between each eruption, the surfaces of many flows were exposed to erosion. By the late Miocene, the basin encompassed an area bounded by Mesozoic granites of the Okanogan highlands on the north, the Precambrian to Mesozoic sequences of the Rocky Mountains to the east, and the folded tertiary sediments of the Cascades and Blue Mountains to the west and south (Deju et al., 1977). As volcanism declined in the late Tertiary, a series of west- to northwest-trending anticlinal ridges formed across the subsiding basin. Broad synclines formed between these ridges, creating the Umatilla, Pasco, Quincy, and several smaller structural basins.

The Columbia River Basalt is tholeiitic. The rock is black to dark gray, dense, and fine-grained, and is composed mostly of microscopic crystals, with some intercrystalline glassy groundmass. The average composition of this basalt is labradorite, 50%; augite, 15%; magnetite, 15%; and brown glass and microlites, 20%. Most of the basalt has an even, microgranular texture, but in a few places the crystals are so small that the texture is flinty or nearly glassy. The textural fabric of the rock indicates that most of the crystallization occurred after the highly fluid lava had come to rest (Newcomb, 1969).

The two most distinctive petrologic structures in the Columbia River Basalt are layers and joints. The layering resulted form the accumulation of successive flows of highly fluid lava of the same general chemical and mineral type. The individual flows are generally separated by one or more features:

- A change in jointing, texture, or color.
- A change in susceptibility to alteration.
- Interbedded sedimentary material.
- A vesiculated top and a flinty basal section.

Joints and fractures traverse the basalt. The main sets of fractures, caused by shrinkage of the solidified rock during cooling, are arranged as vertical columnar joints, flat or sheeting joints, and unsystematic miscellaneous partings. The joints separate some parts of the flows into angular, irregular blocks of all sizes and shapes (Newcomb, 1969). Columnar jointing systems are present in almost every flow.

In addition to the shrinkage joints, the basalt is traversed by regional joints. These long, straight sets of parallel vertical cracks trend in various patterns across most of the basalt. They are believed to be extension fractures (Newcomb, 1969).

The basalt has a thin, oxidation skin on all but newly exposed surfaces. Where basalt has been exposed, it may be weathered to depths of up to 50 or 60 m (Newcomb, 1969).

Stratigraphy of the Pasco Basin. The Pasco basin (Fig. 2-4) was chosen as representative of basins of the Columbia Plateau for three reasons:

- It lies at the depocenter of the regional subsidence and thus comprises the thickest and most complete sequence of basalts.
- It is an attractive potential site for waste storage, since it contains less groundwater than the other basins of the plateau.

- Because the Hanford facility is located there, a greater bank of rock mechanic, hydrologic, and geologic data is available than for other basins.

The minimum thickness of the Miocene basalt sequence in the basin is estimated to be 1500 m (Myers, 1973; Myers and Brown, 1973; Brown and Ledgewood, 1973). The maximum thickness of this sequence is not precisely known; however, where these flows have been penetrated, they overlie older basalts of Oligocene and Eocene age.

There are five principal accumulations of flows in the Columbia River Group of the Pasco basin. The lower two units are the Picture Gorge Basalt and the Imnaha Basalt. The upper three formations, identified on the stratigraphic column in Fig. 2-5, are the Grande Ronde (Lower Yakima), Wanapum (Middle Yakima) and Saddle Mountains (Upper Yakima) basalts. Each of these formations contains numerous individual flows, many interbedded with sandstones, siltstones, tuff, or diatomite. The geographic relationships of these flows are identified in Figs. 2-6 through 2-8. Detailed physical and chemical descriptions of individual flows may be found in a report prepared for the National Waste Terminal Storage Program (NWTSP, 1976).

Snake River Plain.

Description and Geologic History. The Snake River Plain is a structural basin covering an area of about 31,000 km^2 in southern Idaho. As depicted in Fig. 2-9, the basin is approximately 320 km long and 50 to 70 km wide. It consists mainly of an accumulation of basalt flows with intercalated lacustrine and alluvial sediments. The basalt fills a huge graben and is more than 450 m thick (Walker, 1964; Nace et al., 1972).

The eruptions that emplaced the basalt were intermittent, and the sheet of lava that spread out during each event usually solidified before the next sheet was laid down. Each sheet has an upper and lower chilled zone. Commonly, the surface of a flow was exposed to erosion or depostion of sediments before being covered by the succeeding flow (Walker, 1964). The molten basalt was fluid enough to spread many miles over relatively low gradients. The structure, chemistry, and mineralogy of the Snake River Basalt are similar to the Columbia River Basalt.

Geologic data on the basin are limited because of the lack of economic mineralization in the basalt sequence. However, since the siting of the Idaho

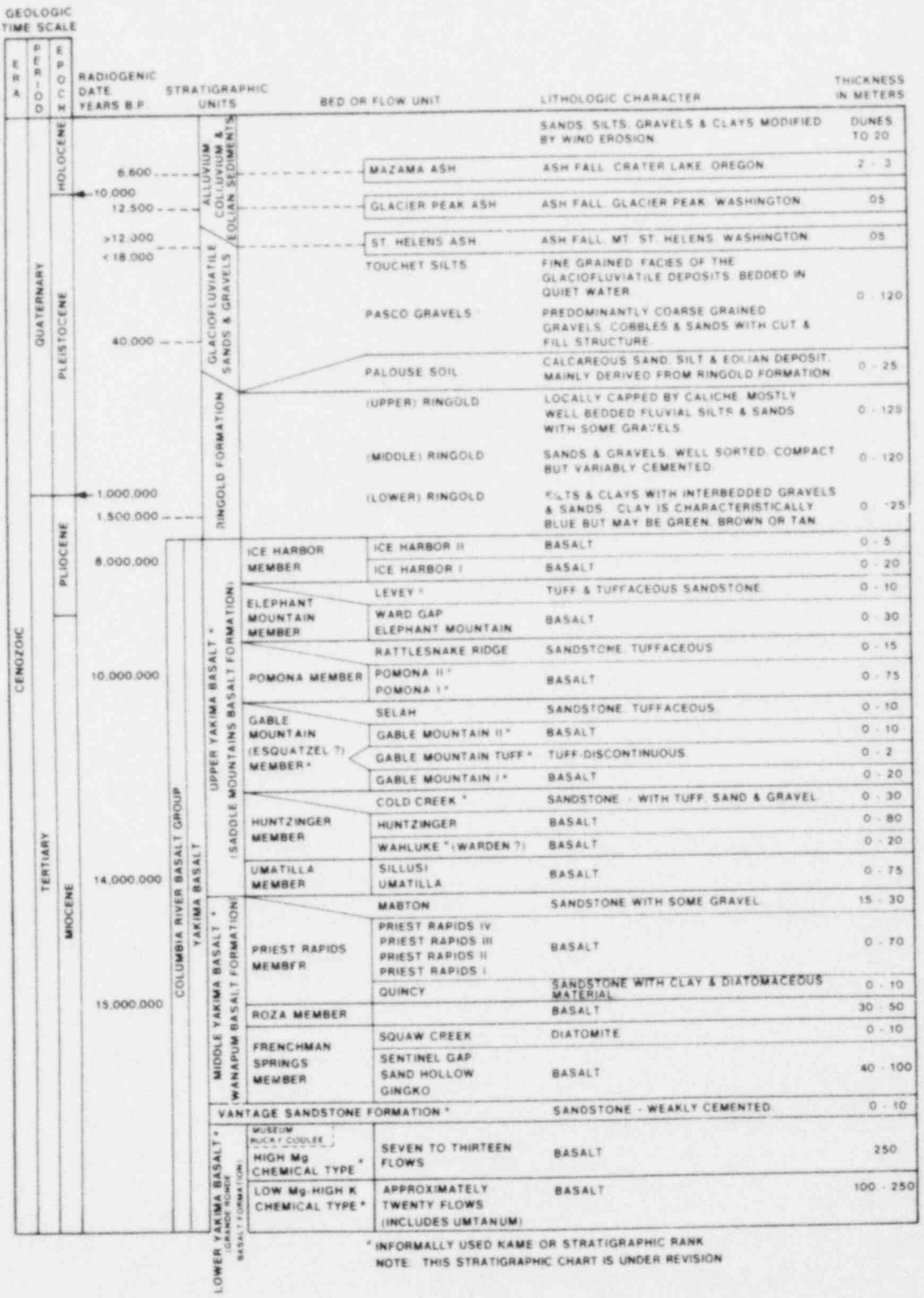

FIG. 2-5. Stratigraphy of the Pasco basin (from NWTSP, 1976).

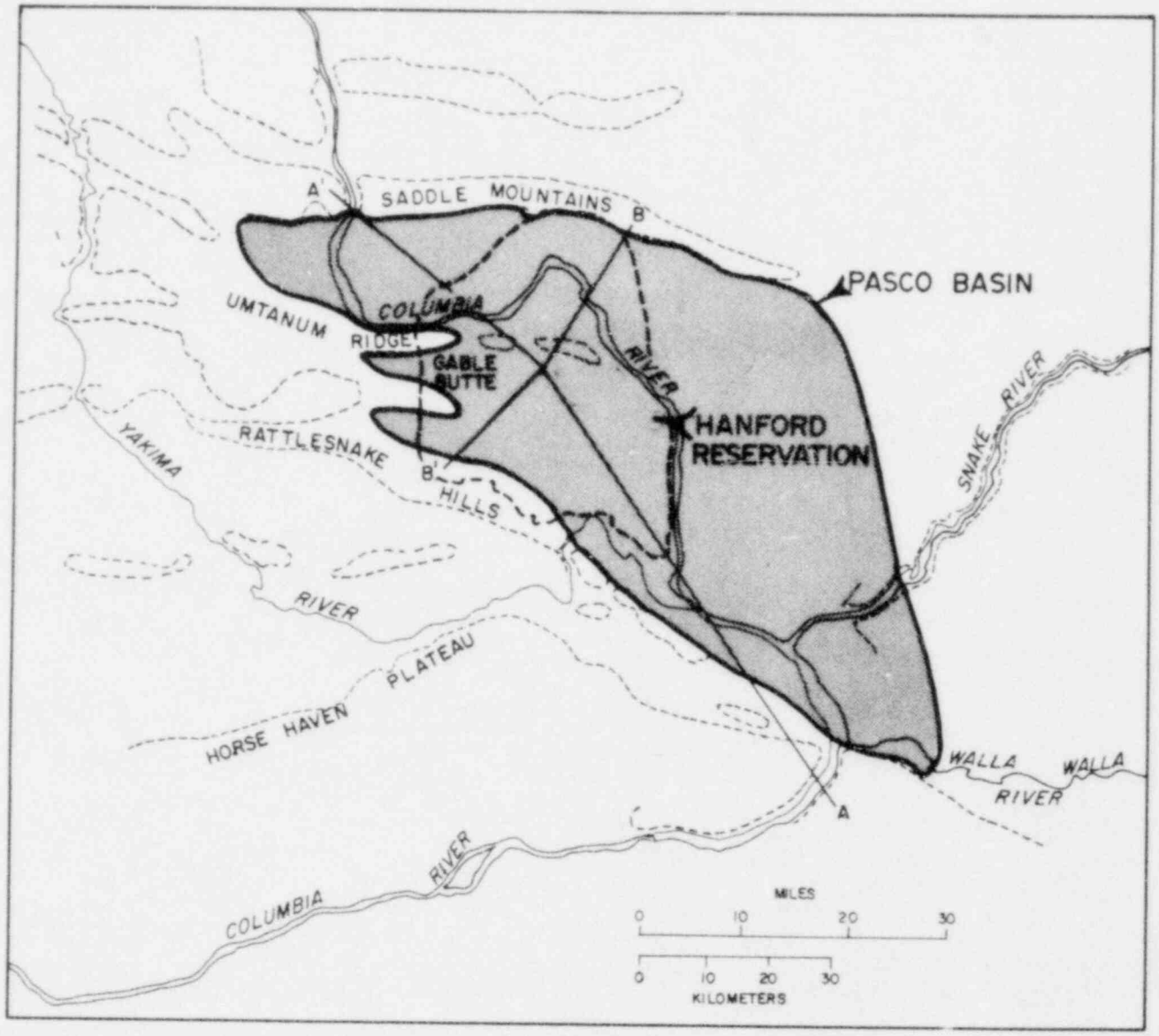

FIG. 2-6. Geography of the Pasco basin (from NWTSP, 1976).

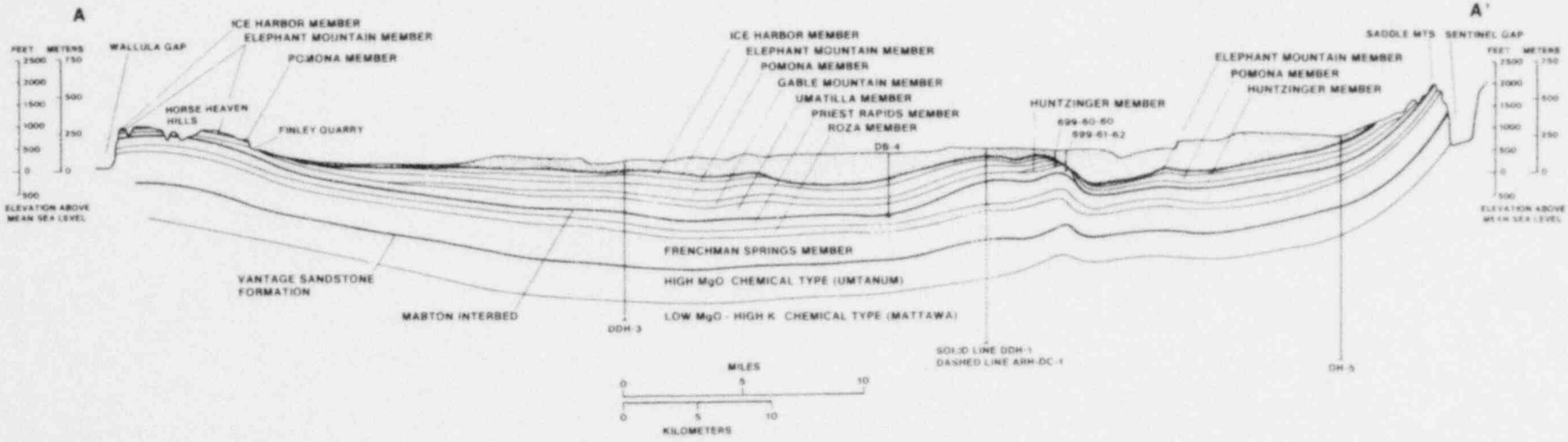

FIG. 2-7. Generalized cross section A-A' of the Pasco basin (from NWTSP, 1976). Line of section is shown in Fig. 2-6

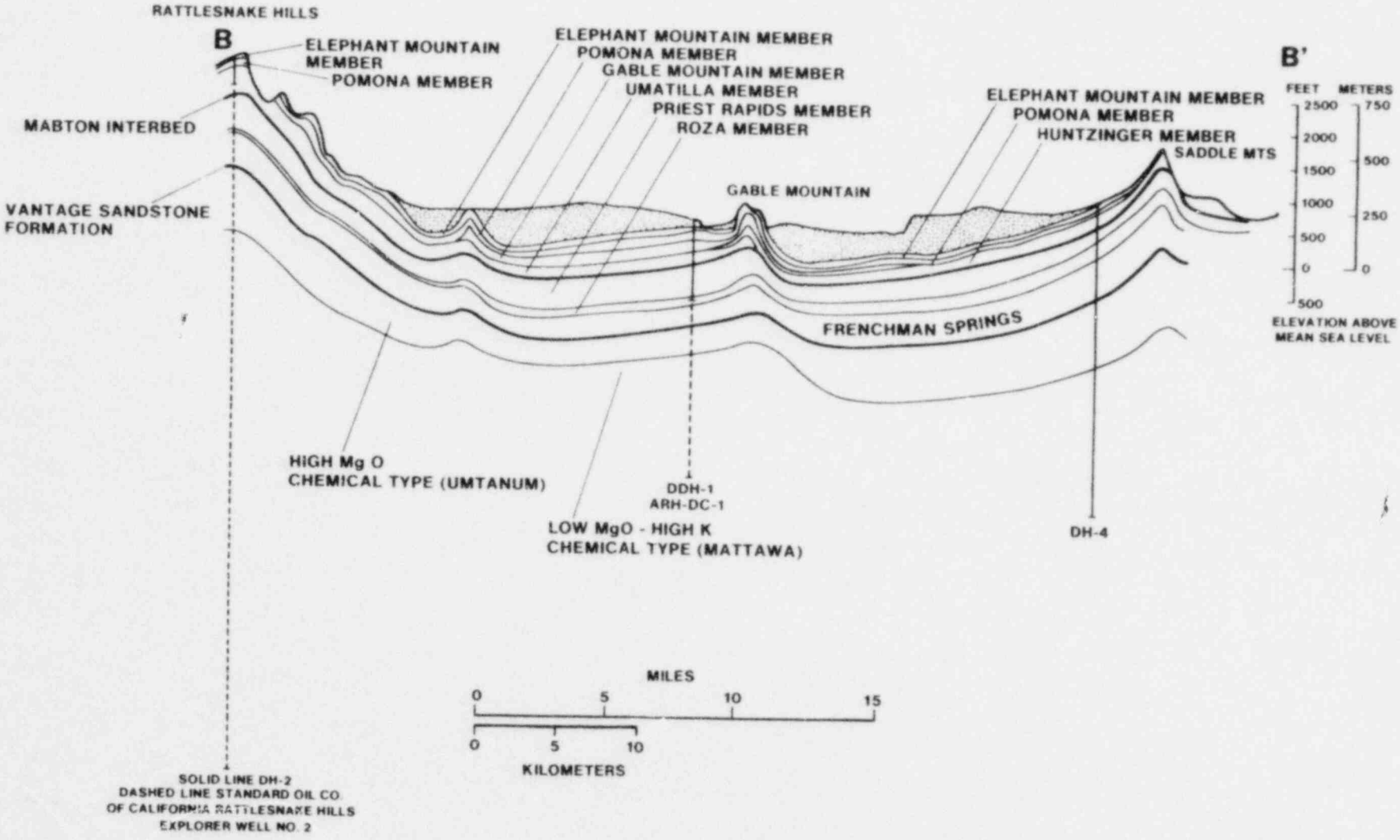

FIG. 2-8. Generalized cross section B-B' of the Pasco basin (from NWTSP, 1976). Line of section is shown in Fig. 2-6.

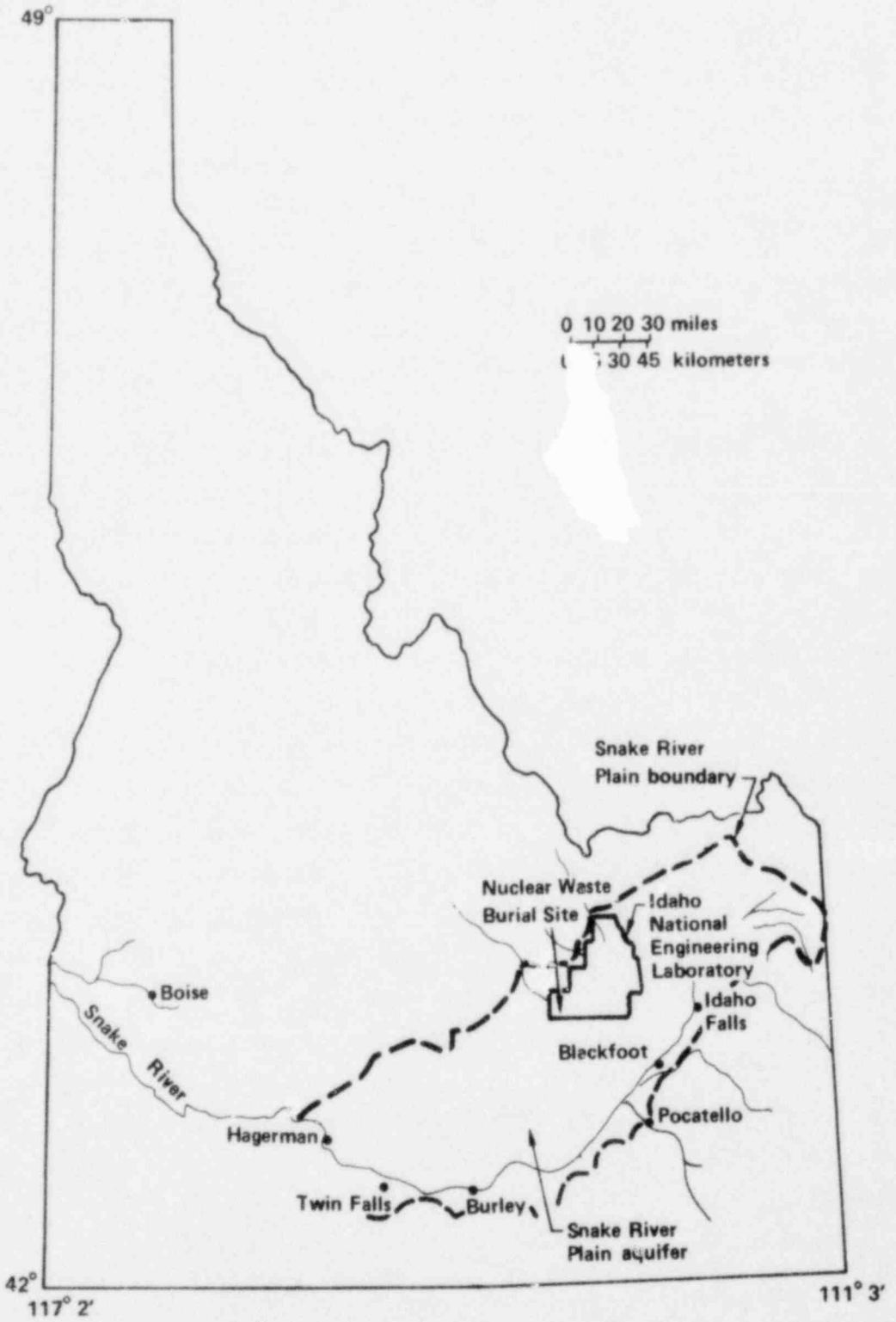

FIG. 2-9. Location of the Snake River Plain aquifer (from Robertson et al., 1974).

National Engineering Laboratory (INEL) on the Snake River Plain in the early 1950s, sufficient work has been sponsored by the Department of Energy and the U.S. Geological Survey to produce a quantitative picture of the basin as a whole and of the INEL site in particular.

The major regional fractures in the basalt are vertical and trend north-south and east-west. It is thought that a north-south-trending geosyncline lay across southern Idaho in late Precambrian time. Sandstones and shales were deposited in this broad depression through the early Ordovician (Crittenden et al., 1971). As the Cordilleran geosyncline developed, principally carbonate rocks were deposited during the later Paleozoic.

Beginning in the Permian and continuing into the Mesozoic, tectonic activity increased in the region. The Idaho batholith was emplaced to the north and west, and the resulting uplift provided a source of detritus for Mesozoic sedimentation on its flanks. By the middle of the Mesozoic, approximately 15,250 m of Paleozoic and 10,700 m of Mesozoic rocks had filled the basin. Uplift and tectonism continued, culminating in the Laramide orogeny during the late Cretaceous.

By early Cenozoic time, deposition had ceased, and erosion of the uplifted sediments had begun. Basin-and-range faulting during the Miocene created a rugged mountain range in southern Idaho, bounded on the north and west by the Idaho batholith and on the east by large basin-and-range horsts and grabens. This topography persisted until the early Pliocene when tectonic events began to create the basin which developed into the Snake River Plain.

A number of theories have been presented for the development of the basin in which the basalts of the Snake River Plain were deposited (Lindgren, 1898; Russell, 1902; Kirkham, 1931; Hamilton, 1963). Currently, the most widely accepted theory postulates the development of a large downfaulted graben inundated by flood basalts. The development of this graben is summarized by Robertson et al. (1974):

> This hypothesis proposes that in the late Miocene the granitic terrain of the Idaho batholith extended southward to the south edge of the present plain where it either thinned considerably or was displaced westward. Tension during the early Pliocene, probably due to subcrustal forces similar to those envisaged by Hamilton and Myers (1966), produced the present Snake River graben into which the southern tip of the batholith subsided
>
> Along with subcrustal tension directly responsible for the grabening, magma developed in the subcrust, perhaps fractionated

from a tholeiite into immiscible rhyolite and olivine basalt (Hamilton, 1965), and erupted along tensional openings in the overlying rocks. Sialic volcanism occurred first and covered the floor of the graben as well as much of the surrounding region with tuff and flows (Idavada Volcanics). Effusive removal of subcrustal material from beneath the graben allowed downfaulting to continue and the Snake River Plain crustal block settled into the mantle. By middle Pliocene time all the rhyolite was gone from the magma chamber and eruption of olivine basalt began. Basalt flows were restricted to filling the graben though some flowed short distances up valleys in the adjoining blocks (Crosthwaite and others, 1970). It is the addition of this subcrustal material to the top of the Snake River graben that accounts for the maintenance of isostasy. [Figure 2-10] depicts these stages in the hypothetical grabening of the Snake River Plain.

Stratigraphy. The sequence of volcanic rock which fills the graben is thought to range from 300 to over 3000 m in thickness (Robertson et al., 1974). Early wells constructed at INEL showed the upper 450 m of the section to consist of a series of thin basalt flows 3 to 25 m thick, interbedded with fluvial, lacustrine, eolian, and pyroclastic sediments. A cross section of the nuclear waste burial site at INEL (Fig. 2-11) identifies the interbedded sediments in the upper portion of the sequence.

In May 1979, the Department of Energy completed a 3159-m geothermal test well (INEL-1) at INEL, approximately 30 km north of the burial site. The upper 745 m of this well penetrated basalt flows and sedimentary interbeds. Below 745 m, a sequence was encountered which consists of rhyolitic welded ash-flow tuffs, air-fall ash deposits, nonwelded ash-flow tuffs, and volcaniclastic sediments. Doherty et al. (1979) suggested that these rocks are part of an intracaldera fill and that a collapsed caldera approximately 25 km in diameter may exist in the region of well INEL-1.

Modoc Plateau Basalts. The Modoc Plateau is the region east of the Cascade Mountains in southern Oregon and northern California and west of the Basin and Range Province. The region consists predominately of a series of north- to northwest-trending block-faulted mountain ranges. Tectonism on the plateau culminated in the Miocene or Pliocene; however, faulting has continued into Recent time. Intervening basins between block-fault ranges have been filled with a series of lava flows ranging in age from Miocene to Recent. These lavas range in composition from rhyolite to basalt and are often interbedded with lacustrine and fluvial mudstones, siltsones, and sandstones, and with

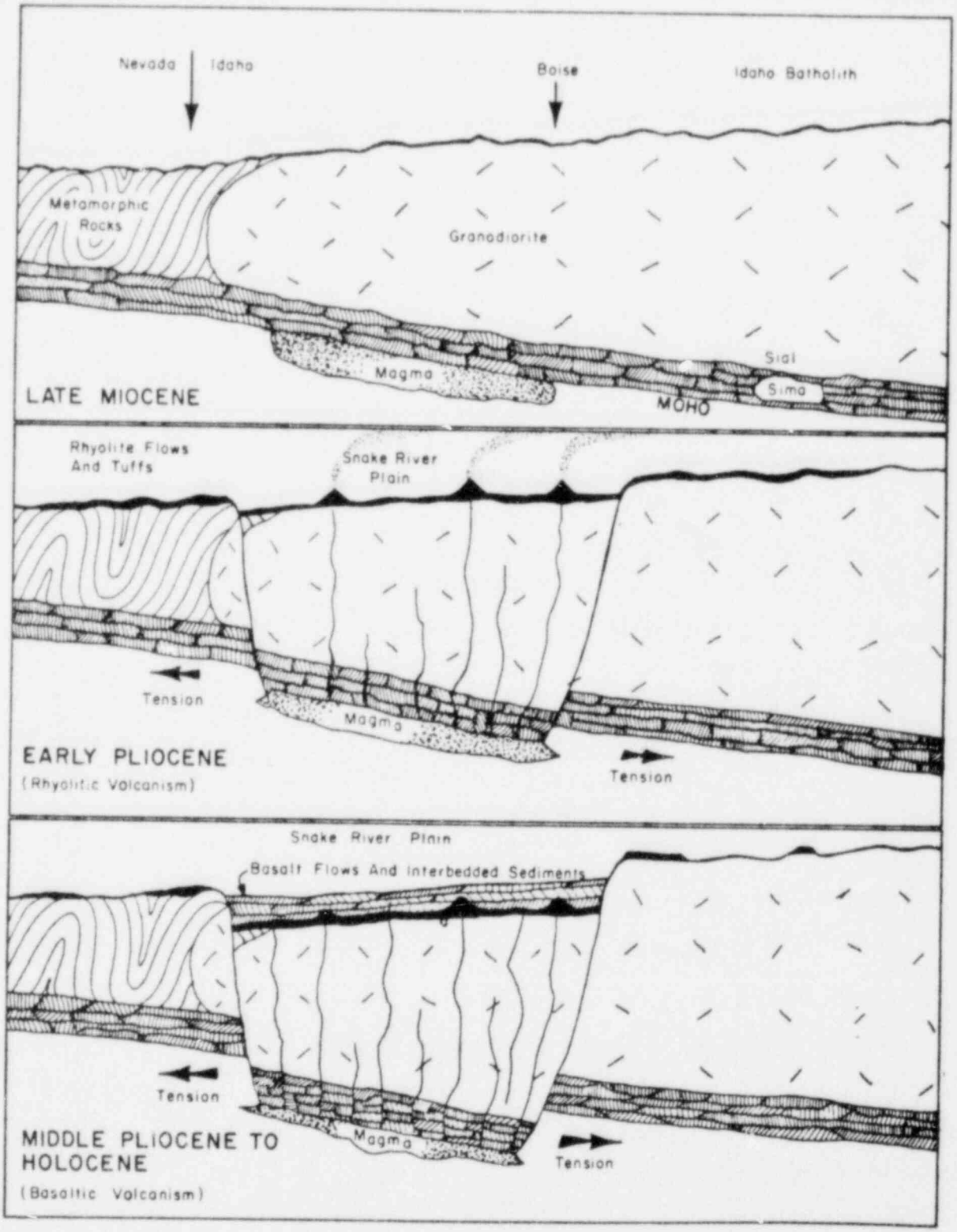

FIG. 2-10. Cross sections showing hypothetical stages of grabening duri. the formation of the Snake River Plain (from Robertson et al., 1974).

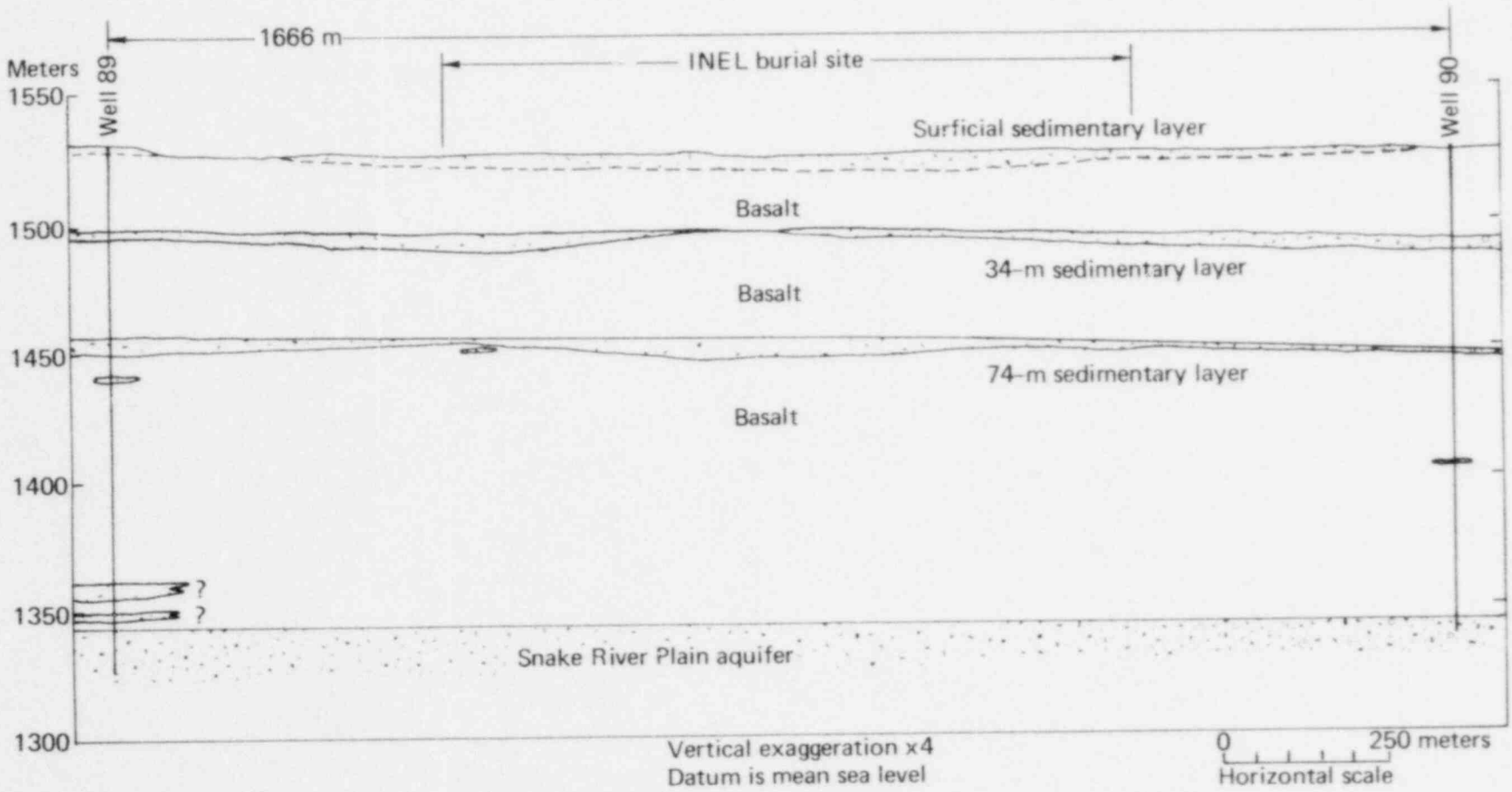

FIG. 2-11. Cross section of INEL burial site (from Barraclough et al., 1976).

volcaniclastic materials. Cinder cones rest on the surface. Because tectonism has been continuous, many of the older flows are now faulted and tilted. The major basalt flows are the Warner Basalt (Miocene), Steens Basalt (Miocene), Picture Rock Basalt (Pliocene), and Hayes Butte Basalt (Pliocene). Every flow does not underlie the entire area. Individual flows commonly fill grabens, and their surfaces are distinguished by pahoehoe or ropy lava structures.

These Tertiary basalts are usually composed of dark gray olivine basalts. Commonly, the texture of the basalt is porphyritic with phenocrysts of olivine or labradorite (Hampton, 1961).

Faults trending north to northwest are common and usually delineate horsts and grabens. These normal high-angle faults show considerable displacement, up to 305 m, and some strike-slip displacement (MacDonald, 1966). The fault surfaces can be undulating or angular. Minor faulting can be seen perpendicular to these faults.

Vertical shrinkage joints are very common, especially in the tops or bottoms of each individual flow. Individual flows range from 3 to 15 m thick. The thickness of the major basalt flows vary from a few tens of meters to over 300 m and generally thin toward the south and east (Piper et al., 1939; MacDonald, 1966; Brown et al., 1962).

GEOMECHANICS

The engineering behavior of basaltic flows is expected to vary widely because of their unique depositional and cooling characteristics. Variations within a flow are largely functions of the flow thickness, which determines the rate of cooling throughout the mass. Normally, thick flows have dense basalt in their lower portions and are jointed. The jointing forms five- or six-sided columns that average 0.6 to 0.9 m across. Cross joints, either inclined or normal to the column, may also be present (ONWI, 1978).

In the Columbia River Basalt, columnar joints are the most common internal structures within individual flows. Although the pattern of columnar jointing varies, both within and between flows, a typical flow usually has a lower zone, which is generally one-third to one-half of the entire thickness of the flow and consists of nearly symmetrical columnar joints, and an upper zone, which is generally one-half to two-thirds of the entire thickness of the

flow and consists of an irregular jointing pattern (see Fig. 2-3, for example). The jointing pattern variations include fanlike columnar joints, plating joints, swirling joints, brickbat joints, and cross joints. Abrupt lateral changes in joint patterns can occur. At depth, most joints and fractures are filled with secondary minerals such as zeolite, amorphous iron-rich silicates, and ferro-magnesium clays. The top of the flow may be a slaggy, ropy, or clinker-type basalt (ONWI, 1978).

The geomechanical behavior of the basalt flows thus depends upon the zone being studied. Potential repository sites would logically be located in the most massive part of the flow, where the joints are the most widely spaced and the strength is the greatest. The behavior of the joints will be a major consideration. Some of the necessary steps in any study of basalt as a potential repository rock are indicated in Table 2-2. The list emphasizes the need to define the major structural properties of the rock mass, as well as the characteristics of the rock on a much smaller scale.

The geotechnical factors that influence design have been summarized very well in a report prepared by Parsons, Brinckerhoff, Quade, and Douglas, Inc. (PBQ&D, 1978). Their discussions make clear the kinds of geomechanical considerations that are important in any repository design. They concluded:

- At high temperatures, the strength of rock diminishes as the rock crystalline structures begin to break down. In basalt, major losses of strength are expected at around 400 to 500°C. Thermal loading must be adjusted so that temperatures do not exceed critical values near the canisters.
- The rock surrounding and overlying the repository will respond to the stresses imposed by the mined excavation and by thermal loading from the implanted waste materials. The repository layout and geometry and the allowable thermal loading must be designed to minimize rock movements.
- When basalt is overstressed, it will fail quickly, with little warning. Accordingly, the main philosophy must be to limit stresses to a value well below the level required for initial failure.

The rest of this section discusses the geomechanical characteristics of basalts in general, providing information about the specific rock types as appropriate. Where data are scanty or lacking, we can only look to work currently underway, especially at Hanford. These current studies include both laboratory and field measurements, as well as a large amount of modeling using analytic, finite element, finite difference, and other types of models.

TABLE 2-2. Requirements of any study of basalt as a potential repository medium (from Deju et al., 1977).

Requirement	Methods
Tectonics and seismology	
Assess the tectonic stability of the region.	Regional geology; field studies; evaluation of seismic records; seismic monitoring; literature survey; geophysical surveys.
Define major faults, fractures, and fissures.	Field studies in outcrops, trenches, and boreholes; remote sensing; literature survey; geophysical surveys.
Document the seismic record.	Examination and documentation of the seismic record, including microearthquake studies.
Assess the structural integrity of the basalt mass.	Field analyses; laboratory and in situ tests; geophysical surveys.
Define the frequency, orientation, and character of major lineaments.	Remote sensing.
Define the frequency and orientation of fractures in basalt.	Core analysis, supplemented by borehole geophysics.
Define the extent of folding and the forces that led to its present state.	Integration of geologic and geophysical data.
Rock properties and stratigraphy	
Define the petrographic, mineralogic, and chemical characteristics of the basalts.	Petrographic, mineralogic, and chemical analyses of selected basalt flows; literature survey.
Assess the stratigraphy and define variations.	Stratigraphic correlation using petrographic, mineralogic, chemical, paleomagnetic, and geophysical techniques.
Define erosional stability over geologic time.	Regional geology, interpretation of observations; geologic history; geomorphological studies.
Define the thermal properties of basalt (expansion, conductivity, and fracture potential).	Laboratory tests on cores under simulated conditions.

continued

TABLE 2-2 continued.

Requirement	Methods
Assess the effect of thermal stress gradients on fractures and basalt properties.	Laboratory tests.
Assess the effect of fractures on the heat transfer properties of the basalt mass.	Laboratory tests.
Examine the effect of radiation on structural integrity of the basalts.	Laboratory tests.

Because of these activities, progress in evaluating and measuring important geomechanical characteristics should be rapid.

Stress

In analyzing the stability of an underground excavation, one must consider the stresses that are applied and the strength of the materials involved. The stresses are of three types:

- In situ stresses--those that exist prior to excavation.
- Stresses induced by the excavation process itself.
- Stresses induced by the materials that are placed within the excavation. Before discussing each of these stresses in detail, we will consider the methods by which stresses are evaluated.

Measurement Techniques. Except in the cases of hydraulic fracturing and flatjack-type measurements, stresses are not measured directly; instead, they are calculated by introducing the results of strain (or displacement) measurements, along with suitable elastic constants, into equations developed from elastic theory. For example, the most common and widely accepted means of obtaining in situ stress fields in the United States is by using a U.S. Bureau of Mines borehole deformation gauge. A 38-mm-diameter hole is drilled, a gauge that measures changes in borehole diameter in three directions is inserted, and the hole overcored with a 150-mm-diameter bit. By measuring the

borehole deformations, knowing the elastic modulus and Poisson's ratio for the rock, and using the equations for a thick-walled cylinder, one can calculate stress magnitudes and directions. Three holes are required to determine the complete stress tension at any point. Because of the overcoring requirement, this technique is generally limited to use in relatively short holes (less than 30 m). Hence, measurements at depth must be obtained from underground openings.

Of the other techniques available, many suffer from both operational and calculational difficulties. Results obtained using several techniques at the same location have generally shown wide variations. These variations may be due to real variations; however, they are more likely due to the instruments, procedures, and evaluation techniques employed. Most techniques, for example, assume that the rock is linearly elastic and isotropic--a good approximation for some rocks, but not for others. The determination of absolute stress or stress changes is complicated by moisture and by temperature variations. For nuclear waste applications, a great deal of development will be required before measurement techniques can be considered adequate.

In Situ Stress. As stated by Hardy and Hocking (1977), "No stress measurements have been recorded in the basalt flows to our knowledge, but in other parts of the U.S. stress measurements have shown a trend toward [the] lithostatic case at depths of around a thousand meters." The stress measurements referred to by Hardy and Hocking were those compiled by Lindner and Halpern (1977), which are shown in Figs. 2-12 and 2-13. Contrary to Hardy and Hocking's statement, no definite trend towards a lithostatic stress field at depth is obvious. Rather, there are only a few widely scattered data points. Figures 2-14 and 2-15 show similar scatters. Clearly, more data are needed; from the few currently available, few quantitative conclusions can be drawn.

Lindner and Halpern fit equations to the data for North America:

$$\sigma_V = (9.42 \pm 13.1)\text{kg/cm}^2 + (0.339 \pm 0.67)\ \text{kg/cm}^2\text{-m}$$
$$= (135 \pm 185)\text{psi} + (1.469 \pm 0.289)\ \text{psi/ft},$$
$$\sigma_H = (43.6 \pm 8.15)\text{kg/cm}^2 + (0.390 \pm 0.72)\ \text{kg/cm}^2\text{-m}$$
$$= (620 \pm 116)\text{psi} + (1.690 \pm 0.311)\ \text{psi/ft},$$

where σ_V is the vertical stress and σ_H is the horizontal stress.

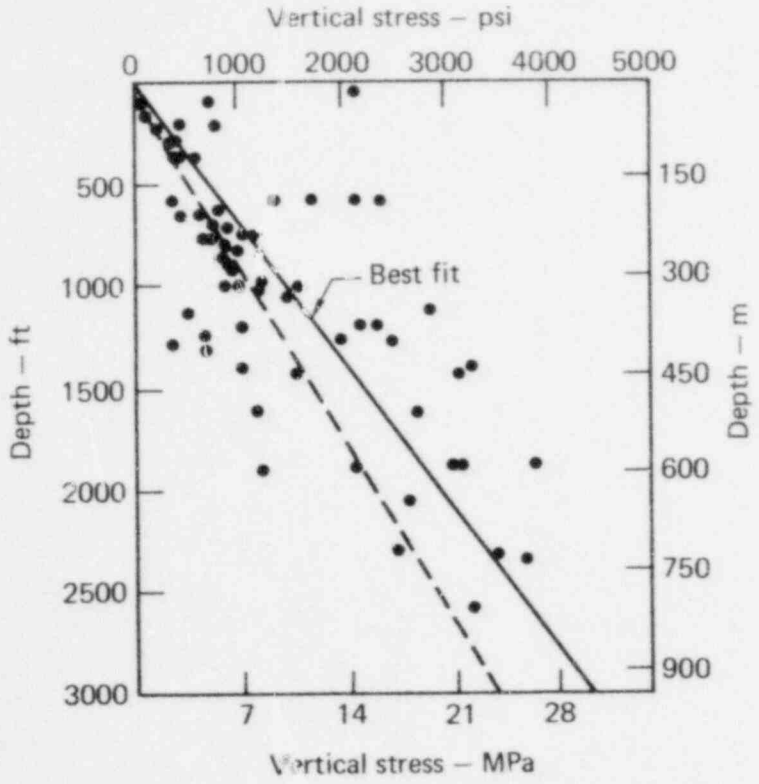

FIG. 2-12. Variation of vertical stress with depth (from Lindner and Halpern, 1977). The dashed line is the predicted vertical stress based on the weight of the overburden (at 175 lb/ft^3).

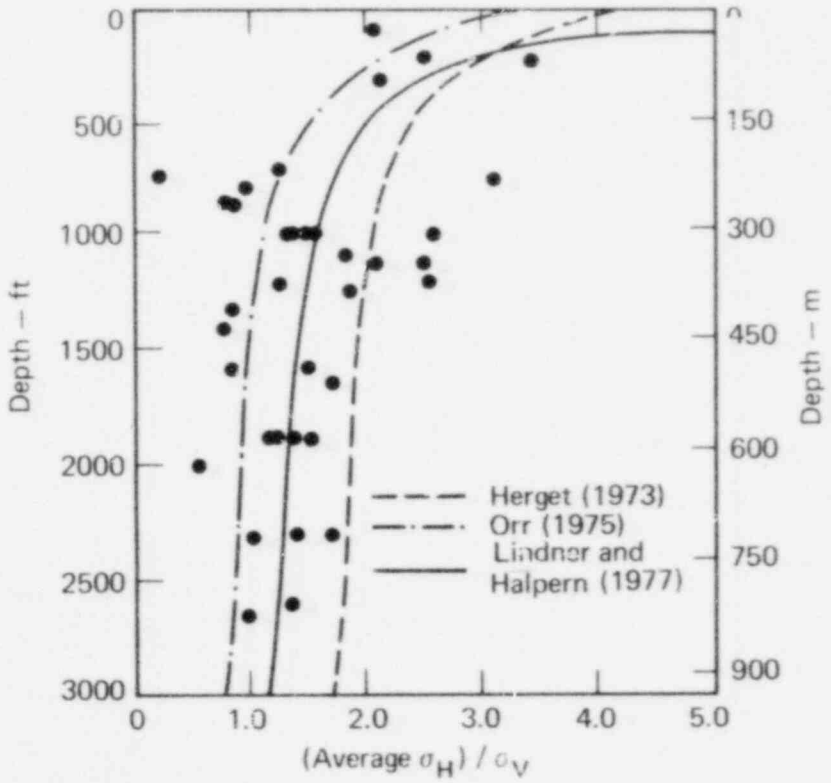

FIG. 2-13. Ratio of the average horizontal stress to the vertical stress (from Lindner and Halpern, 1977). The points represent data from sites where both horizontal and vertical stresses were measured.

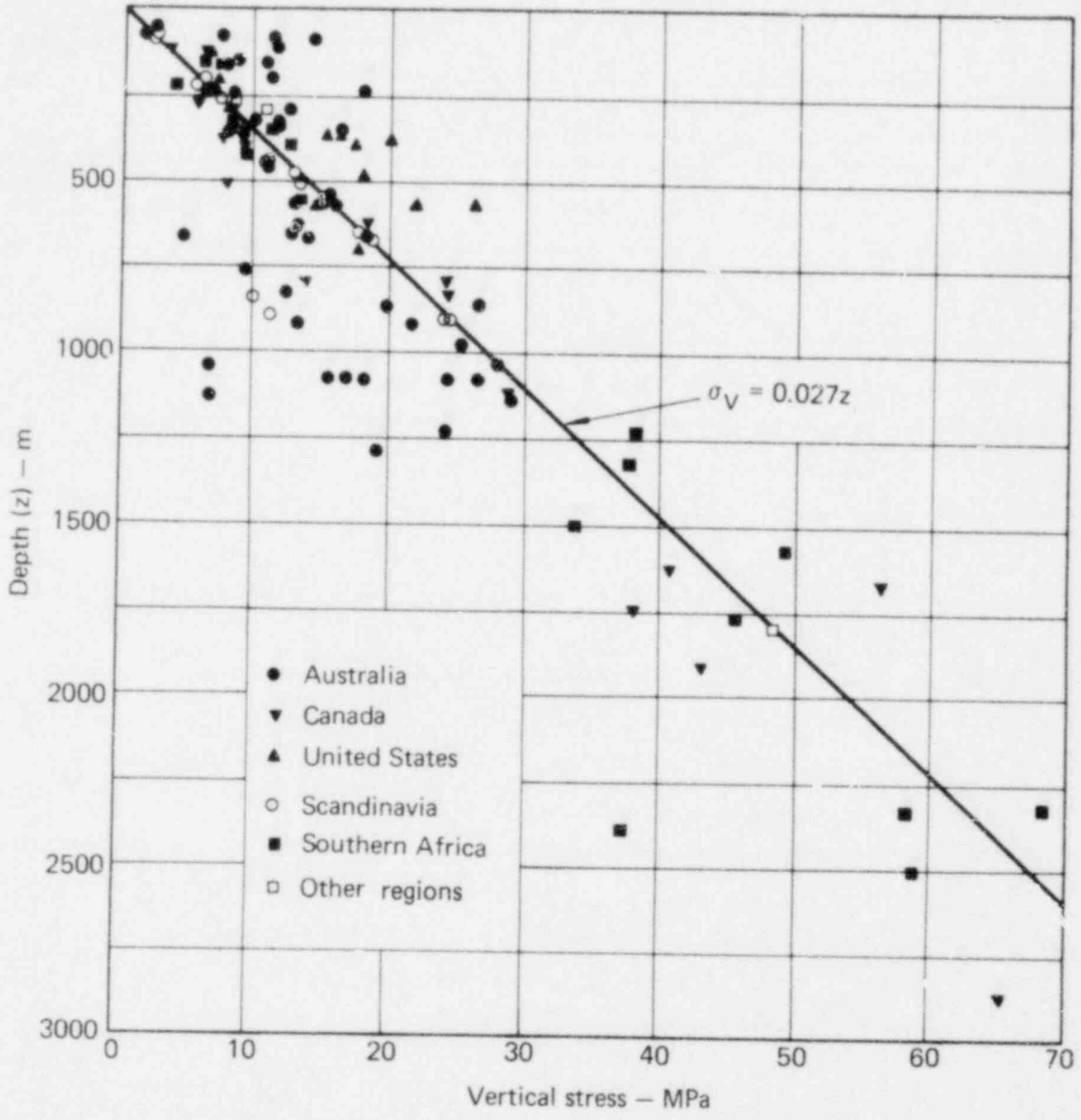

FIG. 2-14. Variation of vertical stress with depth (from Hoek and Brown, in press).

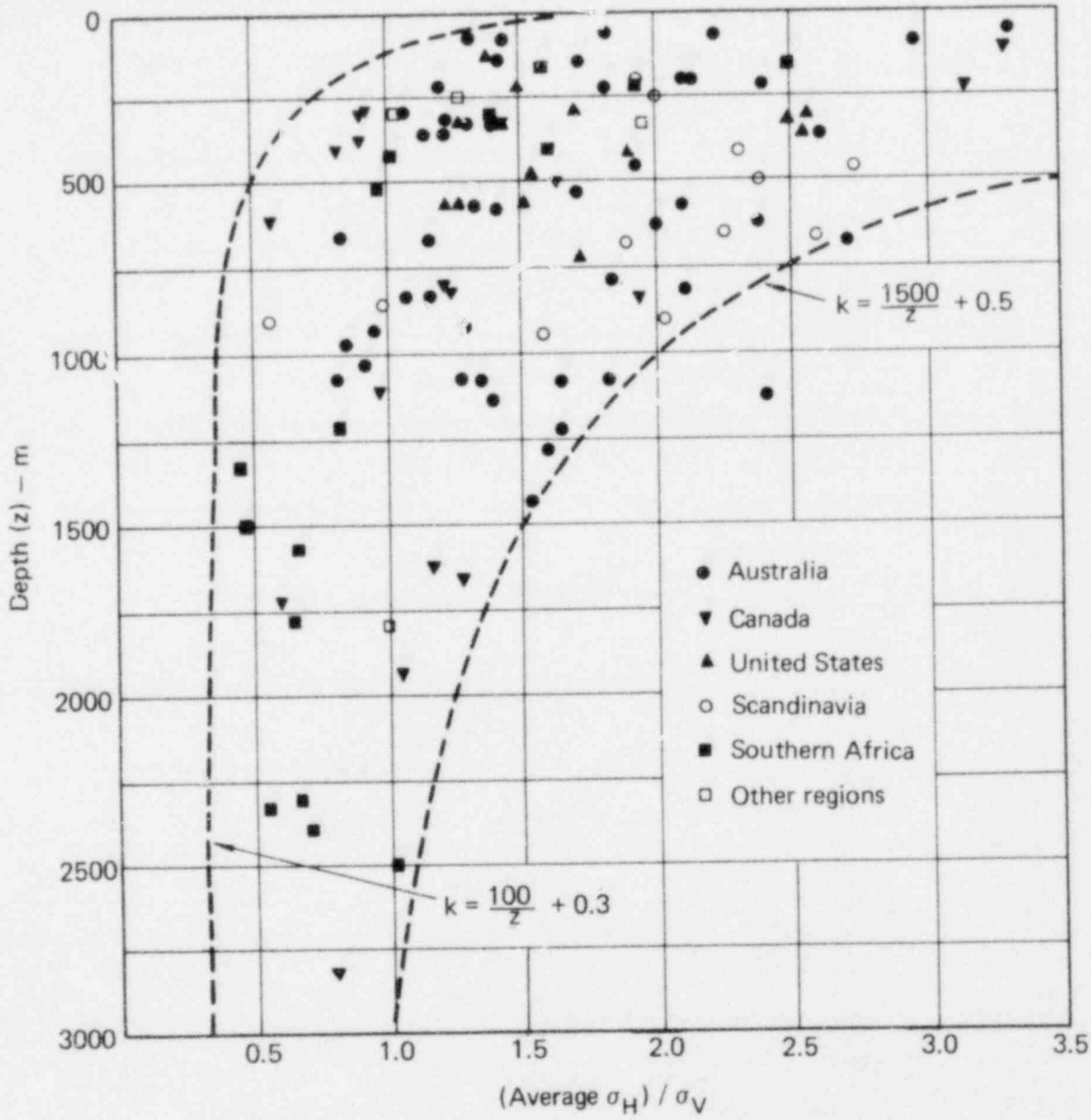

FIG. 2-15. Ratio of the average horizontal stress to the vertical stress (from Hoek and Brown, in press). In the equations for the dashed lines, $k = (\text{average } \sigma_H)/\sigma_V$.

For the horizontal stress, Lindner and Halpern comment, "This curve fit is a poor one. The horizontal stress data indicate considerable scatter. Data vary from three to four times the least-square average, to less than lithostatic. Hence, the curve fit is at best a trend rather than an average that could be utilized in design."

The presence of the basalts themselves is evidence of previous tectonic activity in the area where they are found. Therefore, one might expect to find significant deviations from a stress state calculated on the basis of the weight of the overburden. (Under lithostatic conditions, the three stresses are equal to each other and equal to the weight of the overburden.) The presence of nearby faults, dikes, or other major structures would also affect the in situ stress field.

Stresses Induced by Excavation. Hardy and Hocking (1977) made a two-dimensional analysis of the effect of various in situ stress fields on the stresses around a typical waste repository room. The assumed excavation geometry is shown in Fig. 2-16; the basalt properties used are listed in Table 2-3. For the base case, the initial in situ field stresses were taken as 25 MPa at a depth of 1000 m and the horizontal stress field was assumed to be equal to the vertical.

In Fig. 2-17, the effect of areal thermal loading on the tangential boundary stresses is shown for three points around the periphery of the

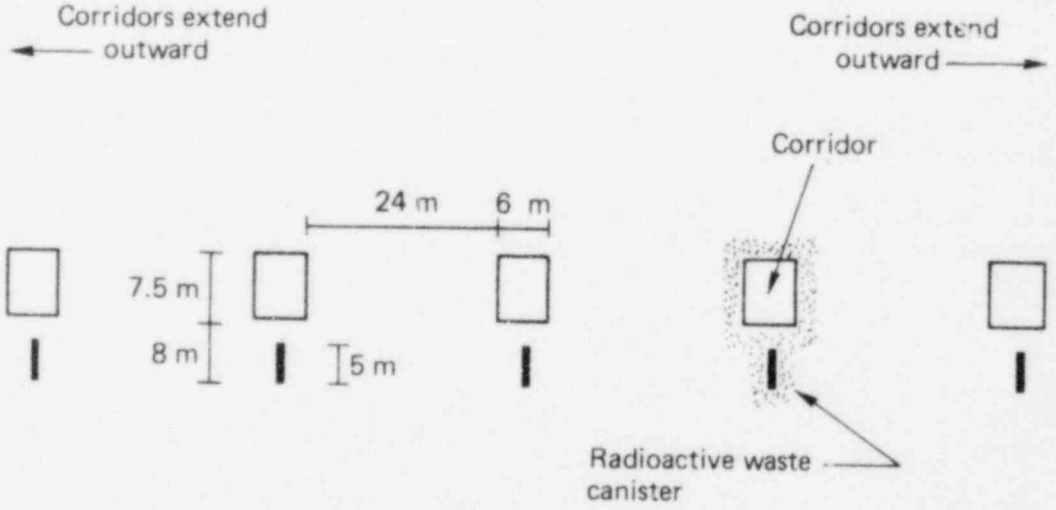

FIG. 2-16. Excavation geometry assumed by Hardy and Hocking (1977) for stress analyses, showing locations of waste canisters.

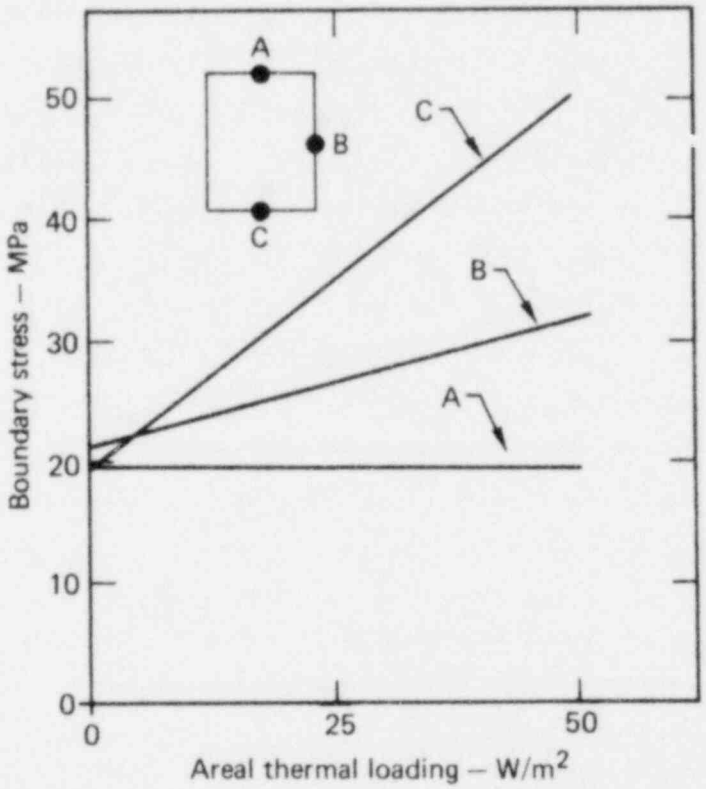

FIG. 2-17. Effect of areal thermal loading on the boundary stresses for the excavation geometry of Fig. 2-16 (from Hardy and Hocking, 1977). Initial horizontal and vertical stresses were taken to be 25 MPa.

TABLE 2-3. Basalt properties assumed by Hardy and Hocking (1977) for base case stress analyses.

Thermal conductivity	1.86 W/m-^{o}C
Specific heat	1030 J/kg-^{o}C
Density	2900 kg/m^{3}
Diffusivity	6.5 x 10^{-7} m^{3}/s
Heat capacity	3.0 x 10^{6} J/m^{3}-^{o}C
Elastic modulus	0.48 x 10^{11} Pa
Poisson's ratio	0.2
Coefficient of linear thermal expansion	5.2 x 10^{-6} ^{o}C^{-1}

corridor. Boundary stresses also depend on the ratio of horizontal to vertical stresses, as shown in Fig. 2-18. When the horizontal in situ stress is equal to one-half the vertical, boundary stresses in the roof and floor are much smaller than when the in situ stresses are equal. In fact, tensile stresses are present in the roof. When the in situ horizontal stress is one and one-half times the vertical, the boundary stresses are much higher in the roof and floor of the corridors than for the base case. The boundary stresses in the side walls are lower than for the base case.

In summary, the boundary stresses in both the roof and floor of the corridor decrease as the ratio of horizontal to vertical in situ stresses decrease. Conversely, the boundary stresses in the sidewall increase as the stress ratio decreases. Hence, it is very important to know at least the ratios of the major principal stresses, and their direction. This information is not currently available.

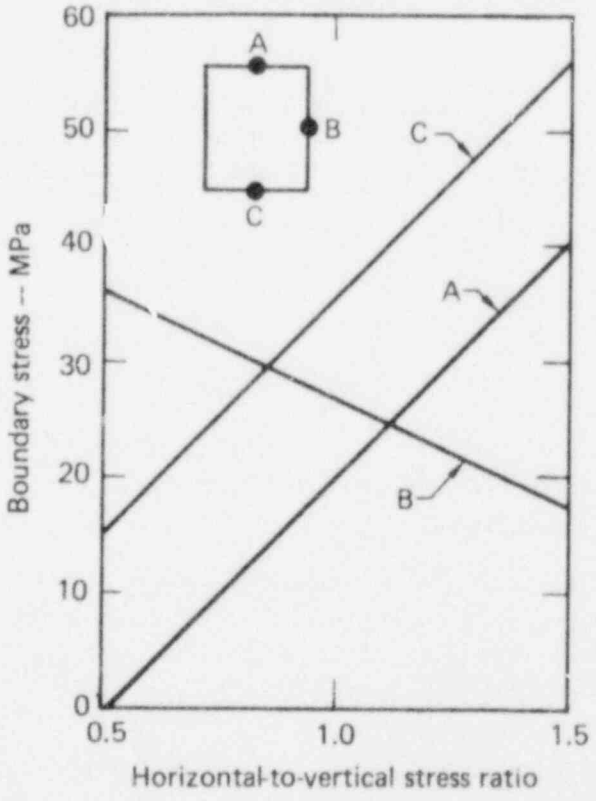

FIG. 2-18. Effect of the horizontal to vertical stress ratio on boundary stresses for the excavation geometry of Fig. 2-16 (from Hardy and Hocking, 1977). Thermal loading was taken to be 25 W/m^2, and the vertical stress was held constant at 25 MPa.

Thermally Induced Stresses. Assuming the excavation geometry illustrated in Fig. 2-16, Hardy and Hocking (1977) calculated the temperature distribution around a corridor after five years (Fig. 2-19). The areal thermal loading was taken as 25 W/m^2, and the air in the room was analyzed as if it were stagnant. No convection or radiation heat-transfer mechanisms were modeled. The magnitude and direction of the thermal stresses at various points in the basalt around the room are illustrated in Fig. 2-20. The magnitudes are indicated by the distances between the ends of the crosses; double-headed arrows denote tensile stresses. Only thermal stresses are presented in Fig. 1-20; no account is taken of in situ stress fields.

Figure 2-21 shows the variation in stress (and temperatures) at the boundary of a corridor. High stresses occur in the corners; however, it should be kept in mind that no reduction in modulus or change in thermal properties has been introduced to account for blasting damage around the corridor.

Hardy and Hocking also calculated the dependence of boundary stresses on Poisson's ratio, Young's modulus, and the coefficient of linear thermal expansion (Figs. 2-22 and 2-23). Raising or lowering Poisson's ratio from its base case value of 0.2 has little effect on the boundary stresses. On the other hand, both Young's modulus and the coefficient of linear thermal expansion have substantial effects, especially at the floor of the corridor. This suggests that an accurate knowledge of Poisson's ratio is not necessary, whereas appropriate values of the coefficient of linear expansion and Young's modulus are of great importance in estimating repository stresses.

Finally, Table 2-4 summarizes the sensitivity of boundary stresses to the parameters studied by Hardy and Hocking. The effects of variation tend to be smallest at the sides of the corridors. These results are strictly qualitative and are not appropriate for detailed design because of insufficient input data. However, the results do suggest which parameters need to be measured accurately.

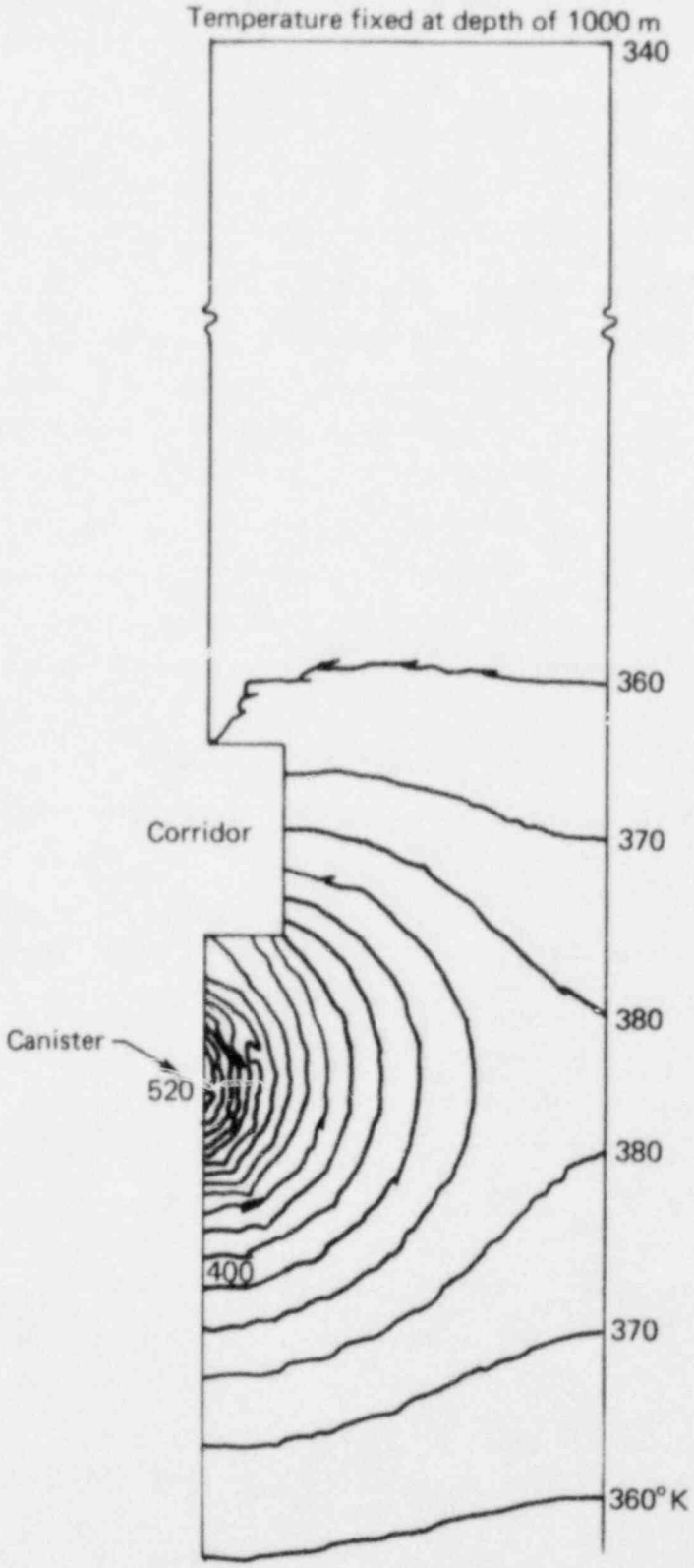

FIG. 2-19. Temperature contours five years after emplacement, assuming a thermal loading of 25 W/m^2 (from Hardy and Hocking, 1977).

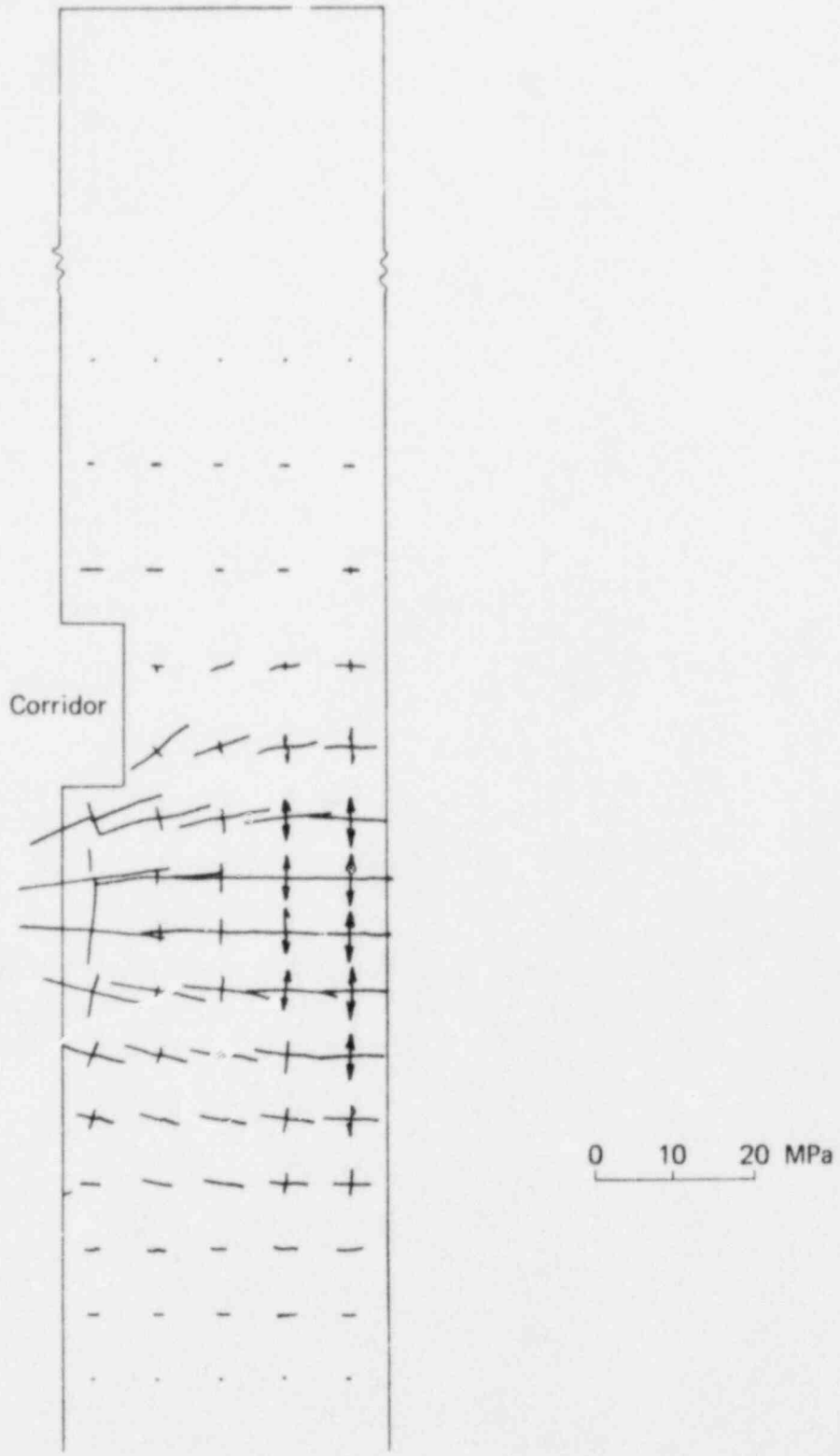

FIG. 2-20. Thermal stresses after five years, assuming a thermal loading of 25 W/m^2 (from Hardy and Hocking, 1977).

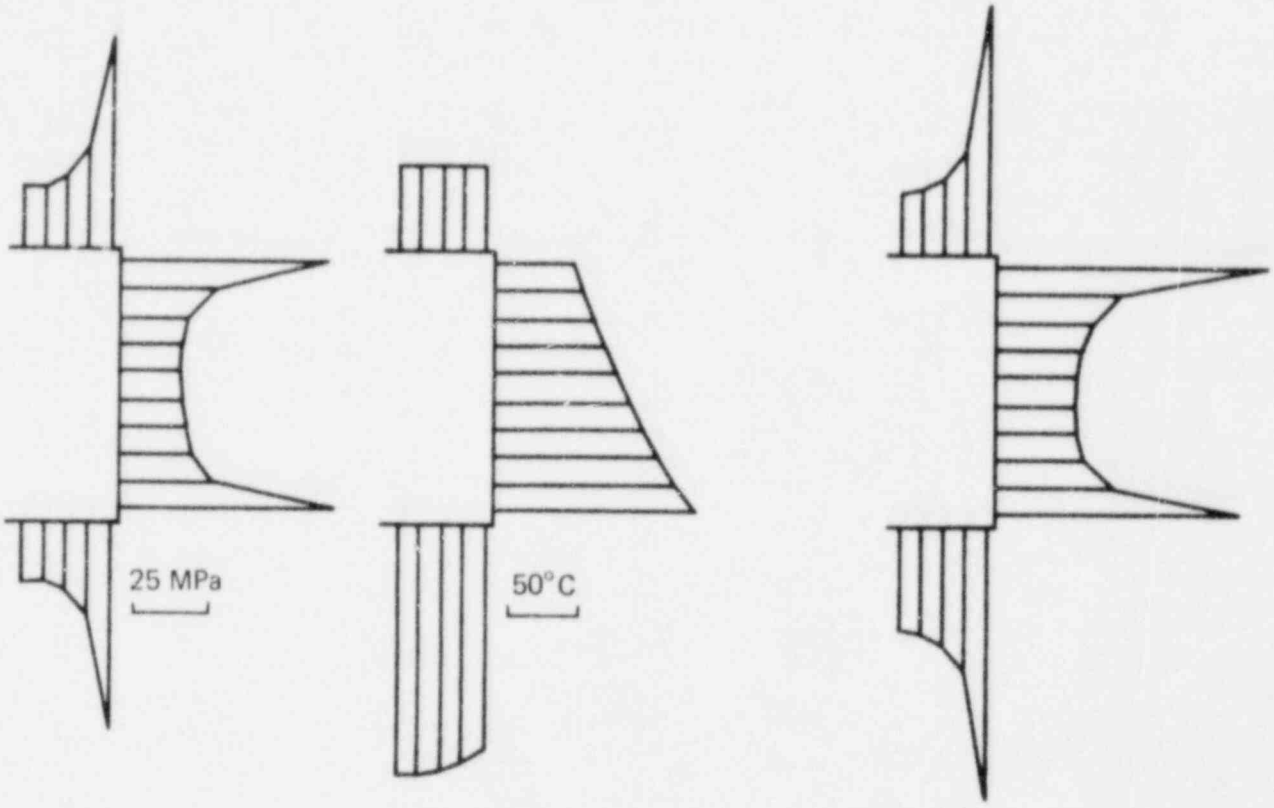

FIG. 2-21. Boundary stresses and temperatures for repository corridor after 5 years, assuming a thermal loading of 25 W/m^2 (from Hardy and Hocking, 1977).

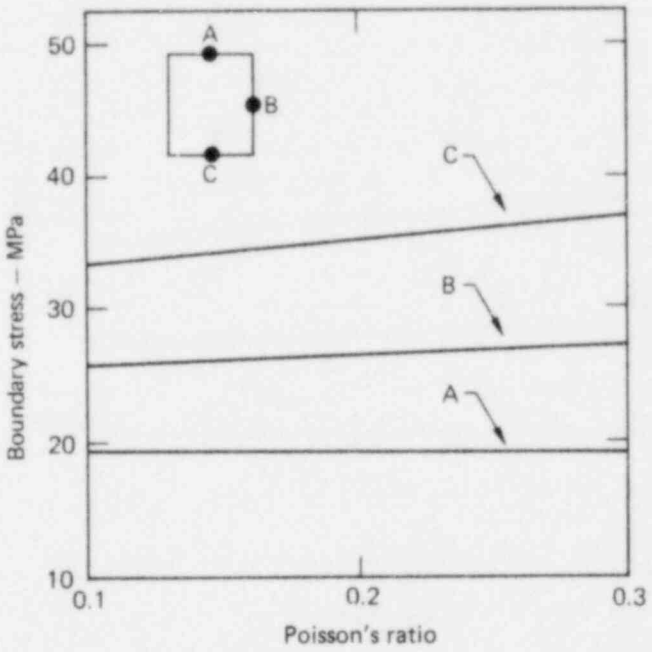

FIG. 2-22. Effect of Poisson's ratio on boundary stresses, assuming a thermal loading of 25 W/m^2 and equal vertical and horizontal stresses (from Hardy and Hocking, 1977).

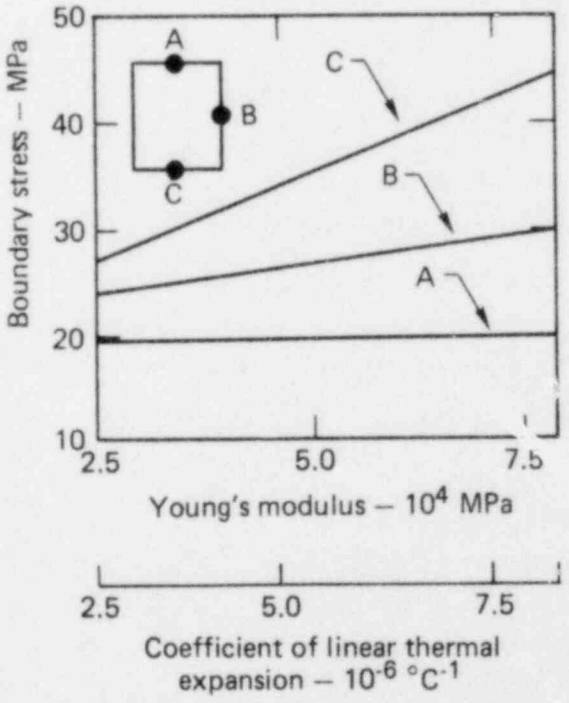

FIG. 2-23. Effects of Young's modulus and the coefficient of linear thermal expansion on boundary stresses, assuming a thermal loading of 25 W/m^2 and equal vertical and horizontal stresses (from Hardy and Hocking, 1977). The effect of each parameter assumes the base case value for the other.

TABLE 2-4. Effects of various factors on boundary stresses (from Hardy and Hocking, 1977).

Assumption	Boundary stress, MPa		
	at A	at B	at C
Base case (Table 2-3)	19.5	26.6	34.9
Thermal loading = 50 W/m^2	19.5	32.0	50.3
E = twice base case	19.8	32.0	51.4
Poisson's ratio = 0.3	19.7	27.0	36.8
Poisson's ratio = 0.1	19.5	25.9	33.2
In situ horizontal stress = 12.5 MPa	-0.7	36.0	14.7
In situ horizontal stress = 37.5 MPa	39.7	17.3	55.1

Mechanical Properties of Intact Rock

Few data are available for the rock strength, Young's modulus, and Poisson's ratio of basalt. The few that are available are for intact rock samples. Furthermore, as shown in Fig. 2-24, rocks classified as basalts have a wide range of compressive strengths and moduli; therefore, it is not possible to adopt generic values for any analysis.

Table 2-5 summarizes data compiled by ONWI (1978). They noted that their information base was rather small and that properties vary widely for "basalts." The modulus varies between 5×10^6 and 16×10^6 psi (34.5 to 110 GPa), for example.

More detailed values, from other sources, for the Dresser Basalt are given in Tables 2-6 and 2-7 for tests conducted under conditions of atmospheric temperature and pressure. As might be expected, the strength increases with the confining pressure. Engineering data for basalts tested from Amchitka Island are given in Tables 2-8 and 2-9. The data in Table 2-9 are for dry rocks. (Moisture can have a significant effect on compressive and tensile strengths. Sharp (1972) compared the properties of Amchitka Island samples that had been air dried for two weeks with those of samples that had

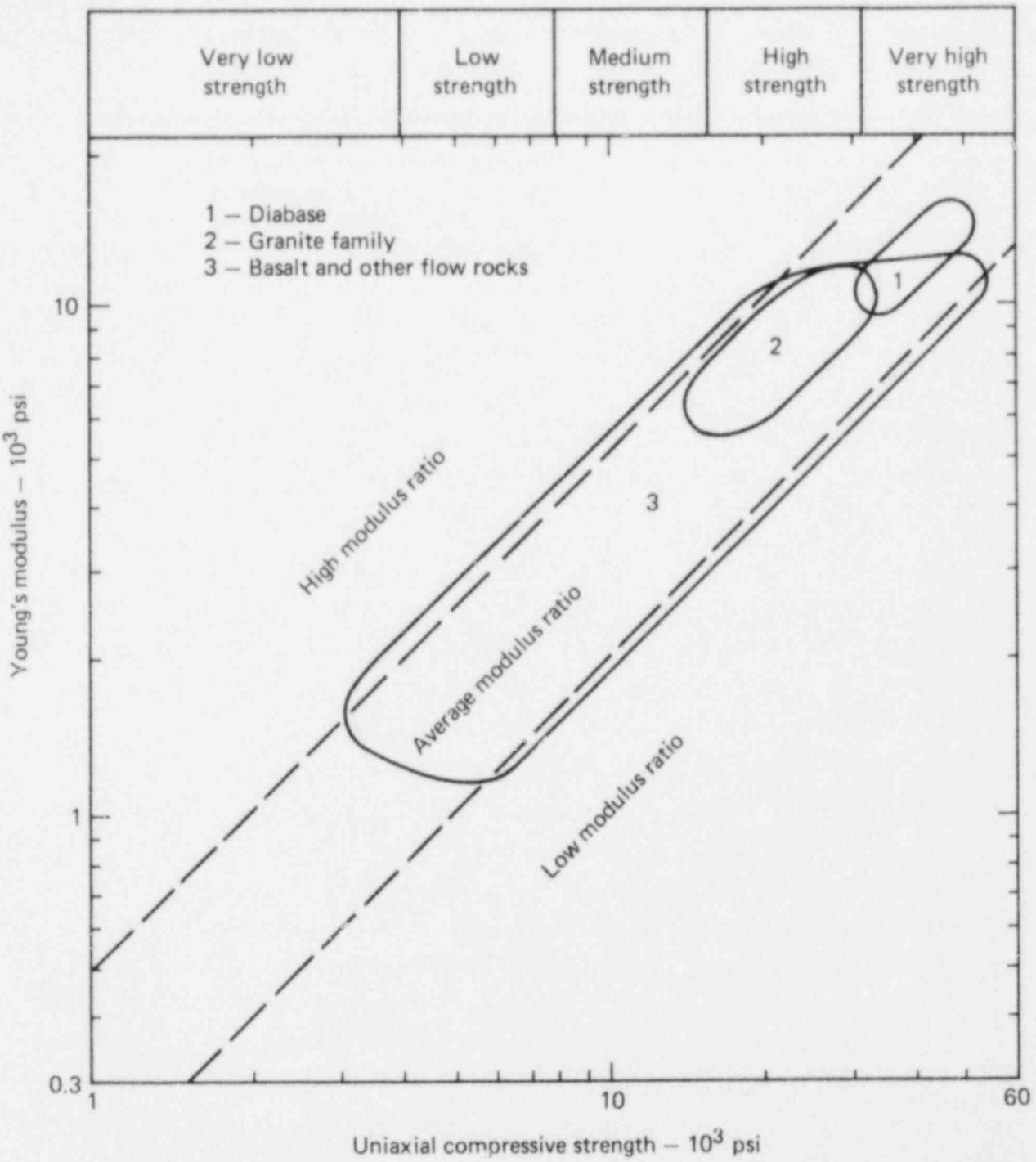

FIG. 2-24. Summary of modulus and strength values found for 176 specimens of igneous rock (from Deere and Miller, 1966).

TABLE 2-5. Intact properties for four basalts (from ONWI, 1978).

	Origin of sample			
	Dresser Basalt	Amchitka Island	Nevada Test Site	Columbia River Basalt
Index properties:				
Unit weight, kg/m^3	3000	2700	2700	2403-3085
Natural moisture content, %	--	--	--	--
Porosity (rock mass), %	0.19	2.8	4.6	--
Stress-strain properties:				
Young's modulus, GPa	93	61.1	34.9	55.2-110
Poisson's ratio	0.264	0.19	0.32	0.22-0.30
Bulk modulus, GPa	--	32.8	--	--
Shear modulus, GPa	4.15	25.7	--	--
Strength properties:				
Uniaxial compressive strength, MPa	440.7	250	148	193.1-400.0
Tensile strength, MPa	22.1	15.5	13.1	12.41-24.14
Thermal properties:				
Coefficient of linear thermal expansion, $10^{-7}\ {}^{o}C^{-1}$	8.9	8.90	--	16.7
Heat capacity, $J/g\text{-}^{o}C$	0.96	0.96	--	0.72-0.96
Thermal conductivity, $W/m\text{-}^{o}C$	1.30	1.30	--	1.00-1.35
Hydrologic properties:				
Permeability		0.0205 m/d	--	9.67×10^{-6} to 3.87×10^{-5} µm/s

TABLE 2-6. Dresser Basalt test results (from Kreck et al., 1974).

	Sample 1		Sample 2		Sample 3		Composite	
	Mean	CV[a]	Mean	CV[a]	Mean	CV[a]	Mean	CV[a]
Porosity, %	0.16	9.0	0.15	0.05	0.25	12.7	0.19	57.3
Permeability, μm/s	$<10^{-4}$	--	$<10^{-4}$	--	$<10^{-4}$	--	$<10^{-4}$	--
Density, g/cm^3	3.02	0.1	3.01	0.7	3.01	0.1	3.01	0.5
Shore hardness	95.0	3.1	93.2	2.5	94.2	1.9	94.1	2.6
Compressive strength, MN/m^2	479	7.91	413	10.7	429	9.16	440	11.0
, 10^3 psi	69.5	7.91	59.9	10.7	62.2	9.16	63.9	11.0
Compressive Young's modulus, GN/m^2	88.5	2.43	82.1	2.18	87.5	2.42	86.1	4.1
, 10^6 psi	12.8	2.43	11.9	2.18	12.7	2.42	12.5	4.1
Tensile strength, MN/m^2	22.9	24	24.0	38.0	17.6	57.0	22.1	39.7
, 10^3 psi	3.33	14	3.48	38.0	2.56	57.0	3.20	39.7
Tensile Young's modulus, GN/m^2	133	9	121	21	105	23	119	20.2
, 10^6 psi	19.2	9	17.6	21	15.3	23	17.3	20.2
Pulse velocity, km/s	6.77	0.3	6.67	0.3	6.72	0.3	6.72	0.7
Bar velocity, km/s	6.12	0.2	5.99	0.4	6.04	0.5	6.05	1.0
Torsional velocity, km/s	3.86	0.2	3.76	0.4	3.80	0.6	3.80	1.2
Dynamic Young's modulus,[b] GN/m^2	113	0.5	108	1.5	109	1.1	110	2.5
Dynamic shear modulus,[c] GN/m^2	44.9	0.4	42.5	1.5	43.4	1.3	43.6	2.6
Poisson's ratio[b]	0.261	1.4	0.266	1.1	0.266	1.5	0.264	1.6

[a]Coefficient of variation, %.

[b]Calculation is based on the assumption of isotropy.

[c]Specimen prepared with the long axis perpendicular to the top face (along z-axis).

TABLE 2-7. Properties of Dresser Basalt (from Morrell and Larson, 1974; Agapito et al., 1977).

Locality	Dresser, Wisc.
Compressive strength, MPa	439
Tensile strength, MPa	14
Shore hardness, scleroscope units	85.8
Apparent density, g/cm^3	3.029
Static Young's modulus, GPa	98.3
Longitudinal velocity, m/s	6669
Bar velocity, m/s	5949
Shear velocity, m/s	3739
Dynamic Young's modulus, GPa	107.2
Poisson's ratio	0.2725
Shear modulus, GPa	42.3
Tensile fracture stress, N/m^2	1.45×10^{-7}
Thermal conductivity coefficient A	1.45×10^{-5}
Thermal conductivity coefficient B	-0.15
Coefficient of thermal expansion, $^oC^{-1}$	3×10^{-6}

TABLE 2-8. Average engineering properties of water-saturated Amchitka Island rocks (from Sharp, 1972).

	Increased moisture, vol%	Compressive strength, MPa	Tensile strength, MPa	Young's modulus, GPa	Violence of rupture
Chitka Point Formation, hornblende pyroxene andesite:					
Av value	3.5	108.69	10.61	22.90	3.1
Max value	15.6	198.25	17.57	56.21	8
Min value	1.2	9.34	0.66	2.00	1
No. of samples	26	20	9	20	23
Std dev	4.0	62.05	5.03	14.76	2.0
Chitka Point Formation, dense flow breccia:					
Av value	6.4	73.95	11.86	17.79	2.8
Max value	10.4	104.72	18.37	31.72	4
Min value	2.4	47.23	5.35	10.21	2
No. of samples	10	5	2	5	5
Std dev	2.9	22.86	9.20	8.34	0.8
Chitka Point Formation, hornblende andesite breccia:					
Av value	7.7	48.42	3.01	14.62	2.0
Max value	17.9	117.92	6.01	25.24	3
Min value	3.2	13.32	1.47	4.00	1
No. of samples	9	8	3	8	7
Std dev	4.5	32.57	2.59	8.21	1.0
Chitka Point Formation, tuff breccia:					
Av value	14.6	49.83	3.06	9.03	2.8
Max value	31.4	116.05	2.12	20.97	7
Min value	6.7	4.49	0.70	1.45	1
No. of samples	26	22	9	11	23
Std dev	7.3	32.42	1.74	5.59	1.6

continued

TABLE 2-8 continued.

	Increased moisture, vol%	Compressive strength, MPa	Tensile strength, MPa	Young's modulus, GPa	Violence of rupture
Banjo Point Formation, breccia:					
Av value	16.6	34.44	6.49	6.76	1.6
Max value	29.2	157.96	17.11	19.03	4
Min value	3.7	9.33	0.92	1.79	1
No. of samples	18	11	7	7	11
Std dev	7.2	42.58	7.38	5.66	1.1
Dense basalts:					
Av value	2.8	123.21	15.17	30.14	5.1
Max value	7.7	196.72	17.54	77.31	9
Min value	1.1	75.48	12.79	14.34	3
No. of samples	10	10	2	7	10
Std dev	2.2	38.22	3.36	18.76	0.0
Amchitka Formation, Kirilof Point glassy breccias:					
Av value	8.1	19.99	2.72	6.90	1.1
Max value	10.7	33.24	14.03	16.00	2
Min value	2.7	12.95	1.86	2.28	1
No. of samples	14	7	6	7	7
Std dev	2.8	8.06	0.69	6.07	0.4
Amchitka Formation, Kirilof Point pillow lavas:					
Av value	9.2	111.90	--	16.28	3.7
Max value	10.5	130.34	--	26.97	4
Min value	7.6	93.67	--	16.97	3
No. of samples	5	3	--	3	3
Std dev	1.1	18.34	--	2.28	0.6

continued

TABLE 2-8 continued.

	Increased moisture, vol%	Compressive strength, MPa	Tensile strength, MPa	Young's modulus, GPa	Violence of rupture
Amchitka Formation, dense older breccias:					
Av value	3.3	196.56	18.15	44.90	6.7
Max value	6.9	304.87	23.65	98.48	6
Min value	0.4	37.90	13.22	11.79	3
No. of samples	17	11	4	11	11
Std dev	1.8	84.08	4.66	24.90	1.6
East Cape quartz diorite:					
Av value	1.7	168.62	12.34	36.28	5.7
Max value	3.0	264.36	15.86	99.17	9
Min value	0.8	41.34	8.07	11.17	3
No. of samples	37	31	6	31	31
Std dev	0.5	62.43	3.13	17.52	1.3

TABLE 2-9. Average engineering properties of air-dried Amchitka Island rocks (from Sharp, 1972).

	Soil hardness	Apparent specific gravity	Air dried pore space, vol%	Compressive strength, MPa	Tensile strength, MPa	Young's modulus, GPa	Poisson's ratio	Rigidity modulus, GPa	Bulk modulus, GPa	Longitudinal velocity, m/s	Shear velocity, ft/s	Violence of rupture	Strain energy, MPa	Internal friction, deg	Magnetic susceptibility, emu/cm³
Chitka Point Formation, hornblende pyroxene andesite:															
Av value	6.0	2.67	3.5	208.66	14.86	47.72	0.23	19.38	29.45	4574.95	2683.46	6.3	0.48	58	[illegible]
Max value	7.0	2.91	15.6	300.22	25.17	91.79	0.36	36.90	109.31	6908.60	3257.09	9	0.93	85	[illegible]
Min value	3.5	2.34	1.2	61.85	4.91	11.03	0.17	4.14	10.83	2468.88	1767.23	1	0.15	20	[illegible]
No. samples	36	105	26	25	53	25	18	18	18	26	10	85	25	25	12
Std dev	1.2	0.13	4.0	74.97	5.12	4.31	0.06	8.97	21.93	1152.14	579.73	2.3	0.22	15.0	595.0
Chitka Point Formation, dense flow breccia:															
Av value	5.2	2.57	6.4	126.67	15.03	30.83	0.18	13.03	16.07	4479.95	2298.50	5.5	0.30	62	1904
Max value	7.5	2.74	10.4	185.16	21.81	54.00	0.22	23.10	27.24	5446.78	2910.54	9	0.56	70	3274
Min value	2.5	2.38	2.4	81.57	8.12	21.24	0.14	9.03	11.03	3712.16	1940.90	1	0.15	53	547
No. samples	18	38	10	8	25	8	7	7	7	10	5	33	7	8	6
Std dev	1.2	0.11	2.9	36.37	4.32	10.69	0.03	4.76	5.86	693.72	384.05	2.6	0.14	6.5	1102.8
Chitka Point Formation, hornblende andesite breccia:															
Av value	4.8	2.47	7.7	91.37	10.35	34.28	0.17	14.62	17.31	3798.11	2754.78	3.7	0.15	61	1953
Max value	6.5	2.59	17.0	138.80	13.77	56.90	0.19	23.93	30.62	4180.03	3335.73	8	0.26	82	7820
Min value	3.5	2.07	3.2	21.41	4.35	8.14	0.15	12.14	13.31	3410.71	2457.90	1	0.004	40	534
No. samples	10	37	9	7	22	7	6	6	6	4	3	29	7	6	4
Std dev	0.8	0.13	4.5	45.22	2.49	14.76	0.02	4.71	5.86	387.10	502.92	2.4	0.09	14.1	326.3
Chitka Point Formation, tuff breccia:															
Av value	4.2	2.24	14.6	82.30	6.02	23.17	0.22	9.52	13.79	3181.50	1937.31	3.1	0.18	58	2353
Max value	7.5	2.55	31.4	154.00	14.28	60.28	0.43	16.48	61.72	4351.32	2444.19	8	0.46	80	2930
Min value	1.5	1.73	6.7	17.05	1.06	4.07	0.11	3.10	3.24	1828.80	1380.13	1	0.003	30	1487
No. samples	40	128	26	25	69	25	21	21	21	21	8	99	25	25	11
Std dev	1.7	.19	7.3	48.17	3.64	11.52	0.10	3.93	12.90	701.95	388.62	2.4	0.16	12.9	404.1
Banjo Point Formation, breccia:															
Av value	4.0	2.27	16.6	118.83	6.81	29.38	0.22	12.07	17.59	3218.69	2155.85	2.5	0.28	60	2554
Max value	7.5	3.09	29.2	339.49	29.54	81.03	0.37	34.48	66.00	5651.60	3141.88	8	0.92	70	3563
Min value	1.5	1.93	2.7	9.18	1.43	3.31	0.11	2.02	3.24	1177.14	1254.56	1	0.003	40	787
No. samples	35	82	18	14	49	14	8	8	8	71	4	68	13	15	10
Std dev	1.4	0.29	7.2	125.96	7.00	20.76	0.10	13.03	31.86	1255.47	818.39	2.4	0.33	16.3	907.4
Dense basalts:															
Av value	5.4	2.73	2.8	249.91	15.51	61.10	0.19	25.65	32.83	4415.33	3234.84	5.9	0.56	60	2750
Max value	7.5	2.93	7.7	356.35	25.43	91.93	0.21	27.65	51.93	5860.39	3630.17	9	0.99	80	6020
Min value	2	2.17	1.1	124.45	6.56	32.21	0.17	21.52	27.38	3279.05	2920.40	1	0.12	30	1088
No. samples	28	63	10	9	43	9	7	7	7	14	4	53	9	10	5
Std dev	2.1	0.21	2.2	73.20	5.18	16.90	0.01	5.66	8.34	884.22	293.83	2.8	0.28	15.5	1587.2
Amchitka Formation, Kirilof Point glassy breccia:															
Av value	4.7	2.24	8.1	38.03	3.43	12.76	0.27	5.03	9.24	3317.14	1726.39	1.4	0.11	63	907
Max value	7.5	2.34	10.7	55.65	5.12	30.00	0.40	11.93	20.76	4421.12	2315.87	—	0.50	70	2539
Min value	3.5	2.15	2.7	18.79	2.15	4.41	0.20	4.21	6.29	2396.64	1406.04	1	0.02	48	401
No. samples	25	61	14	10	49	10	6	6	6	15	4	60	10	10	6
Std dev	0.9	0.04	2.8	10.79	0.70	6.76	0.07	2.83	5.38	699.82	404.77	0.8	0.14	8.7	8212

continued

TABLE 2-9 continued.

	Soil hardness	Apparent specific gravity	Air dried pore space, vol%	Compressive strength, MPa	Tensile strength, MPa	Young's modulus, GPa	Poisson's ratio	Rigidity modulus, GPa	Bulk modulus, GPa	Longitudinal velocity, m/s	Shear velocity, ft/s	Violence of rupture	Strain energy, mPa	Internal friction, deg	Magnetic susceptibility, emu/cm^3
Amchitka Formation, Kirlof Point pillow lavas:															
Av value	5.8	2.42	9.2	161.76	13.89	30.76	0.18	13.03	16.00	3930.70	2433.22	6.8	0.46	60	2976
Max value	7.0	2.54	10.5	186.52	23.90	39.03	0.18	16.69	19.72	4621.07	---	9	0.71	70	3076
Min value	4.5	2.32	7.6	148.90	6.63	24.55	0.17	12.14	14.90	3331.77	---	3	0.29	40	2875
No. samples	10	25	5	3	19	3	2	2	2	4	1	22	3	3	2
Std dev	1.3	0.07	1.1	21.44	4.46	7.45	0.01	3.24	3.45	661.11	0	1.6	0.22	17.3	---
Amchitka Formation, dense older breccia:															
Av value	6.7	2.77	3.3	3.85	20.01	46.64	0.25	18.69	31.10	4960.01	2700.22	6.9	0.76	67	3165
Max value	7.5	2.95	6.9	373.38	36.00	69.72	0.38	29.31	[illegible]	6096.00	3088.54	9	1.39	75	7747
Min value	2.5	2.56	0.4	65.71	8.01	18.00	0.19	12.69	[illegible]	3219.60	2200.05	1	0.12	44	727
No. samples	29	72	17	16	41	16	10	10	10	18	7	58	16	17	8
Std dev	0.9	0.08	1.8	93.67	7.22	15.72	0.06	5.59	5.93	833.32	316.99	2.2	0.37	7.3	2481.9
East Cape quartz diorite:															
Av value	7.0	2.71	1.7	229.52	16.40	49.31	0.28	19.24	37.38	5060.59	2897.73	6.2	0.59	64	2666
Max value	7.0	2.86	3.0	332.29	27.69	76.76	0.40	45.80	151.03	6226.76	3450.03	9	1.04	70	3607
Min value	6.5	2.58	0.8	43.42	7.87	19.66	0.11	13.38	15.24	3464.05	2441.45	1	0.05	40	1787
No. samples	55	174	37	34	90	33	22	22	22	27	12	134	33	34	16
Std dev	0.2	0.05	0.5	69.45	4.29	12.69	0.07	6.48	28.07	34.31	252.07	2.3	0.24	16.1	486.7

been submerged in water for one week. Wet compressive strengths declined by at least 30%--for quartz diorite and pillow lavas--and as much as 67%--for the Banjo Point Breccia. Tensile strengths showed greater variation: it did not decline significantly for "dense basalts," but it declined by 70% for the andesite breccia.)

Data for basalt tested from the Nevada Test Site are shown in Figs. 2-25 through 2-27. Figure 2-26 shows the relationship between strength and confining pressure for basaltic rocks of different porosities. The strength can be seen to depend strongly on the porosity. Figure 2-27 shows only an insignificant variation in Poisson's ratio with confining pressure for Test Site basalt.

Values for the strength of samples from the Hanford reservation are shown in Table 2-10. Of particular interest are the results from rock zone RM 4, which illustrate the large effect of jointing on strength.

Tables 2-11 and 2-12 and Figs. 2-28 and 2-29 summarize the physical properties of Columbia Plateau basalts. The figures show large variations in strength with porosity and density, the values of which depend strongly on the position of the sample within the flow. The same type of behavior for Test Site basalt is shown in Fig. 2-30.

Tables 2-13 through 2-15 list some additional values for geomechanical properties of basaltic rock samples.

In summary, only sparse data are currently available on the mechanical properties of basalt. Those that are available suggest great variability in compressive strength and modulus, and less variation in Poisson's ratio. All three parameters vary with porosity and density.

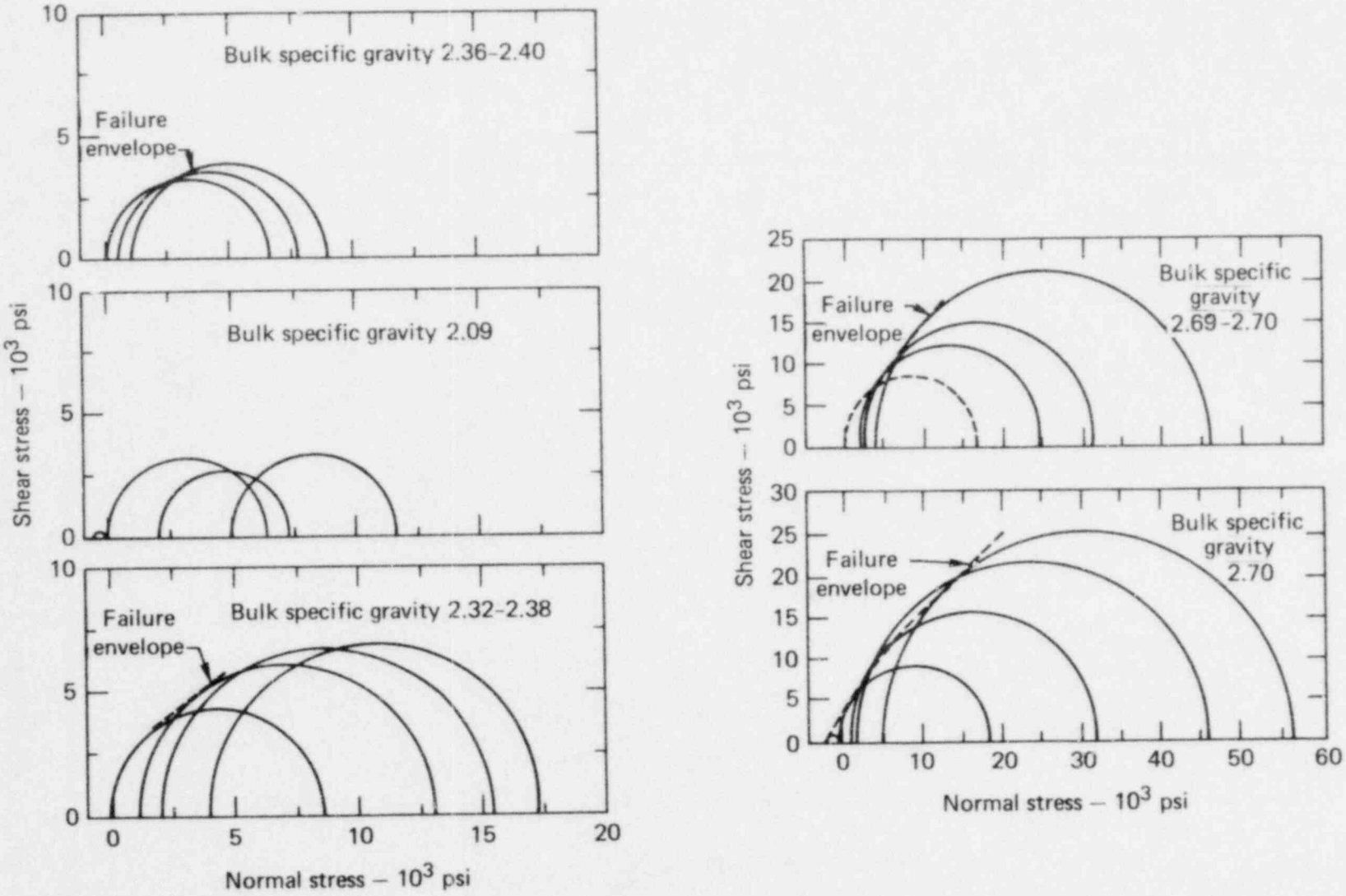

FIG. 2-25. Mohr circles for vesicular (left) and dense (right) basalts (from Lutton, 1968).

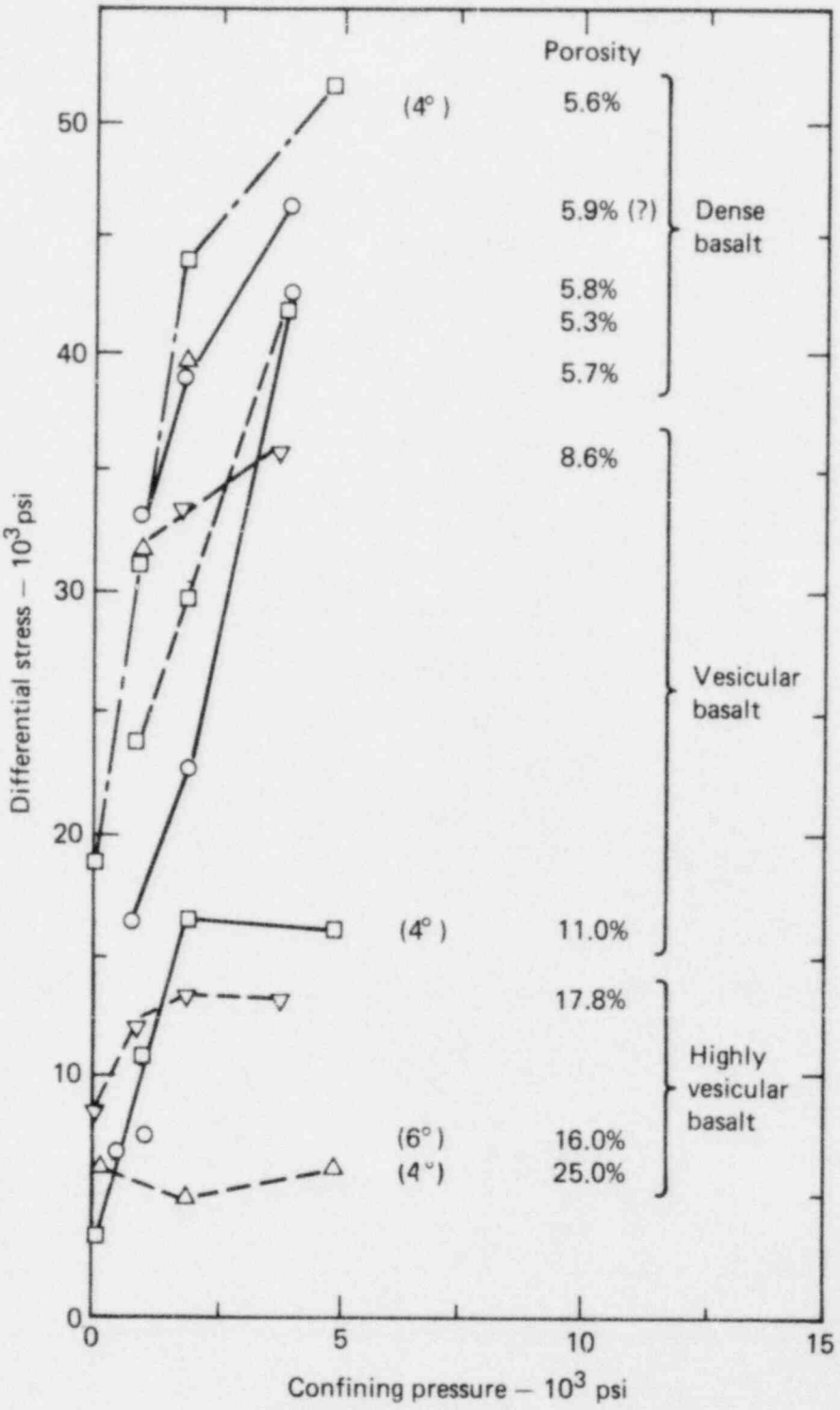

FIG. 2-26. Relationship between strength and confining pressure for basaltic rocks of different porosities (from Lutton, 1968).

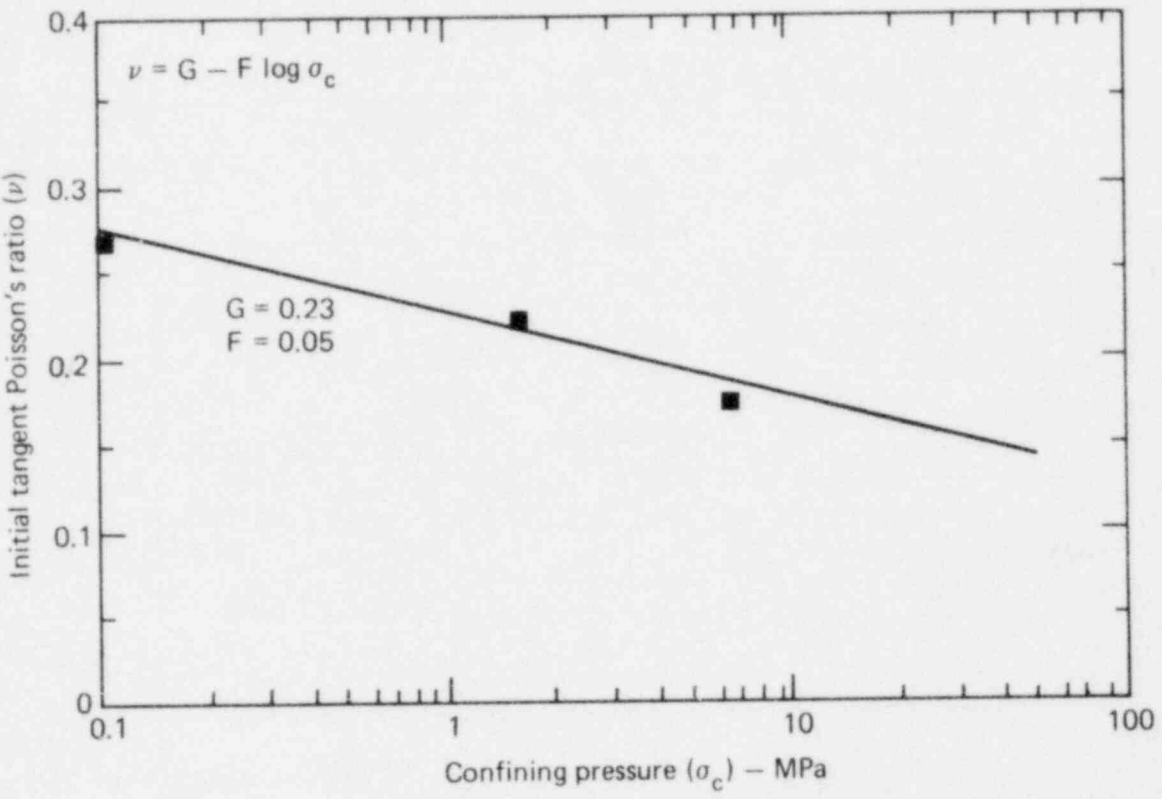

FIG. 2-27. Variation of initial tangent Poisson's ratio with confining pressure for Nevada Test Site basalt (from Stowe, 1969).

TABLE 2-10. Summary of triaxial compression strength tests on core from the Hanford reservation (from Agapito et al., 1977).

Rock zone	Number of tests	Confining pressure, MPa	Average strength, MPa
RM 1	3	0.0	212
	3	3.5	287
	3	7.0	305
	3	14.0	350
	3	21.0	400
RM 2 (solid)	2	0.0	266
	2	7.0	361
	2	14.0	481
	1	21.0	562
	1	28.0	638
RM 1 (with slip planes)	1	0.0	143
	1	7.0	179
	1	14.0	252
	2	21.0	331
	2	28.0	390
RM 3 (all specimens contained many open vugs and pores)	3	0.0	69
	2	7.0	93
	3	14.0	145
	3	21.0	172
	3	28.0	152
RM 4 (solid)	2	0.0	216
	2	7.0	307
	1	14.0	434

continued

TABLE 2-10 continued.

Rock zone	Number of tests	Confining pressure, MPa	Average strength, MPa
RM 4 (with joints)	1	0.0	16
	1	7.0	168
	2	14.0	281
	3	21.0	310
	2	28.0	333

TABLE 2-11. Summary of rock properties for basalts from the Columbia Plateau (DH-100 series samples) (from Agapito et al., 1977). All failed samples fractured across their matrix and structure.

Depth, ft	Secant elasticity,[a] GPa	Compressive strength, MPa	Absorption, wt%	Specific gravity
88.3	43	81	3.9	2.57
101.9	53	98	3.7	2.61
120.9	23	216	2.1	2.74
148.7	22	83	3.9	2.58
152.8	22	137	3.7	2.62
181.6	30	194	2.5	2.65

[a]For first cycle of loading, 7 MPa stress.

TABLE 2-12. Summary of rock properties for basalts from the Columbia Plateau (DH-200 series) (from Agapito et al., 1977).

Depth, ft	Secant elasticity,[a] GPa	Poisson's ratio[a]	Compressive strength, MPa	Absorption, wt%	Specific gravity	Porosity
133.21	45	0.09	176	1.6	2.76	4.4
135.58	74	0.16	204	0.8	2.78	2.2
148.75	59	0.05	109	4.1	2.56	10.4
149.75	49	0.31	39	5.3	2.46	12.9
166.06	54	0.10	125	1.5	2.73	4.2
166.42	55	0.14	104	1.5	2.73	4.0
232.69	58	0.14	180	1.5	2.68	4.2
233.50	66	0.22	192	1.1	2.70	3.1
235.54	36	0.10	179	2.3	2.65	6.0
239.53	--	--	139	3.1	2.58	8.0
239.31	--	--	125	3.7	2.54	9.4
120.33	77	0.18	293	0.2	2.86	0.6
133.60	72	0.26	229	0.3	2.88	0.9
147.98	80	0.23	241	0.2	2.90	0.6

[a]For first cycle of loading, 7 MPa stress.

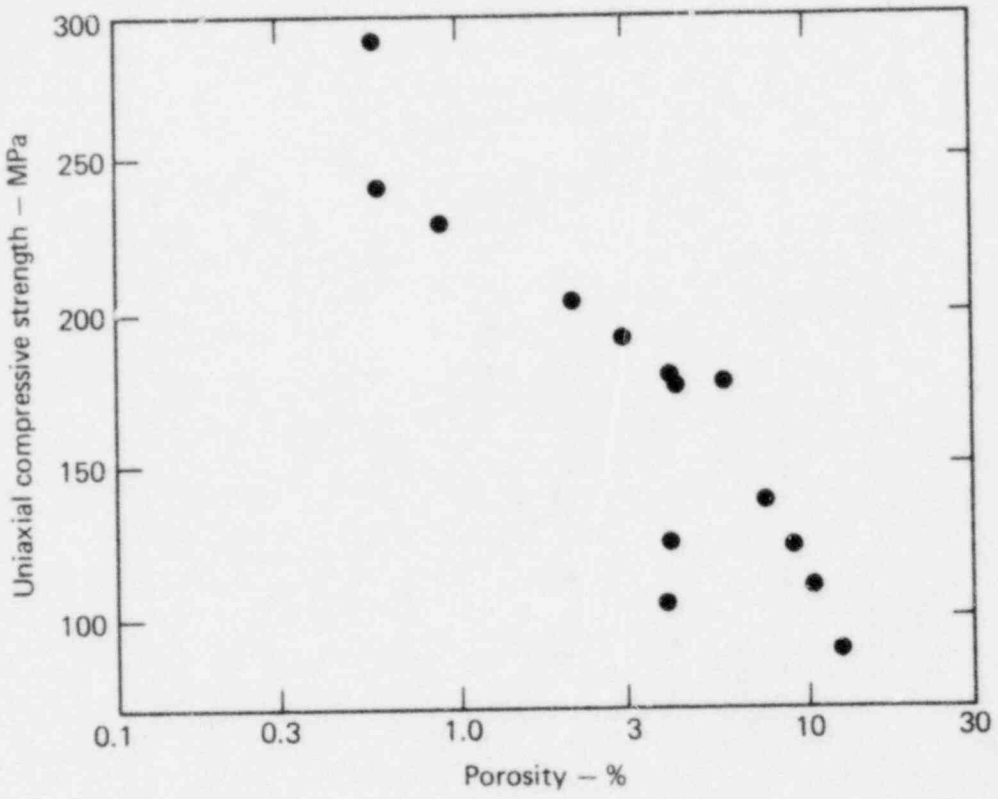

FIG. 2-28. Dependence of compressive strength on the porosity of Columbia Plateau basalts (from Agapito et al., 1977).

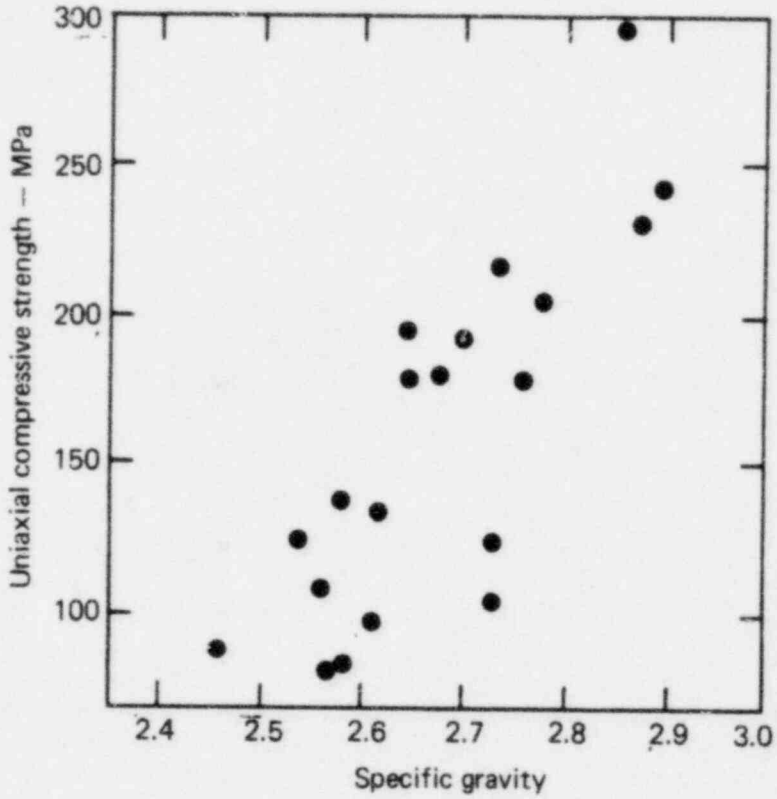

FIG. 2-29. Dependence of compressive strength on the specific gravity of Columbia Plateau basalts (from Agapi ' et al., 1977).

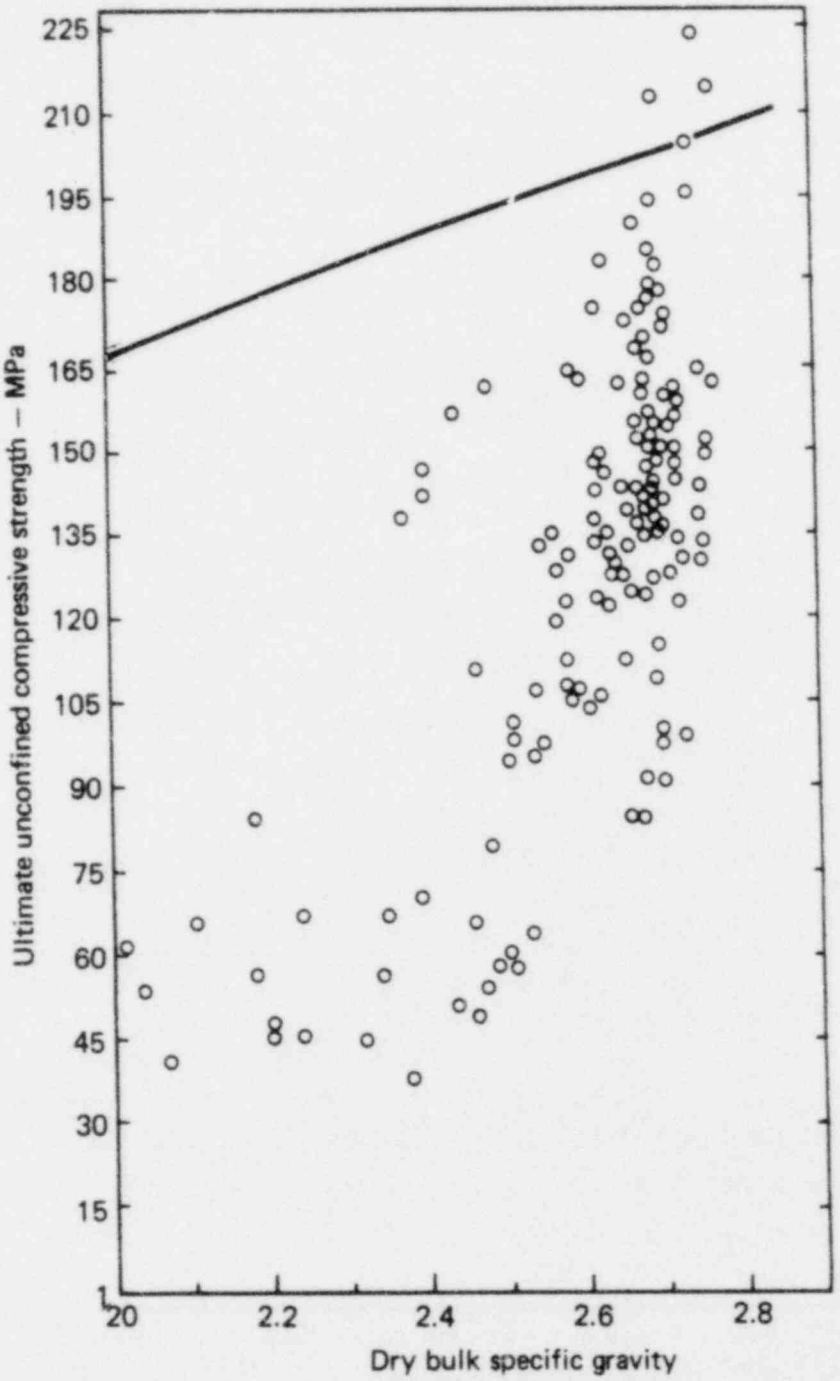

FIG. 2-30. Dependence of compressive strength on the specific gravity of Nevada Test Site basalts (from Sandia, 1962). The solid line represents the predicted strength, based on the reduction of cross-sectional solid area and assuming that void-free basalt has a specific gravity of 2.85 and a strength of 206.9 MPa.

TABLE 2-13. Strength data on various basalts (from Agapito et al., 1977).

Rock	Crushing strength, MPa	Cohesive strength, MPa	Tan ϕ[a]
Miocene basalt, Ore.	169	32	1.2
Miocene basalt, Ore.	219	44	1.1
Andesite hyperstene	133	29	1.0
Andesite hyperstene	129	28	1.0
Dresser Basalt	440	--	--
Dresser Basalt	363	--	--
Knippa Basalt	262	--	--

[a]Tangent of angle of internal friction.

TABLE 2-14. Elastic properties of various basalts (from Agapito, et al., 1977).

Rock	Young's modulus, GPa	Poisson's ratio
Basalt, Ostritz, Germany	11.5	--
Basalt, Champion mine, Mich.	61	--
Basalt, Champion mine, Mich.	85	--
Dresser Basalt, Wisc.	88.5	0.26
Frederick Diabase	99	--
Karroo Dolerite	84	--
Gabbro, norites, diabases	78-99	0.11-0.31

TABLE 2-15. Geomechanical properties of various basalts.[a]

Rock type and origin	Stress-strain properties					Strength properties		Reference
	Young's modulus, GPa	Density, g/cm^3	Bulk modulus, GPa	Shear modulus, GPa	Poisson's ratio	Uniaxial compressive strength, MPa	Tensile strength, MPa	
Vesicular basalt, South Coulee dam site, Columbia Basin project, Wash.	38.6(NR,5)	2.58(0.4,6)			0.14(NR,5)	82.1(37.9,2)		Brandon, 1976
Basalt, no location		3.07(2.95-3.15)						Morris and Johnson, 1967
Basalt, no location	40.4(79.2,9)	2.66(0.65,16)						Judd, 1969
Basalt, Mich.	6.15	2.85		26.8		230.3		Windes, 1949
Basalt, Mich.		2.97		33.9		268.3		Windes, 1949
Basalt, Mich.	70.3	2.9[illegible]		29.6		358.6		Windes, 1949
Basalt, Mich.						257.9		Windes, 1949
Basalt (altered), Mich.						81.4		Windes, 1949
Heavily altered amygdular, zeolitic basalt, Mich.		2.04			0.04	171.7		Windes, 1950
Heavily altered amygdular, epidotized basalt, Mich.	40.7	2.70		18.5	0.09	119.3		Windes, 1950
Basalt, Sec 32, T. 38 S., R. 4 E., Medford, Ore.	62.3(32.4,6)	2.72(0.11,14)			0.234	168.6(68.1,3)		USBR, 1953
Basalt, Columbia Plateau	70.3(60.7-111.7)	2.9(2.4-3.1)			0.26(0.22-0.28)	200(0-4000)	14(0-23)	Deju et al., 1978
Vesicular basalt, Kayna dam site, Bombay, India	36.2(NR,3)	2.54(0.5,4)			0.13(NR,3)	68(60.3,3)	2.2(2.8,6)	Brandon, 1976
Glassy basalt, Black Canyon dam site, Boise, Idaho	32.2(NR,6)	2.62(0.16,10)			0.10(NR,6)	60(39.3,3)	1.1(0.69,2)	Brandon, 1976

continued

[a]Values are presented in the form A(B,C), where A is either the single value reported, the mean, or the range of values (A_1-A_2); B is either the difference between the maximum and minimum reported values or the range of values (B_1-B_2); and C is the number of samples tested. Both B and C or C alone may be absent. NR signifies "not reported."

TABLE 2-15 continued.

Rock type and origin	Stress-strain properties					Strength properties		Reference
	Young's modulus, GPa	Density, g/cm^3	Bulk modulus, GPa	Shear modulus, GPa	Poisson's ratio	Uniaxial compressive strength, MPa	Tensile strength, MPa	
Basalt, South Coulee dam site, Columbia Basin project, Wash.	50.7(NR,3)	2.8(0.13,5)			0.18(NR,3)	171.7(NR,1)		Brandon, 1976
Vesicular basalt, South Coulee dam site, Columbia Basin project, Wash.	59.3(NR,6)	2.62(0.04,10)			0.21(NR,6)	95.9(44.1,3)		Brandon, 1976
Vesicular basalt, South Coulee dam site, Columbia Basin project, Wash.	42.1(NR,6)	2.47(0.24,12)			0.19(NR,6)	61.4(7.03,3)		Brandon, 1976
Heavily altered amygdular, calcitized basalt, Mich.	60.0	2.80			0.15	342.1		Windes, 1950
Dense basalt, Tupia dam, Brazil	73.1	3.00			0.21	104.8		Kulhany, 1975
Dense basalt, Bonita dam, Brazil	61.0	2.97			0.19	137.4		Kulhany, 1975
Dense basalt, Turamirin dam, Brazil	42.8	2.71			0.16	133.0		Kulhany, 1975
Dense basalt, Mussa quarry, Brazil	44.0	2.68			0.19	126.8		Kulhany, 1975
Very dense, fine-grained basalt, Howard Prarie dam, Ore.	61.8	2.73			0.23	194.1		Kulhany, 1975
Lower Granite Basalt (massive, compact), Medford, Ore.	50.2	2.73			0.24	228.1	26.3	Kulhany, 1975
Little Goose Basalt (massive, compact) Walla Walla, Wash.	77.2				0.27	296.1	11.1	Kulhany, 1975
John Day Basalt (compact to vesicular)	83.4				0.29	355.1	14.5	Kulhany, 1975
Basalt	38.8	2.86			0.16	146.1		Kulhany, 1975

Thermal Properties

Several numerical techniques are available for calculating the thermal distributions around an excavation due to the emplacement of radioactive waste. In general, these techniques require as input the density, specific heat, thermal conductivity, and/or the thermal diffusivity of the basalt surrounding the emplacement site. The induced thermal fields are superimposed upon the geothermal gradient at the point of interest. A geothermal gradient from a hole at the Hanford facility is shown in Fig. 2-31.

The density must be known, since it controls the initial stress gradient and is needed to estimate thermal diffusivity. Table 2-16 summarizes the values obtained for the density of some basalts. There is considerable variability, as one might expect from the characteristics of basalt, and the tabulated values must be used cautiously.

Many tests have been performed to determine thermal parameters for basalt as functions of temperature. Thermal properties for Hanford basalt, for

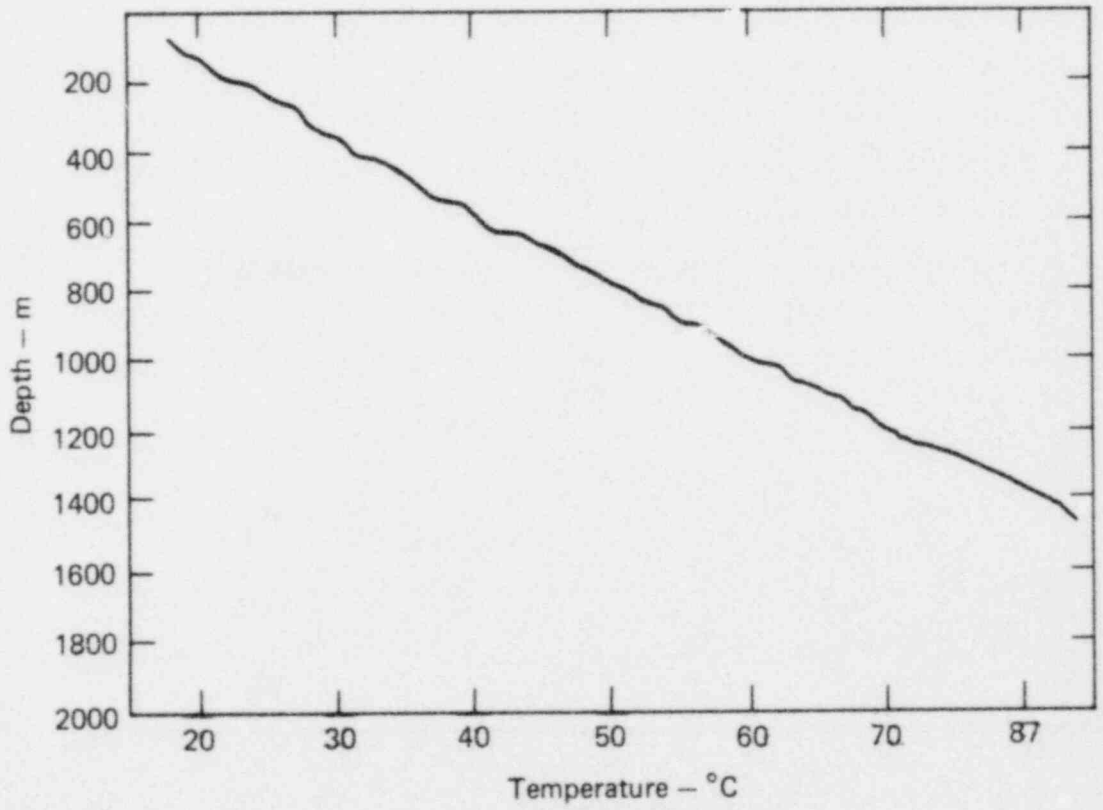

FIG. 2-31. Subsurface temperature as a function of depth in the DC-1 drill hole at the Hanford reservation (from NWTSP, 1976, Vol. 1).

TABLE 2-16. Density of some basalts (from Agapito et al., 1977).

Rock type	Density, g/cm^3
Basalt	2.4-3.1
Gabbros, norites, diabase	3.0
Dresser Basalt	3.02

example, are shown as functions of temperature in Tables 2-17 and 2-18. Values for the thermal conductivity and thermal diffusivity of basaltic rocks, as collected by Agapito et al. (1977), are shown in Tables 2-19 and 2-20.

An equation for the inverse thermal conductivity as a function of temperature for Dresser Basalt is given in Fig. 2-32. The curve fits the data for three of the five blocks tested. Values for the specific heat of several rock types as functions of temperature are given in Fig. 2-33. Both the thermal conductivity and the specific heat are strongly dependent on the chemical composition of the rock.

Using numerical models, it is possible to show the effect of uncertainty in each thermal property on the thermal distribution around a repository. For example, the effect of the thermal conductivity of the basalt layer on the cavern temperature is shown in Fig. 2-34. Increasing the thermal conductivity causes a large reduction in the maximum cavern temperature.

As this survey suggests, relatively little information regarding the thermal properties of basalt is presently available. At least one study on Hanford basalts is underway (at the Colorado School of Mines), and the results shown be available soon.

TABLE 2-17. Thermal properties of Hanford basalts as functions of temperature (from NWTSP, 1976).

Temperature, ^{o}C	Density, kg/m^3	Heat capacity, $J/g\text{-}^{o}C$	Thermal diffusivity, $10^{-3}\ m^2/h$	Thermal Conductivity, $W/m\text{-}^{o}C$
Sample 1005, depth = 306 m:				
37.8	2941.3	0.728	1.91	1.12
93.3	2944.5	0.779	1.87	1.19
149	2947.7	0.829	1.82	1.24
204	2949.3	0.879	1.77	1.28
260	2952.5	0.929	1.73	1.32
316	2955.7	0.980	1.68	1.30
Sample 1084, depth = 330 m:				
37.8	2660.9	0.737	1.86	1.02
93.3	2662.5	0.783	1.81	1.04
149	2665.7	0.825	1.76	1.07
204	2667.3	0.867	1.70	1.09
260	2670.5	0.908	1.64	1.11
316	2672.1	0.950	1.50	1.12

TABLE 2-18. Heat capacity for Hanford basalts at different temperatures (from ONWI, 1978). The values were taken originally from different sources.

Temperature, °C	Heat capacity, J/g-°C
20-100	0.837
100	0.963
200	1.005
300	1.047
37.8	0.728-0.737
93.3	0.779-0.783
148.8	0.825-0.829
204.4	0.867-0.879
260	0.908-0.929
315.6	0.950-0.980

TABLE 2-19. Thermal conductivity of several basaltic rocks (from Agapito et al., 1977).

Rock	Temperature, °K	Thermal Conductivity, W/m-°C
Basalt	--	1.8-2.2
Basalt (Japan)	--	1.4
Gabbro, norites, diabase	273-373	1.7-2.6
Columbia Plateau Basalt	373	1.53
Dresser Basalt	373	3.0
Diabasic basalt	303	1.69
Diabasic basalt	348	1.73

TABLE 2-20. Thermal diffusivity of several basaltic rocks (from Agapito et al., 1977).

Rock	Thermal Conductivity, 10^{-7} m^2/s
Gabbro	5.2
Fine-grained diabase	5.8
Silicified diabase	8.1
Basalt (Japan)	7.0
Gabbro (Japan)	8.0
Dresser Basalt	10.0
Columbia Plateau Basalt	6.5

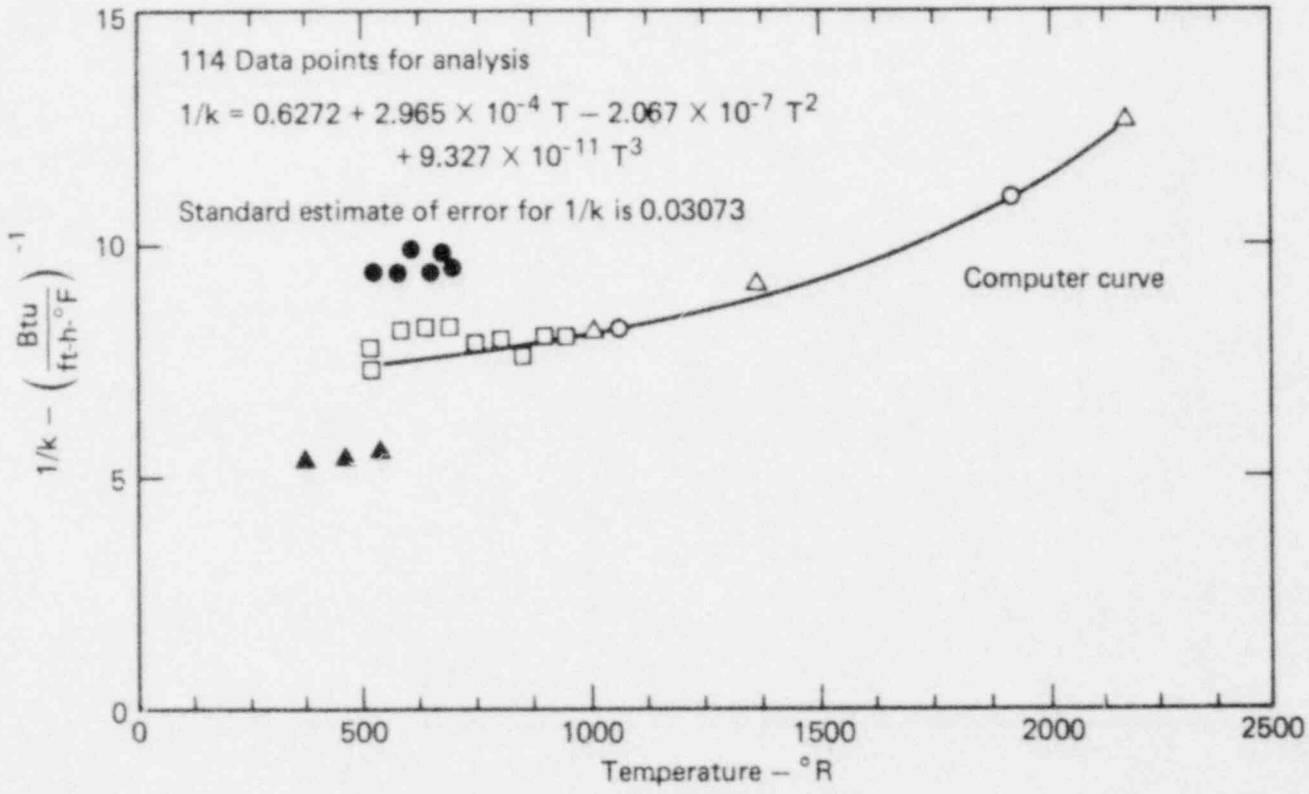

FIG. 2-32. Inverse thermal conductivity (1/k) as a function of temperature for Dresser Basalt (from Morovelli and Veith, 1965). The different symbols represent five sample blocks; the closed circles and triangles were not used for the computer fit.

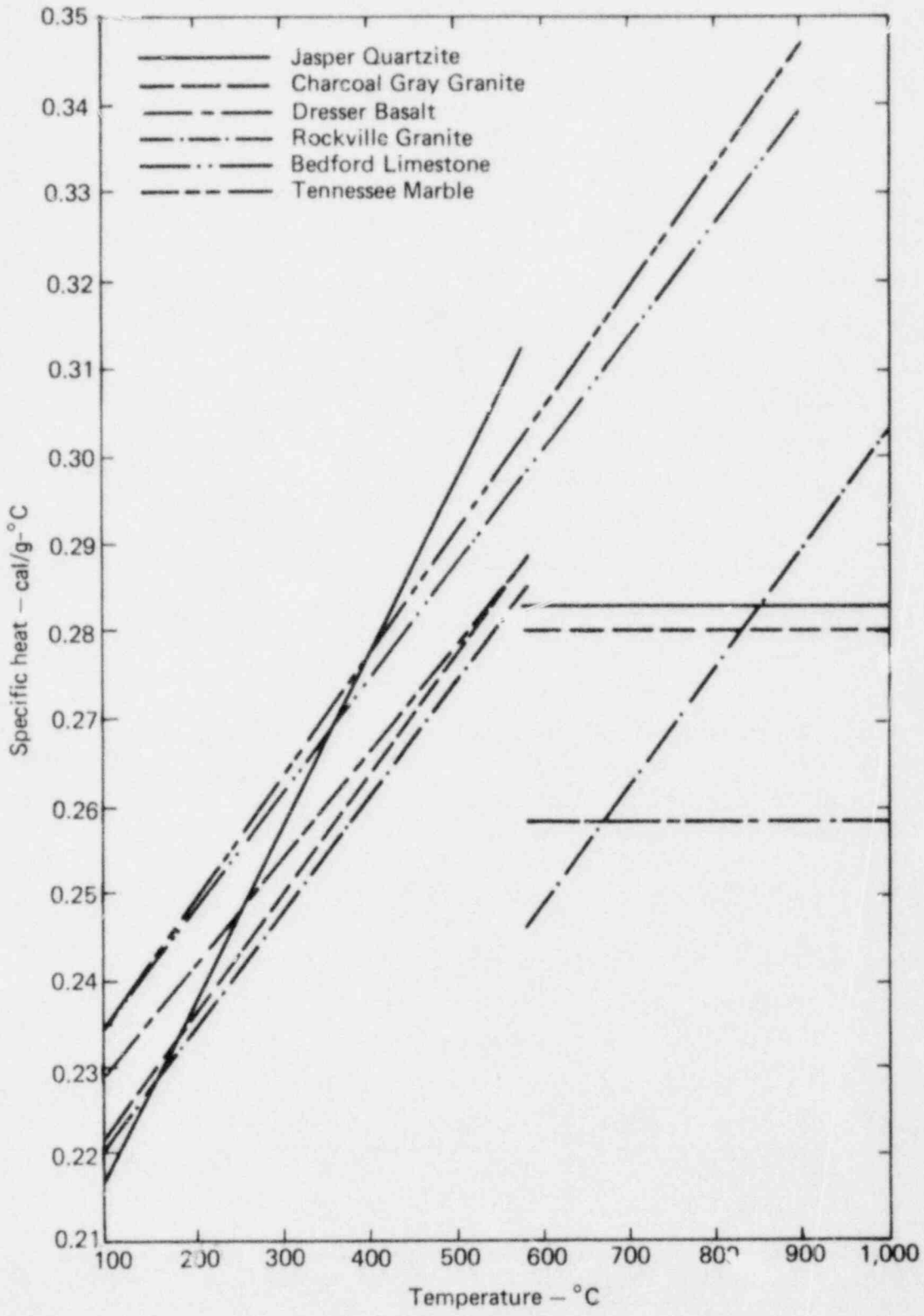

FIG. 2-33. Specific heats for six rock types (from Lindroth and Krawza, 1971).

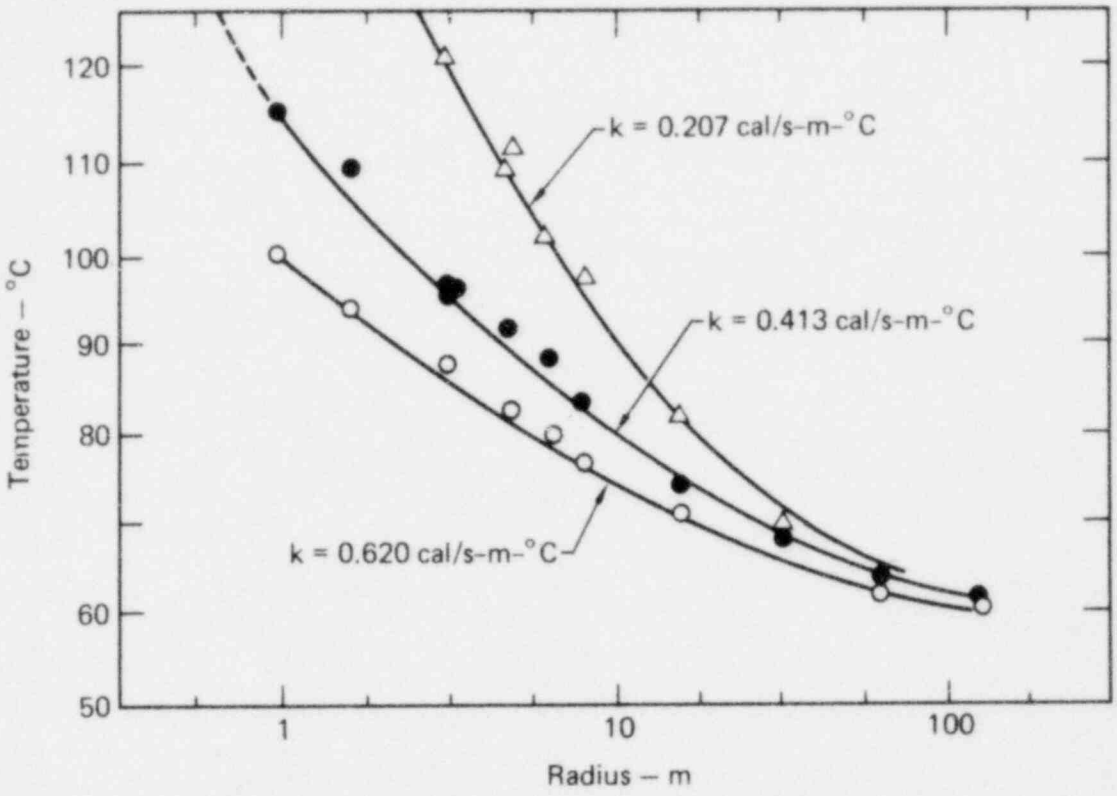

FIG. 2-34. Cavern temperature vs cavern radius for various values of the thermal conductivity k (from NWTSP, 1976, Vol. 1). The heat generation rate was taken to be 54.0 cal/s-m-^{o}C.

Thermoelastic Properties

Elastic properties include Poisson's ratio, Young's modulus, and the coefficient of linear thermal expansion. Tables 2-21 through 2-24 and Fig. 2-35 show the effect of temperature on the elastic modulus and Poisson's ratio of various basalts and basaltlike rocks. For Dresser Basalt, an increase in temperature from 297 to 866^{o}K is accompanied by a reduction in modulus from 100 to 66 GPa. For the same temperature range, Poisson's ratio is reduced by about half.

Little data is currently available regarding the relationship between compressive strength and temperature. Figure 2-36 reveals that under static loading, the strength of Dresser Basalt decreases dramatically between 0 and 400^{o}K but then levels off. The twofold decrease in strength between room temperature and 400^{o}K is of great importance, since the rock near a waste canister would undergo such a change.

TABLE 2-21. Influence of temperature and pressure on the elastic properties of some basaltic rocks.

Rock and origin	Density, kg/m^3	Temperature, ^oK	Pressure, MPa	Young's modulus, GPa	Poisson's ratio
Basalt, hornblende, Chaffee County, Colo.	2586	298	50	67.5	0.246
			500	70.8	0.269
		573	50	63.7	0.240
			500	69.7	0.276
"San Marcos" Gabbro, Escondido, Calif.	2[illegible]	298	50	96.0	0.363
			500	99.8	0.375
		573	50	88.3	0.334
			500	98.1	0.370
Gabbro, bylownite, Duluth, Minn.	2885	298	50	90.1	0.343
			500	95.3	0.362
		573	50	78.1	0.303
			500	90.1	0.344
Gabbro, hornblende, location unknown	2933	298	50	98.1	0.378
			500	105.4	0.407
		573	50	87.8	0.345
			500	103.7	0.403

TABLE 2-22. Experimental values of Young's modulus and Poisson's ratio at elevated temperatures for Dresser Basalt (from Wingquist, 1969).

Temperature, ^oK	Elastic modulus, GPa	Poisson's ratio
297	100.7	0.24
395	98.6	0.24
533	95.1	0.22
644	87.6	0.19
755	83.4	0.18
811	79.9	0.16
866	66.5	0.11

TABLE 2-23. Elastic moduli for Dresser Basalt (from Wingquist, 1969).

	Temperature, °C								
	24	121	260	371	482	538	593	704	815.5
Young's modulus, GPa:									
Sample 1	103.4	101.4	97.9	89.0	84.8	--	67.0	49.0	48.5
Sample 2	99.3	97.2	93.1	86.2	82.1	80.0	65.0	44.6	44.9
Sample 3	99.3	97.9	94.5	86.9	82.8	80.0	67.7	48.3	48.1
Mean	100.7	98.6	95.2	87.6	83.4	80.0	66.6	47.3	47.2
Std dev	2.41	2.21	2.48	1.45	1.45	0.0	1.38	2.41	1.93
Shear modulus, GPa:									
Sample 1	41.7	40.7	40.1	37.2	36.0	--	30.4	23.1	22.8
Sample 2	40.0	39.1	38.1	36.0	34.8	34.1	29.5	20.6	21.6
Sample 3	40.5	39.9	38.8	36.6	35.4	34.3	30.3	22.9	22.6
Mean	40.7	3.99	39.0	36.6	35.4	34.2	30.1	22.2	22.3
Std dev	0.828	0.828	1.03	0.621	0.621	1.38	0.483	1.38	0.690
Poisson's ratio:									
Sample 1	0.24	0.25	0.22	0.19	0.18	--	0.10	0.06	0.06
Sample 2	0.24	0.24	0.22	0.20	0.18	0.17	0.10	0.08	0.04
Sample 3	0.23	0.23	0.22	0.19	0.17	0.16	0.12	0.06	0.06
Mean	0.24	0.25	0.22	0.19	0.18	0.16	0.11	0.07	0.05
Std dev	0.01	0.01	0.00	0.01	0.01	0.01	0.01	0.01	0.01

TABLE 2-24. Properties of Dresser Basalt (from Lehnhoff and Scheller, 1975).

Temperature, ^{o}C	Young's modulus, 10^5 MPa	Poisson's ratio	Coeff. of thermal expansion, 10^5 $^{o}C^{-1}$
24	1.007	0.24	0.290
122	0.9860	0.24	0.500
260	0.9510	0.22	0.770
371	0.8760	0.19	0.940
482	0.8340	0.18	1.020
538	0.7990	0.16	1.080
593	0.6650	0.11	1.160
700	0.0010	0.10	1.160

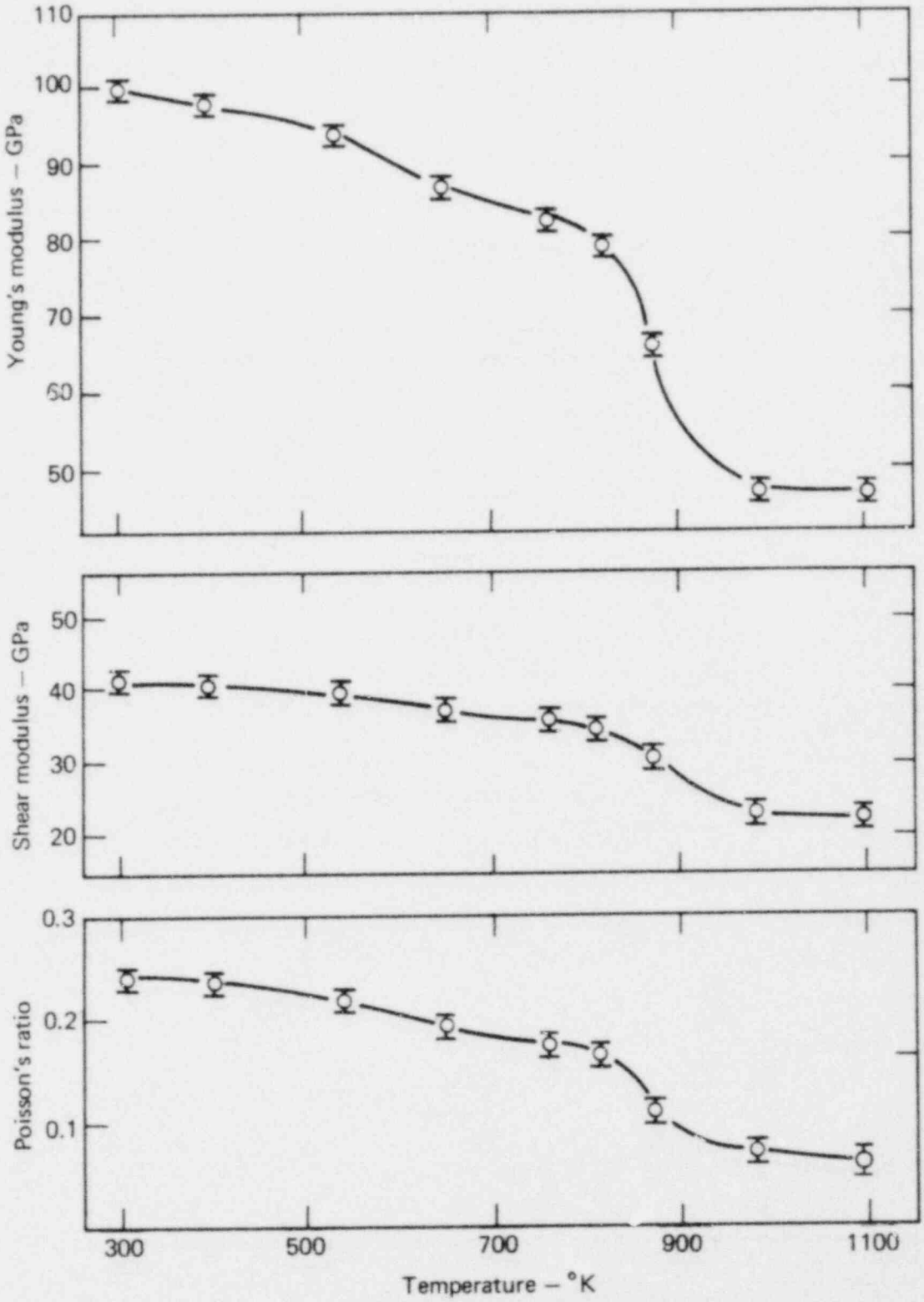

FIG. 2-35. Elastic moduli and Poisson's ratio as functions of temperature for Dresser Basalt (from Wingquist, 1969).

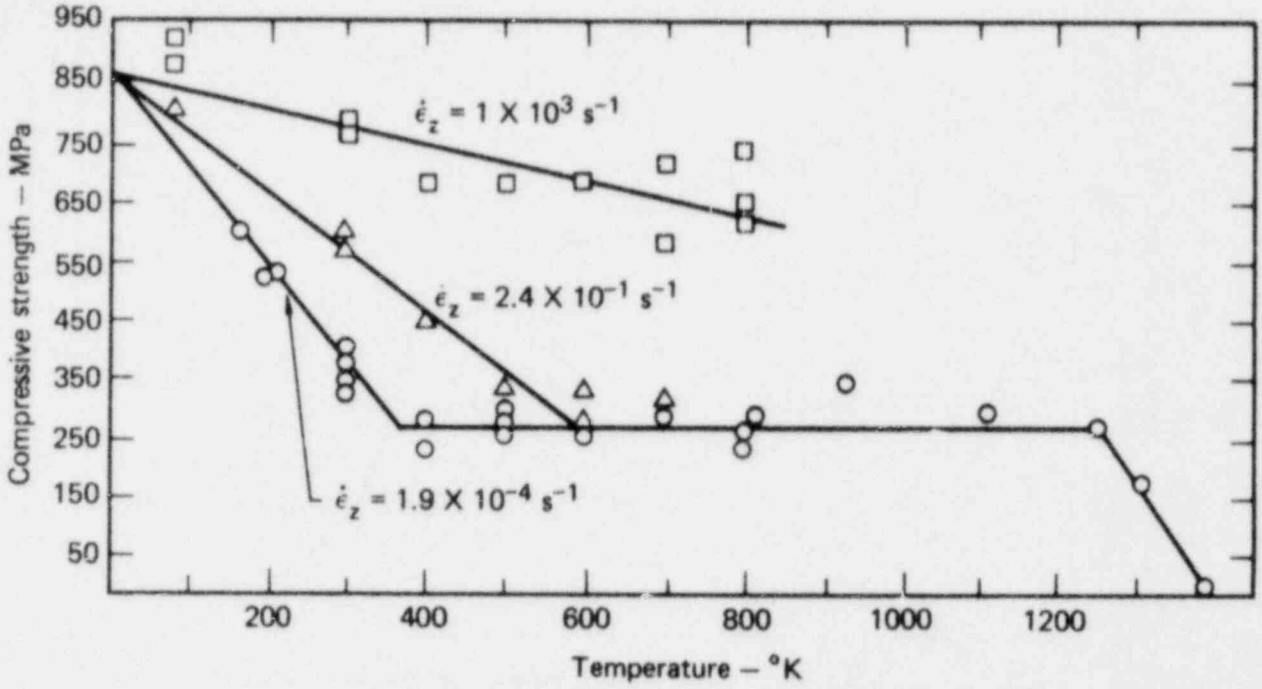

FIG. 2-36. Influence of temperature and strain rate on the strength of Dresser Basalt (from Krumer, 1968).

Average values of the coefficient of linear thermal expansion for a number of rocks are given in Table 2-25. This coefficient, however, has been found for most rocks to depend on temperature, as shown for Dresser basalts in Table 2-24.

If there is any gap between the canister and the rock (as will most certainly be the case in any practical situation), thermally induced stresses and displacements can cause the material directly around the canister to degrade or spall as it is heated. The effects of this thermal degradation can be evaluated by numerical models. Hardy and Hocking (1977), for example, examined the influence of changes in the thermal conductivity which result from the failure of the basalt. The coupling between thermal and mechanical response, which was used to model the effects of borehole decrepitation, was based on a volumetric strain-dependent thermal conductivity (Fig. 2-37). Hardy and Hocking argued that this type of coupling is supported by observation, since during rock failure microcracks and void spaces develop and hence the volumetric strain increases. The development of such voids in the rock will lead to a reduced thermal conductivity, thereby restricting the flow of heat from the canister into the rock. The assumed conductivity-strain relationship leads to a radial variation in the thermal conductivity, as shown in Fig. 2-38.

TABLE 2-25. Coefficient of linear thermal expansion for several basaltic rocks (from Agapito et al., 1977).

Rock type	Expansion coefficient 10^{-6} $^{o}C^{-1}$
Basalts, gabbros, diabase	5.4
Basalt ($300^{o}K$)	4.3-6.5
Fairfax Diabase	5.9
Cape Neddick Gabbro	8.5
Dresser Basalt	2.9-11.6

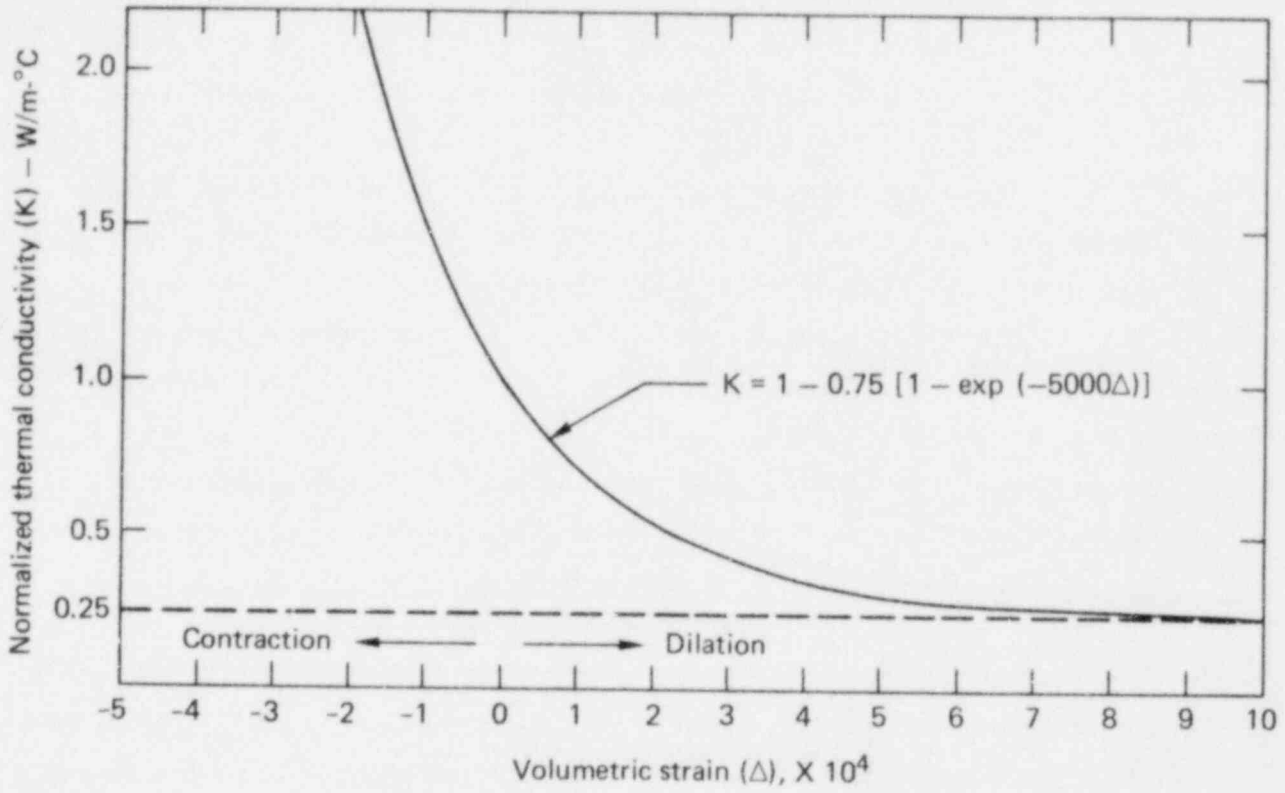

FIG. 2-37. Thermal conductivity-volumetric strain relationship assumed by Hardy and Hocking (1977).

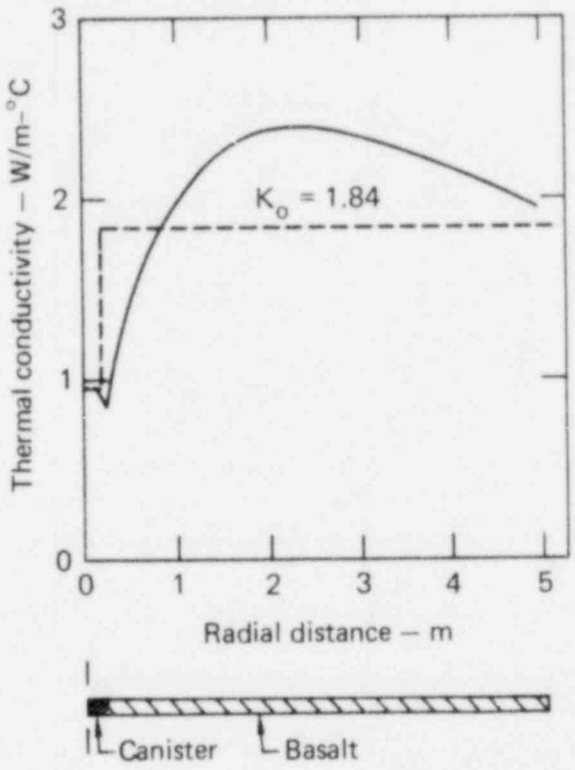

FIG. 2-38. Thermal conductivity as a function of radial distance after 28 days. This curve illustrates the result of Hardy and Hocking's (1977) analysis, which assumed the conductivity-strain relationship of Fig. 2-37.

The expected temperatures for the case with thermomechanical coupling can be compared with the case for constant thermal conductivity (Fig. 2-39). The comparison shows that, for a 1-kW heat source, the reduced thermal conductivity of the rock adjacent to the canister causes a 20% increase in the canister temperature. This cannot be considered significant. For higher thermal outputs, however, increased rock failure could produce a more extensive zone of reduced conductivity, thus leading to thermal runaway. No laboratory data are available to support the thermal conductivity-volumetric strain curve shown in Fig. 2-37, but since its consequences are so severe (breakdown of waste forms, greatly reduced canister life, etc.), data must be made available.

A summary of thermomechanical properties for basalt as prepared by Agapito et al. is given in Table 2-26.

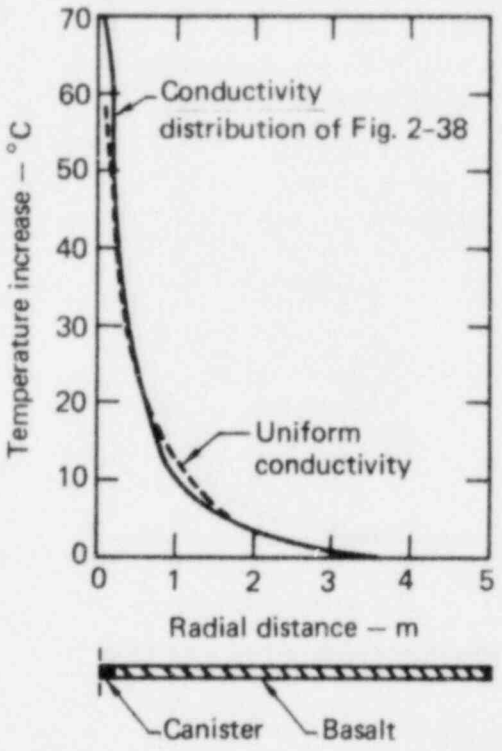

FIG. 2-39. Comparison of temperature distributions for two cases: uniform conductivity and the conductivity distribution of Fig. 2-38 (from Hardy and Hocking, 1977).

TABLE 2-26. Summary of thermomechanical basalt properties (from Agapito et al., 1977).

Property	Estimated value	Range	Major influence
Density, g/m^3	2.9×10^6	2.4×10^6 to 3.1×10^6	Porosity
Diffusivity, m^2/s	6.5×10^{-7}	5.2×10^{-7} to 8.0×10^{-7}	Porosity
Thermal conductivity, W/m-^oC	1.5	1.4-4.28	
Specific heat, kJ/kg-^oC	1.0	0.95-1.05	
Thermal expansion coefficient, $^oC^{-1}$	5.4×10^{-6}	2.9×10^{-6} to 11.6×10^{-6}	Temperature
Young's modulus, GPa	70	61-112	
Poisson's ratio	0.26	0.22-0.28	
Uniaxial compressive strength, MPa	200	0-400	Porosity, jointing
Angle of internal friction, deg	55	45-60	Jointing
Tensile strength, MPa	14	0-23.0	Jointing

Other Considerations

Because of the elevated temperatures and the long life of the repository, the possibility of long-term creep deformation must be considered. Unfortunately, the time-dependent behavior of basalt over the temperature and stress ranges of interest for radioactive waste disposal is not well documented.

The compressive strength as a function of creep rate for Amchitka basalt is shown in Table 2-27. Dense basalts appear to have a low uniaxial creep rate and seem to exhibit a minimum average amount of irrecoverable strain. Some creep curves for basalt, as presented by Iida et al. (1960), are shown in Fig. 2-40. All of the tests represented were performed at approximately room temperature.

TABLE 2-27. Creep and failure characteristics of Amchitka Island rocks under uniaxial compressive stress (from Sharp, 1972).

	Creep rate,[a] microstrains/h	Irrecoverable strain,[b] %
Chitka Point Formation, hornblende pyroxene andesite:		
Av value	1.3	4.7
Max value	4.0	10.9
Min value	0.1	0.2
No. of samples	5	5
Std dev	1.4	4.4
% variation	106	92
Chitka Point Formation, dense flow breccia:		
Av value	1.3	21.2
Max value	--	--
Min value	--	--
No. of samples	1	1
Std dev	--	--
% variation	--	--
Chitka Point Formation, tuff breccias:		
Av value	2.8	5.4
Max value	3.0	8.9
Min value	0.8	1.6
No. of samples	3	3
Std dev	1.2	8.6
% variation	56	68
Banjo Point Formation, breccia:		
Av value	1.0	4.7
Max value	1.8	10.0
Min value	0.5	0.4
No. of samples	6	6
Std dev	0.5	3.1
% variation	47	67

continued

[a]Extrapolated to 200 minutes.

[b]After loading to one-half ultimate strength.

TABLE 2-27 continued.

	Creep rate,[a] microstrains/h	Irrecoverable strain,[b] %
Dense basalt:		
Av value	1.0	2.7
Max value	1.1	4.5
Min value	0.9	0.8
No. of samples	2	2
Std dev	--	--
% variation	--	--
Amchitka Formation, Kirilov Point glassy breccia:		
Av value	2.8	9.0
Max value	3.0	10.6
Min value	2.6	7.3
No. of samples	2	2
Std dev	--	--
% variation	--	--
Amchitka Formation, Kirilov Point pillow lavas:		
Av value	0.9	1.7
Max value	1.4	2.1
Min value	0.4	1.3
No. of samples	2	2
Std dev	--	--
% variation	--	--
Amchitka Formation, dense older breccia:		
Av value	1.7	5.4
Max value	2.5	8.2
Min value	0.7	2.6
No. of samples	4	4
Std dev	1.0	2.5
% variation	58	46

continued

TABLE 2-27 continued.

	Creep rate,[a] microstrains/h	Irrecoverable strain,[b] %
East Cape quartz diorite		
Av value	1.5	11.6
Max value	3.0	17.1
Min value	0.4	4.6
No. of samples	5	5
Std dev	1.1	5.7
% variation	71	51

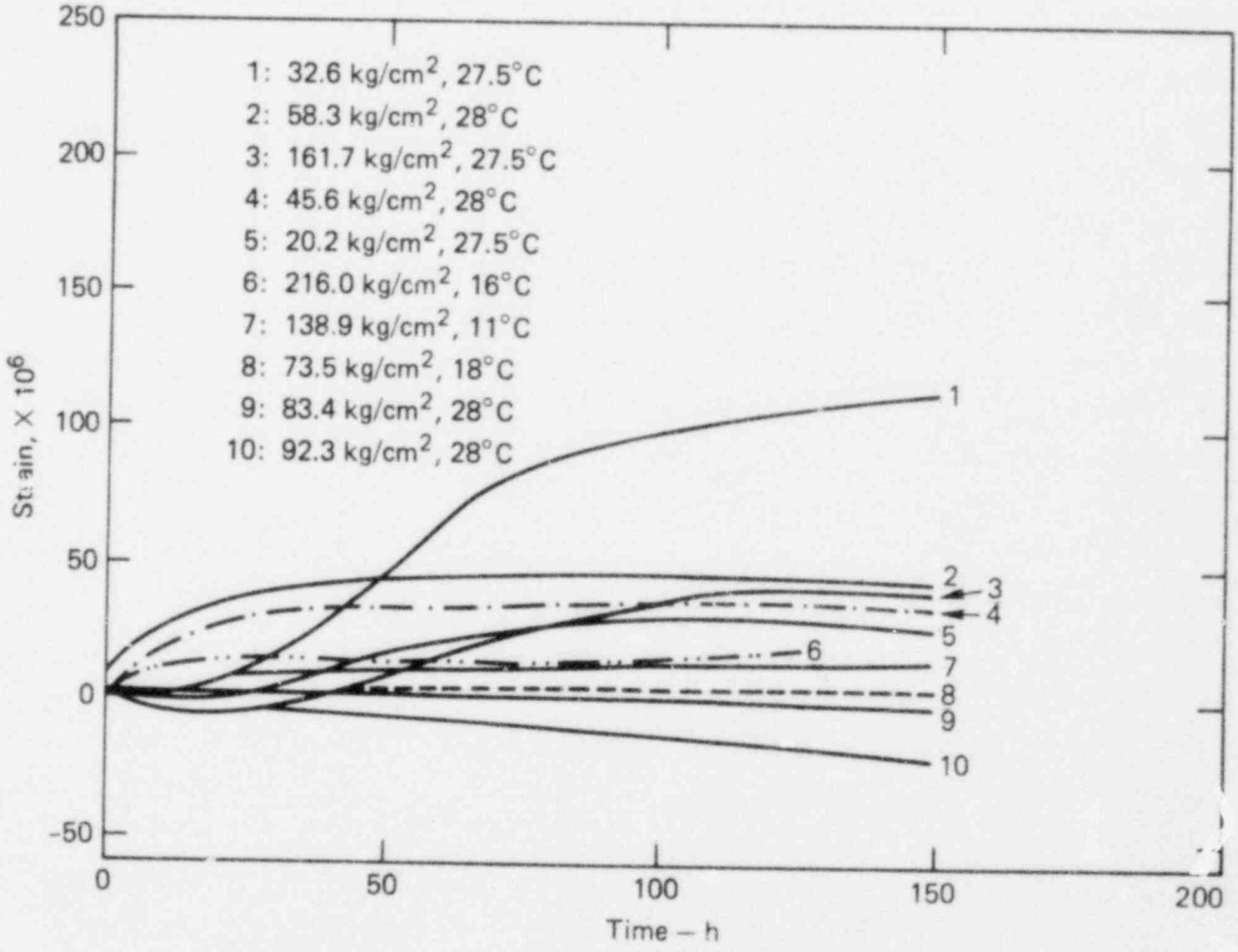

FIG. 2-40. Creep curves for basalt (from Iida et al., 1960).

Scaling of Laboratory Results

As described earlier, basalt can vary considerably in the flows, both horizontally and vertically. A significant structural characteristic of many basalts, one that varies widely, is their jointing pattern. Because of jointing, among other factors, it is expected that intact properties of basalt will be considerably different from the rock-mass properties, which will be products of the complex interaction of the intact rock, the joint system, joint filling, and water.

In their report, ONWI (1978, Vol. 7) presented a discussion of how one might infer rock-mass values from intact values. They concluded that, for two important design parameters, namely Young's modulus and unconfined compressive strength, the rock-mass values are typically much smaller than the intact values. The ratio of the former to the latter value is the reduction factor. Reduction factors can be evaluated by directly measuring rock-mass properties, but no large-scale field tests have been reported in the literature. Among the structural variations that must be accounted for by reduction factors are those listed in Table 2-28.

The rock-mass properties of a typical dense basalt, representative of the lower portion of a thick flow, are given in Table 2-29. The moduli and

TABLE 2-28. Partial description of typical structures in basalt (from ONWI, 1978).[a]

	Sample A	Sample B	Sample C	Sample D
Type of joint	Joint	Joint	Joint	Joint
Filling	Hematite	Nontronite	Calcite	Clean
Orientation	0/85	100/90	230/80	160/10
Opening width	Tight	Tight	Tight	Tight
Spacing	>2 m	0.3-2 m	0.1-2 m	0.1-1 m
Waviness	Planar/rough	Planar/rough	Planar/rough	Planar/rough
Lengths of joints	≈6 m	≈4.5 m	≈9 m	≈3 m

[a]The typical rock quality designation for all samples was >95%; the typical fracture frequency was 0.5 to 6 per meter (horizontal) and 0.3 to 3 per meter (vertical).

TABLE 2-29. Intact properties for a typical dense basalt (from ONWI, 1978, Vol. 7).

	Intact value	Rock-mass value
Index properties:		
Density, g/cm^3	3.01	2.88
Porosity, %	2.0	0.6
Stress-strain properties:		
Young's modulus	69	12.4
Poisson's ratio	0.26	0.26
Strength properties:		
Uniaxial compressive strength, MPa	276	124
Tensile strength, MPa	16	0
Thermal properties:		
Coefficient of linear thermal expansion, 10^{-6} $^oC^{-1}$	1.7	1.7
Heat capacity, J/g-^oC, at:		
0^oC	0.71	0.71
100^oC	0.80	0.80
200^oC	0.92	0.92
300^oC	0.96	0.96
Thermal conductivity, W/M-^oC, at:		
0^oC	1.12	1.12
50^oC	1.19	1.19
100^oC	1.26	1.26
150^oC	1.32	1.32
200^oC	1.38	1.38
300^oC	1.47	1.47
400^oC	1.56	1.56

strength characteristics were determined by using reduction factors. The reduction factor for Young's modulus was based in part on the work of Panek (1970), which related the reduction factor to the fracture spacing and the width of the excavation. Joint spacing was taken to average about two feet in basalt. Jointing was considered to be less significant in reducing the value of rock-mass strength, hence the value of 0.45 for the reduction factor. Both of the reduction factors were based largely on intuition.

The nonlinear failure curve recommended by ONWI for a typical basaltic rock mass at room temperature is shown in Fig. 2-41. The unit weight of the basalt rock mass was taken to be 2880 kg/m^3. Thermal properties at depth were assumed to be similar to the intact properties.

Although ONWI assumed isotropic behavior, anisotropic behavior should be investigated at the design stage for a specific repository. For instance, detailed geological mapping and in situ testing will be required at the actual

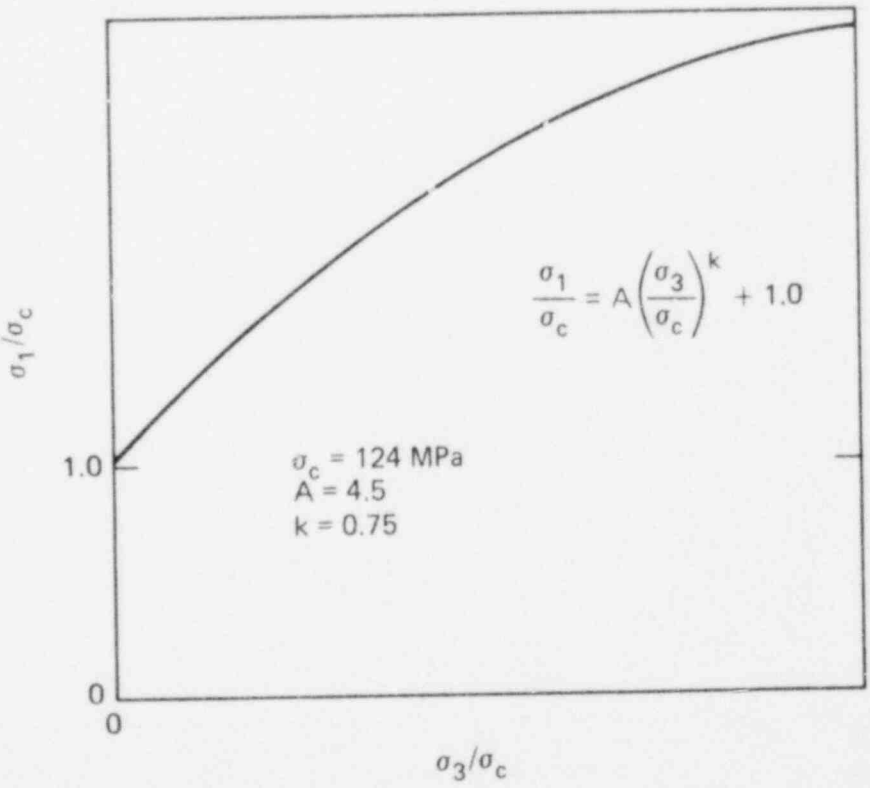

FIG. 2-41. Nonlinear failure curve for basaltic rock mass (from ONWI, 1978). The rock strength (σ_1) depends on the confining stress (σ_3) and the assumed unconfined rock-mass strength (σ_c).

site of the underground repository. Furthermore, since the value of the unconfined rock-mass strength was based on an estimated reduction factor, the failure curve of Fig. 2-41 must be used cautiously.

In Table 2-29, in which intact properties are compared to rock-mass properties for a typical dense basalt, ONWI offered no justification for the reduction factors (other than those for modulus and compressive strength). Thermal expansion, for example, is indicated to be the same for the intact rock and the rock mass. This is probably far from the case. The presence of joints in a rock mass influences its elastic properties, strength, thermal conductivity, and thermal expansion coefficient. The stress across the joint influences all these properties, and since the stress of the joints will change during the mining of the repository, the response of the joints during and after this stress change is of primary concern. The effect of joints on several rock properties is shown in Figs. 2-42 through 2-44. No quantitative information was found on joint stiffness, either shear stiffness or normal

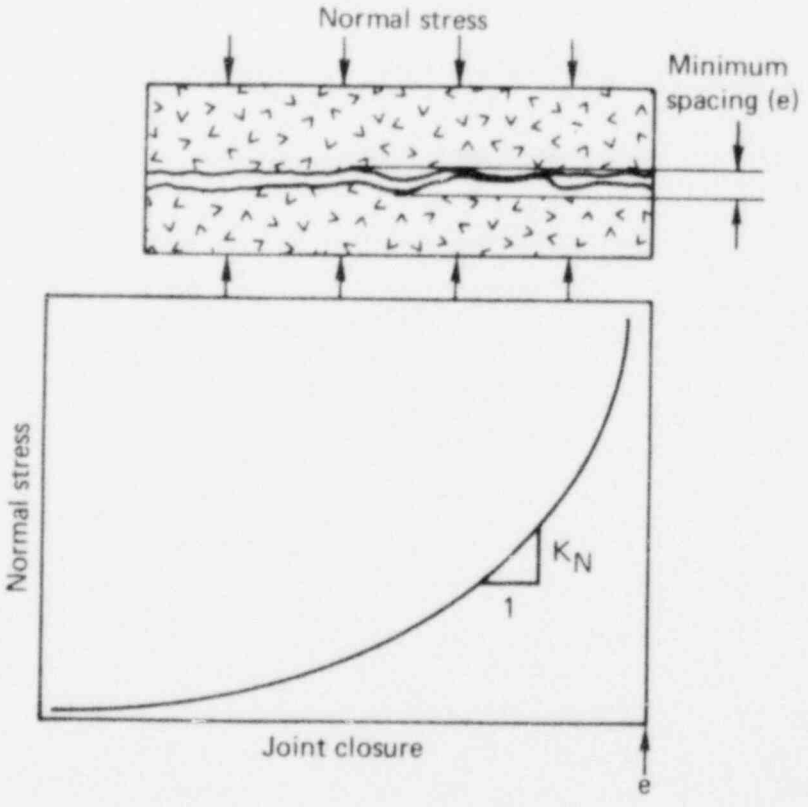

FIG. 2-42. Influence of normal stress and joint closure on the normal stiffness (K_N) of a joint (from Agapito et al., 1977).

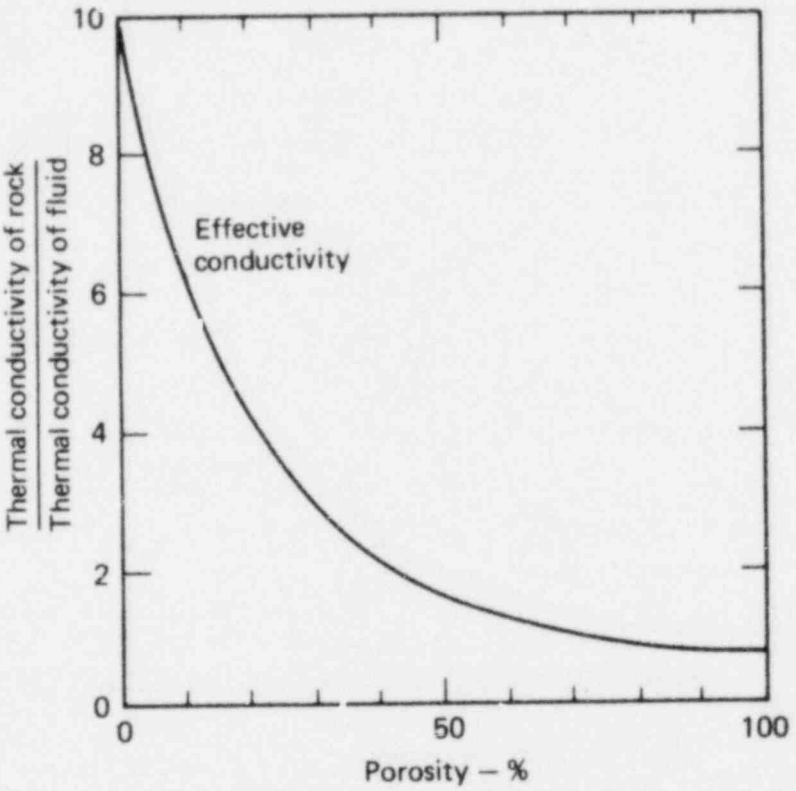

FIG. 2-43. Idealized relationship for the thermal conductivity of porous material with fluid-filled joints (from Agapito et al., 1977).

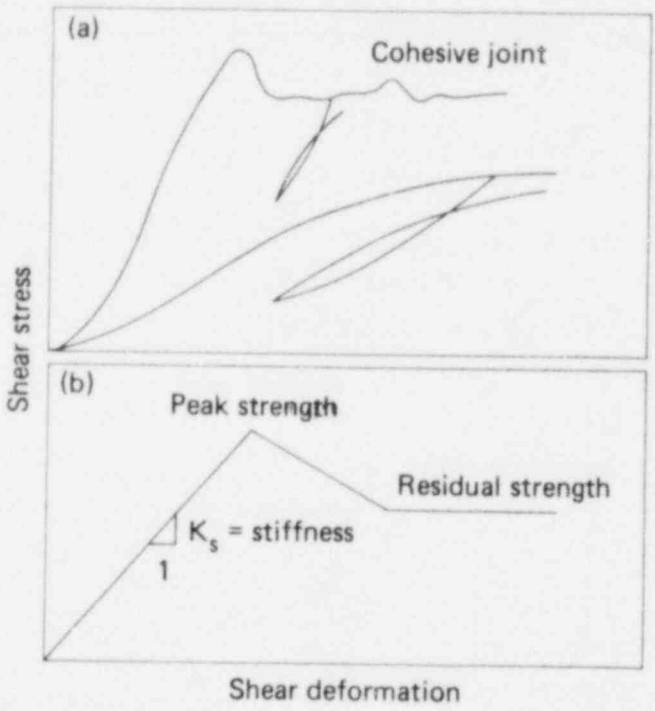

FIG. 2-44. Typical shear stress and shear deformation response of joints (from Agapito et al., 1977). (a) Experimental responses of two joints, (b) idealized representation of joint response.

stiffness. Coulson (1970) has performed shear strength testing on artificial surfaces which were cut and sandblasted, then lapped with various grades of material. The data shown in Fig. 2-45 thus constitutes the current data base for basalt regarding the behavior of joints.

Before scoping studies and detailed quantitative evaluations can be made, the mechanical, thermal, and thermal-mechanical properties of basalt must be determined, both in situ and in the laboratory under carefully controlled conditions. Currently, the data required for any significant modeling do not exist. The modelers, however, should be working in close cooperation with the experimentalists to construct the experiments required to provide the input data. (For more on the modelers' role, see Chapter 3 of this volume.)

HYDROLOGY

Groundwater flow in a basalt sequence occurs through both porous intergranular and nonporous fractured media. The mechanics of flow through both will be discussed in Chapter 3. This section presents a summary of the hydrologic characteristics of basalt flows and discusses porosity, permeability, and groundwater flow regimes through basalt sequences of the Columbia Plateau, the Snake River Plain, and the Modoc Plateau.

Porosity, Hydraulic Conductivity, and Groundwater Flow Regimes

Variations in hydraulic conductivity (K) and porosity (ϕ) among flows, and even within single flows, is so great that assigning average values of K and ϕ for a generic basalt would be arbitrary and misleading. However, some generalizations about groundwater flow through basalt may be offered without trying to assign definitive or representative values for hydrologic parameters.

The permeability of basaltic sequences is highly anisotropic. Horizontal components of permeability generally greatly exceed vertical components. Furthermore, within a given flow, permeabilities are generally much greater near the upper and lower margins of the flow than in its center. While jointing in the entablature and lower colonnade does contribute to groundwater flow, permeabilities of Zones I, II, and VII of the flow unit (Fig. 2-3) are generally much higher. Principal flow regimes within a basalt sequence may be categorized as follows:

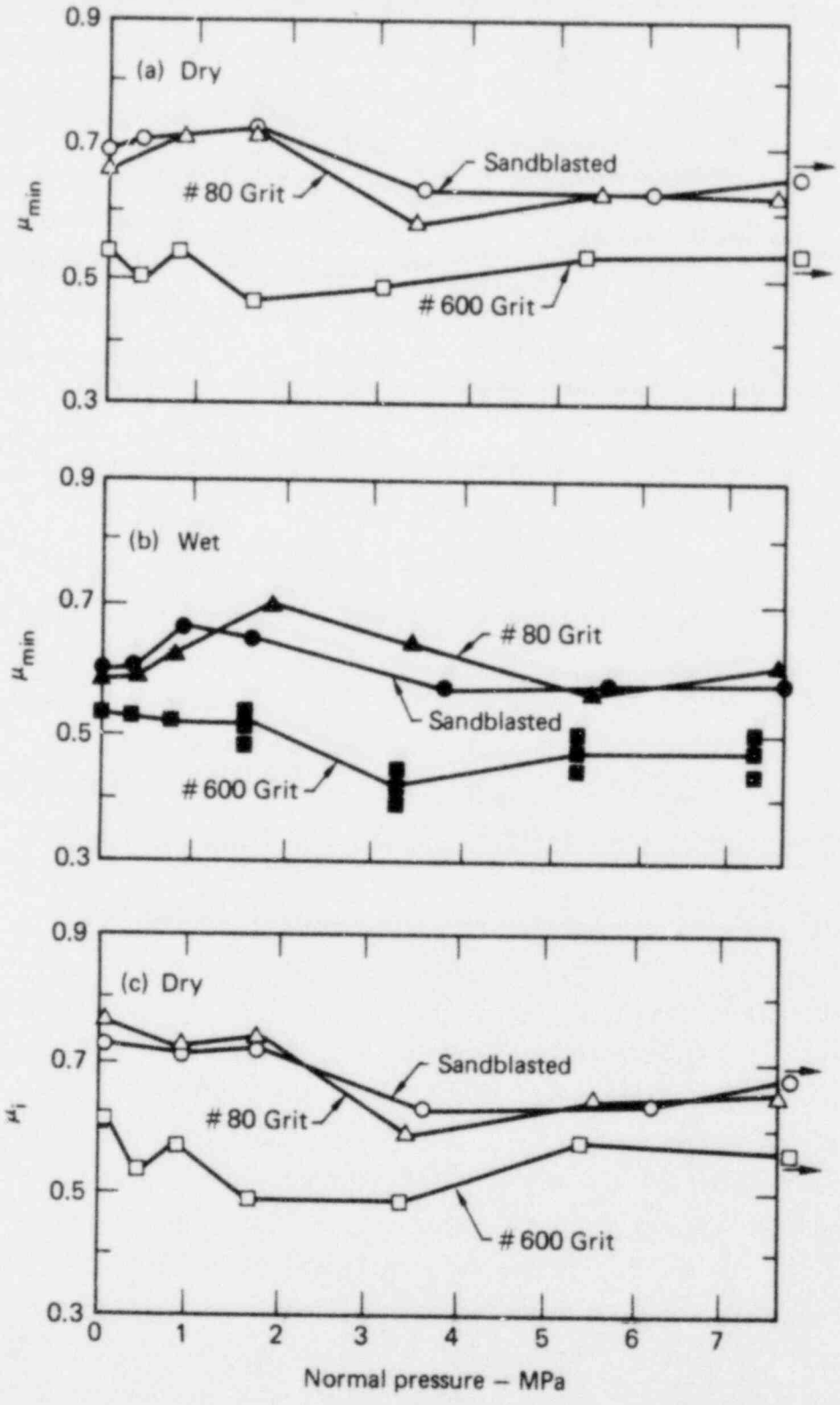

FIG. 2-45. Coefficients of friction as functions of normal pressure for lower-granite basalt (from Coulson, 1970). (a) and (b) minimum coefficients, (c) and (d) initial coefficients, (e) and (f) residual coefficients.

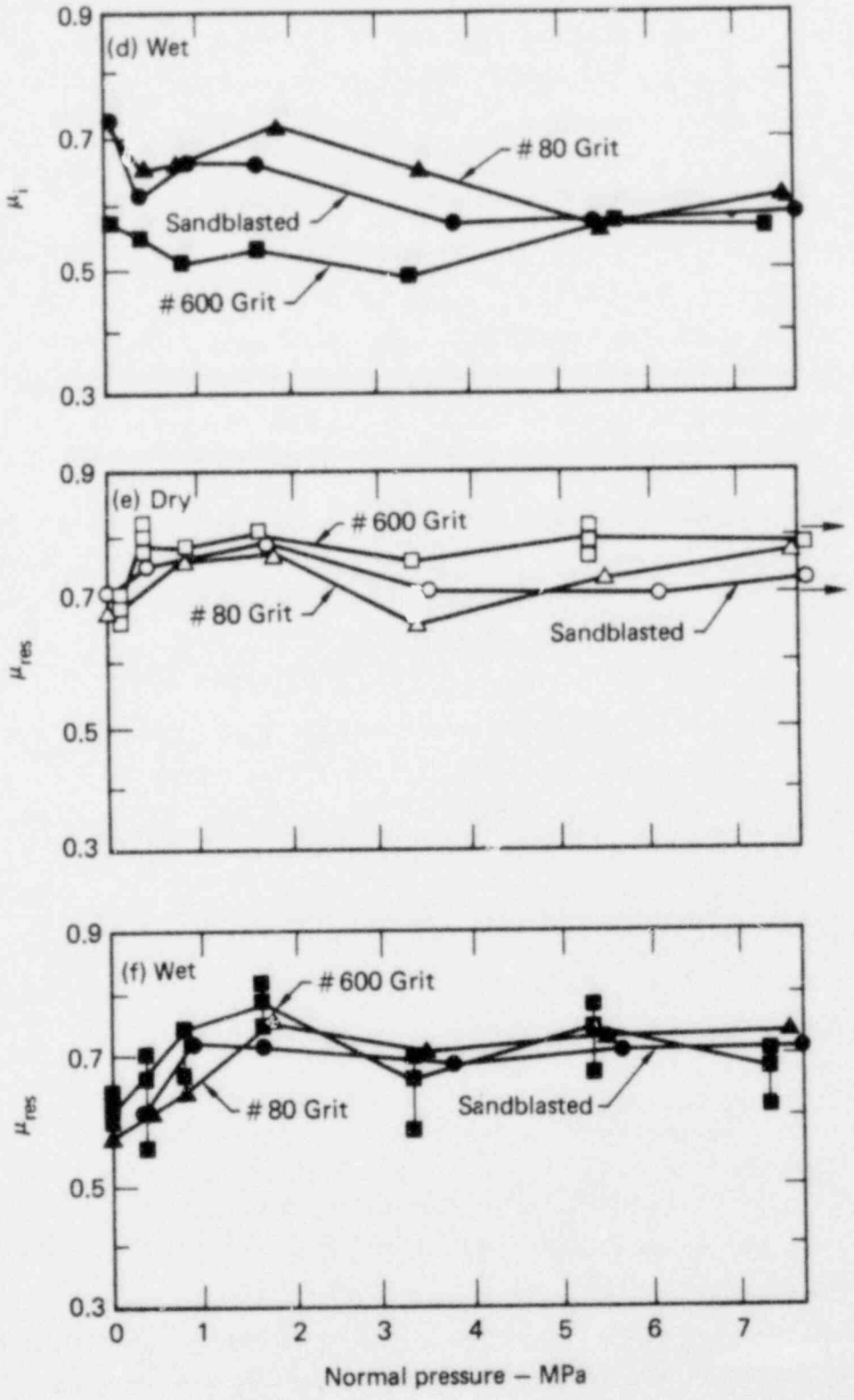

FIG. 2-45 continued.

- Interflow regions. Interfaces between flows, or the interfaces between flows and interbeds, provide some of the most permeable regimes for flow within the basaltic sequence. Rubble zones, scoria, weathered surfaces, fracture-connected vesicles, and interflow voids in Zones I and II on the upper surface of a flow and in Zone VII of an overlying flow often provide highly pervious media.

- Interbeds. Interbeds, or sediments deposited between volcanic events, are highly varied in character. Fluvial sands and gravels, as well as some sandy lacustrine deposits, constitute highly permeable zones between lava flows. On the other hand, interbeds composed of lacustrine silts and clays are much less permeable and often act as aquitards or aquicludes in the sequence.

- Joints. Joints in flows on the Columbia Plateau range from less than a centimeter to several meters in width. These joints are the principal means of vertical movement of groundwater through a basalt sequence and are also often an important means of horizontal flow.

- Other features. Lava tubes, breccia pipes, and fault zones all form localized features which can dominate groundwater flow. However, these features are uncommon in the northwest basalts, thus reducing their importance for regional flow. A waste repository will probably not be sited near highly permeable groundwater conduits such as these.

Ranges of values of hydraulic conductivity, measured in various basalts of the northwest United States, are summarized in Fig. 2-46. Specific hydrologic data for a few Columbia River basalts will be presented later in this section.

Hydrology of the Columbia River Basalt (Pasco Basin Sequence)

The Pasco basin has often been suggested as a potential site for a deep repository, because it appears to possess the smallest quantity of usable ground water per unit surface area of any of the structural basins (Deju et al., 1977). The basin has numerous thin beds of clay-rich sediment and saprolite, which were deposited between outpourages of Columbia River Basalt. This material has since plugged pore and fracture spaces, reducing the rate of groundwater movement and hydraulically separating individual interflow zones. Pumping data from the Columbia River Basalt within the Pasco basin show that

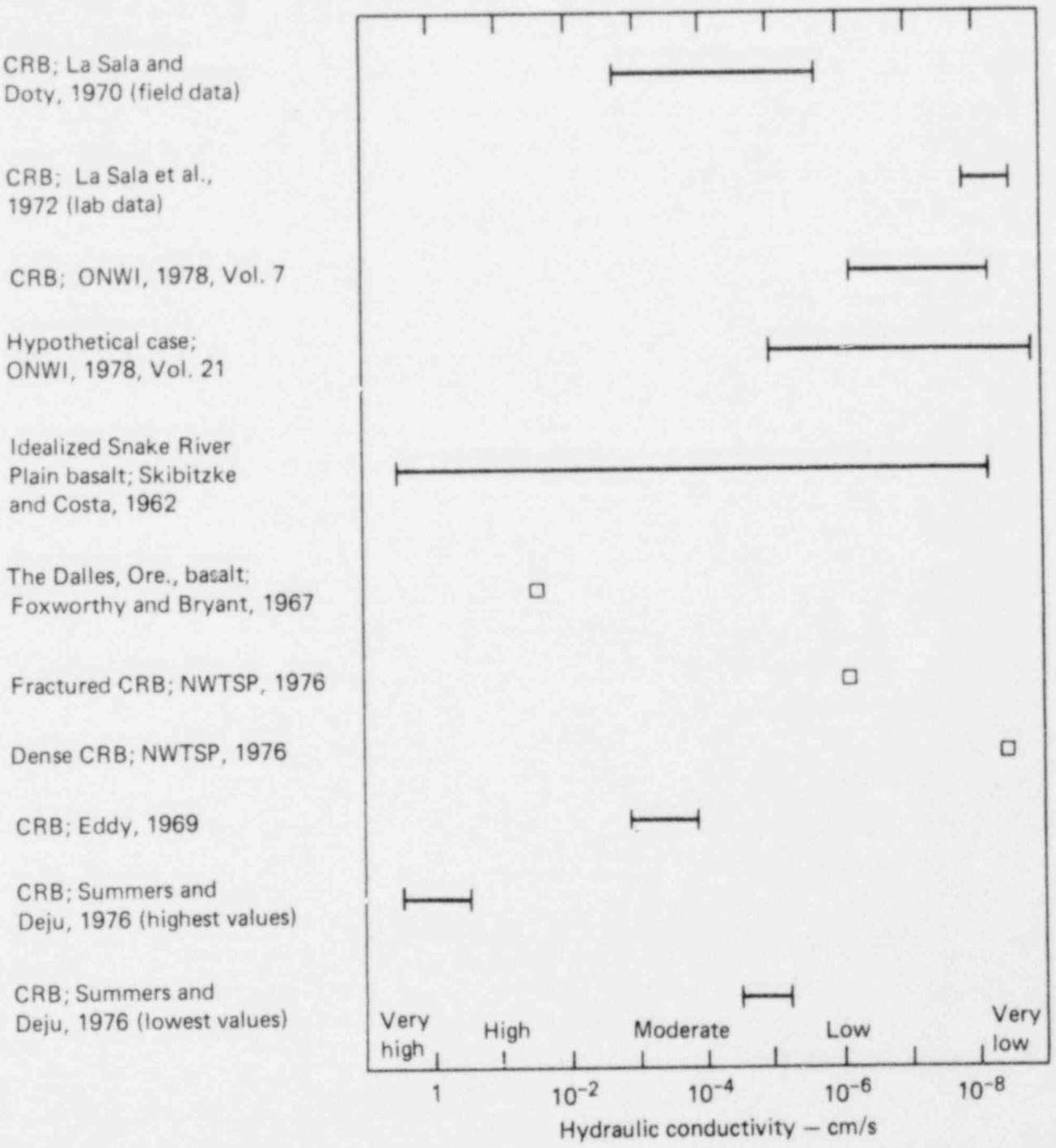

FIG. 2-46. Hydraulic conductivity data from basalts in the northwest United States. CRB denotes Columbia River Basalt.

no large amounts of water have been obtained. The basalts themselves offer zones as thick as 200 m that are fully dry (Deju et al., 1977).

Since the siting of the Hanford facility in the Pasco basin, more hydrologic data on deep rock units have been collected for this area than for most of the remainder of the plateau. Testing of the deep basalts at Hanford began in 1969 with the drilling of well ARH-DC-1. Since then, several more wells have been constructed, and additional wells have been proposed (Apps et al., 1978, 1979). The results of the tests conducted at the DC-series wells at Hanford constitute much of the geologic and hydrologic data available for the basin and for the deep basalts of the Plateau in general.

At Hanford an unconfined aquifer overlies the basalts. This aquifer consists of the basal portions of the glaciofluvial sediments and extends downward to the clay layers at the base of the Ringold Formation. These layers act as an effective aquitard, confining waters in lower formations. A large body of data is available on the shallow sedimentary aquifer. Summaries of these data are found in the reports of the NWTSP (1976) and the Committee on Radioactive Waste Management (CRWM) (1978).

Of principal significance to the deep burial of nuclear waste are the confined aquifers at Hanford. These comprise the lowermost portion of the Ringold Formation and the underlying Columbia River Basalt Group. The general hydrologic characteristics of the stratigraphic sequence at Hanford are summarized in Fig. 2-47.

General Characteristics of Groundwater Flow. Within the sequence of Miocene basalt flows, the zones of highest permeability, as determined from packer tests of the Hanford test wells, are the interflow zones separating basalt flows. These interflow zones consist of rubble and porous sediments deposited between flow events. The central volume of most basalt flows is quite dense and has a very low permeability. Fractures, formed during the cooling of the molten rock or during subsequent structural deformation, are the dominant hydraulic interconnection between basalt units. In many instances, secondary mineralization has effectively sealed these fractures to further groundwater movement. In addition, fracture spacing diminishes as depth increases. The hydraulic separation of individual water-bearing strata is apparent when the water levels at the top and bottom of some basalt flows are compared (Deju et al., 1977). Figure 2-48 illustrates this confinement of individual zones of higher permeability in the Hanford well ARH-DC-1.

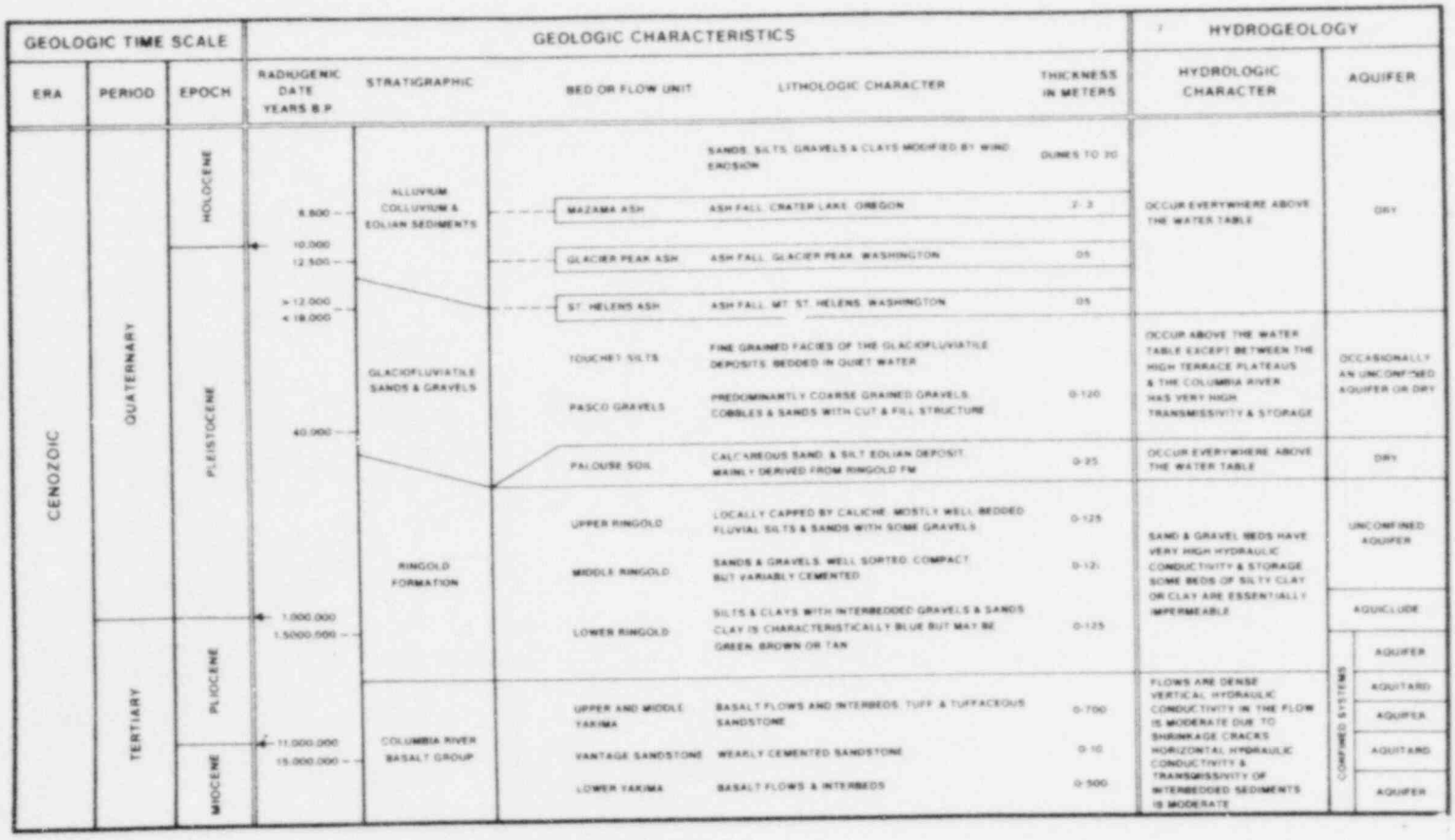

FIG. 2-47. Hydrostratigraphic characteristics of the Pasco basin (from NWTSP, 1976).

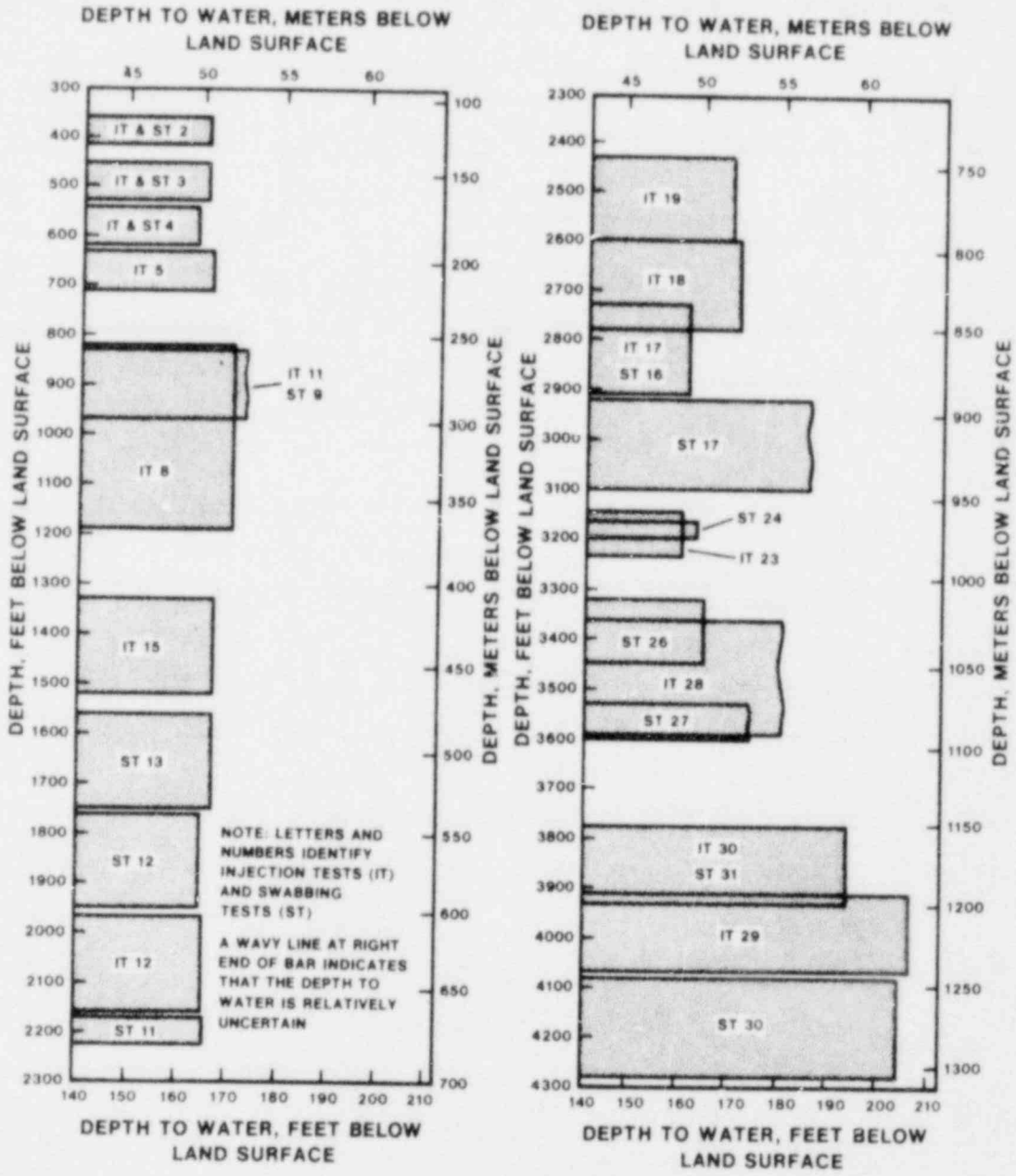

FIG. 2-48. Approximate undisturbed groundwater heads, measured in 1969, for isolated water-bearing zones in well ARH-DC-1 (from NWTSP, 1976).

Porosity. The porosity of rocks in the flood basalt sequence is not well defined. Porosity within flows is primarily attributable to fracturing and voids in rubble zones at the flow margins. If the fractured rock is vesicular, effective porosity is increased by the volume of vesicles that are parted by fractures. For basalt penetrated by borehole ARH-DC-1, values of mean porosity were calculated by a commercial logging firm as follows: dense, 1%; vesicular, 5%; and zone of close fractures, 10% (Fenix and Scisson, 1969). These estimates were developed using log interpretation principles designed for sediments with intergranular porosity. They are not determinations of effective porosity and should be considered only order-of-magnitude estimates.

Hydraulic Conductivity. Although additional well-testing work continues (Apps et al., 1978, 1979), the bulk of published data on the hydraulic conductivity of the basalt sequences in the Pasco basin is from tests of well ARH-DC-1. This well penetrated the basalts to a depth of 1725 m, and in-hole permeability tests were conducted to 1305 m. In addition, laboratory permeability tests were conducted on core samples from specific zones of interest.

Those zones identified in packer tests of well ARH-DC-1 as having the highest hydraulic conductivities are identified in Table 2-30. These zones

TABLE 2-30. Principal zones of high hydraulic conductivity in well ARH-DC-1 (from CRWM, 1978).

Depth, m	Description of beds	Hydraulic conductivity, m/d	Zone thickness, m
147	Sands/sands and clay		
181	Sands/sands and clay		
226	Sands/sands and clay	0.4-1.0	4.6-33
254	Sands/sands and clay		
344	Flow breccia		
626	--	2.7	2
803	Sands and tuff	0.6	3.7
983	Scoria or breccia	2	3
1210	Fractured basalt	0.5	15

have hydraulic conductivities ranging from 0.4 to 2.7 m/d. In the intervening zones, hydraulic conductivities were found to be much lower. The CRWM (1978) has classified the intervening materials and has assigned representative hydraulic conductivities to each class:

- Basalt, dense or with healed joints: about 67% of aggregate thickness, mean hydraulic conductivity about 6×10^{-4} m/d.
- Basalt, vesicular: about 7% of aggregate thickness, mean hydraulic conductivity about 9×10^{-4} m/d.
- Basalt, weathered or jointed: about 17% of aggregate thickness, hydraulic conductivity about 3×10^{-3} m/d.
- Tuff or sand: about 9% of aggregate thickness, mean hydraulic conductivity about 6×10^{-2} m/d.

To summarize, all the cited values of conductivity for water-yielding segments are of the order of 1 m/d; those for the remainder of the confined-water zone range between about 10^{-1} and 10^{-4} m/d. All the basalt in the confined-water zone of the Hanford reservation must be considered potentially transmissive, at least to some degree, for dissolved radioactive waste constituents.

In a report prepared for the NWTSP (1976), ranges are presented for the hydraulic properties of both the uppermost confined aquifer (Table 2-31) and various forms of basalt from the Lower Yakima flows (Table 2-32). In the Lower Yakima basalts, in situ measurements of hydraulic conductivity were found to be as low as 10^{-6} m/d for dense basalt.

Laboratory tests of cores taken from well ARH-DC-1 show the hydraulic conductivities to be about two orders of magnitude smaller than the average values determined from injection tests (Table 2-33). The difference in these measurements is explained by La Sala and Doty (1970):

> These differences in values of hydraulic conductivity result because these two types of tests measure different characteristics of the rocks. The field values of hydraulic conductivity were determined on a large volume of in-place rocks. The basalt, as can be seen in outcrops, is cut by shrinkage cracks and other fractures which are capable of transmitting water. The field hydraulic conductivities, therefore, apply not only to the ability of the basalt flows to transmit water through intergranular pore spaces, but also through fractures. The laboratory tests were made on small cylinders of rock that were selected to be free of open fractures and, therefore, indicate the hydraulic conductivity dependent on movement through intergranular pore spaces. The results of the tests indicate that the hydraulic conductivity of basalt flows results mainly from fractures.

TABLE 2-31. Hydraulic characteristics of the uppermost confined aquifers of the Pasco basin (from NWTSP, 1976). The porosity ranged between 0.3 and 0.4 (30% and 40%). The vertical hydraulic conductivity in the interbeds ranged between 5×10^{-4} and 20×10^{-4} m/d. The storage coefficient approached the compressibility of water.

Well number	Transmissivity		Hydraulic conductivity	
	in ft^2/d	in m^2/d	in ft/d	in m/d
Lower Ringold Formation:				
699-84-35P	4	0.4	0.11	0.03
699-24-1P	90	8.3	5	1.5
699-S11-E12	40	3.7	0.5	0.15
699-20-E12P	350	32	7	2.1
Mean	120	11	3	0.91
Rattlesnake Ridge:				
199-B3-2P	3.5	0.3	0.25	0.08
199-H4O2	3	0.3	0.3	0.09
699-140E6Q	600	55	30	9.1
Mean	200	18	10	3.0
Mabton:				
DH-8	600-2000	55-180	20-60	5.0-20.0

TABLE 2-32. Hydrologic characteristics of Lower Yakima Basalt flows and interbeds (from NWTSP, 1976).

	Hydraulic conductivity		Transmissivity		Effective porosity[a]	Storage coefficient
	in ft/d	in m/d	in ft^2/d	in m^2/d		
Dense basalt	1×10^{-5} to 3×10^{-3}	3×10^{-6} to 9×10^{-4}	1×10^{-4} to 3×10^{-2}	9×10^{-6} to 3×10^{-2}	0.1-1	1×10^{-5} to 1×10^{-6}
Vesicular basalt	1×10^{-3} to 1×10^{-2}	3×10^{-4} to 3×10^{-3}	1×10^{-2} to 1	9×10^{-4} to 9×10^{-2}	5	$<1 \times 10^{-4}$
Fractured, weathered, or brecciated basalt	3×10^{-3} to 5	3×10^{-4} to 1.5	1×10^{-2} to 500	9×10^{-4} to 46	10	$<1 \times 10^{-3}$
Interbed	3×10^{-3} to 10	9×10^{-4} to 3	3×10^{-2} to 100	3×10^{-3} to 9	20	$<1 \times 10^{-2}$

[a]Volume percent.

TABLE 2-33. Summary of laboratory analyses of rock cores from test well ARH-DC-1 (from NWTSP, 1976).

Core depth, m	Hydraulic conductivity, m/d	Porosity, %
725.7-726.8	1.12×10^{-5}	9.8
847.0-847.3	1.18×10^{-5}	10.5
898.1-899.2	9.5×10^{-6}	25.4
953.1-953.4	5.79×10^{-6}	2.1
1306.0-1306.2	1.12×10^{-5}	10.9

Although the bulk of the permeability data currently available on basalts of the Pasco basin has been taken from well ARH-DC-1, some additional data are available. Tests conducted at Hanford on well RSH-1 in 1976 yielded hydraulic conductivity values ranging from 2.5×10^{-5} to 1.5×10^{-2} m/d (Raymond and Tillson, 1968). In tests run in 1978 on well DC-6 at Hanford, hydraulic conductivities ranged form 9.5×10^{-5} to 0.3 m/d (Apps et al., 1979).

Vertical Permeability. Little work has been done to determine the vertical component of permeability in the Columbia basalts. Vertical permeability is difficult to evaluate in situ since deep wells run parallel to vertical joint systems. Ledgerwood and Deju (1976), using data obtained by La Sala et al. (1972), suggested the vertical components of permeability to be approximately one-tenth the horizontal permeability. Tanaka et al. (1974), in a modeling study of an area north of Hanford, attempted to match hydraulic conductivity to head response in an effort to develop a suitable value for vertical conductivity. Tanaka concluded that the vertical component of K should be between 3×10^{-7} and 1×10^{-5} m/d. Deju et al. (1977) concluded that hydraulic conductivities in the central volume of a dense, thick basalt are usually about 10^{-11} or 10^{-12} m/d. An understanding of permeability anisotropies is critical to effective modeling of a deep repository. Further work on directional components of permeability needs to be done.

Vertical Hydraulic Gradients. In 1972, five piezometers were installed in well ARH-DC-1, as depicted in Fig. 2-49. These piezometers have been

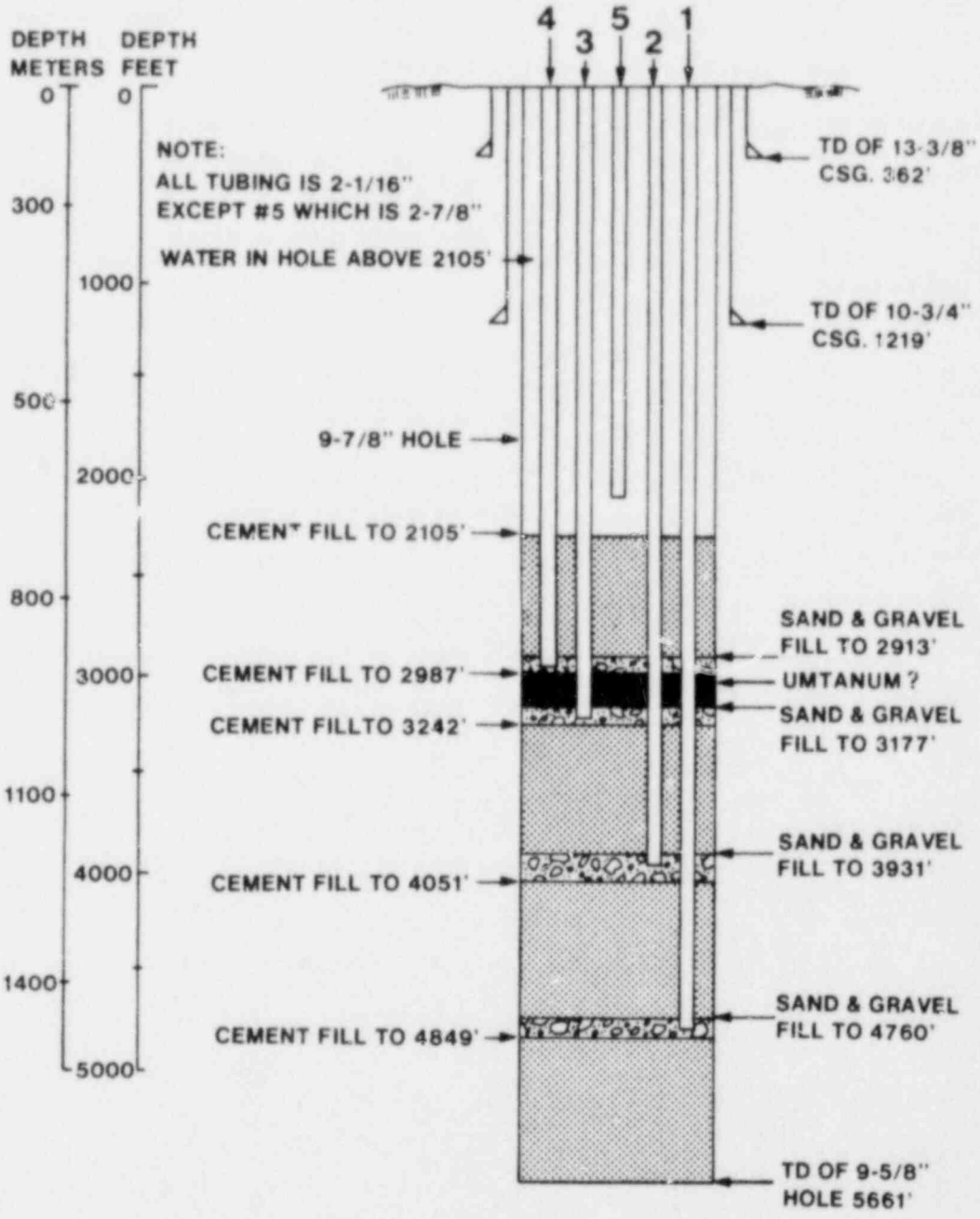

FIG. 2-49. Piezometers installed in well ARH-DC-1 (from NWTSP, 1976).

monitored more or less continuously since. Data from these piezometers indicate a potential interconnection of basalt beds above the 888-m level. This is confirmed by the uniformity of the piezometric surfaces measured in the injection tests summarized in Fig. 2-48. Data collected form 1972 to 1976 also indicate an interconnection of beds in the 970-to-1480-m interval. Separating these two apparent flow regimes is the Umtanum flow unit.

During 1978, additional wells in the DC sequence were constructed, as shown in Fig. 2-50. Although work with this series of wells continues and full data are not yet published, Apps et al. (1979) suggested that there are errors in piezometer readings from well DC-1, caused by leakage through cement seals between piezometers 1, 2, and 3. Readings from well DC-1 indicated that units below the Umtanum flow were hydraulically connected and that there was an upward gradient across this flow unit. Piezometric readings made in well DC-2, 40 ft from DC-1, confirm the hydraulic connection of beds above the Umtanum, but show a sharp downward gradient immediately below this flow, followed by a sharp upward gradient at a point approximately 1000 ft below the Umtanum. As illustrated in Fig. 2-51, this pattern of gradient reversals was also found in well DC-6. While some dense basalts within the Columbia River Group are sufficiently impermeable to allow different heads to be maintained on various portions of the aquifer, this does not signify an absolute hydraulic discontinuity between these aquifers. The head differential between beds continues to drive waters across the "confining layer" at a rate proportional to the hydraulic conductivity of the strata and at a velocity inversely proportional to its effective porosity.

Storage Coefficients. Available data on storage coefficients of basalts are minimal. Estimates for confined basaltic flows, based on data from well ARH-DC-1, are summarized in Table 2-34. These results, drawn from a single well, are at best only order-of-magnitude estimates.

La Sala and Doty (1970) observed that "the storage coefficients of basaltic rocks should generally be smaller [than those observed in well ARH-DC-1] and, for the most dense, most competent rocks, should approach the value for the compressibility of water."

Average Velocity of Groundwater. Average velocities for groundwater in various zones of basalt have been estimated by La Sala and Doty (1970)

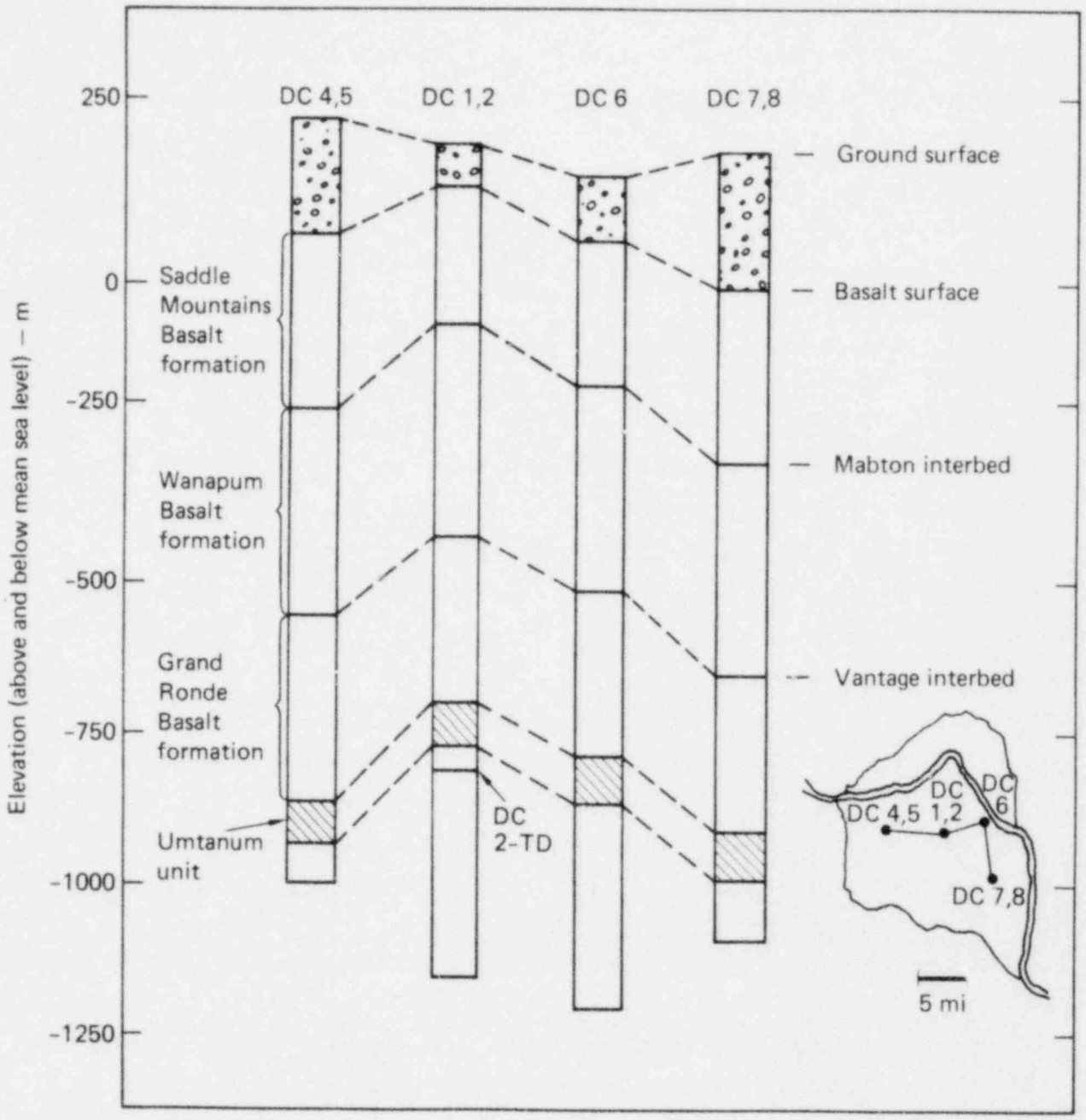

FIG. 2-50. Generalized basalt stratigraphy within the Pasco basin (from Apps et al.,1979).

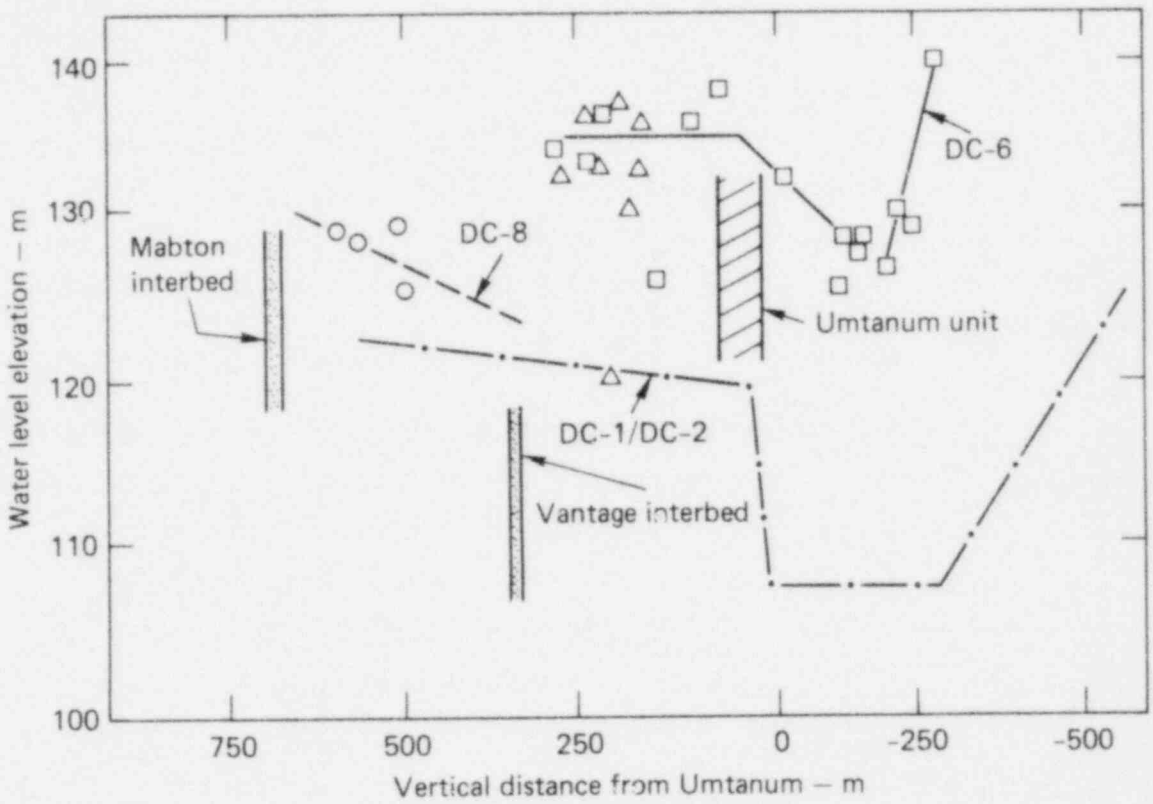

FIG. 2-51. Hydraulic pressure data from the Pasco basin (from Apps et al., 1979). Different symbols signify data from different investigators.

TABLE 2-34. Storage coefficients computed from hydraulic test data from well ARH-DC-1 (from La Sala and Doty, 1976).

Depth interval, m	Storage coefficient
110.3-126.8	6.6×10^{-5}
405.4-463.3[a]	1.8×10^{-3}
536.4-594.4	6.3×10^{-4}
958.9-986.3	1.4×10^{-6}

[a]The comparatively high storage coefficient for this interval may largely reflect the characteristics of two sections of sand interlayered with the basaltic rocks.

(Table 2-35). They concluded that average velocity ranges from 2×10^{-2} dh/dl to 20 dh/dl m/d, where dh/dl is the gradient. Assuming a mean gradient in the confined aquifer at Hanford of 6×10^{-4} m/m (CRWM, 1978), average velocities of groundwater would range from 1×10^{-5} to 1×10^{-2} m/d.

La Sala and Doty based their estimates on minimal porosity data and limited information on hydraulic conductivity. Current programs should better define average groundwater velocities.

Regional Groundwater Systems. Detailed piezometric surface maps indicating the direction of groundwater flow have been developed for the unconfined and the shallow confined aquifers in the Pasco basin (CRWM, 1978). However, little is known of the direction of migration through deep basalts and interbeds. La Sala and Doty (1970) discussed the effects of groundwater flow through the deep basalts and interbeds and their potential recharge and discharge areas. Their investigations were based upon meager data, and the results remain unsubstantiated (NWTSP, 1976).

Hydrology of the Snake River Plain Basalts

Groundwater flow in the Snake River Plain aquifer occurs principally along the upper and lower contacts of successive basaltic flow, which have large and irregular fractures, fissures, and other voids (Robertson et al., 1974). The tops of many flows core-drilled at INEL are highly vesicular, with numerous intersecting fractures, resulting in high porosity and permeability. The centers of the flows are relatively dense and significantly less porous and permeable (Barraclough et al., 1976). The

TABLE 2-35. Relative groundwater velocities in generalized rock units of well ARH-DC-1 (from La Sala and Doty, 1970).

Rock type	Relative groundwater velocity, m/d
Interbedded sand	5
Fracture zone in basalt	20
Vesicular zone in basalt	2×10^{-2}
Dense basalt	5×10^{-2}

lowermost portion of the flow is vesicular and fractured, though to a lesser degree than the flow top. Like basalts in other regions, the flows of the Snake River Plain exhibit columnar jointing.

Groundwater flow paths are not well defined in the rhyolitic ash flow sequence below 745 m. Doherty et al. (1979) noted that most of the rhyolitic rocks are devitrified and dense. Nearly all fractures in recovered core are sealed by alteration products, including calcite, quartz, hematite, pyrite, a septechlorite mineral, and a variety of other clays. Although most of the fractures, joints, and vesicles in the rhyolite rocks have been filled by products of hydrothermal alteration, there may be large-scale fracture features conducive to the flow of groundwater at these depths. Doherty et al. (1979), in their study of geothermal potential, state, "Porous and fractured rocks in ring fracture zones [around the collapsed caldera] provide channel ways for circulation and storage of water, and therefore, rocks in these zones may be likely targets for further geothermal explorations."

Hydraulic Conductivity. Few reliable hydraulic conductivity data exist for the Snake River Plain aquifer. Data are available only from water-well tests and from tests at INEL on wells generally less than 500 m in depth. These data suggest that the greatest permeabilities may be found in the upper 200 m of the aquifer and that permeabilities may significantly decline from this point downward (Robertson et al., 1974). However, insufficient deep-well data are available to fully confirm this conclusion.

Pumping tests conducted by Norvitch et al. (1969) on irrigation wells penetrating the basalt aquifer showed transmissivities to range from 1.25×10^4 to 1.25×10^5 m^2/d and to average 6×10^4 m^2/d. In similar tests at INEL, transmissivities ranged for 3.7×10^2 to 2.2×10^5 m^2/d, averaging 2.5×10^4 m^2/d (Robertson, et al. 1974).

Barraclough et al. (1976), in well tests at INEL, found hydraulic conductivity to vary substantially within very short distances: they observed values between 30 and 3000 m/d. Barraclough et al. further observed that vertical components of permeability are significantly less than horizontal components. Corroboration can be found in the results of King (1968). In tests of a 30-m-thick section of basalt, he found horizontal conductivities to average 17 m/d, while vertical components averaged 4.5 m/d. His data, however, were insufficient to allow generalizations about the rock mass as a whole.

The sedimentary interbeds within the Snake River Plain aquifer generally have more homogeneous hydraulic properties, greater porosity, greater capillary pressure, and lower permeability than the basalt. (Barraclough, et al. 1976). Unlike the Columbia River region, sedimentary interbeds in the Snake River Plain aquifer are generally barriers to the downward movement of groundwater. Vertical hydraulic conductivities measured from cores of the 34- and 73-m interbeds at the INEL burial site are summarized in Table 2-36.

The basalt-sediment interface is suspected of having vertical permeabilities even lower than those of the interbeds. Barraclough et al. (1976) suggests:

> An additional and even greater constraint occurs at the base of each sedimentary layer, at the sediment-basalt interface. This is caused by the discontinuity of pore spaces from the sediment to the basalt, due both to the lower porosity of the basalt and to the relatively great distances between its fractures. In other words, at the interface, perhaps only 10% of the basalt surface is composed of permeable openings, and these are partially filled by sediment. The other 90% is virtually impermeable. This, in effect, provides a thin skin that is estimated to have one-tenth or less of the permeability of the sediments alone.

In many areas of the Snake River Plain, the vertical permeabilities of sediments lying above the zone of water saturation are sufficiently low to allow perched water tables to exist locally. Perched waters have been identified at the burial site at INEL. However, leakage of the TRA disposal ponds at INEL and the subsequent contamination of the Snake River Plain aquifer indicate that some vertical leakage does occur through the sediments.

Storage Coefficients. The literature provides few estimates of storage coefficients for the Snake River Plain aquifer. Norvitch et al. (1969) determined the average storage coefficient for that portion of the aquifer penetrated by water wells on the plain to range from 0.001 to 0.2. In later work at INEL, pumping test data on wells less than 500 m deep showed the storage coefficient of the penetrated section to range from 0.01 to 0.06.

Average Velocity of Groundwater. With the minimal data available, average flow rates are difficult to assess. Tracer tests at INEL identified zones with flow rates of 1 to 7 m/d; however, these rates are not necessarily representative of velocities throughout the aquifer. Barraclough et al. (1976) suggested that the average effective porosity of the upper 610 m of the

TABLE 2-36. Vertical hydraulic conductivities for sedimentary interbeds of the Snake River Plain aquifer (from Barraclough et al., 1976).

Well no.	Depth zone[a]	Vertical hydraulic conductivity, m/d
87	C	2.5×10^{-2}
87	C	3.2×10^{-1}
88	C	1.3×10^{-1}
88	C	3.5×10^{-5}
88	C	8×10^{-7}
88	C	3.1×10^{-6}
89	C	1.6×10^{-7}
89	C	6.1×10^{-5}
89	C	5.9×10^{-6}
90	C	2.9×10^{-2}
91	A	1.3×10^{-2}
91	B	3.0
91	C	7.1×10^{-1}
91	C	2.6×10^{-1}
92	A	5.5×10^{-4}
92	C	2.7
92	C	2.7×10^{-2}
92	C	2.1×10^{-6}
93	A	2.6×10^{-4}
93	C	5.5×10^{-2}
94	A	2.7×10^{-4}
94	A	9.6×10^{-6}
94	B	7.6×10^{-1}
94	C	1.6×10^{-2}
94	C	2.3×10^{-1}
94	C	7.3×10^{-5}
94	C	5.5×10^{-5}
95	A	7.9×10^{-3}
95	A	5.3×10^{-1}
95	B	1.5×10^{-1}

continued

[a]Depth A signifies 0-8 m; B, 23-38 m; and C, 69-84 m.

TABLE 2-36 continued.

Well no.	Depth zone	Vertical hydraulic conductivity, m/d
95	B	3.1×10^{-6}
95	C	2.8×10^{-1}
95	C	9.3×10^{-1}
96	A	5.9×10^{-1}
96	B	6.7×10^{-6}
96	C	1.9×10^{-3}

aquifer is 5 to 10%. Utilizing Barraclough's conclusion and gradients estimated by Mundorff et al. (1964), Robertson et al. (1974) estimated the average flow through a 1-km section of the aquifer on the south edge of INEL to be 2 m^3/s. This is equivalent to a flow of 0.18 $m^3/d/m^2$ normal to the direction of flow, or assuming an 8% effective porosity, an average flow velocity of 2.4 m/d.

Regional Groundwater System. Data from irrigation wells across the Snake River Plain indicate that water in the upper 500 m of the aquifer migrates in a generally southwesterly direction (Mundorff et al., 1964; Robertson et al., 1974). The flow pattern is shown in Fig. 2-52. Little if any work has been done to delineate the rate and direction of movement of deeper waters. Although regionally deeper waters probably also migrate southwesterly, the directions of groundwater flow may vary locally.

At INEL, Barraclough, Robertson, and others have studied in detail the groundwater flow patterns at the burial site and disposal ponds. These studies, summarized in Barraclough et al. (1976), describe flow in the upper three basalt series and in the sedimentary interbeds. While regional water movement through the area was to the southwest, local movement at the burial site was northeasterly. This was attributed to recharge from the Big Lost River and its flood diversion areas to the west.

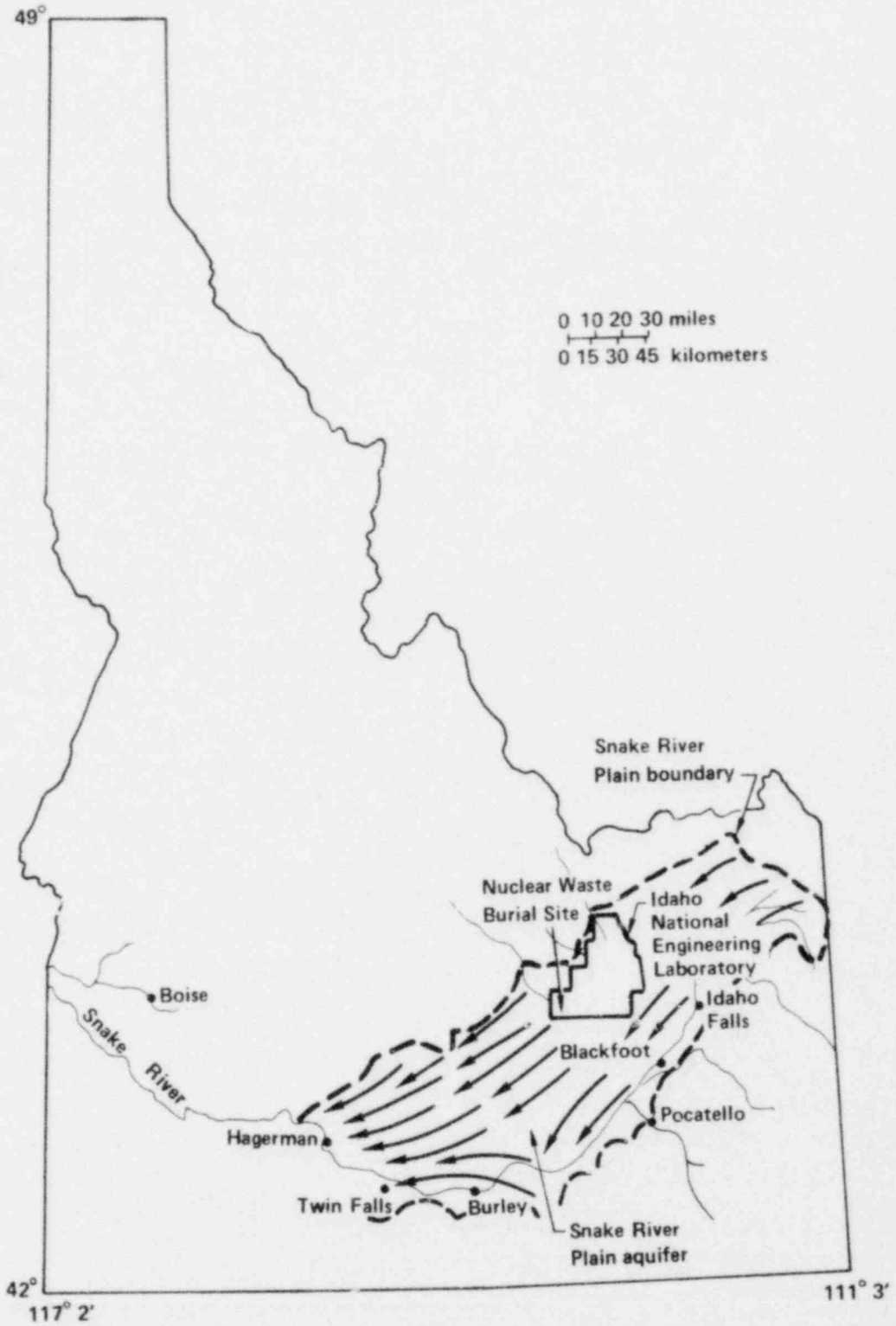

FIG. 2-52. Regional groundwater flow in the Snake River Plain aquifer (from Robertson et al., 1974).

Hydrology of the Modoc Plateau Basalts

The intact basalt of the Modoc Plateau has low porosity and permeability. Most groundwater flow occurs in breccia layers between flow units, and in clinker zones, vesicular zones, joints, or lava tunnels (Mack, 1960; Wood, 1960; Brown and Newcomb, 1962; Foxworthy, 1961; Newcomb, 1961). Faults in the basalt flows usually form vertical conduits that enhance permeability, rather than barriers to horizontal flow. Interbeds are discontinuous and generally are of only local significance.

Specific hydrologic data on the aquifer are sparse. Although sustained well yields of 50 to 100 gal/min are common, well production is highly variable. Brown and Newcomb (1962) observed transmissivities between 1050 and 3720 m^2/d and storage coefficients between 1.4×10^{-3} and 2.4×10^{-3}.

Regionally, groundwater occurrences in the Modoc Plateau are restricted to many structural basins or grabens between block-fault sequences. These basins are surrounded by crystalline rock of low permeability, which provide little recharge. Most recharge occurs through precipitation or seepage from irrigation facilities or streams.

REFERENCES: CHAPTER 2

Agapito, J. F. T., M. P. Hardy, and D. R. St. Laurent, 1977, Geo-Engineering Review and Proposed Program Outline for the Structure Design of a Radioactive Waste Repository in Columbia River Basalt, Rockwell International, Hanford, Wash., RHO-ST-6.

Apps, J. A., N. G. W. Cook, and P. A. Witherspoon, 1978, An Appraisal of Underground Radioactive Waste Disposal in Argillaceous and Crystalline Rocks: Some Geochemical, Geomechanical, and Hydrogeological Questions, Lawrence Berkeley Laboratory, Berkeley, Calif., LBL-7047.

Apps, J., T. Doe, B. Doty, S. Doty, R. Galbraith, A. Kearns, B. Kohrt, J. Long, A. Monroe, T. N. Narasimhan, P. Nelson, C. R. Wilson, and P. A. Witherspoon, 1979, Geohydrological Studies for Nuclear Waste Isolation at the Hanford Reservation, Volume II: Final Report, Lawrence Berkeley Laboratory, Berkeley, Calif., LBL-8764.

Barraclough, J. T., et al., 1976, Hydrology of the Solid Waste Burial Ground, as Related to the Potential Migration of Radionuclides, Idaho National Engineering Laboratory, U.S. Geol. Survey Open File Report 76-471.

Brandon, J. R., 1976, Rock Mechanics Properties of Typical Foundation Rock Types, Engineering and Research Center, Bureau of Reclamation, REC-ERC-74-10.

Brown, D. J., and R. K. Ledgerwood, 1973, Stratigraphy and Structure of Yakima Basalt in Pasco Basin, Washington, Oregon Department of Geology and Mineral Industries Bulletin 77, pp. 171-181.

Brown, S. G., et al., 1962, Ground Water Resources of Cow Valley, Malheur County, Oregon, U.S. Geol. Survey Water Supply Paper 1619-M, pp. M1-M35.

Carmichael, I. S. E., F. J. Turner, and J. Verhoogen, 1974, Igneous Petrology (McGraw-Hill, New York).

Committee on Radioactive Waste Management (CRWM), 1978, Radioactive Wastes at the Hanford Reservation, A Technical Review (National Academy of Sciences), ERDA contract E-11-2708/4.

Coulson, J. H., 1970, The Effects of Surface Roughness on the Shear Strength of Joints in Rock, Corps of Engineers NTIS AD714244.

Crittenden, M. D., Jr., F. E. Schaeffer, D. E. Trimble, and L. A. Woodward, 1971, "Nomenclature and Correlation of Some Upper Precambrian and Basal Cambrian Sequences in Western Utah and Southeastern Idaho," Bull. Geol. Soc. Am. 82, 581.

Crosthwaite, C., A. Thomas, K. L. Dyer, 1970, Water Resources in the Big Lost River Basin, South Central Idaho, U.S. Geol. Survey Open File Report 1970-93.

Deere, D. U., and R. P. Miller, 1966, Engineering Classification and Index Properties for Intact Rock, Air Force Weapons Lab, Kirkland AFB, N.M., AFWL-TR-65-116.

Deju, R. A., P. A. Eddy, M. W. Grutzeck, and C. W. Myers, 1977, Environmental Factors Needed to Establish the Geotechnical Feasibility of Storing Radioactive Waste in Columbia River Basalts, Rockwell International, Hanford, Wash., RHO-ST-8.

Deju, R. A. et al., 1978, Structural Considerations in the Design of a Repository to Store Radioactive Waste in Basalt Formations, Rockwell International, Hanford, Wash., RHO-SA-10.

Doherty, D. J., L. A. McBroome, and M. A. Kuntz, 1979, Preliminary Geological Interpretation and Lithologic Log of the Exploratory Geothermal Test Well (INEL-1), Idaho National Engineering Laboratory, Eastern Snake River Plain, Idaho, U.S. Geol. Survey Open File Report 79-1248.

Eddy, P. A., 1969, "Geohydrology of the Columbia Basin Project Area, Washington," abstract in Northwest Sci. 43 (1), 35.

Fenix and Scisson, 1969, Exploratory Report, Exploratory Hole ARH-DC-1, Atlantic Richfield Hanford Company, Richland, Wash.

Foxworthy, B. L., 1961, Deformed Basaltic Caprock as an Aquifer at Cow Valley, Oregon, U.S. Geol. Survey Professional Paper 424-C, pp. C150-C151.

Hamilton, W., 1963, "Overlapping of Late Mesozoic Orogens in Western Idaho," Bull. Geol. Soc. Am. 74, 779.

_____, 1965, Geology and Petrogenesis of the Island Park Caldera of Rhyolite and Basalt, Eastern Idaho, U.S. Geol. Survey Professional Paper 504-C.

Hamilton, W., and W. B. Myers, 1966, "Cenozoic Tectonics of the Western United States," Rev. Geophys. 4, 509.

Hampton, E. R., 1961, Geologic Factors that Control the Occurrence and Availability of Ground Water in the Fort Rock Basin, Lake County, Oregon, U.S. Geol. Survey Professional Paper 383-B.

Hardy, M. P., and G. Hocking, 1977, Numerical Modeling of Rock Stresses within a Basaltic Nuclear Waste Repository: Phase II--Parametric Design Studies, report EY-77-C-06-1030, submitted to Rockwell Hanford Operations.

Herget, G., 1973, "Variation of Rock Stresses with Depth at a Canadian Iron Mine," Int. J. Rock Mech. Min. Sci. 10, 37.

Hess, H. H., and A. Poldervaart, 1967, Basalts (Interscience, London).

Hoek, E., and E. T. Brown, Underground Excavation Engineering (The Institution of Mining and Metallurgy, London), in press.

Holmes, A., 1965, Principles of Physical Geology (Ronald Press, New York), 2nd ed.

Iida, K., T. Wada, Y. Aida, and R. Schichi, 1960, "Measurements of Creep in Igneous Rocks," J. Earth Sci., Vol. 8.

Judd, W. R., 1969, Strain Distribution around Underground Openings: Statistical Methods to Compile and Correlate Rocks, Properties, and Preliminary Results, Purdue University Technical Report 2.

King, L. G., 1968, Mathematical Models for Underground Injection of Gaseous Wastes into the Vadose Zone, Battelle Memorial Institute, Cleveland, Ohio, BNWL-945.

Kirkham, V. R. D., 1931, "Snake River Downwarp," J. Geol. 39, 456.

Kreck, W. W., F. A. Henderson, and K. E. Jhelmstad, 1974, A Standard Rock Suite for Rapid Excavation Research, U.S. Bureau of Mines Report of Investigation 7865.

Krumer, A., 1968, "The Effect of Stress Rate and Temperature on the Strength of Basalt and Granite," Geophys. 33(3).

Kulhany, F. H., 1975, "Stress Deformation Properties of Rock and Rock Discontinuities," Engin. Geol. 9, 327.

La Sala, A. M., Jr., and G. C. Doty, 1970, "Preliminary Evaluation of Hydrologic Factors Related to Radioactive Waste Storage in Basaltic Rocks at Hanford," U.S. Geol. Survey Admin. Report, in Nucl. Sci. Abst. 25(21), Art 48606.

Ledgerwood, R. K., and R. A. Deju, 1976, Hydrology of the Uppermost Confined Aquifers Underlying the Hanford Reservation, Atlantic Richfield Hanford Company, Hanford, Wash., ARH-SA-253.

Lehnhoff, T. F., and J. D. Scheller, 1975, "The Influence of Temperature Dependent Properties on Thermal Rock Fragmentation," Int. J. Rock Mech. 12, 255.

Lindgren, W., 1898, Geologic Atlas of the United States, Boise Folio, Idaho, U.S. Geol. Survey Folio 45.

Lindner, E. N., and J. A. Halpern, 1977, "In Situ Stress: An Analysis," in

Proc. 18th U.S. Symposium on Rock Mechanics, Keystone, Colo. (Colorado School of Mines Press).

Lindroth, D. P., and W. G. Krawza, Heat Content and Specific Heat of Six Rock Types at Temperature to 1000° C, U.S. Bureau of Mines Report of Investigation.

Lutton, R. J., 1968, "Comparison of Strengths of Dense and Vesicular Types of Basalt," Bull. Assoc. Engin. Geol. 5 (1).

MacDonald, G. A., 1966, "Geology of the Cascade Range and Modoc Plateau," in Geology of Northern California, E. H. Bailey, Ed., California Division of Mines Geol. Bulletin No. 190, pp. 65-96.

Mack, S., 1960, Geology and Ground-water Features of Shasta Valley, Siskiyou County, California, U.S. Geol. Survey Water Supply Paper 1484.

Morovelli, R. L., and K. F. Veith, 1965, Thermal Conductivity of Rock: Measured by the Transit Line Source Method, U.S. Bureau of Mines Report of Investigation 6604.

Morrell, R. J., and D. A. Larson, 1974, Tunnel Boring Technology: Disc Cutter Experiments in Metamorphic and Igneous Rocks, U.S. Bureau of Mines Report 7952.

Morris, D. A., and A. I. Johnson, 1967, Summary of Hydrologic and Physical Properties of Rock and Soil Materials as Analyzed by the Hydrologic Laboratory of the USGS, U.S. Geol. Survey Water Supply Paper 1839-D.

Mundorff, M. J., E. G. Crosthwaite, and C. Kilburn, 1964, Ground Water for Irrigation in the Snake River Basin in Idaho, U.S. Geol. Survey Water Supply Paper 1654.

Myers, C. W., 1973, Yakima Basalt Flows near Vantage, and from Core Holes in the Pasco Basin, Washington, University of California, Santa Cruz, Ph.D. dissertation.

Myers, C. W., and D. J. Brown, 1973, "Stratigraphy of the Yakima Basalt in the Pasco Basin, Washington," abstract in Geol. Soc. Am. (Cordilleran Section) 5(1), 80.

Nace, R. L., M. Deutsch, and P. T. Voegeli, 1972, Physical Environment of the National Reactor Testing Station, Idaho--A Summary, U.S. Geol. Survey Professional Paper 725-A.

National Waste Terminal Storage Program (NWTSP), 1976, Preliminary Feasability Study on Storage of Radioactive Wastes in Columbia River Basalts, Atlantic Richfield Hanford Co., Hanford, Wash., ARH-ST-137.

Newcomb, R. C., 1961, Ground Water in the Western Part of the Cow Creek and Soldier Creek Grazing Units, Malheur County, Oregon, U.S. Geol. Survey Water Supply Paper 1475-E.

_____, 1969, Effect of Tectonic Structure on the Occurrence of Ground Water in the Basalt of the Columbia River Group of The Dalles Area, Oregon and Washington, U.S. Geol. Survey Professional Paper 383-C.

Norvitch, R. F., C. A. Thomas, and R. G. Maditon, 1969, Artificial Recharge to the Snake Plain Aquifer: An Evaluation of Potential and Effect, Idaho Department of Reclamation Water Information Bulletin 12.

Office of Nuclear Waste Isolation (ONWI), 1978, Technical Support for GEIS: Radioactive Waste Isolation in Geologic Formations, Oak Ridge, Tenn., Y/OWI/TM/-36.

Orr, C. M., 1975, "High Horizontal Stresses in Near-Surface Rock Masses," in Proc. Sixth Regional Conference for Africa, Soil Mechanics and Foundation Engineering.

anek, L. A., 1970, "Effect of Rock Fracturing on the Modulus as Determined by Bore Hole Dilation Tests," in Proc. Second International Congress on Rock Mechanics, Belgrade.

Parsons, Brinckerhoff, Quade, and Douglas, Inc. (PBQ&D), 1978, Technical Support for GEIS: Radioactive Waste Isolation in Geologic Formations, report to Office of Nuclear Waste Isolation, Oak Ridge, Tenn.; published as ONWI (1978).

Piper, A. M., et al., 1939, Geology and Ground Water Resources of the Harney Basin, Oregon, U.S. Geol. Survey Water Supply Paper 841.

Raymond, J. R., and D. D. Tillson, 1968, Evaluation of a Thick Basalt Sequence in South-Central Washington, Battelle Pacific Northwest Laboratories, Richland, Wash., BNWL-776.

Robertson, J. B., R. Schoen, and J. T. Barraclough, 1974, The Influence of Liquid Waste Disposal on the Geochemistry of Water at the National Reactor Testing Station, Idaho, 1952-1970, U.S. Geol. Survey Report UC-70.

Rodrigues, F. P., 1970, "Anisotropy of Granites," in Proc. Second International Congress on Rock Mechanics, Belgrade.

Russell, I. C., 1902, Geology and Water Resources of the Snake River Plain of Idaho, U.S. Geol. Survey Bulletin.

Ryan, M. P., 1974, "Fracture Mechanisms and Columnar Basalts," in Rock Mechanics (Pennsylvania State University, University Park), pp. 247-251.

Sandia Laboratories, 1962, Project Buckboard, 20-Ton and 1/2-Ton High Explosive Cratering Experiments in Basalt Rock, final report.

Sharp, R. R., 1972, A Geological Engineering Evaluation of an Underground Nuclear Test Site, University of Arizona, Ph.D. dissertation.

Skibitzke, H. E., and J. A. da Costa, 1962, The Ground-Water Flow System in the Snake River Plain, Idaho--An Idealized Analysis, U.S. Geol. Survey Water Supply Paper 1536-D.

Stowe, R., 1969, Strength and Deformation Properties of Granite, Basalt, Limestone, and Tuff at Various Loading Rates, U.S. Army Engin. Waterways Exp. Station Miscellaneous Paper C-69-1.

Summers, W. K., and R. A. Deju, 1974, A Preliminary Review of the Regional Hydrology of the Hanford Reservation, Raul A. Deju Associates, Richland, Wash., CA-168-RAD-4.

Tanaka, H. H., A. J. Hansen, Jr., and J. A. Skrivan, 1974, Digital-Model Study of Ground-Water Hydrology, Columbia Basin Irrigation Project Area, Washington, Washington State Dept. of Ecology Water Supply Bulletin 40.

U.S. Bureau or Reclamation (USBR), no date, Physical Properties of Some Typical Foundation Rocks, Concrete Laboratory Report SP-39.

Walker, E. H., 1964, Subsurface Geology of the National Reactor Testing Station, Idaho, U.S. Geol. Survey Bulletin 1133-E.

Windes, S. L., 1949, Physical Properties of Mine Rock, Part I, U.S. Bureau of Mines Report of Investigation 4459.

_____, 1950, Physical Properties of Mine Rock, Part II, U.S. Bureau of Mines Report of Investigation 4727.

Wingquist, C. F., 1969, Elastic Moduli of Rock at Elevated Temperatures, U.S. Bureau of Mines Report of Investigation 7269.

Wood, P. R., 1960, Geology and Ground-Water Features of the Butte Valley Region, Siskiyou County, California, U.S. Geol. Survey Water Supply Paper 1491.

Yoder, H. S., Jr., and C. E. Tilley, 1962, "Origin of Basalt Magmas--An Experimental Study of Natural and Synthetic Rock Systems," J. Petrol 3(3), 342.

CHAPTER 3

GRANITES

The term granitic rock generally signifies any coarse-grained, light-colored igneous rock containing quartz. In its broadest usage, it may be loosely applied to certain metamorphic rocks and to quartz-free, light-colored igneous rocks. Although its broad, undefined use can be confused with the very specific rock name granite, the term granitic rock has attained a wide casual acceptance. Perhaps the reason for this acceptance is that it groups three important igneous rock types that have similar petrographic, tectonic, and genetic characteristics. These types are the granites, monzonites, and granodiorites, which commonly occur as batholiths, huge rock bodies covering hundreds of square kilometers.

Together, granite, monzonite, and granodiorite constitute a major portion of the earth's igneous terrane. Although less common rocks are sometimes included in the definition of granitic rock, this report uses the term for the three major common rock types.

GEOLOGY

Classification and Composition of Granitic Rocks

Granitic rocks, and igneous rocks in general, are classified according to texture and mineralogy. Texture is the more obvious and less complicated means of classification. All igneous rocks are either phaneritic (coarse grained) or aphanitic (fine grained); if two distinct grain sizes are present, they are also said to be porphyritic. Granitic rocks are phaneritic; some are also porphyritic. However, in phaneritic rocks, the relative differences in grain sizes are not great, and the physical properties of the rock are not greatly affected.

The classification of granitic rocks based on mineralogy is shown in Fig. 3-1. The scheme is based on a changing ratio of potassium feldspar

Essential minerals		Potassium Feldspar 2/3 total feldspar			Potassium Feldspar 1/3 - 2/3 total feldspar			Plagioclase Feldspar 2/3 total feldspar	
		Quartz > 10%	Quartz < 10% Feldspathoid < 10%	Feldspathoid > 10%	Quartz > 10%	Quartz < 10% Feldspathoid < 10%	Feldspathoid > 10%	Potassium Feldspar 10% total feldspar Quartz 10%	Potassium Feldspar 10% total feldspar Sodic Plagioclase Quartz 10%
Characterizing accessory minerals		Chiefly: Hornblende, Biotite, Pyroxene, Muscovite Also: Sodic Amphiboles, Aegirine, Cancrinite Sodalite, Tourmaline			Chiefly: Hornblende, Biotite, Pyroxene Also: Sodic Amphiboles, Aegirine			Chiefly: Hornblende, Biotite, Pyroxene (in Andesite) Also: Pyroxene Feldspathoid Sodic Amphiboles	
Average chemical composition %	SiO_2	71.5	60.4	56.0	66.0	57.0	54.1	65.3	61.6
	Al_2O_3	14.0	17.0	19.2	15.8	17.1	21.0	16.1	16.2
	Fe_2O_3	1.5	2.7	2.9	2.3	3.4	1.8	2.1	2.5
	FeO	1.4	2.9	1.6	1.3	3.6	3.3	2.3	3.8
	MgO	0.6	1.8	0.6	1.0	2.3	1.1	1.7	2.8
	CaO	1.6	3.7	2.0	2.8	5.4	3.2	3.9	5.4
	Na_2O	3.4	4.2	8.5	3.7	4.7	6.2	3.8	3.4
	K_2O	4.3	5.1	5.3	4.2	3.7	5.9	2.7	2.1
Phaneritic	Equigranular	Granite	Syenite	Nepheline Syenite	Quartz Monzonite	Monzonite	Nepheline Monzonite	Granodiorite	Quartz Diorite

FIG. 3-1. Mineral composition of granitic rocks (from Travis, 1955).

($K_2AlSi_3O_8$) to plagioclase feldspar ([Ca,Na]Al[Al,Si]Si_2O_8). As the percentage of SiO_2 increases, potassium feldspars become dominant. Also, the amount of quartz increases and the calcium to sodium ratio of the plagioclases decreases.

Average mineral compositions for granites, monzonites, and granodiorites, the three major granitic rock types, are given in Table 3-1. (Table 3-1 and Fig. 3-1 were taken from different sources; hence, the percentages differ somewhat.) Even though variations occur in the types and percentages of minor minerals present, the real differences in the rocks are the percentages of the potassium and plagioclase feldspars. In fact, all three rock types could have the same minor minerals and still maintain their identity.

Since all granitic rocks consist of about 80% feldspar, and since the various feldspars have similar physical properties, all granitic rocks have similar physical properties.

Granitic rocks are unique in having a tremendously varied suite of trace elements. The number and variety is different with each rock body, but almost all bodies contain at least a trace concentration of some rare elements. Much of the world's mineral wealth is associated with granitic rock bodies that concentrated rare metals during formation. These metals, other rare elements, and a few compounds, such as water, do not have the molecular properties necessary to fit the structures of common minerals that form during rock crystallization. This saves these elements and compounds for the low-temperature end of the igneous process, where granitic rocks crystallize.

Structure and Genesis of Granitic Rock Bodies

Granitic rock bodies occur in any of the many forms assumed by plutonic igneous rocks. Their coarse grain size requires the slow cooling of a deep subsurface environment and precludes formation by any surface volcanic mechanism. Although dikes, sills, stocks, and other smaller bodies are common, by far the greatest volumes of granitic rock now exposed at the earth's surface occur as continental shield complex and orogenic belt batholiths. Batholiths are igneous rock bodies with an exposed surface area in excess of 100 km^2. Their vertical dimensions are so great that no lower boundaries have been located. These great rock bodies tend to be composed of granite, monzonite, and/or granodiorite. The less common granitic rock types are only rarely found in large bodies.

TABLE 3-1. Average chemical and mineral compositions for granite, quartz monzonite, and granodiorite (from Huang, 1962). The table summarizes the analysis of 72 granites, 121 quartz monzonites, and 137 granodiorites.

	Composition, wt%		
	Granite	Quartz monzonite	Granodiorite
Chemical constituents:			
SiO_2	72.08	69.15	66.88
TiO_2	0.37	0.56	0.57
Al_2O_3	13.86	14.63	15.66
Fe_2O_3	0.86	1.22	1.33
FeO	1.67	2.27	2.59
MnO	0.06	0.06	0.07
MgO	0.52	0.99	1.57
CaO	1.33	2.45	3.56
Na_2O	3.08	3.35	3.84
K_2O	5.46	4.58	3.07
H_2O	0.53	0.54	0.65
P_2O_5	0.18	0.20	0.21
Mineral constituents:			
Quartz, SiO_2	29.2	24.8	21.9
Orthoclase, $KAlSi_3O_8$	32.2	27.2	18.3
Albite, $NaAlSi_3O_8$	26.2	28.3	32.5
Anorthite, $CaAl_2SI_2O_8$	5.6	11.1	16.4
C	0.8	--	--
$CaSiO_3$	--	--	--
$MgSiO_3$	1.3	2.5	3.9
$FeSiO_3$	1.7	2.2	2.9
Magnetite, Fe_2O_4	1.4	1.9	1.9
Imenite, $FeTiO_3$	0.8	1.1	1.1
Apatite, $Ca_5(PO_4)_3(F,OH,Cl)$	0.4	0.5	0.5

Description of Occurrences

The nine areas shown in Fig. 3-2 were selected for analysis in this report. Certain specific geologic information for some of these areas is lacking; futhermore, consideration of the geology of an area the size of a batholith requires generalization of a great many variables. These generalizations are unimportant when more than 100 km^2 are involved, but when 1 to 5 km^2 are under study, they may not be at all applicable.

FIG. 3-2. Granitic occurrences chosen for this study.

An example of this problem is the intensity and depth of fracturing at a specific site. References on an entire batholith may generalize by saying, for example, that there are three "well defined" joint trends. The references may not mention minor or local fracturing at all. However, once a specific site is chosen, we may find that locally this "well-defined" joint pattern is nonexistent or that it is oriented differently; or a local structure may have caused extremely fine granulation of the rock. Depth of fracturing is even more difficult to determine. It almost always requires drill hole data, which are necessarily site specific.

The solution to this problem is simply to work with the generalizations and the more consistent properties of the rock. Once local areas are chosen for study, specific data can be gathered.

Front Range Uplift.

Location and Geology. The Front Range uplift extends from southern Colorado to southern Wyoming along the eastern slope of the Rocky Mountains (Fig. 3-3). Elevations range from 1500 to over 4000 m. The rugged terrain is typical of youthful erosion surfaces superimposed on recently uplifted igneous and metamorphic complexes.

An outline of the geologic history of the area begins with the 1.7-billion-year-old metamorphic complex. Sediments deposited prior to this time were metamorphosed into the Idaho Springs series and intruded by the Boulder Creek granodiorite batholiths. Major intrusions and diastrophism occurred again at 1.4 billion years (the Silver Plume granitic suite) and at 1.1 billion years (the Pikes Peak Granite). During the Phanerozoic, uplift occurred during the Carboniferous, the Cretaceous, and the Tertiary. Uplift is still in progress and the present elevations are due to this recent period. Terrestrial and marine sedimentary rocks deposited throughout the Phanerozoic are still found. The last period of igneous intrusion, responsible for volcanism and many small granitic rock bodies, began in the Cretaceous and continued through the late Tertiary.

The various Precambrian intrusives are the major granitic rocks of the Front Range uplift. These occur in an almost continuous series of batholiths along its length. Their total area is many million square kilometers.

The southern Tarryall region, which lies about 100 km west of Colorado Springs, Colorado, is typical of the geology and petrology of the Front Range

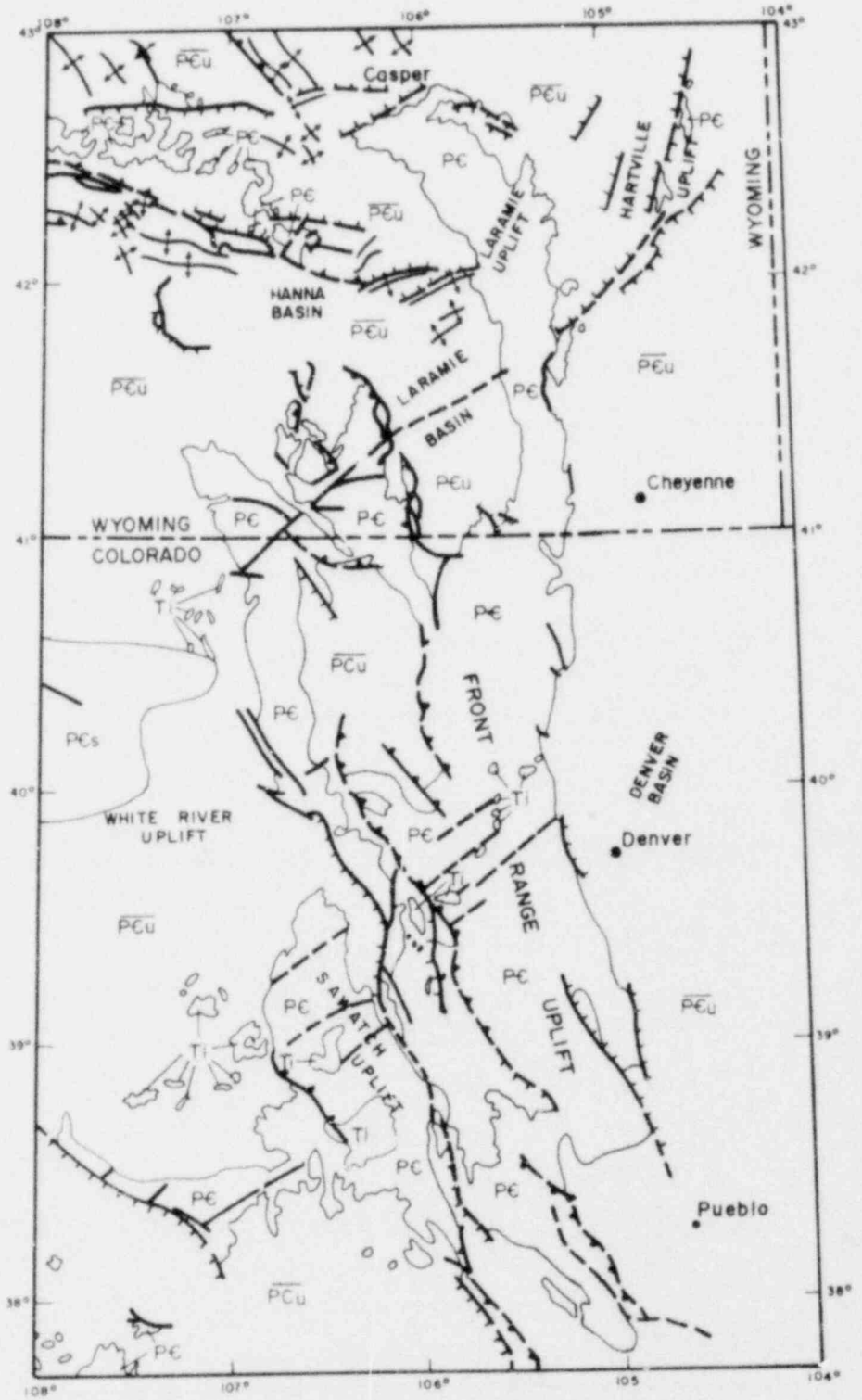

FIG. 3-3. Bedrock geology of the Front Range uplift. A key to the symbols appears on the following page.

KEY TO THE SYMBOLS

Ti	Tertiary and younger intrusive rocks
Tv	Tertiary volcanics
Mzi	Mesozoic intrusive rocks
$\overline{Mzi}$	Mesozoic intrusive rocks not exposed
$\overline{P}M_k$	Paleozoic and Mesozoic sedimentary and volcanic rocks
$\overline{PM_k}$	Paleozoic and Mesozoic sedimentary and volcanic rocks not exposed
P€s	Precambrian supracrustal sedimentary rocks
$\overline{P€s}$	Precambrian supracrustal sedimentary rocks not exposed
$\overline{P€su}$	Precambrian supracrustal rocks of undetermined composition in subsurface
P€	Precambrian granites and granitic gneisses
$\overline{P€}$	Precambrian granites and granitic gneisses not exposed
$\overline{P€u}$	Precambrian rocks of undetermined composition in subsurface
U	Ultramafic rocks

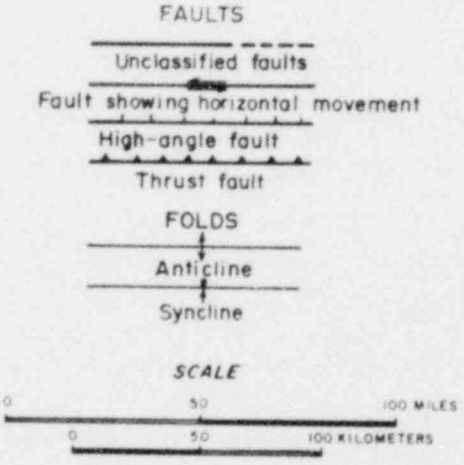

FIG. 3-3 continued.

uplift (Hawley and Wobus, 1977). This region is underlain by a large and varied suite of Precambrian intrusive igneous rocks, locally covered by a recently deposited veneer of sediments of the Tertiary and Quaternary periods. Most of the intrusive rocks are related to one of the three main granitic series of the Front Range: the Boulder Creek Granodiorite, the Silver Plume Quartz Monzonite, and the Pikes Peak Granite.

Petrology. The composition of the Boulder Creek Granodiorite varies widely from biotite-quartz diorite to granite. Three main lithology types can be distinguished: quartz diorite, granodiorite, and quartz monzonite.

The dominant unit of the Boulder Creek rocks is a quartz monzonite. Texturally, the rock can usually be classed as a gneiss because of the foliation that separates the light and dark minerals. The potassium feldspar present is microcline; the major plagioclases are oligoclase and andesine; and quartz makes up roughly 30% of the rock. Biotite is the main ferromagnesian mineral, and accessory zircon, apatite, magnetite, and sphene occur with it.

The Silver Plume Quartz Monzonite is a massive to flow-foliated, plutonic igneous rock correlated with the Silver Plume Granite of the central Front Range. It occurs in igneous intrusions as large as 13 km^2 and in many dikes. Three varieties of the Silver Plume Quartz Monzonite are recognized, according to differences in grain size and structure: fine to medium grained, fine grained, and medium to coarse grained. All three are found in the Front Range plutons. The medium- to coarse-grained type forms separate plutons; the two finer-grained varieties commonly occur together in the same pluton. The rock is generally red and porphyritic, and contains microclines, oligoclase, quartz biotite, and muscovite, with accessory apatite, zircon, monzite, and opaque oxides.

The Pikes Peak Granite forms massive, sharp-walled plutons. The major Pikes Peak batholith covers at least 3100 km^2. A smaller batholith of Pikes Peak Granite, the Tarryall Mountains mass, underlies a 245-km^2 area. Pikes Peak Granite consists of a coarse sub-equigranular granite, coarse porphyritic granite, and a heterogeneous medium- to coarse-grained granite. The batholiths also contain small dikes of pegmatite or aplite and irregular masses of fine-grained granite. The granite averages approximately 50% microcline, 30% quartz, 15% sodic plagioclase, and 5% biotite.

Only thin soils have developed since the last uplift. In areas where closely spaced joints occur, there has been significant mechanical and

chemical weathering. The granitic rocks were exposed to intense weathering during the late Paleozoic and mid-Tertiary. Paleosoils over 25 m thick can be found where the old surface has been preserved.

Structure. The Front Range area has undergone at least three major Precambrian deformations and three Phanerozoic uplifts. The granitic rocks and, to a great extent, the entire area are affected most by the Precambrian tectonics. Three major regional trends occur: northwest, northeast, and east. Intense folding and fracturing follow all three, but the northwest trend is the major one. The northeast trend is noted for its mineralization during the Tertiary. All trends have continued to be active into recent times.

Bighorn Uplift.

Location and Geology. The exposure of granitic rocks in the Bighorn uplift, located just west of Buffalo and Sheridan, Wyoming, occupies an area of about 3100 km^2 (Fig. 3-4). Its shape is roughly elliptical, about 100 km long and 48 km wide at its greatest width. The Precambrian granitic rocks are

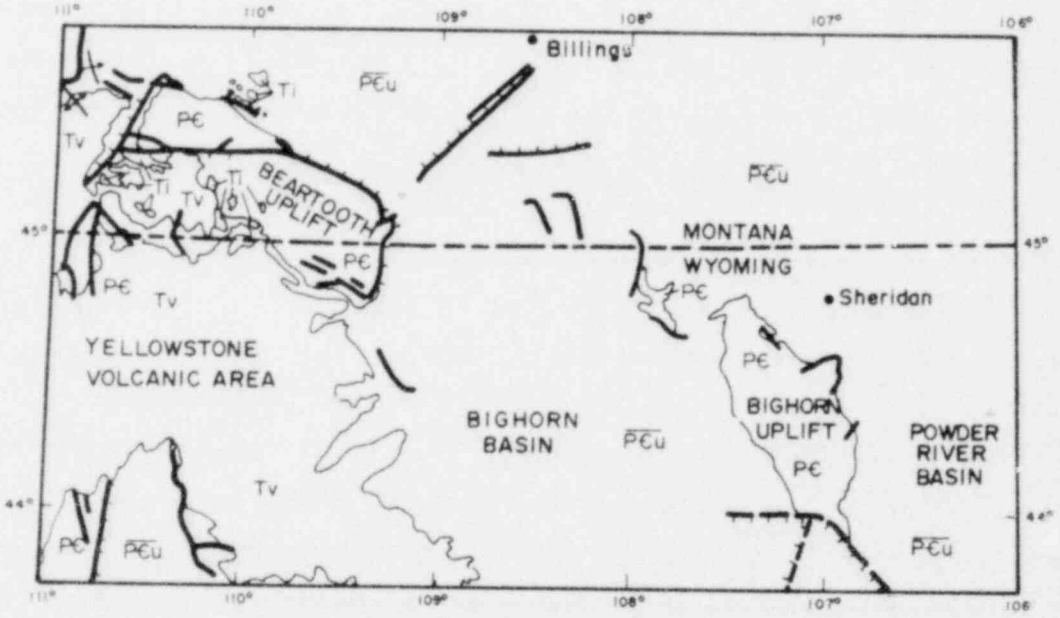

FIG. 3-4. Bedrock geology of the Beartooth and Bighorn uplifts. See Fig. 3-3 for a key to the symbols.

in contact with the Cambrian Deadwood Formation on all sides. In a few localities, its boundary is defined by faults, along which it is in contact with various formations.

The central portion of the uplift comprises mainly older, metamorphic Precambrian gneiss. At the northern and southern ends of the uplift, the major rocks are red to grey, younger Precambrian, igneous granitics. These range in composition from granite to quartz diorite, and even though there has been some mobilization, they have mostly been formed in place through granitization of the older rocks (Osterwald, 1955).

Petrology. Classified according to color, the granitics consist largely of two varieties, a moderately coarse-grained red granitic rock and a medium- to fine-grained gray granitic rock. The boundary between the two rock types is gradational, and both are believed to have originated from the same magma. The feldspar in the red granite is mainly orthoclase and microcline with some oligoclase. Quartz is also a major constituent. The red color is caused by the dissemination of small particles of iron minerals in the orthoclase. In some areas, the gray rock contains a higher proportion of more calcic plagioclase and grades into a quartz monzonite or quartz diorite. Common accessory minerals in the gray granite are apatite, magnetite, titanite, rutile, and zircon. Much of the gray granite shows evidence of shearing. In weathered portions of the rock, biotite is commonly altered to chlorite, and some of the feldspar is altered to kaolinite and sericite (Osterwald, 1955; Darton, 1906).

Texture of both rock types is typified by migmatization and twin microshearing, gneissic foliation, and various sizes of inclusions. These are all common in granitic rocks that have been granitized in place or formed from replacement by metasomatic fluids.

Structure. A widespread joint system is prevalent throughout the granitic outcrop area. This causes the granitics to weather into rounded blocky boulders. Dikes are common. They are either granitic, granite aplites and pegmatites, or diabasic. No pattern has been discerned.

Major faulting and folding is generally confined to the margins of the granitic rocks. Thrust, normal, and reverse faults occur with mainly dip movement. These and the simple folds of the overlying sediments reflect the movement of the uplift that produced the Bighorn Mountains.

Beartooth Uplift.

Location and Geology. The Precambrian Beartooth uplift is located in south-central Montana, north and east of Yellowstone National Park (Fig. 3-4). The felsic batholithic mass trends northwest and is approximately 97 km long and 48 km wide. The granitic core of the Beartooth uplift was formed by granitization of early Precambrian sediments about 2.7 billion years ago. The uplift that formed the present Beartooth Mountains started in the Cretaceous and continued into the Tertiary. The volcanism that is still evident in Yellowstone Park began with the later stages of the uplift.

Petrology. The rocks of the granitic core consist mainly of granitic gneiss and granodioritic gneiss. The granitic gneiss consists of about equal amounts of quartz, microcline, and sodic plagioclase. Minor minerals are biotite, muscovite, magnetite, ilmenite, chlorite, apatite, zircon, and epidote. The granodioritic gneiss is nearly half plagioclase with 43% quartz. Microcline is almost totally absent. Minor minerals are similar to the granitic gneiss. Both rocks are foliated.

Structure. The major structural trend in the Beartooth Mountains is northwest. The present mountains parallel it; there are Precambrian dikes that follow it; and the prominent Cooke City and Stillwater structures also follow it. The only major variation in this trend is the Cretaceous-Tertiary bounding faults and folds at the ends of the elongated uplift.

Wolf River Batholith.

Location and Geology. The Precambrian (1.5-billion-year-old) Wolf River batholith underlies an area of about 9300 km^2 in northeastern Wisconsin (Fig. 3-5). It is surrounded on three sides by older Precambrian plutonic and volcanic rocks of the central and northeastern Wisconsin complexes. The batholith is not apparently related to an orogeny, and it is epizonal (formed near the surface). Evidence for this conclusion includes widespread development of porphyritic texture, local occurrences of chilled margins, and sharp, discordant intrusive contacts with country rocks. Adjacent metavolcanic and metasedimentary rocks have been contact metamorphosed to hornblende-hornfels, pyroxene-hornfels facies (Van Schmus et al., 1975).

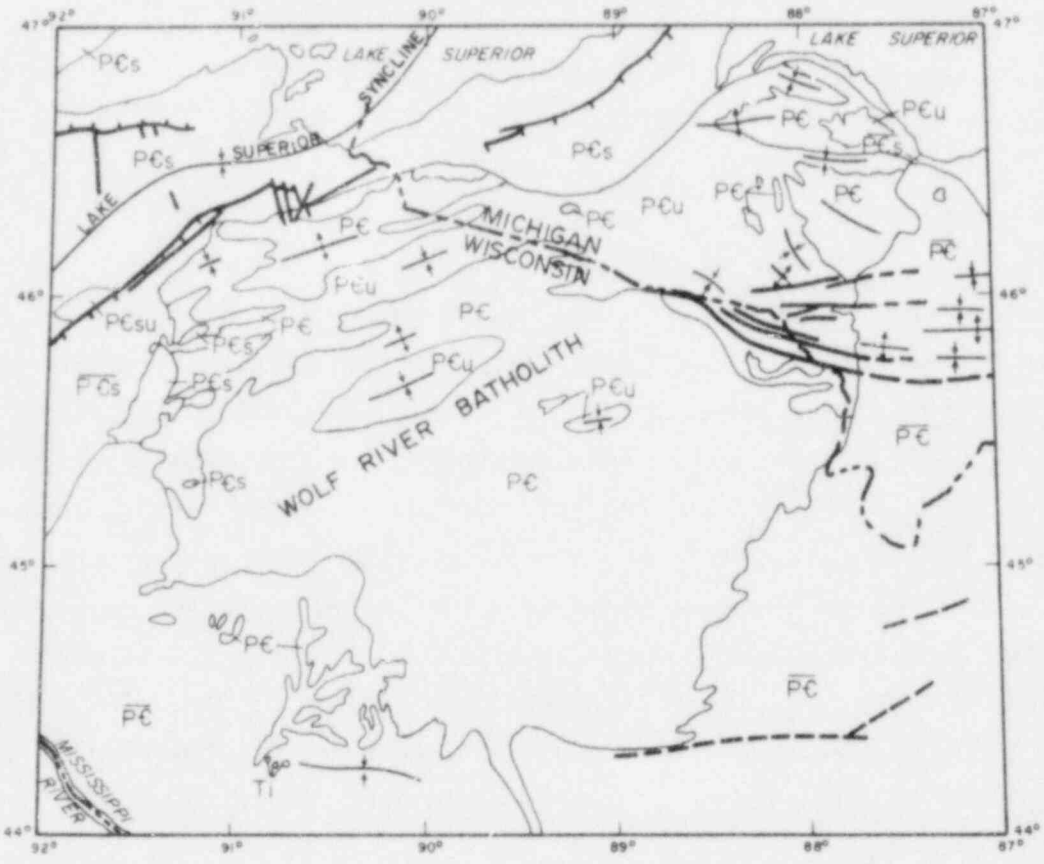

FIG. 3-5. Bedrock geology of the Wolf River batholith. See Fig. 3-3 for a key to the symbols.

Petrology. The Wolf River batholith contains mappable units of granite, quartz monzonite, syenite, monzonite, quartz and feldspar porphyry, and monzonite porphyry. Quartz monzonite is the most common and the most extensively exposed rock type.

Although a porphyritic texture is the most extensively developed in certain rock types of the batholith, Rapakivi texture is more spectacular. The Wolf River batholith is lithologically similar to the Rapakivi massifs of Finland, and the classic texture (ellipsoidal potassium feldspar mantled by plagioclase) is well developed in the Wisconsin quartz monozonites.

Perthitic alkali feldspar and quartz are the most abundant minerals in the batholith, which also contains smaller amounts of sodic plagioclase, iron-rich biotite and amphibole, and (locally) olivine and pyroxene (Van Schmus et al., 1975). Typical accessory minerals are fluorite, zircon, apatite, allanite, ilmenite, and magnetite.

Jointing and Fracturing. Although numerous and well-developed near the surface, fractures diminish in size and number with depth. Major fracture patterns in the batholith are oriented N. 75° W., N. 30° E.; and N. 30° W., N. 85° E. (Bell and Sherrill, 1974).

Sierra Nevada Batholith.

Location and Geology. The Sierra Nevada batholith comprises a group of many granitic plutons which, collectively, form the northwest-trending Sierra Nevada mountain range in east-central California (Fig. 3-6). The batholith is approximately 644 km long and 80 km wide, and covers approximately 77,700 km^2. The Sierra Nevada batholith was probably formed during the Mesozoic era when the upper layers of the earth's crust were depressed into deeper, more mafic regions. The more siliceous rocks melted, migrated upward, and crystallized to form the batholith. For this reason, the base of the granitic batholith grades into ultramafic rocks at an approximate depth of 35 km. Th batholith has been block-faulted on the east and tilted westward, so that sedimentary rocks lap onto the west side, forming gentle slopes, while the east side is steep.

Petrology. At least two parent magmas formed the batholith. The eastern side of the batholith is 200 $\pm$ 20 million years old (Triassic period). Individual plutons there consist mainly of quartz monzonites and diorites (Bateman et al., 1963). Plutons on the western side are from the Jurassic period. They generally consist of quartz diorites and granodiorites. The mineralogy of this massive batholith is difficult to typify, because the composition of the rocks commonly vary from alaskite to quartz diorite within the same subsidiary pluton. However, the rocks commonly have equigranular, porphyritic, or seriate texture, and contain plagioclase, quartz, potassium feldspar, hornblende, biotite, and muscovite (in order of descending abundance).

Structure. The Sierra Nevada batholith is thought to occupy the trough of a large synclinorium. The dominant trend within this structure is N. 40° W., or parallel with the range itself. All the major strike, normal, and reverse faults follow this trend and all faults have a main strike-slip component.

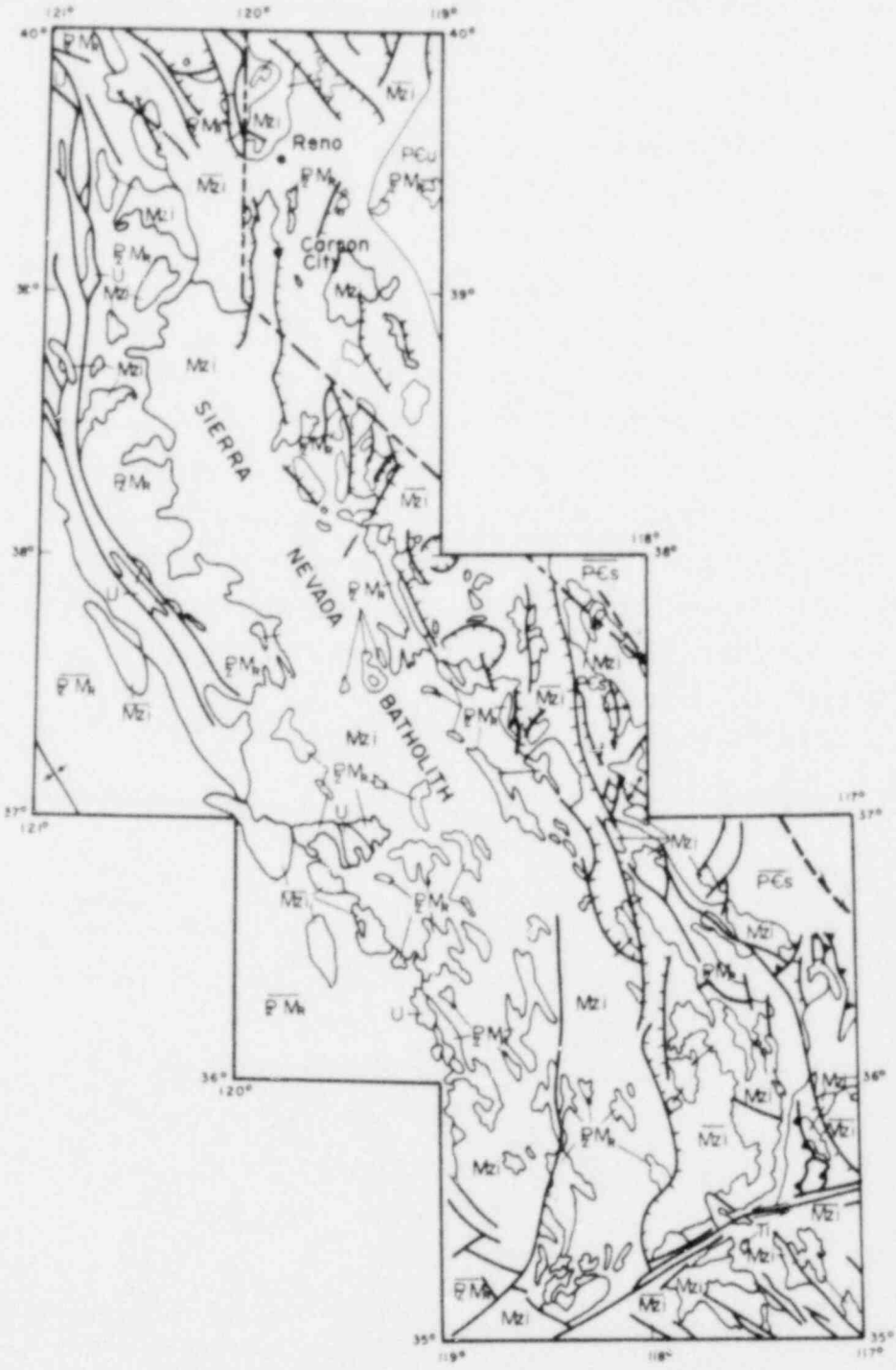

FIG. 3-6. Bedrock geology of the Sierra Nevada batholith. See Fig. 3-3 for a key to the symbols.

Southern California Batholith.

Location and Geology. The Southern California batholith has been described as a huge, composite injection dike (Larsen and Schmidt, 1958). Formed during the middle Cretaceous period, the batholith is located in the southern part of California and northern Mexico. The granitic mass is elongated in a northwesterly direction and covers approximately 207,200 km^2 (Fig. 3-7).

Petrology. Like the Sierra Nevada batholith, the Southern California batholith is composed of several individual plutons. It consists of what is thought to be a single magma series with rocks ranging from gabbro to granite. The most common rock composition of the batholith is quartz diorite. The mineral percentages of a typical quartz diorite are quartz, 18%; microcline, 7%; oligoclase, 58%; biotite, 7%; amphibole, 8%; and magnetite, 1%. Grain size is irregular; oligoclase forms the larger grains, microcline and quartz occur as the small grain and interstitial material.

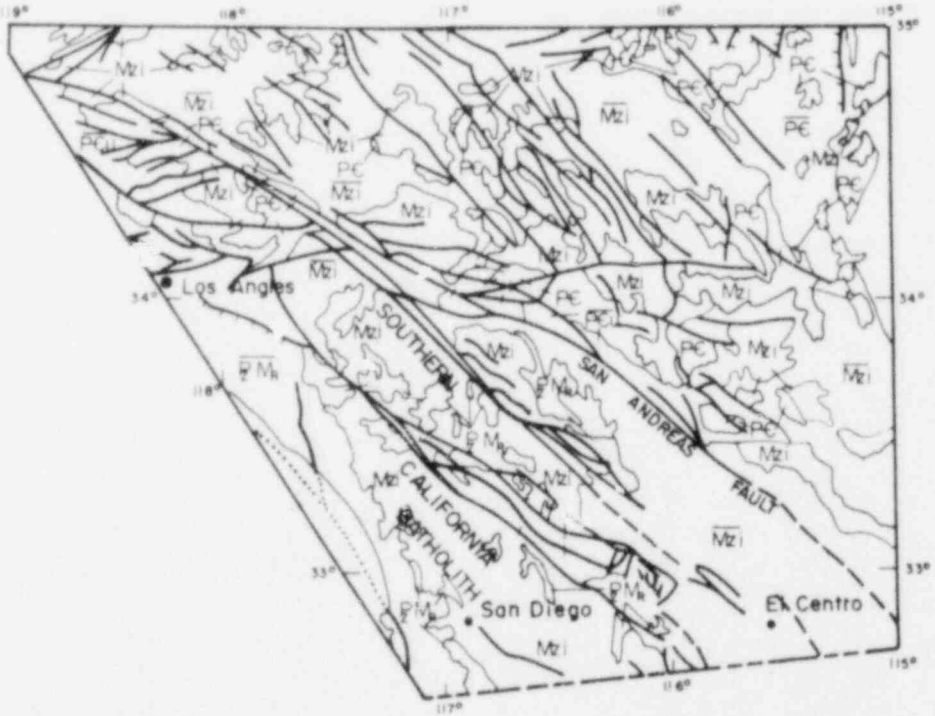

FIG. 3-7. Bedrock geology of the Southern California batholith. See Fig. 3-3 for a key to the symbols.

Structure. The main trend of the Southern California batholith is northwesterly. Excluding the Transverse Ranges in the same area, this is typical of the rest of Southern California. All the sediments and metamorphics that host the batholith, and most of the linear features within the batholith, strike parallel to this trend. Individual intrusives are elongate to the northwest, as are inclusions, gneissic foliation, and mineral zones within the intrusions.

References show that the few faults mapped within and adjacent to the granitics also trend northwest. No reference was found for jointing or minor fracture patterns. However, these certainly exist and no doubt also follow the regional trend (Larsen, 1948).

Northern Washington Batholiths.

Location and Geology. The Colville, Chelan, Loon Lake, and Cathedral batholiths cover about 181 km^2 in a nearly circular area in northeastern Washington (Fig. 3-8). The four comparably sized batholiths merge toward the south and are considered to be contemporaneous (Hutting et al., 1961). Age dating of the batholiths is difficult, because few cross-cutting relationships

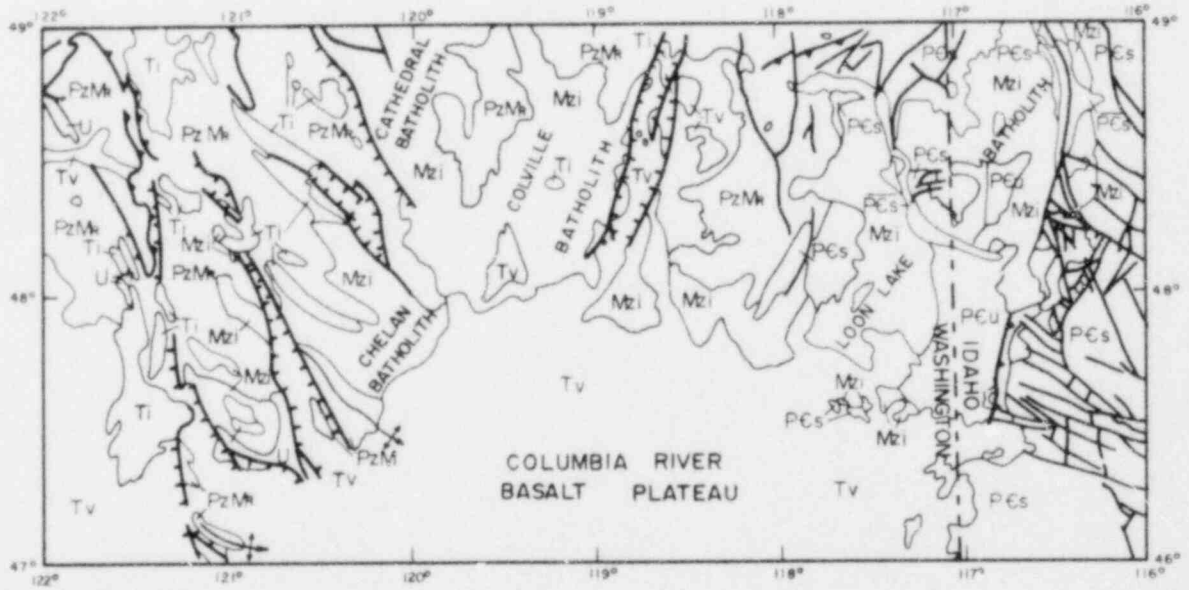

FIG. 3-8. Bedrock geology of the Northern Washington batholiths. See Fig. 3-3 for a key to the symbols.

between the batholiths and surrounding strata are evident. It is commonly believed that the four Mesozoic batholiths are from the Cretaceous period. Granitization produced the igneous as well as the gneissic rocks (Campbell, 1940; Krauskopf, 1941; Crowder, 1959; Hutting et al., 1961).

Petrology. In these four batholiths, rock composition ranges from alaskite to granodiorite (Pardee, 1918; Waters and Krauskopf, 1941). The centers of the batholiths commonly consist of light to pinkish grey, medium-grained, porphyritic granite. This granite is composed of orthoclase phenocrysts, quartz, plagioclase, and a smaller amount of biotite. Toward the edges of each batholith, granodiorite and quartz diorite become the most common rock types, with hornblende content increasing to 30% of the total rock. Lamprophyre and pegmatite dikes commonly intersect the edges of the batholiths.

Quartz diorite gneisses display an unusual, but widespread, swirled foliation in the Chelan and Colville batholiths (Waters, 1938; Waters and Krauskopf, 1941). The texture of the rocks near the contacts of the batholiths varies. The Cathedral batholith border lacks the foliated and cataclastic structure of the Chelan batholith. The Cathedral batholith is the only pluton with extensive contact metamorphism, which produced a very unusual breccia (up to four miles thick), with hornblende schist as the xenoliths (Waters, 1938).

Jointing and Fracturing. Northwest-trending faults which have had many episodic displacements are common. Joint patterns are less consistent than the fault patterns. Three sets of widely spaced joints (two vertical and one horizontal) are common throughout (Pardee, 1918).

Idaho Batholith.

Location and Geology. The Idaho batholith, of middle Cretaceous age, extends from central Idaho into western Montana (Fig. 3-9). It underlies a roughly rectangular area of about 41,440 km^2 (Larsen and Schmidt, 1958). The Idaho batholith is relatively flat-topped and is about 836 km long and 137 km wide at its widest point. It is bounded on the north, east, and west by older rocks, while the southern contact is with younger rocks, chiefly

FIG. 3-9. Bedrock geology of the Idaho and Boulder batholiths. See Fig. 3-3 for a key to the symbols.

lavas of Tertiary age. The batholith is in an area of high, rugged mountains, yet over large areas weathering is so deep that the geologic character of the rock cannot be determined.

Petrology. The Idaho batholith is made up of several individual rock units. The extreme range in petrology of the rock units is from quartz gabbro to granite, but many rock types occur in very small amounts. The range in petrology of the main rock mass is from quartz diorite to quartz monzonite (Larsen and Schmidt, 1958). The average composition is a granodiorite with major quartz, potassium feldspar, and plagioclase, and minor biotite. Muscovite hornblende and pyroxene are rare, and sphene and apatite are accessories (Ross, 1963). Generally, the rocks are coarse grained. Some, especially the quartz monzonites and some of the granodiorites, contain phenocrysts of microcline and microperthite as much as 8 cm long. The large phenocrysts are unevenly distributed and are abundant in parts of some rock bodies and absent in others. The principal dark minerals of the gabbro are pyroxene and secondary hornblende, those of the tonalite are hornblende with some biotite. The quartz monzonites are almost entirely biotite (Larsen and Schmidt, 1958).

The greater part of the Idaho batholith was probably intruded as a unit or as a number of large, intimately related units. Changes in fabric and composition are common, but in many places the different varieties merge into each other without mappable boundaries. The changes record movement in the magma, differentiation, and late-stage modifications during the long period required for so large a mass to move into position and consolidate.

Structure. Because of the size of the Idaho batholith, the structure and interrelations of the various plutons are complex. Anderson (1952) divided it into two distinct age groups. The old rocks are related to the Sierra Nevada orogeny granitics of Washington and Oregon. These cover the entire range of compositions from diorite to granite, but granodiorite and quartz monzonite are most common. The younger plutons are also quartz monzonite and granodiorite; however, they are Cretaceous to Eocene.

Once in place, the Idaho batholith played an important role in the crustal deformation that occurred in the western United States during the early Tertiary. Along the edges of the batholith, the compressional forces were transmitted to the surrounding rocks and there produced great thrust faults and tight folds.

Within the batholith, northwest-trending thrusts were complemented by northeast shear zones. The shear zones tend to have strike-slip movement and

are accompanied by normal faulting. Where these shears are aligned with regional transverse zones, major strike-slip shears developed. The Coeur d'Alene's Osburn Fault is an example (Anderson, 1948).

Local fracturing intensities are related to the major structures. Where a major thrust or shear occurs, the rocks are much more fractured and jointed than elsewhere.

Boulder Batholith.

Location and Geology. The Boulder batholith of southwestern Montana is an elongated mass 100 km long and 50 km wide, trending north-northeastward around Butte, Montana (Fig. 3-9). This batholith is of late Cretaceous age and consists of plutons of quartz monzonite, granodiorite, and other granitic rocks. It is believed to be a relatively thin mesozonal batholith that was injected into a shallow floor of premagmatic rocks and then covered mainly by its own volcanic ejecta. Geologic field relations and gravity data suggest that the average thickness of the batholith is perhaps 5 km (Hamilton and Myers, 1974).

Petrology. The composition of igneous rocks in the Boulder batholith varies from syenogabbro to alaskite, but approximately 75% of the batholith is Butte Quartz Monzonite, which contains the following mineral percent ranges: quartz, 15-40%; plagioclase, 20-48%; feldspar, 15-45%; biotite, 1-12%; and accessories, 1-3%. Accessories include magnetite, sphene, zircon, apatite, allanite, and rutile. Texture is generally equigranular; however, porphyries with potassium feldspar phenocrysts up to 3 cm long do occur (Becraft et al., 1962).

Structure. The thin disklike structure of the Boulder batholith presented by Hamilton and Myers (1974) does contrast with the classic, thick, no-bottom batholith shape. However, their theory is based on inward dipping structures and floorlike features that appear to lie beneath the batholith at its north and south edges. This shape makes this batholith the equivalent, on a much larger scale, of a lopolith.

The area of Montana underlain by the Boulder batholith was caught up in the extensive eastward thrusting that took place in the Cretaceous and

Tertiary. In addition, smaller scale thrusting has occurred along the top of the batholith chamber in conjunction with intrusion. Hence, thrust faulting, with accompanying strike-slip, shear zones, and other union faulting, is common.

On a smaller scale, individual areas have well-developed joint and fracture patterns. Many dikes, veins, shear zones, and faults trend east, northeast, and north. Yet, in the same area, no pattern for the well-developed joints could be identified.

GEOMECHANICS

This section presents a review of the major rock mechanics considerations which affect the evaluation of granite as a potential nuclear waste disposal site. Its aim is not to be exhaustive, rather to present the major effects and trends of the principal parameters. Definitions of the major terms used in this discussion may be found in the appendix to this chapter.

The most important considerations in designing the excavations for an underground repository for radioactive waste are the safety, stability, and longtime security of the excavations. Ideally, one would like to take the results of laboratory experiments performed on small samples of rocks and insert these values into theoretical analyses, thus to predict the stability of the openings created. Such an approach, however, has not proven to be realistic for a major underground structure. It is limited by the effects of size and geologic structure on the strength of the rock.

Unfortunately, as will be discussed later, there is a great lack of information regarding the effect of sample size on the property measured. Nonetheless, because of the great expense of large-scale in situ testing, the primary source of information regarding the properties of rock are obtained from laboratory measurements. Many properties can be adequately described by such laboratory testing procedures. Unfortunately, others cannot. Much work remains to be done on the procedures by which the input parameters for predictor models can be generated on the basis of laboratory data.

It is clear from a review of available data that all of the thermal, thermoelastic, and mechanical properties of rock are functions of temperature. Until recently, however, most rock properties were determined only at room temperature. The effects of temperature variations on several properties are summarized in Table 3-2, with particular reference to the

TABLE 3-2. Temperature dependence of rock properties and the effects of temperature on cavern stability (from Tsui, 1979).

	Temperature dependence	Consequence of temperature increase
Thermal properties:		
Conductivity and diffusivity	Decrease with increasing temperature.	Combined effect increases thermal gradient, hence increases thermal stress. Stability thus decreases.
Specific heat	Increases with increasing temperature.	
Density	Negligible in nonporous rock.	
Thermoelastic properties:		
Coefficient of linear thermal expansion	Increases with increasing temperature.	Increases thermal stress, hence decreases stability.
Young's modulus and Poisson's ratio	Decrease with increasing temperature.	(1) Decreases thermal stress, hence increases stability. (2) Increases radial deformation.
Mechanical properties:		
Strength parameters	Decrease with increasing temperature.	Decreases stability.
Stress-strain behavior	Ductility and flow tendency increase with increasing temperature.	Increases radial deformation.

stability of an underground opening (Tsui, 1979). Both conductivity and diffusivity decrease with increasing temperature. Specific heat, on the other hand, increases with increasing temperature. These changes, taken together, increase the thermal gradient and hence increase thermal stress. The coefficient of linear thermal expansion increases with increasing temperature, likewise increasing thermal stress and decreasing the stability of an opening. Young's modulus and compressive strength decrease with increasing temperature; these changes combine to reduce structural stability.

Attempts have been made to classify rocks generically and to discuss physical properties in the same way. One type of strength classification is shown in Fig. 3-10 for several rock types (Deere and Miller, 1966). Even for small laboratory samples, the strength of granite varies about threefold. The difference between intact rock properties and rock-mass properties is even greater. These variability and scaling considerations should be kept in mind during the following discussions.

In Situ Stresses

The stability of any underground opening is determined by the strength of the rock materials and by the stresses applied. These stresses include those existing in the ground prior to excavation, those induced during the excavation process, and those induced after completion of the excavation, such as the long-term effects of radioactive waste. This section discusses the state of stress in the vicinity of a potential repository prior to excavation.

In general, the vertical component of the in situ stress has a value close to that given by the weight of the overburden. It is, of course, influenced by variations in topography and by the time which has passed since the rock was deposited. Horizontal stresses, on the other hand, are highly variable. In situ measurements of stress fields have revealed that the horizontal components can range from approximately one-third of the vertical stress to several times the vertical stress. These measurements have been compiled by Hoek and Brown (in press), as shown in Fig. 3-11. Note that the envelope at a 1000-m depth, which might be typical for a repository, shows horizontal stress variations from about 0.5 to 1.75 times the vertical stress. The exact stress state is highly site dependent; therefore, the stress field must be carefully measured at the location of interest. The

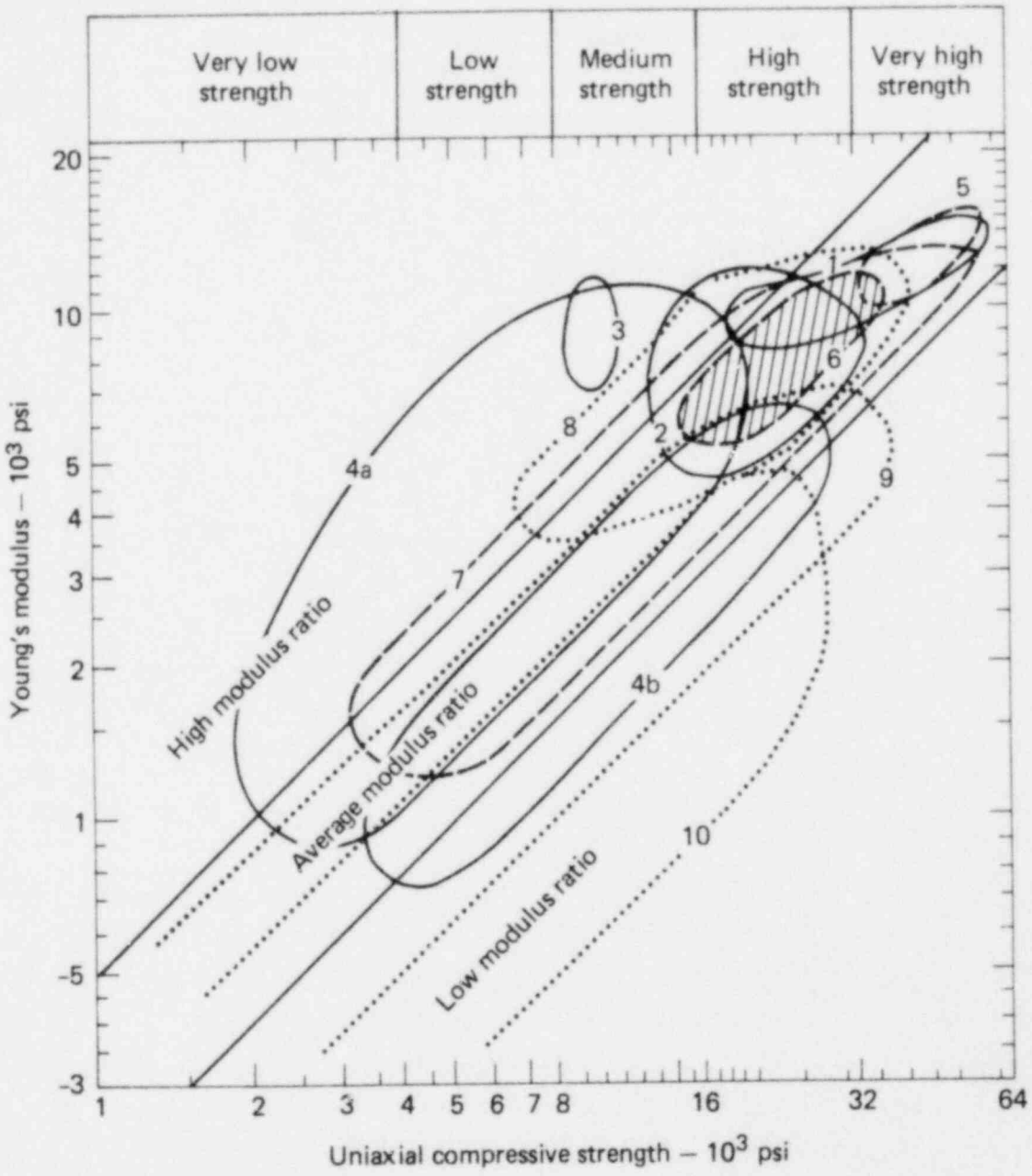

Metamorphic
- 1 Quartzite
- 2 Gneiss
- 3 Marble
- 4a Schist, steep foliation
- 4b Schist, flat foliation

Igneous
- 5 Diabase
- 6 Granite
- 7 Basalt and other flow rocks

Sedimentary
- 8 Limestone and Dolomite
- 9 Sandstone
- 10 Shale

FIG. 3-10. Engineering classification of intact rock, based on uniaxial compressive strength and modulus ratio (from Deere and Miller, 1966).

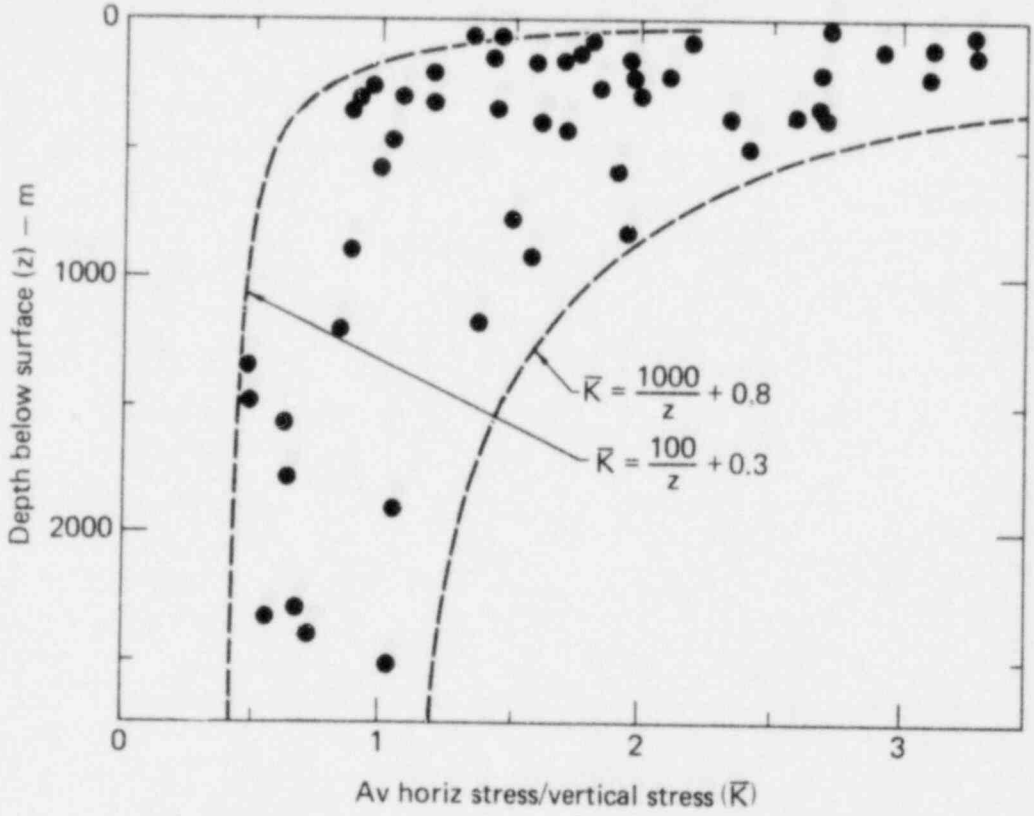

FIG. 3-11. Compilation of measurements of the virgin state of stress in rock (from Hoek and Brown, in press).

stability of an opening will vary considerably, depending on whether the major principal stress is vertical or horizontal. The best design shape of the opening will change accordingly.

Table 3-3 shows the relationship of the stresses for various ages of rock in Ontario. For Devonian rocks, the horizontal stress is expected to be less than or equal to the vertical, whereas, for the older Silurian, Ordovician, and Precambrian rocks, the horizontal stress is expected to be greater than the vertical stress.

A plot of stress variation with depth for Precambrian (primarily granitic) rocks is shown in Fig. 3-12 for a number of locations. There is a wide variation, but most of the sites and tests reveal a horizontal stress greater than the vertical. Figures 3-13 and 3-14 show the results of some stress measurement work which was done at the Stripa mine in Sweden (Carlsson, 1978). The variation in principal stress magnitude is shown in Fig. 3-13. The principal stress magnitude appears to vary threefold over a hole length of

TABLE 3-3. Stress conditions for rocks in Ontario, Canada (from Tsui, 1979; Lee, 1978).

Geological period	Probable stress conditions[a]
Devonian	$\sigma_v \geq \sigma_h$ (?)
Uplift (20 million years)	
Silurian	$\sigma_h >> \sigma_v$
Ordovician	$\sigma_h >> \sigma_v$
Uplift (500 million years)	or $\sigma_h \simeq \sigma_v$
Precambrian	$\sigma_h > \sigma_v$

[a] σ_h = horizontal stress; σ_v = vertical stress.

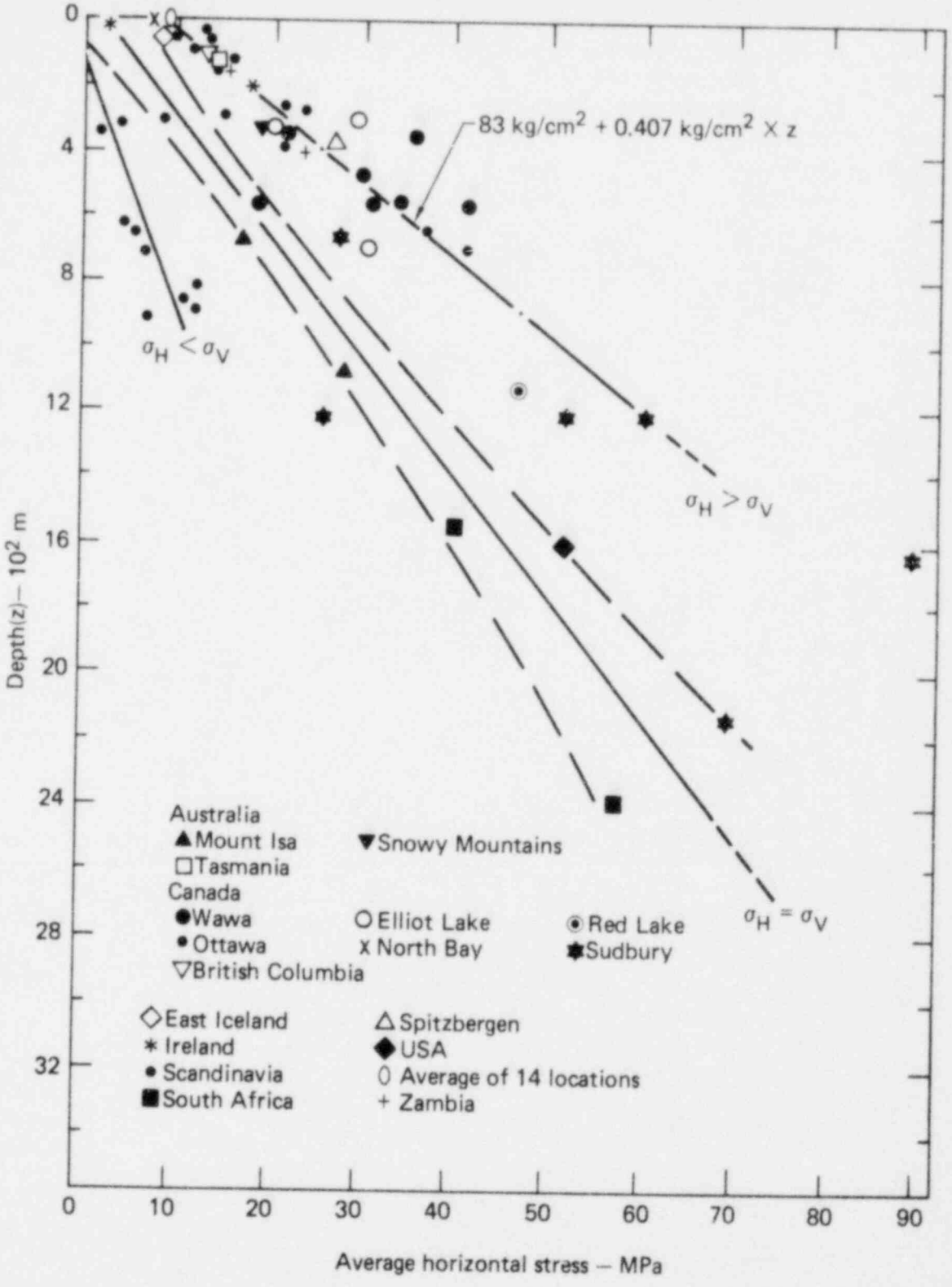

FIG. 3-12. Increase of average horizontal stress with depth in Precambrian rocks (from Lee, 1978; Tsui, 1979).

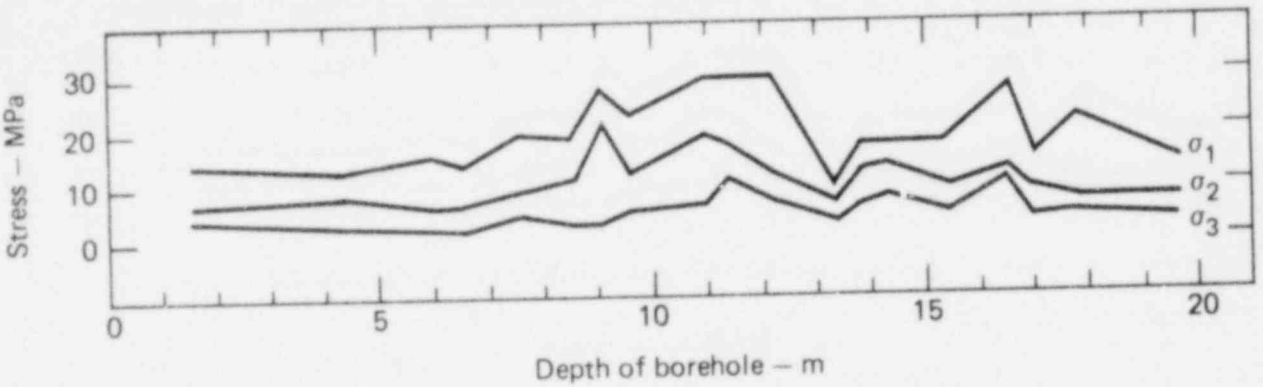

FIG. 3-13. Variation of principal stresses in a borehole at the Stripa mine, Sweden (from Carlsson, 1978).

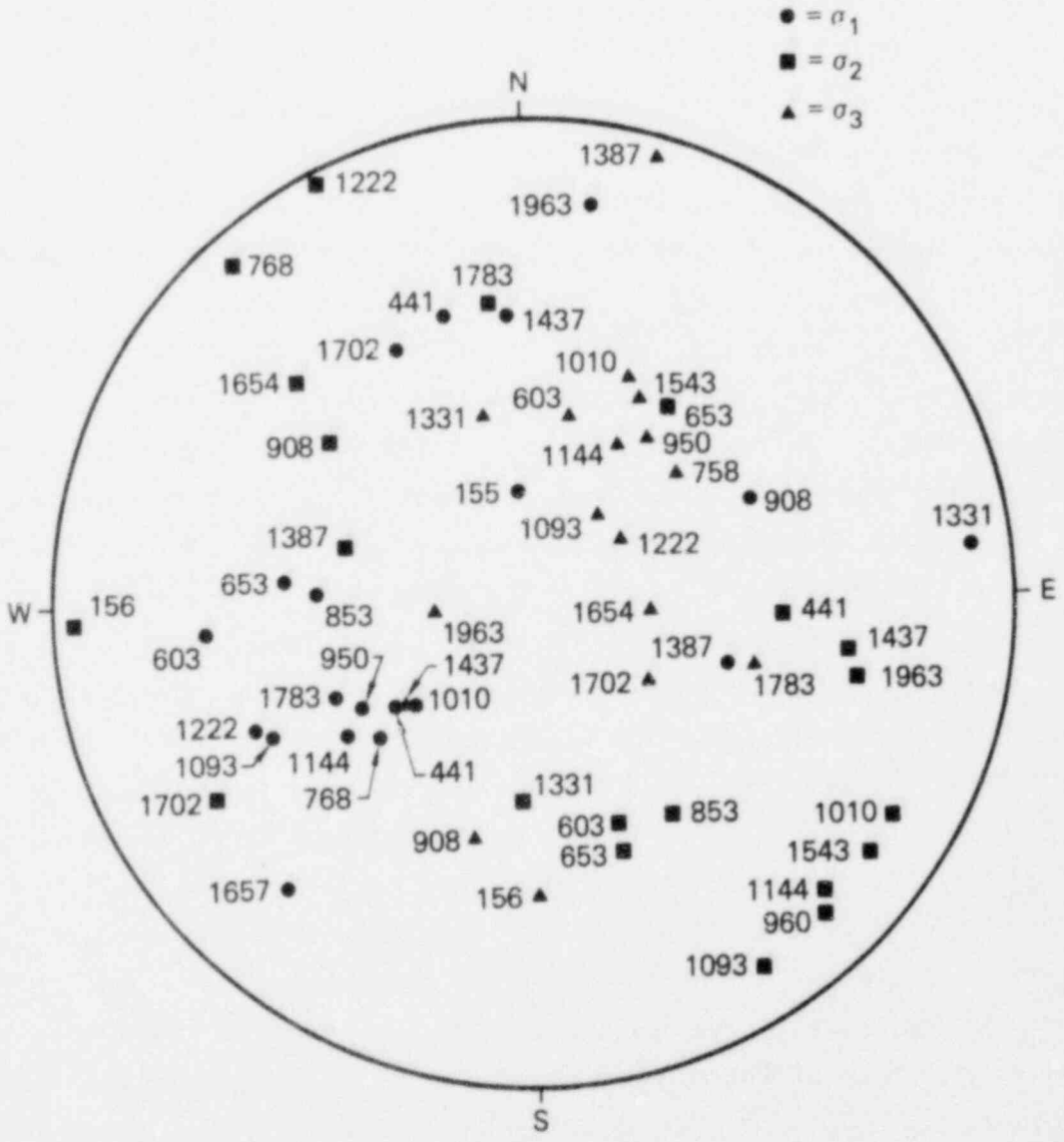

FIG. 3-14. Direction of the principal stresses at different measurement points at the Stripa mine, Sweden (from Carlsson, 1978). The depth of measurement in the borehole is indicated on a Wulff net lower hemisphere.

about 5 m. Variability in principal stress direction is shown in Fig. 3-14. Again, the variation is considerable. In general, stress fields are found to be not only site specific but also significantly variable even within a specific rock mass.

Mechanical Properties

Mechanical properties which are normally considered in any description of a rock material include index properties (such as unit weight or density), moisture content, porosity, stress-strain relationships (which yield Young's modulus and Poisson's ratio), and rock strength as measured by the compressive and tensile strengths.

A summary of properties for intact granite is given in Table 3-4. These values were collected during a literature review of published reports. Even properties such as unit weight, which is normally considered relatively constant for granite, varies considerably (from 2310 to 3040 kg/m^3). Other properties vary much more widely. (Tensile strength is shown to vary from about 3.5 to 55 MPa; however, those samples which were already broken were, of course, not tested. Thus, the variation should actually be from 0 to 55 MPa.)

A second summary of properties for granite is shown in Table 3-5. The granitic rock types and locations marked with asterisks are from quarries. As a group, they can be considered typical granites. They were selected for special mention because of their lack of jointing, lack of weathering, homogeneous nature, uniform coloring and texture, and their proximity to the surface. Some of these quarries exhibited very high in situ stress fields. Table 3-6 presents a comparison of rock properties from the Climax stock at the Nevada Test Site and the Stripa mine in Sweden. Notice that for any particular site, the variation in properties is much smaller than the range established for a generic granite.

The most common test performed in rock mechanics work is the uniaxial compression test from which one can obtain Young's modulus (the ratio of stress to resultant strain) and Poisson's ratio (the ratio of lateral to longitudinal strain). At the edge of an underground opening, the confining pressure is zero. As one progresses away from the opening, the stress state becomes triaxial. The two minor principal stresses may or may not be equal.

TABLE 3-4. Properties of intact granite (from ONWI, 1978).

	Mean value	Range
Index properties:		
Unit weight, kg/m^3	2646.5	2306.9-3043.8
Natural moisture content (intact), %	--	0-0.32
Porosity (rock-mass), %	1.6	0.05-11.2
Stress-strain properties:		
Young's modulus, GPa	50.3	15.9-83.4
Poisson's ratio	0.18	0.045-0.39
Strength properties:		
Uniaxial compressive strength, MPa	175.1	35.2-353.1
Tensile strength, MPa	6.3	3.4-55.9
Thermal properties:		
Coefficient of linear thermal expansion, $^oC^{-1}$	2.5×10^{-6}	1.67×10^{-6} to 3.34×10^{-6}
Heat capacity, J/g-^oC	0.92	0.67-1.38
Thermal conductivity, W/m-^oC, at:		
0^oC	2.86	
50^oC	2.70	
100^oC	2.56	
150^oC	2.44	
200^oC	2.34	
300^oC	2.15	
400^oC	1.99	

TABLE 3-5. Summary of geomechanical properties of granitic rocks.[a] See text for explanation of granites marked by asterisks.

Rock type and origin	Stress-strain properties					Strength properties		Reference
	Young's modulus, GPa	Density, g/cm^3	Bulk modulus, GPa	Shear modulus, GPa	Poisson's ratio	Uniaxial compressive strength, MPa	Tensile strength, MPa	
Granite (coarse-grained), Polehill power plant, Loveland, Colo.	26.6 25.4	2.63(0.03,9)				72.1 52.6	2.63(0.03,9) 0.02(0.0002,9)	USBR, 1953
Pegmatite granite, Polehill power plant, Loveland, Colo.:		2.62(0.09,27)						
Group A Group B	19.0				0.10	42.7(29.2,3) 58.2(0.69,2)		USBR, 1953
Slightly altered granite, Grand Coulee pumping project, Grant County, Wash.	7.59				0.13(NR,3)	56.9 26.3		USBR, 1953
Slightly altered granite, Grand Coulee pumping project, Grant County, Wash.	8.97 8.28	2.61(0.04,18)			0.126(NR,3)	64.8 33.2		USBR, 1953
Granite, Grand Coulee pumping plant, Grant County, Wash.	32.6 12.4	2.63(0.07,32)			0.14(NR,3)	148.8		USBR, 1953
Granite, Nevada Test Site						64.8		Kunar, 1968
Granite, no location	31.0-58.6				0.15-0.24		2.99-4.8	Richey, 1963
Granite, Valencia County, N.M.	77.9(NR,2)	3.0				154.5		USBR, 1953
Granite, N.M.	77.9	2.80		32.3	0.27			Blair, 1955
Granite (gneisses), Ga.	19.2	2.66		10.3		200.0	2.8	Blair, 1955
Granite, Bridge Canyon dam site, Mohave County, Ariz.	53.8(NR,5)	2.66(0.06,15)			0.08	144.8(66.2,4)	5.6(1.9,4)	Brandon, 1976
Granite, Valencia County, N.M.	7.24(NR,2)	2.59(0.06,2)			0.07	25.5(9.7,2)		Br[illegible]on, 1976
Granite (weathered), no location		2.74(NR,8)						Morris and Johnson, 1967

continued

[a]Values are presented in the form A(B,C), where A is either the single value reported, the mean, or the range of values (A_1-A_2); B is either the difference between the maximum and minimum reported values or the range of values (B_1-B_2); and C is the number of samples tested. Both B and C or C alone may be absent. NR signifies "not reported."

TABLE 3-5 continued.

Rock type and origin	Stress-strain properties					Strength properties		Reference
	Young's modulus, GPa	Density, g/cm^3	Bulk modulus, GPa	Shear modulus, GPa	Poisson's ratio	Uniaxial compressive strength, MPa	Tensile strength, MPa	
Granite, Unaweep granite site, Grand Junction, Colo.	21.9	2.69			0.08	164.8	4.17	Blair, 1956
Granite, Vt.	28.9	2.66		15.9				Windes, 1949
Granite, Md.	54.6	2.65		25.4		251.0		Windes, 1949
Granite, Nev.	51.3	2.63		22.5		272.4		Windes, 1949
Granite, N.C.	24.2	2.60		12.3		209.7		Windes, 1949
Granite, no location	48.1(71.65,93)				0.20(0.35,75)		6.62(16.6,22)	Judd, 1969
Granite, no location	52.1	2.67			0.16	202.7		Kulhany, 1975
Quadarrama Granite	24.4					62.8		Kulhany, 1975
Fremont Canyon Granite (coarse-grained)	64.1	2.62			0.14		8.62	Kulhany, 1975
Salida Granite	70.7	2.64			0.18	324.1		Kulhany, 1975
Porphyritic granite, Mitidieri Quarry	69.06	2.74			0.24	91.7		Kulhany, 1975
Granite, Valinnos Quarry	65.8	2.72			0.18	107.2		Kulhany, 1975
Granite, Cantareira Quarry	64.1	2.81			0.25	111.3		Kulhany, 1975
Tourmaline granite, Piccicacco Quarry	75.5	2.65			0.16	127.1		Kulhany, 1975
Pikes Peak Granite (coarse-grained, weathered)	33.4	2.67			0.37	88.9	3.93	Kulhany, 1975
Pikes Peak Granite (dense, medium- to fine-grained)*	70.6	2.67	62.0	27.0	0.31	226.1	11.9	Kulhany, 1975
Barre Granite (dense, medium-grained)*	72.4	2.64	43.1	29.7	0.22	234.5	7.59	Kulhany, 1975
Silver Plume Granite, Straight Creek tunnel site, pilot bore, Colo.	60.4(44.1,40)				0.205(0.31,38)	264.9 386.2		Hurr and Richards, 1974
Quartz monzonite, Straight Creek pilot bore, Colo.	52.4	2.67(NR,30)	52.4	19.3	0.33			Carroll et al., 1966
Quartz monzonite, Climax stock, Nevada Test Site	61.4-69.7	2.6-2.66	53.8	20.0	0.21-0.22	210.3		Carroll et al., 1966

continued

TABLE 3-5 continued.

Rock type and origin	Stress-strain properties					Strength properties		Reference
	Young's modulus, GPa	Density, g/cm^3	Bulk modulus, GPa	Shear modulus, GPa	Poisson's ratio	Uniaxial compressive strength, MPa	Tensile strength, MPa	
Monzonite porphyry, Grand Coulee pumping plant, Grant County, Wash.	41.4(3.4,3)	2.57(0.05,16)			0.18(NR,3)	124.8(0.08,140)		USBR, 1953
Colville Granite (slightly colored)*	11.0	2.61	6.20	4.82	0.20	64.8	3.24	ONWI, 1978
Colville Granite (unaltered)*	35.9	2.63	17.2	15.9	0.15	144.8	7.45	ONWI, 1978
Monzonite porphyry, Grand Coulee pumping plant, Grant County, Wash.	42.8				0.6	170.6		USBR, 1953
Quartz monzonite, Mont.		2.75				112.4		Blair, 1956
Quartz diorite, Bridge Canyon dam site, Mohave County, Ariz.	47.2(NR,2)	2.71(0.15,5)			0.07(NR,2)	118.6(19.3,2)	8.21	Brandon, 1976
Quartz diorite, Garden Valley dam site, Boise, Idaho	25.5(11.45,3)				0.104(NR,3)	87.4(9.7,3)		USBR, 1953
Quartz diorite gneiss, Bridge Canyon dam site, Mohave County, Ariz.	61.7(NR,4)	2.83(0.09,9)			0.11(NR,4)	81.4(13.1,3)	13.5(2.69,3)	Brandon, 1976
Diorite gneiss, Sec a, T. 6 S., R. 77 W.	68.4(13.4,2)	2.86(0.27,10) 2.87(0.09,3)			0.88(NR,2)	64.2(NR,1) 104.4(NR,1)		USBR, 1953
Diorite, no location	69.7(72.4,12)	2.82(0.48,5)						Judd, 1969
Mineralized diorite, Utah	71.7(24.1,5)	2.71(0.08,5)		28.8(9.17,5)	0.26(0.08,5)	246.9(40.0,5)		Windes, 1950
Diorite, Mich.	98.6(23.7,5)	2.91(0.20,2)		35.9(12.6,2)	0.29(0.06,5)	227.6(0.09,2)		Blair, 1956
Diorite (gneissic-diorite-gabbro), N.Y.	71.1(31.6,2)	3.03(0.01,2)		32.5(9.45,2)		230.0(87.6,2)		Windes, 1949
Granodiorite, Tumut Pond dam site, Snowy Mountains project, Australia	63.1(NR,6)	2.71(0.05,14)			0.16(NR,6)	126.9(50.3,3)	1.45(0.97,3)	Brandon, 1976
Pegmatite, Morrow Point Dam, Montrose, Colo.	18.5-20.6	2.64(NR,4)			0.05-0.07	56.9	6.00	Dodd, 1967
St. Cloud grey grandiorite (Precambrian)*	71.3	2.72	46.5	28.6	0.25	282.1	6.97	ONWI, 1978

TABLE 3-6. Comparison of rock properties from two locations (from Ramspott, 1979).

Property	Climax stock quartz monzonite[a]	Stripa mine Swedish granite[b]
Dry density, g/cm^3	2.6-2.66	2.6
Porosity, %	0.7-1.1	1.7
Compressive strength, MPa	210	217
Young's modulus, GPa	61.4-69.7	51.3
Poisson's ratio	0.21-0.22	0.23
Thermal conductivity, $W/m-^oC$	3.0	3.5

[a]Data from Maldonado, 1977; Obert, 1963; Wright, 1967.

[b]Data from Pratt et al., 1978.

Figure 3-15 shows the effect of confining pressure on the stress-strain curve. Figure 3-16 depicts the variation of Young's modulus and fracture stress with confining pressure for Stripa granite. The modulus varies by about 15% as the confining pressure increases from 0 to 30 MPa. The compressive strength, on the other hand, increases from about 200 to about 550 MPa. Therefore, whereas the modulus is relatively insensitive, the compressive strength is very dependent upon the confining pressure.

Tensile strength, as determined in the laboratory, is very dependent upon the sample selection, the sample size, and the method used for measurement. (Samples with preexisting fractures, which would produce a tensile strength of zero, are discarded prior to testing.) An indirect way of determining tensile strength is the Brazilian test. It is also the easiest technique and the one most often employed. However, the results obtained are about twice those obtained using a straight-pull-type tension test. Both tests supposedly measure the same property.

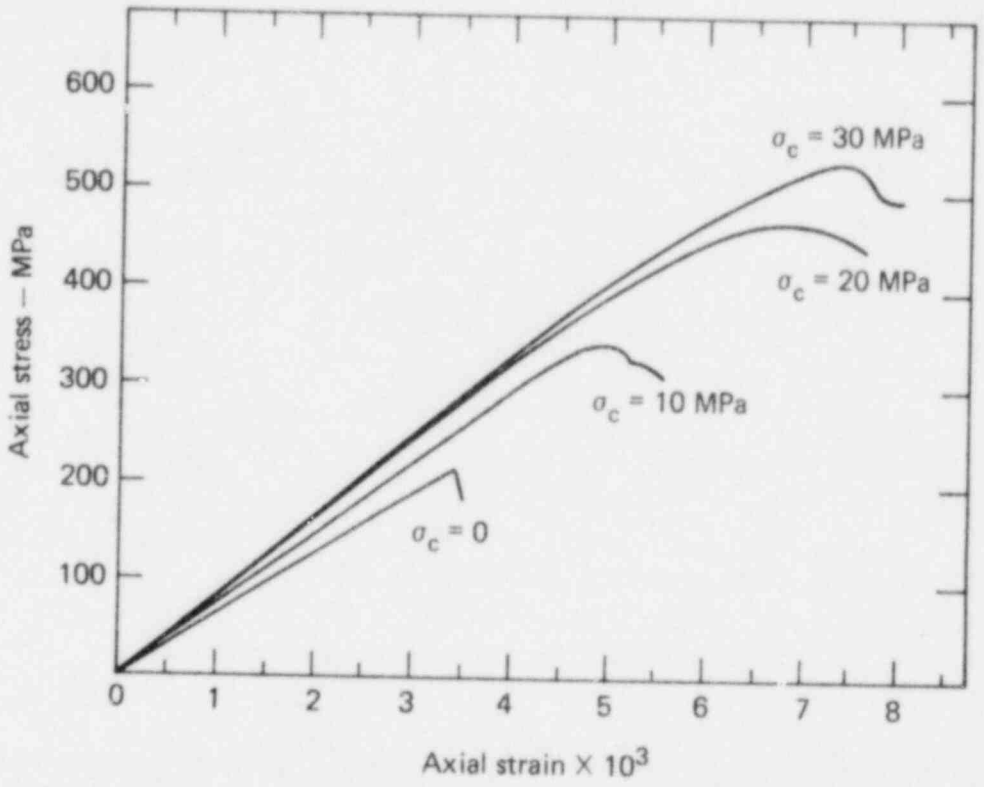

FIG. 3-15. Axial stress-strain plots for confining pressures of 0, 10, 20, and 30 MPa (from Swan, 1978).

Thermal Properties

Failure Modes. When the surface of an underground opening is exposed to a heat source, heat transfer takes place from the source to the rock mass by conduction, and possibly by radiation. Thermal transients, or a time-dependent temperature distribution, are generated across a heated zone in the rock around the opening. The temperature distribution is dependent upon a combination of three thermal properties--conductivity, density, and specific heat. These properties can be characterized by a single thermal parameter known as diffusivity.

If an analytic solution to the temperature distribution is sought, one must assume that the rock mass is a continuum and that the thermal properties of the rock are independent of temperature and spatial location. If the assumption of temperature independence is rejected, the problem becomes nonlinear, thus requiring numerical methods. Numerical techniques are

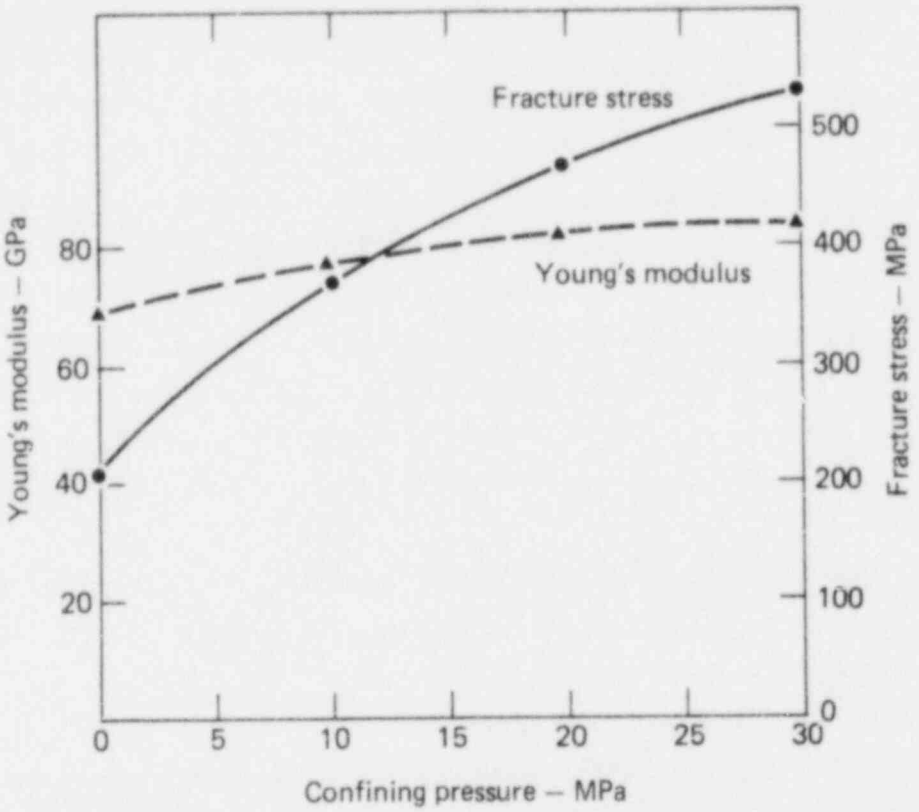

FIG. 3-16. Variation of Young's modulus and fracture stress with confining pressure (from Swan, 1978).

currently available, but the appropriate values of the necessary thermal properties are lacking.

The variation in thermal properties for intact rock samples is generally rather high. In describing rock-mass properties, the problem can become even more severe. If a piece of homogeneous material is free from constraint and is heated uniformly, no stresses are generated, even though the material changes size due to thermal expansion. However, in a rock mass that is subjected to a temperature gradient, thermal stresses are induced. The stress is due both to geometric constraint and to differences in the thermal expansion coefficients of the various constituents within the rock. These intergranular thermal stresses can develop independently of the existence of a thermal gradient or the geometric constraints. They can cause cracking along grain boundaries and also within the grains themselves. Such cracking can significantly affect both the mechanical and thermal properties of the rock. As noted earlier, rock strength decreases with temperature. We now see that stresses increase as well. When the thermally induced stress field is imposed

upon the existing stress field (that due to the in situ stresses and the excavation-induced stresses), the total may exceed the strength of the rock.

Another type of thermally induced failure is spalling. This is a progressive failure induced by thermal shock or a sudden application of heat. (Thermal loading of rock using the jet piercing system has been used for many years as a technique for rock removal.) Hence, for waste repository considerations, one must consider several thermal failure modes and have a very clear understanding of the thermal properties of the rock, on both a small and a large scale. These properties can vary widely between crystalline rock types, and even within the same rock type.

Values for Thermal Properties. Thermal conductivity has been measured for many years. It depends upon both rock temperature and pressure, though there are few data regarding the pressure dependency. The variation of thermal conductivity with temperature, however, is shown for various rocks in Figs. 3-17 through 3-19. Generally, a very rapid decrease in thermal conductivity occurs between 0 and 250^{o}C. Thereafter, the rate of decrease is considerably slower. This lower temperature range is precisely that of most repositories, however. As shown in Table 3-7, there can be a rather large range of conductivities at any temperature for a group of samples. For any one rock, the variation is generally about 30%, but can be as great as 100%. Hasan (1978) also compiled data on thermal conductivity as a function of temperature. The many values reported near room temperature ranged between 1.51 and 4.48 W/m-^{o}C. He also proposed a best fit for Barre and Westerly granites decreasing smoothly from about 2.5 W/m-^{o}C at 27^{o}C to about 1.2 W/m-^{o}C at 750^{o}C.

As mentioned earlier, one of the factors that must be considered is the spallability of the rock, since it affects the conditions directly surrounding the borehole. The piercing rating or spallability index of a number of different rocks is presented in Table 3-8. The spallability or piercing index is based on a scale from 1 to 10, where 1 indicates the greatest degree of spallability. Granites generally have high piercing indexes.

Specific heats of rocks are determined by heating specimens of known weights to a given temperature, then measuring the heat content of the rock by calorimetric methods. Figure 3-20 shows the variation of specific heat with temperature for several different rock types. The rather strange behavior of

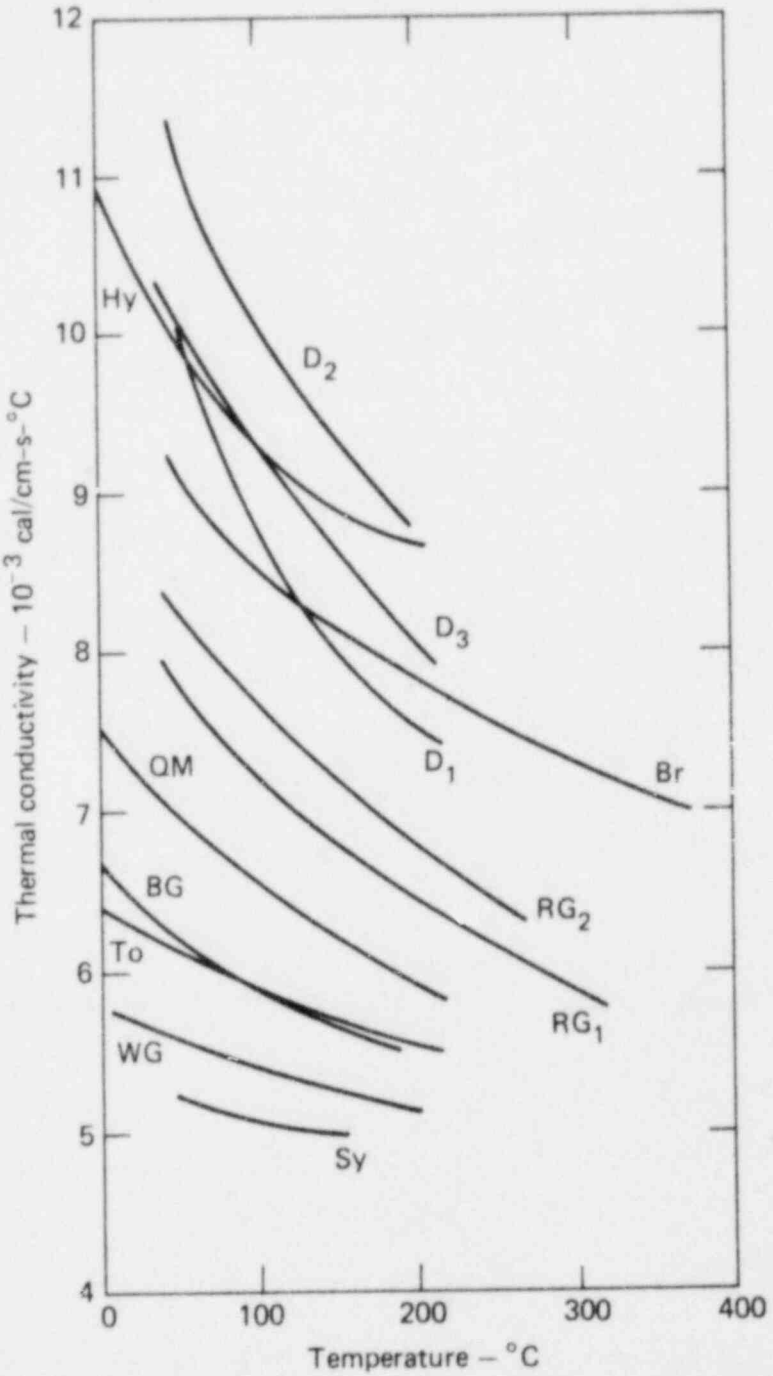

Sy Syenite, Ontario
WG Westerly Granite
To Tonalite, California
BG Barre Granite
QM Quartz monzonite, California
RG Rockport Granite
BR Bronzitite
Hy Hypersthenite
D Dunite

FIG. 3-17. Variation of thermal conductivity with temperature (from PBQ&D, 1976).

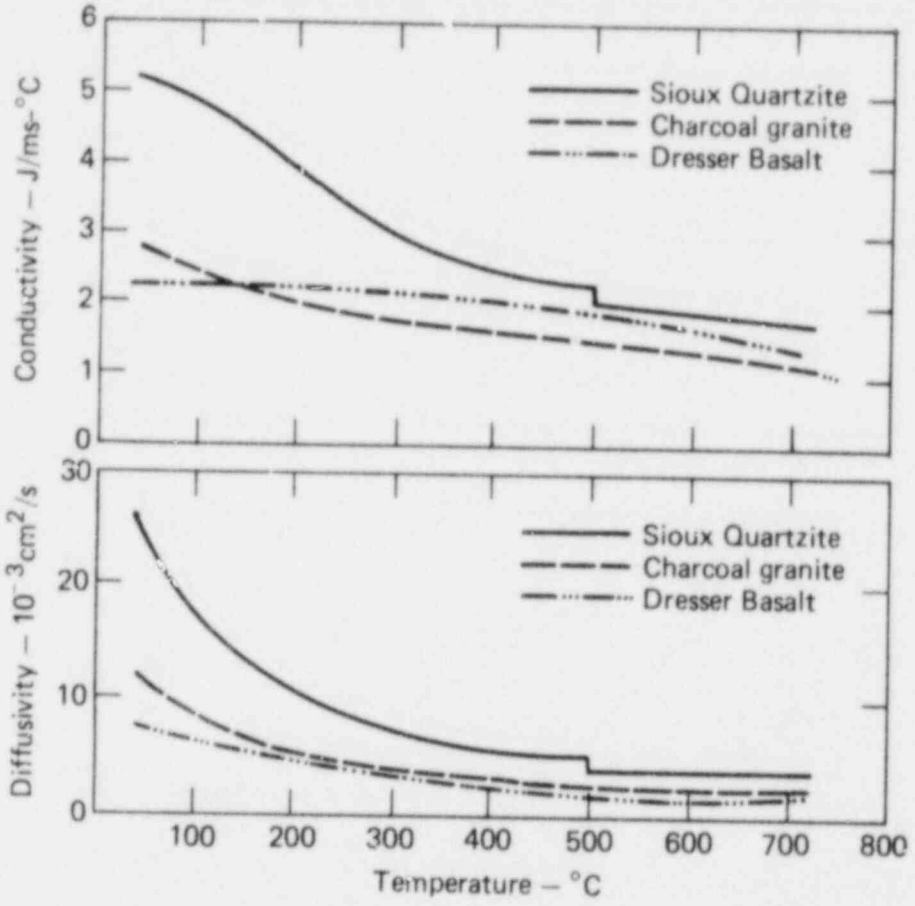

FIG. 3-18. Variation of thermal conductivity and diffusivity with temperature (from Thirumalai, 1970).

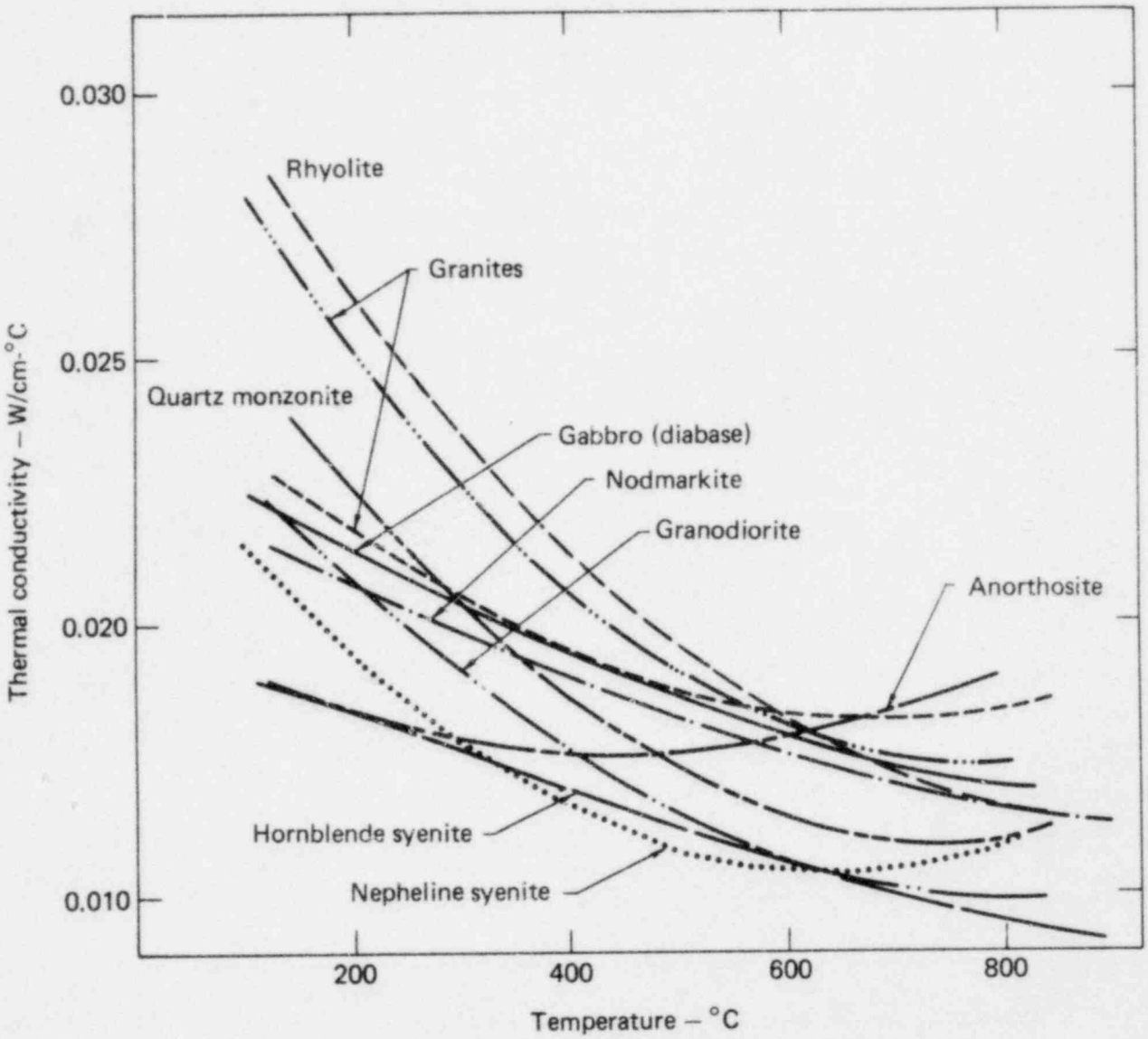

FIG. 3-19. Thermal conductivity of selected igneous rocks (from Mirkovich, 1968).

TABLE 3-7. Thermal conductivity, in 10^{-3} cal/cm-s-^{o}C, of rocks (from Lee, 1978). The measurements were made at about 20^{o} unless otherwise noted. Only cases in which there are five or more measurements from a single lithologic unit are included.

Rock type and origin	Number of determinations	Mean value	Range
Granite and quartz monzonite, Adams Tunnel, Colo.	59	7.89	6.7-8.6
Granite, Loetschberg Tunnel, Switzerland	12	7.77	6.2-9.0
Granodiorite, Steamboat Springs, Nev.	5	6.64	6.2-6.9
Granodiorite, Grass Valley, Calif.	14	7.61	7.0-8.3
Quartz-feldspar porphyry, Jacoba bore, Orange Free State, South Africa (25^{o}C)	5	8.0	7.6-8.6
Syenite and syenite porphyry, Kirkland Lake, Ontario	37	7.66	6.3-9.5
Altered rhyolite, Timmins, Ontario	6	8.23	7.4-8.8
Norite, Sudbury, Ontario	5	6.42	5.5-7.3
Serpentinized periodotite, Thetford mines, Quebec	5	6.34	5.7-7.0
Agglomerate, Roodepoort bore, Transvaal, South Africa	5	7.4	7.1-8.0
Karoo dolerite, Kestell bore, Orange Free State, South Africa (35^{o}C)	9	4.8	4.0-5.5
Ventersdorp lava, Jacoba bore, Orange Free State, South Africa (25^{o}C)	9	7.4	6.3-8.6
Ventersdorp lava, Roodepoort bore, Transvaal, South Africa	15	7.2	6.4-8.0
Portage Lake lava, Calumet, Mich.:			
Dense flows	27	5.01	4.1-6.6
Amygdaloidal tops	10	6.4	5.5-9.0
Porphyrite and diabase, Grass Valley, Calif.	21	7.14	6.2-8.2
Quartz diorite gneiss, Adams Tunnel, Colo.	17	7.75	6.6-8.5
Injection gneiss and schist, Adams Tunnel, Colo.	41	7.74	4.0-11.0
Gneiss, Gotthard Tunnel, Switzerland	15	6.68	5.1-8.0
Gneiss, Simplon Tunnel, Switzerland:			
Perpendicular	22	6.34	4.6-7.7
Parallel	8	8.90	6.0-11.4

continued

TABLE 3-7 continued.

Rock type and origin	Number of determinations	Mean value	Range
Gneiss, Simplon Tunnel, Switzerland:			
Perpendicular	8	5.74	4.1-6.8
Parallel	7	7.50	6.8-8.9
Gneiss, Chester, Vt.:			
Perpendicular	9	6.24	4.9-8.7
Parallel	9	8.33	6.1-10.4
Amphibolite, Homestake mine, Lead, S.D.	6	6.92	6.1-9.1
Calcareous mica phyllite, Homestake mine, S.D.:			
Perpendicular	7	7.89	6.5-9.0
Parallel	9	11.83	9.5-14.0
Quartzite, Homestake mine, S.D.	6	16.05	14.2-17.6
Witwatersrand quartzite, Gerhardminnebron bore, Transvaal, South Africa (two experiments, 25°C)	17 21	14.3 14.5	8.7-19.2 10.4-18.9
Witwatersrand quartzite, Roodepoort bore, Transvaal, South Africa	7	10.1	7.4-12.7

TABLE 3-8. Composition and thermal properties of several igneous Canadian rocks and minerals (from Clark et al., 1969).

Rock class[a]	Mineral composition, %					Texture	Piercing Index	% Therm. exp. to 500°C	Specific heat, W/s-g-°C	Density, g/cm^3
	Quartz	K-felds	Na-felds	Ca-felds	Ferromagnesians and miscellaneous					
Gabbro (diabase)	--	12 (graphic)	--	46 (An_{50})	24 aug; 11 hbde biot; 7 mag	M. diabasic-hypidiomorphic	2	0.45	0.945	2.98
Nepheline syenite	--	23	52	--	2 mag; 23 nepheline	M. hypidiomorphic	9	0.82	0.991	2.98
Rhyolite	23	52	51	--	3 mag	F. alletriomorphic	10	0.74	0.991	2.67
Hbde. syenite	--	73 (perthite)	17	--	9 hbde; 2 biot; 3 mag	M. hypidiomorphic	4	0.63	0.958	2.64
Nordmarkite	9	69 (perthite)	8	--	7 hbde; 2 aug; 1 mag + hematite	C. panidiomorphic	5	0.68	0.966	2.66
Anorthosite	--	1	--	97 (An_{50})	1 aug; 1 mag	C. hypidiomorphic	2	0.40	0.979	2.83
Granite	34	31	31	--	3 biot	M. hypidiomorphic	9	0.82	0.996	2.65
Granodiorite	21	4	--	51 (An_{50})	12 hbde; 9 biot; 8 epidote + sphene	M. hypidiomorphic	6	0.82	0.991	2.77
Granite	33	29	25	--	10 biot	M. hypidiomorphic	8	0.82	0.991	2.66
Quartz monzonite	27	20	--	42	10 biot; 1 muscovite	C. panidiomorphic	7	0.85	0.991	2.68

[a]All homogeneous except the second granite entry, which was coarsely gneissic.

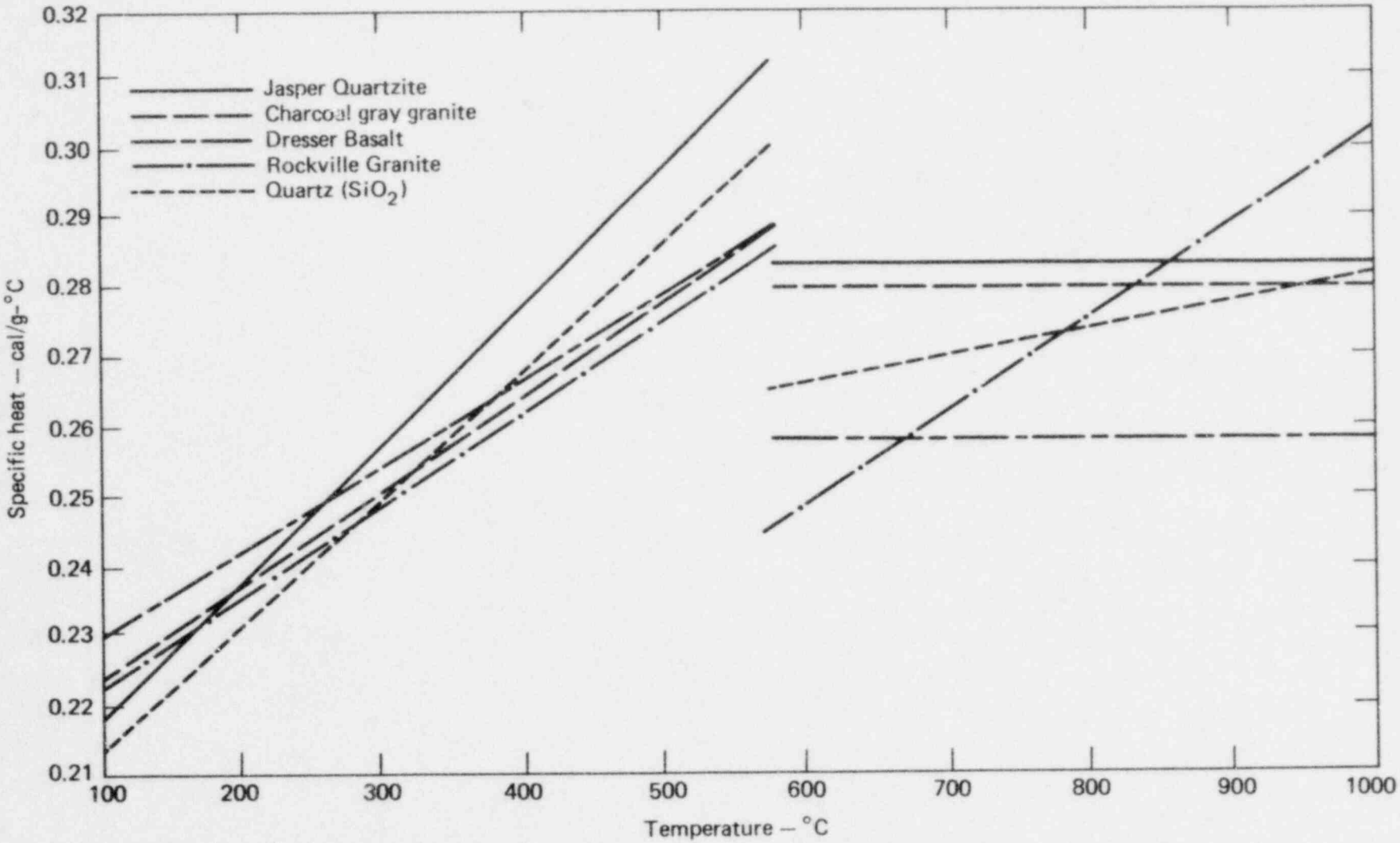

FIG. 3-20. Variation of specific heat with temperature (from PBQ&D, 1976; Lindroth and Krawza, 1971).

quartz in the vicinity of 573°C is due to the transformation of quartz from the alpha to the beta form. Over the temperature range shown in Fig. 3-20, the specific heat varies by about 25%. Some additional values for mean specific heats between 25 and 625°C are given in Table 3-9.

The effect of temperature on the density of relatively nonporous rocks such as granites is negligible. For other rocks, however, the density may decrease with increasing temperature as a result of moisture changes.

Thermal diffusivity is a derived quantity which depends on thermal conductivity, specific heat, and density. The results presented in Figs. 3-21 through 3-23 reveal that the thermal diffusivity decreases with increasing temperature to at least 600°C. Above this temperature, as shown in Fig. 3-23, the diffusivity may increase slightly.

The fusion temperatures of the rock, which may or may not be necessary considerations in nuclear waste disposal decisions, are shown in Table 3-10. The temperatures are in the range of about 1100 to 1300°C, well above the proposed operating temperatures for repositories.

TABLE 3-9. Specific heats of various samples (from Clark et al., 1969). The values given are the means for two calorimetric runs between 25 and 625°C for each sample.

Common designation	Specific heat, cal/g-°C
Granite	0.241
Anorthosite (Peribonka black)	0.234
"Nepean sandstone"	0.246
"Diabase"	0.226
Nepheline syenite	0.237
"Basalt"	0.236
"Rhyolite"	0.237
Syenite (Sienna red)	0.229
Nordmarkite (Scots green)	0.231

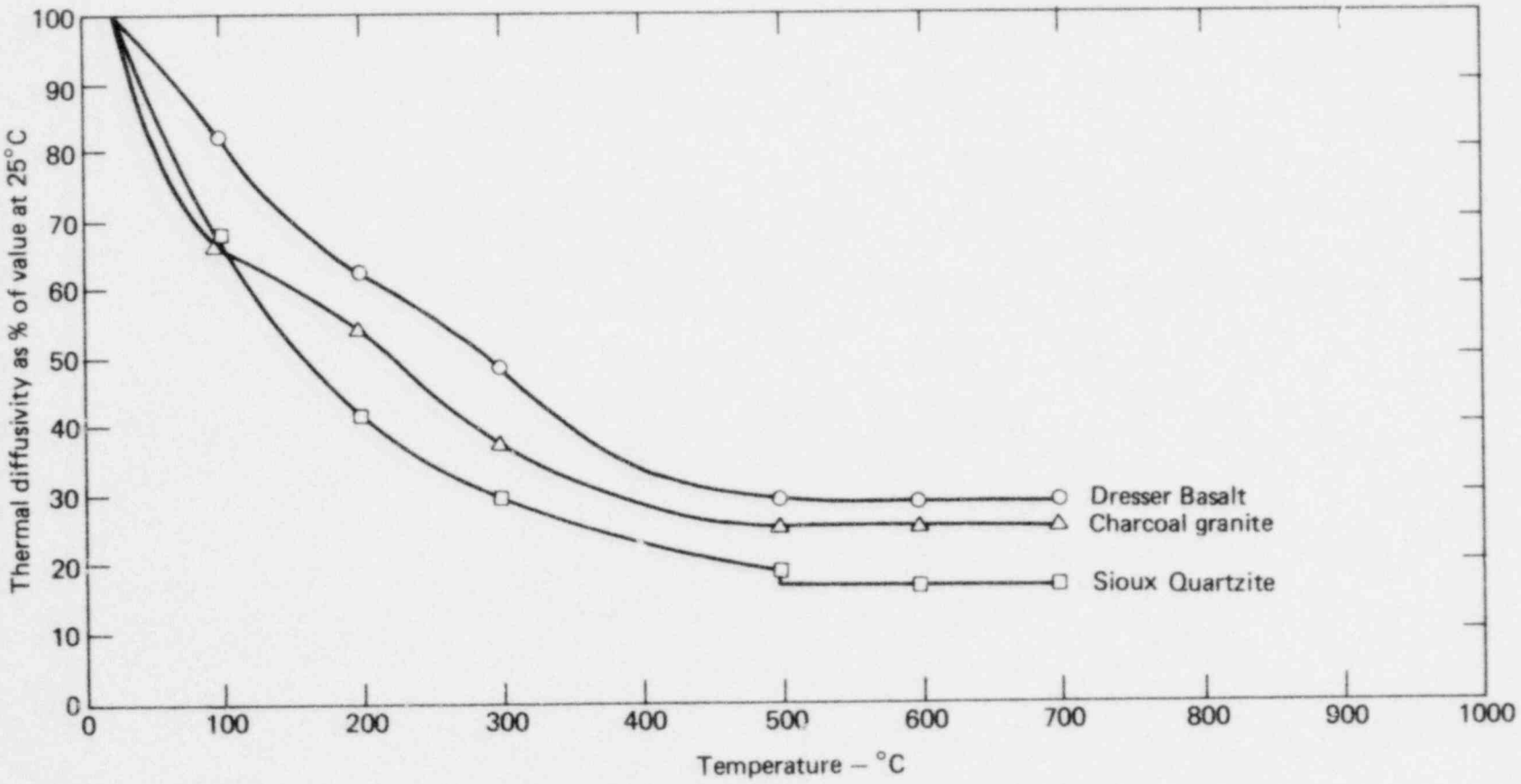

FIG. 3-21. Variation of normalized thermal diffusivity with temperature (from Thirumalai, 1970).

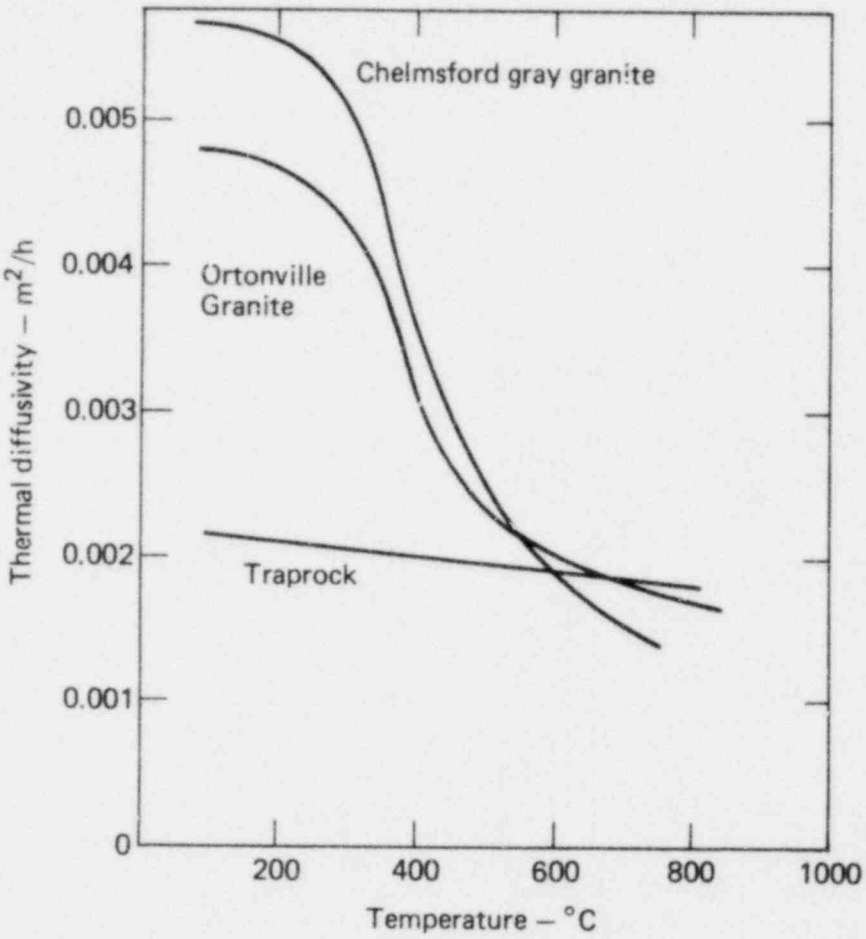

FIG. 3-22. Thermal diffusivity of eight air-dried rocks as a function of temperature (from Hanley et al., 1978).

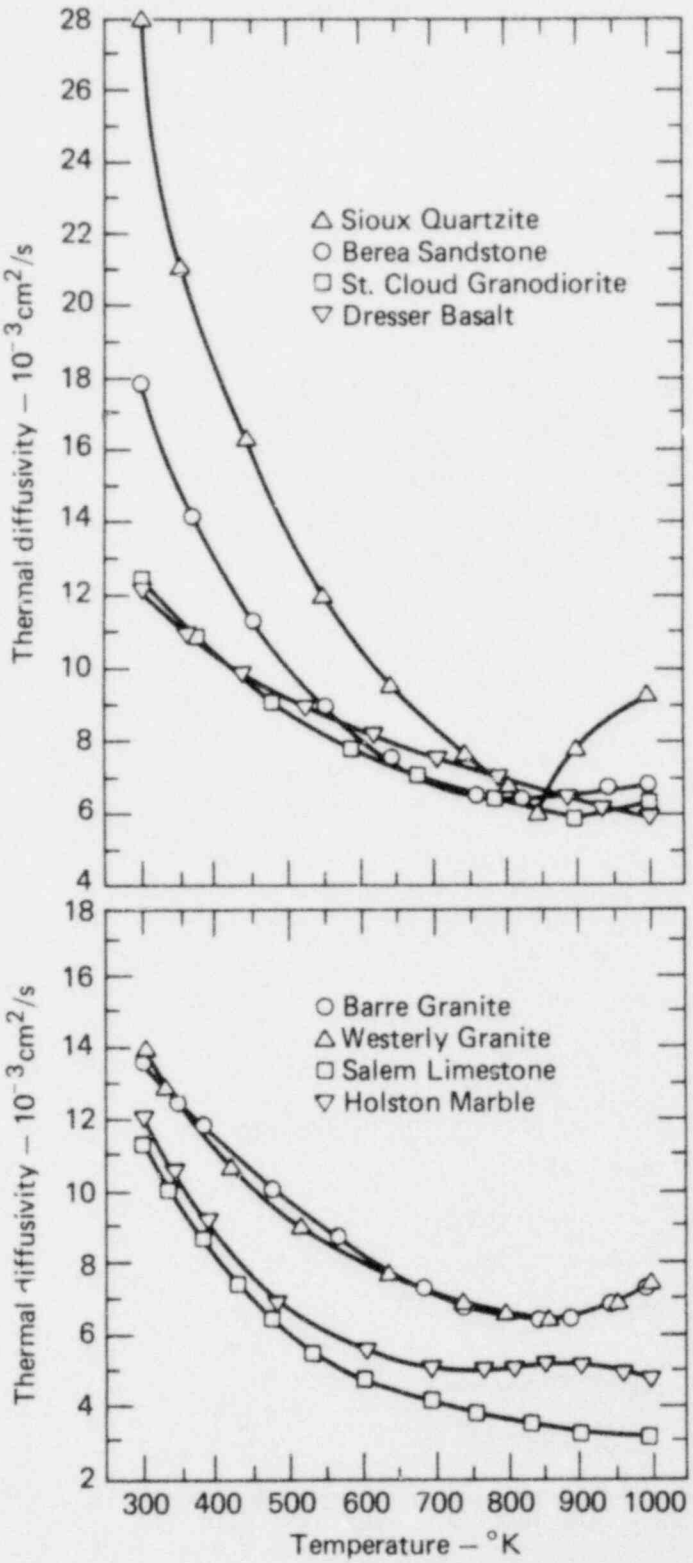

FIG. 3-23. Variation of thermal diffusivity with temperature (from Freeman et al., 1963).

TABLE 3-10. Fusion temperatures for various rocks (from Clark et al., 1969).

Rock type and origin	Fusion temp, °C	Pyrometric cone equivalent (P.C.E.) No.
Crystalline igneous rocks		
Basalt (traprock), N.J.	1152-1168	C-3
Diabase traprock ("black granite"), French Creek Granite Co.	1168-1186	C-4
Medium red granite, Leeds County, Ontario	1168-1186	C-4
White granite (high mica content), Chelmsford, Mass.	1168-1186	C-4
Opalescent granite, Cold Springs, Minn.	1201-1222	C-6
Grey granite, Norway	1215-1240	C-7
Grey granite, Salisbury, N.C.	1236-1263	C-8
Collins pink granite, Salisbury, N.C.	1236-1263	C-8
"Syenite," Lake Asbestos, Quebec	1236-1263	C-8
Red granite, Wausau, Wisc.	1236-1263	C-8
Melrose pink granite, Guenette, Quebec	1236-1263	C-8
Granite gneiss, Mount Wright, Quebec	1236-1263	C-8
Grey granite, Chelmsford, Mass.	1285-1305	C-10
Quartz-rich crystalline igneous rocks (more than 10% quartz)		
Granite, Stanstead, Quebec	1198-1221	C-5 1/3
"Granite" (Stanstead grey), Stanstead, Quebec	1201-1222	C-6
Granite (Saguenay red), Lake St. John, Quebec	1177-1196	C-5
Granite (Vermilion pink), Vermilion Bay, Ontario	1207-1232	C-6 1/2
"Rhyolite," Havelock, Ontario	1215-1240	C-7
Quartz-poor crystalline igneous rocks (less than 10% quartz)		
"Basalt," Havelock, Ontario	1149-1165	C-2 2/3
"Diabase," Bell's Corners, Ontario	1164-1179	C-3 2/3
Anorthosite (Peribonca black), Peribonca River, Quebec	1297-1319	C-11 1/3
Syenite (Sienna red), Rawcliffe, Quebec	1168-1186	C-4
Nordmarkite (Scots green), Mount Megantic, Quebec	1167-1184	C-3 4/5
Nepheline syenite, Methen Township, Ontario	1168-1186	C-4

Thermoelastic Properties

Thermoelastic properties include the effect of temperature on strength, Young's modulus, Poisson's ratio, and the linear coefficient of thermal expansion. Figure 3-24 shows a typical stress-strain plot for an uniaxial compression test conducted at 150°C on Stripa granite (Swan, 1978). Even at this elevated temperature, the relationship between stress and strain is stil fairly linear. Figure 3-25 shows the change in ultimate compressive strength with temperature for a number of different rock types, including four granites. The very severe decrease which occurs at about 1100°C corresponds to the fusion temperature for these rocks. Otherwise, over the temperature range of principal interest (from 20 to 400°C), the decrease in strength varies, depending on the rock, from 0% to approximately 50%.

Figures 3-26 and 3-27 show the change in strength with temperature and confining pressure. These tests were all done at a confining pressure of

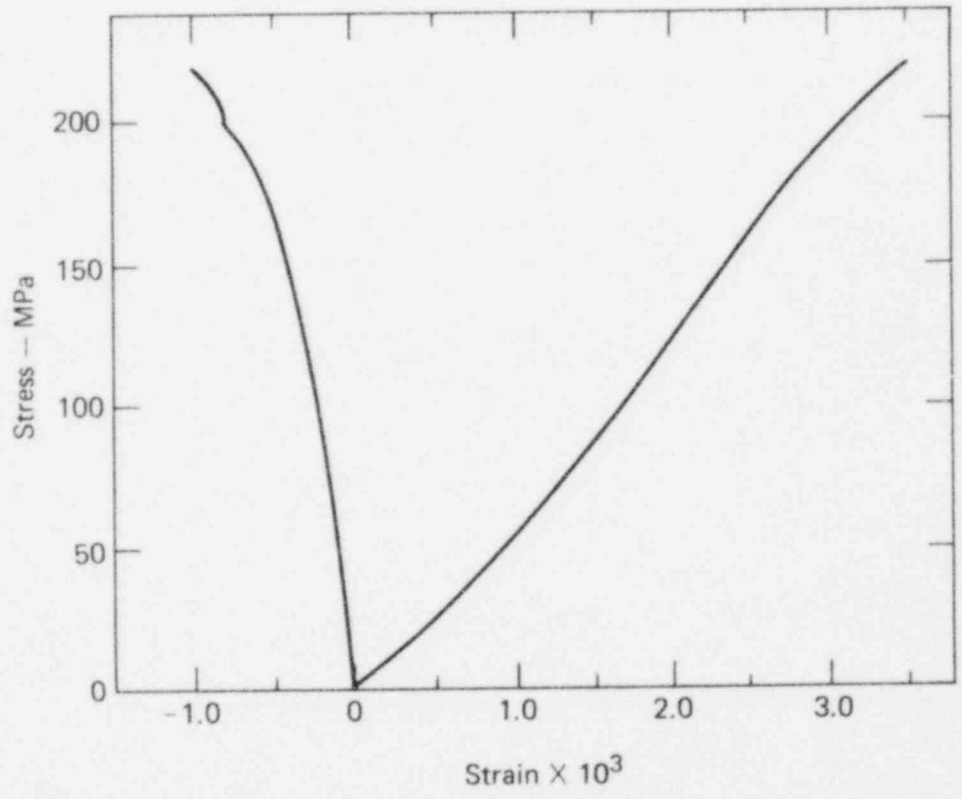

FIG. 3-24. Typical stress-strain plot from a uniaxial test at 150°C (from Swan, 1978).

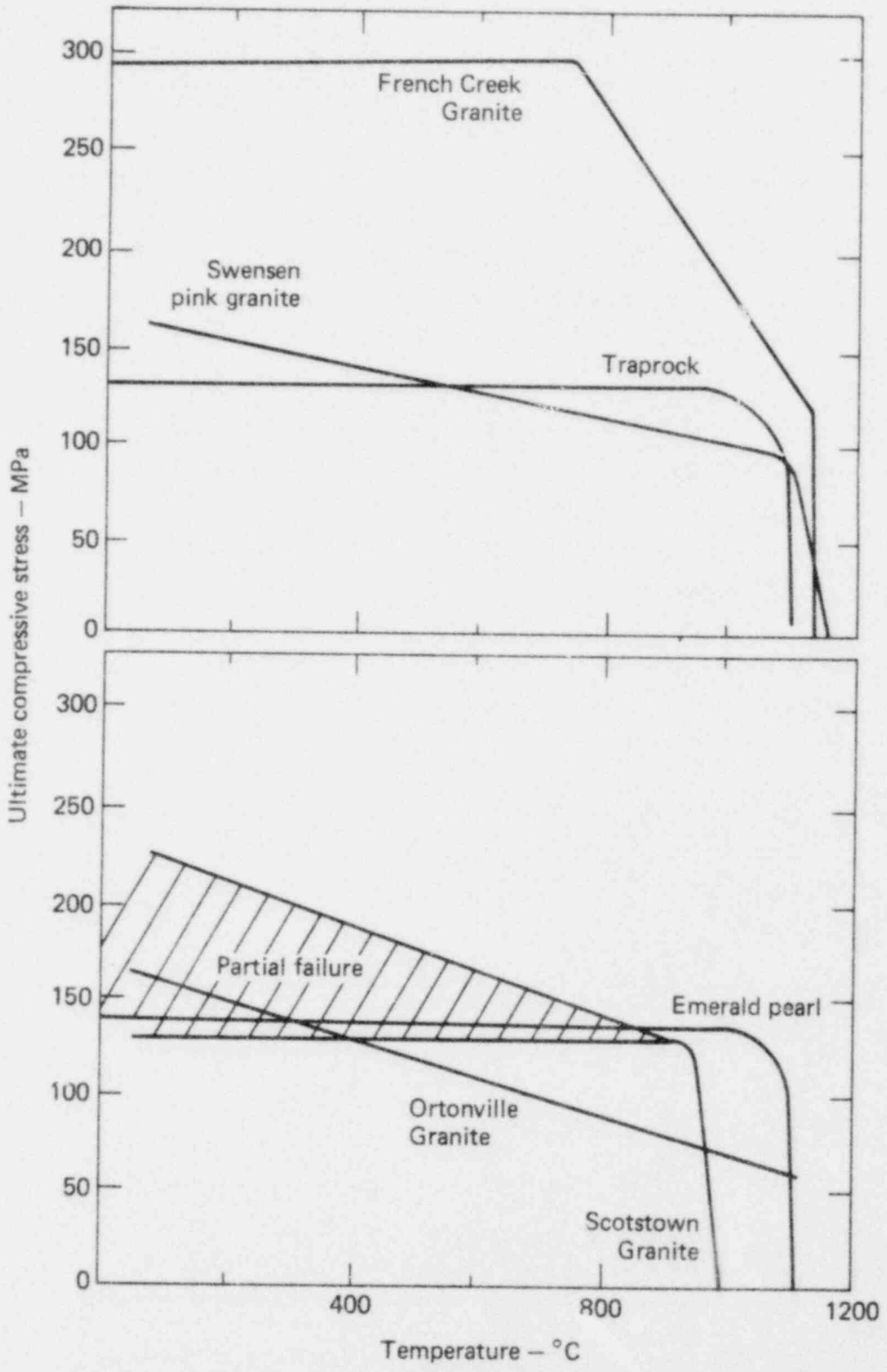

FIG. 3-25. Variation of ultimate compressive stress with temperature (from Freeman et al., 1963).

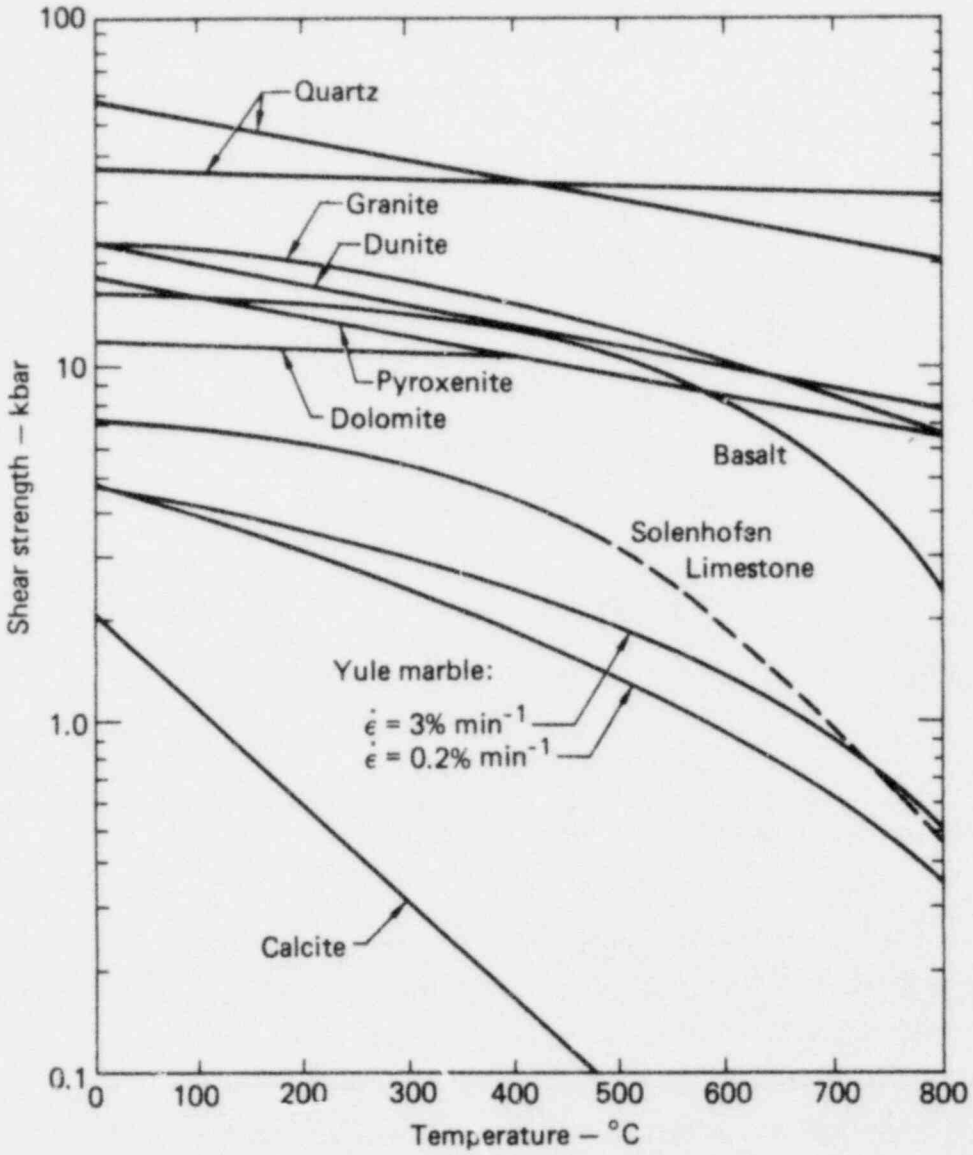

FIG. 3-26. Strengths of rocks and minerals as functions of temperature at 5 kbar (from Griggs et al., 1960). The two curves for quartz reflect tests along two different axes: the flatter curve for compression perpendicular to a rhombohedral face, the second curve for compression parallel to the c-axis.

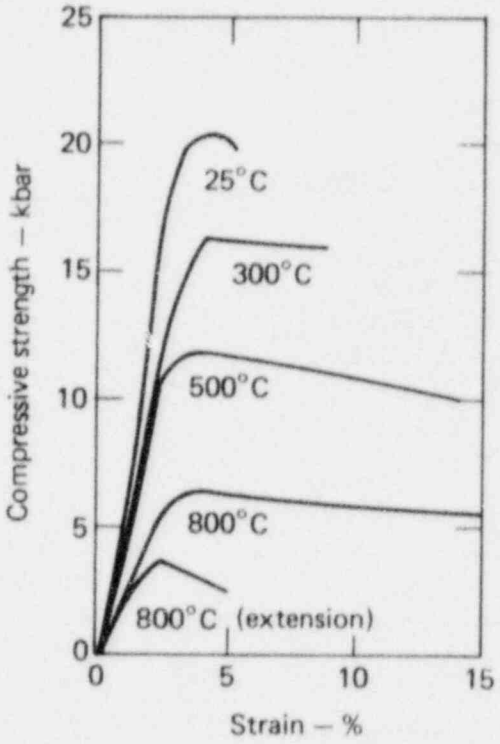

FIG. 3-27. Effect of temperature on the stress-strain curves for granite (from Griggs et al., 1960).

5 kilobars. Note that for the granite shown in Fig. 3-26 the decrease in strength between 0 and 400°C is relatively small. In Fig. 3-27, the compressive strength is plotted as a function of strain. With increasing temperatures at 5 kilobars, the rocks become much more plastic and the deviatoric stress required to cause extension becomes much smaller.

Figures 3-28 and 3-29 show Young's modulus and Poisson's ratio as functions of temperature for Stripa granite. The error bars indicate 90% confidence limits for these laboratory tests. Between 0 and 200°C, Young's modulus decreases by approximately 30%, and Poisson's ratio decreases about 50%. The variations of Young's modulus, shear modulus, and Poisson's ratio with temperature are shown for four rock types in Fig. 3-30. Between room temperature and 400°C, Young's modulus for charcoal granite decreases by about 50%. Poisson's ratio appears to change from positive to negative, which is rather unusual. Ongoing work will help clarify some of these relationships. In general, both the uniaxial and triaxial compressive strengths of granite decrease markedly with increasing temperature. Both the elastic modulus and Poisson's ratio are reduced.

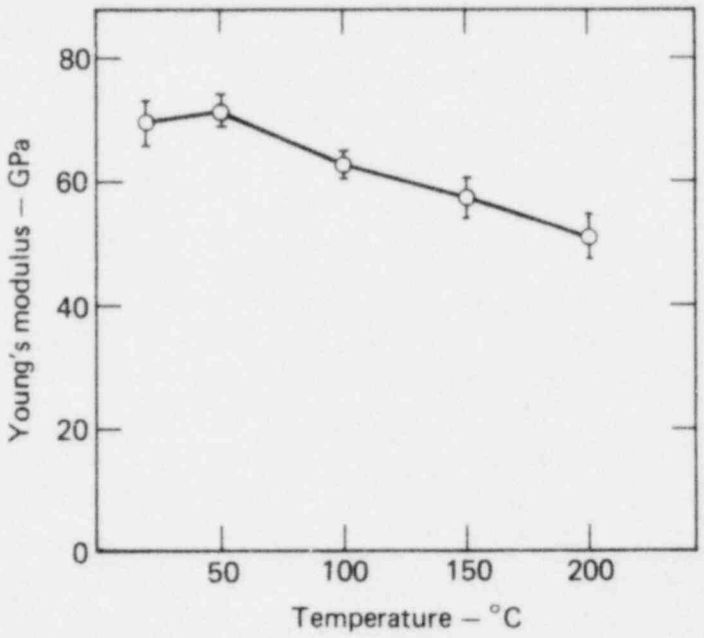

FIG. 3-28. Young's modulus as a function of temperature (from Swan, 1978). The error bars indicate 90% confidence limits.

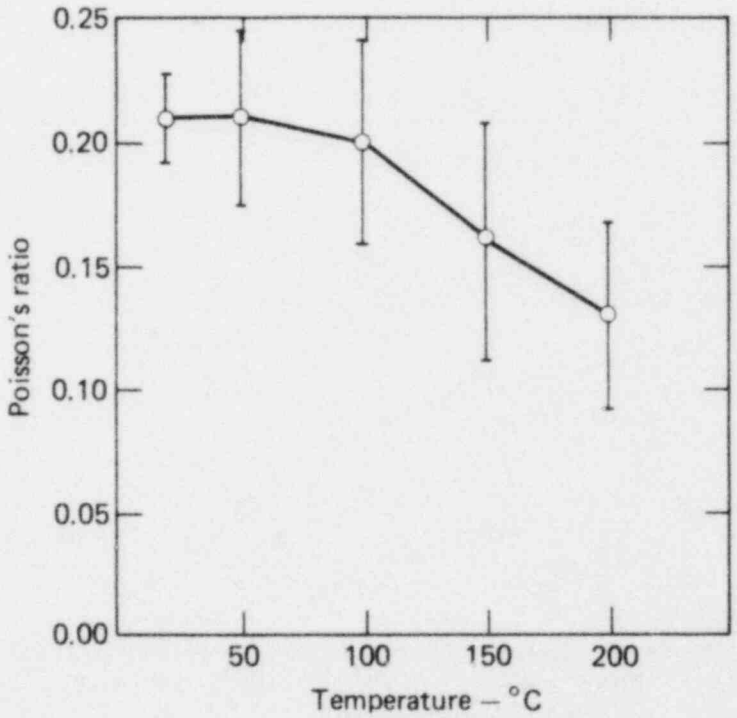

FIG. 3-29. Poisson's ratio as a function of temperature (from Swan, 1978). The error bars indicate 90% confidence limits.

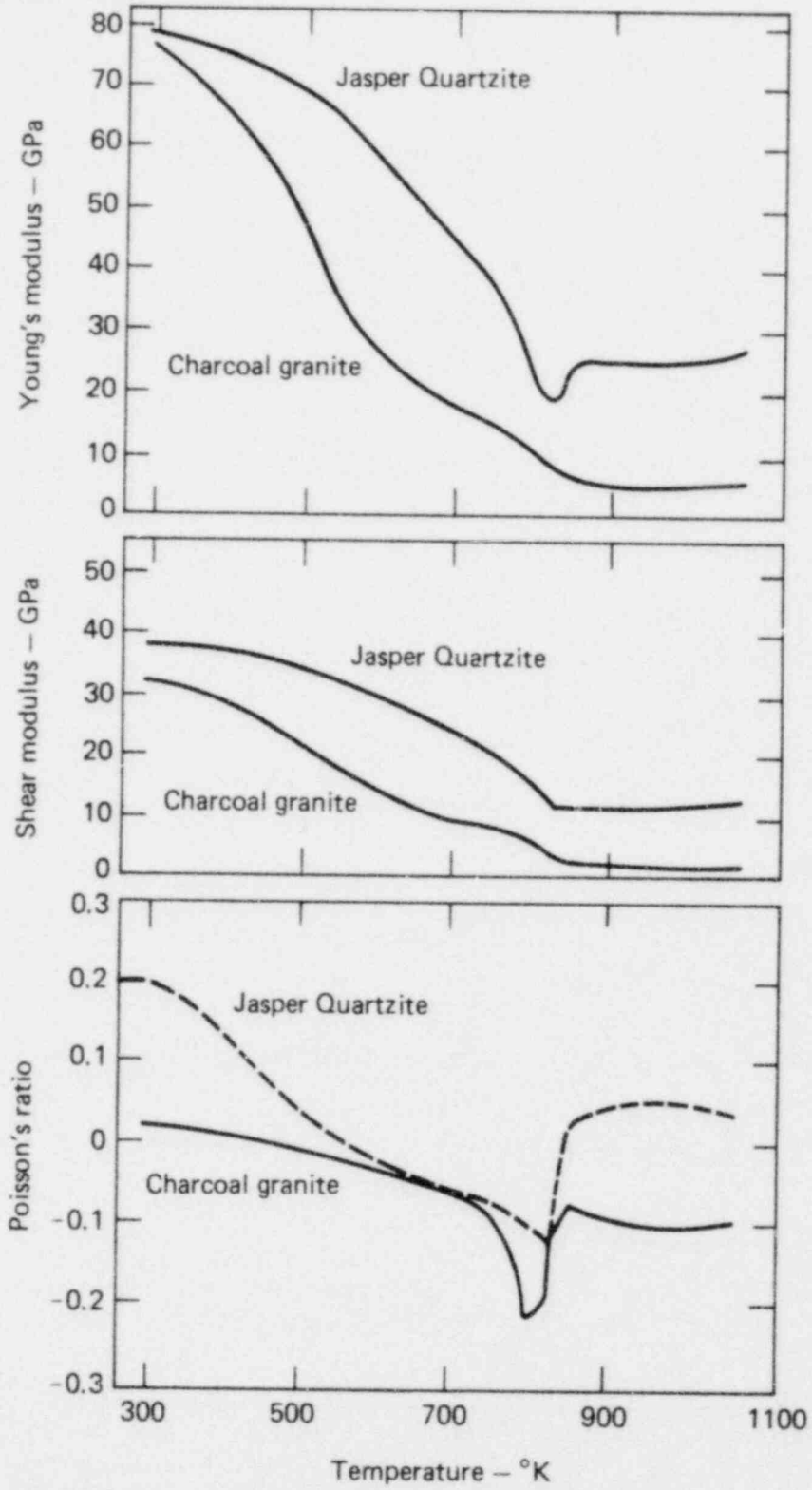

FIG. 3-30. Variations of Young's modulus, shear modulus, and Poisson's ratio with temperature (from Wingquist, 1970).

The coefficient of linear thermal expansion is very important for the calculation of both the displacements and the stresses that will result from the thermal field around a waste repository. The degree of temperature dependence of thermal expansion varies widely among different rocks, as shown in Figs. 3-31 and 3-32, and in Table 3-11. Thermal expansion coefficients for granite are also affected by the alpha-beta inversion temperature (573°C) of quartz (Fig. 3-32). It is interesting to note in Table 3-11 that the values for most granites or granite-type rocks are relatively similar over a wide temperature range.

The variation in percent volume expansion for some common igneous minerals, shown in Fig. 3-33, illustrates the reason for high thermal stresses in quartz-rich rocks, such as igneous rocks. This difference in volume expansion is exploited in thermal rock removal processes. The rock removal rate and average linear expansion for several quartz-rich and quartz-poor rocks are shown in Tables 3-12 and 3-13, respectively. The percent elongation as a function of temperature is shown in Figs. 3-34 and 3-35 for rocks having various spallability indexes. Most granitic rocks have a very good spallability and therefore would be expected to spall under high thermal gradients.

Table 3-14 shows the effect of the combination of heat and moisture on the strength of granite. When granite was tested at 240°C in a dry nitrogen atmosphere, the compressive strength was 135.9 MPa. In an atmosphere saturated with water vapor, the strength dropped to 41.4 MPa. Unfortunately, few test data are currently available on the effect of environmental conditions on the strength of rocks. However, this can be an extremely important consideration in evaluating the long-term competence of a repository.

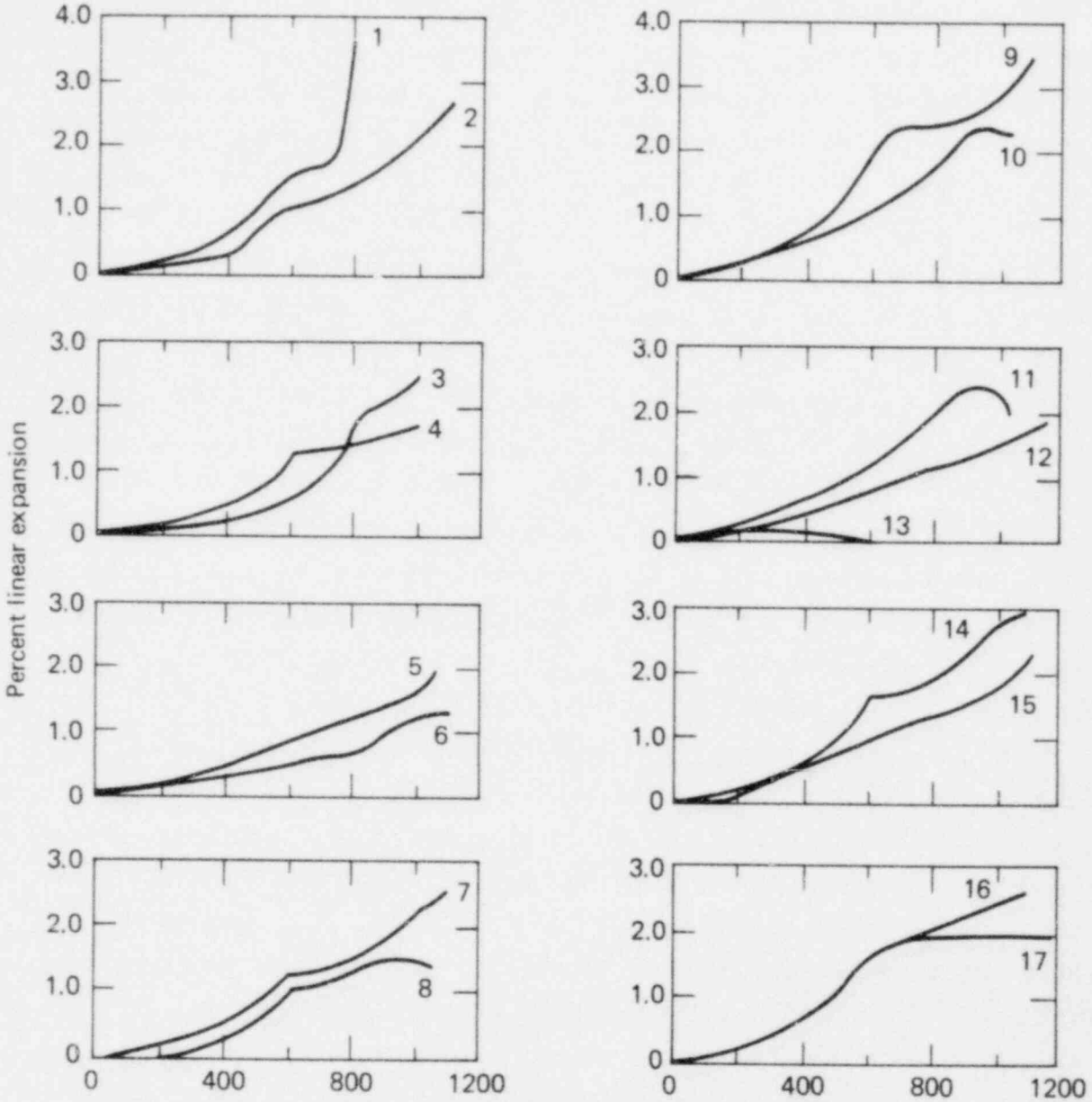

1 Chelmsford white granite
2 Syenite, poor piercing
3 Woodleaf Granite
4 Opalescent granite
5 Emerald pearl
6 Traprock
7 Scotstown Granite
8 Minnesotaite
9 Swenson pink granite
10 Dolomite
11 Limestone
12 French Creek Granite
13 Serpentine
14 Chelmsford gray granite
15 Syenite, good piercing
16 Ortonville Granite
17 Quartzite

FIG. 3-31. Variation with temperature of the extent of linear thermal expansion (from Freeman et al., 1963).

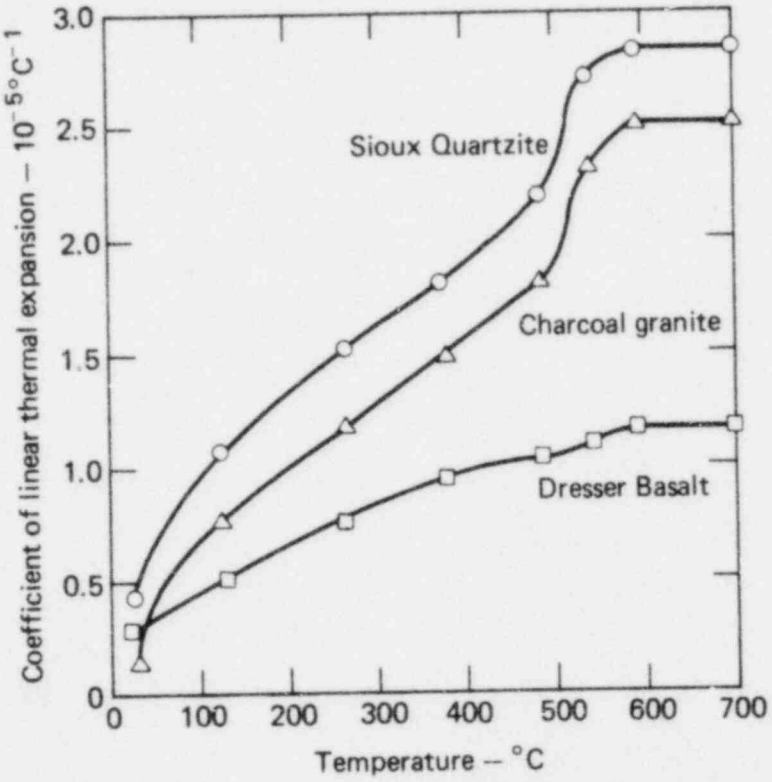

FIG. 3-32. Variation with temperature of the coefficient of linear thermal expansion (from Lehnhoff and Scheller, 1975).

TABLE 3-11. Measured coefficients of volumetric thermal expansion (from Swan, 1978).

Rock type	Coeff of volumetric thermal expansion, 10^{-6} $^{o}C^{-1}$	
	at 25°	at 400°
Chelmsford Granite	21.5	73.3
Westerly Granite	24.8	67.0
Wausau Granite	19.9	71.5
Graniteville Granite	25.1	76.8
Red River Quartz Monzonite	21.1	75.0

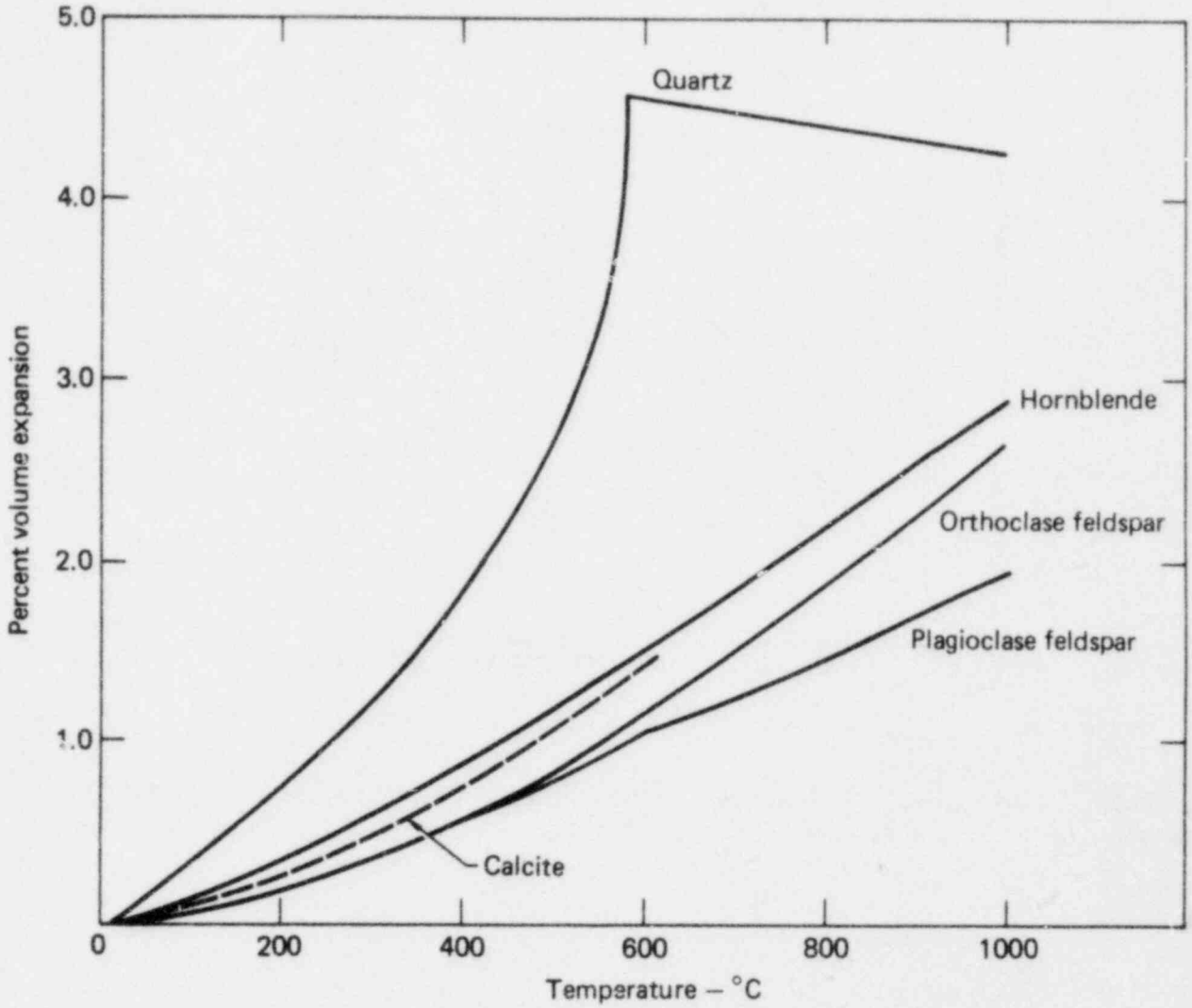

FIG. 3-33. Variation with temperature of the volume thermal expansion of some common minerals (from Skinner, 1966).

TABLE 3-12. Mineralogical composition, rock removal rate, and percent elongation at 600°C for quartz-rich (>10% quartz) crystalline igneous rocks (from Clark et al., 1969; Geller et al., 1962).

Rock type	Granite	Granodiorite	Quartz monzonite	Granite	Granite	Graphic granite
Composition, %:						
K-feldspar[a]	21.2	3.8	19.5	28.6	31.1	51.5
Plagioclase	44.8	50.5	41.4	23.0	31.3	20.5
Perthite[b]	--	--	--	2.4	0.9	--
Quartz	29.3	20.6	27.4	33.5	32.8	23.2
Amphibole	0.1	12.0	--	--	--	0.1
Other mafics	--	2.0	0.3	0.6	0.4	0.6
Biotite	2.9	9.4	9.9	9.8	2.9	1.0
Muscovite	1.7	--	1.1	0.3	0.1	0.6
Magnetite	--	--	0.3	--	0.3	2.5
Carbonate	--	--	0.1	0.3	--	--
Others	--	1.7	--	1.5	0.2	--
Rock removal rate, $in.^3/ft^3$ O_2	1.0	1.5	2.4	3.1	3.1	3.4
% elongation at 600°C	1.4	2.0	1.4	1.5	1.6	1.5

[a]Includes both orthoclase and microcline.

[b]Intergrown plagioclase and potassic feldspar.

TABLE 3-13. Mineralogical composition, rock removal rate, and percent elongation at 600°C for quartz-poor (<10% quartz) crystalline igneous rocks (from Clark et al., 1969; Geller et al., 1962).

Rock type	Basalt (saussurite)	Gabbro (diabase)	Anorthosite	Syenite	Nordmarkite	Neph. syenite
Composition, %:						
K-feldspar[a]	--	6.0	0.5	--	--	23.0
Plagioclase	17.8	46.2	98.0	17.4	7.6	52.3
Perthite[b]	--	--	--	69.2	73.3	--
Nepheline	--	--	--	--	--	23.0
Quartz	5(?)	6.2	--	--	9.4	--
Pyroxene	19.7	23.8	1.0	--	1.8	--
Amphibole	--	5.0	0.3	8.8	6.7	--
Other mafics	52.1	4.9	--	--	--	--
Biotite	--	1.0	0.2	2.3	0.1	--
Muscovite	--	--	--	--	--	0.2
Magnetite, Hem.	5.2	6.9	0.2	2.3	1.1	1.5
Carbonate	0.2	--	--	--	--	--
Rock removal rate, $in.^3/ft^3$ O_2	0.4	0.6	1.0	1.5	2.0	3.9
% elongation at 600°C	0.5	0.75	0.55	0.82	1.0	1.15

[a]Includes both orthoclase and microcline.

[b]Intergrown plagioclase and potassic feldspar.

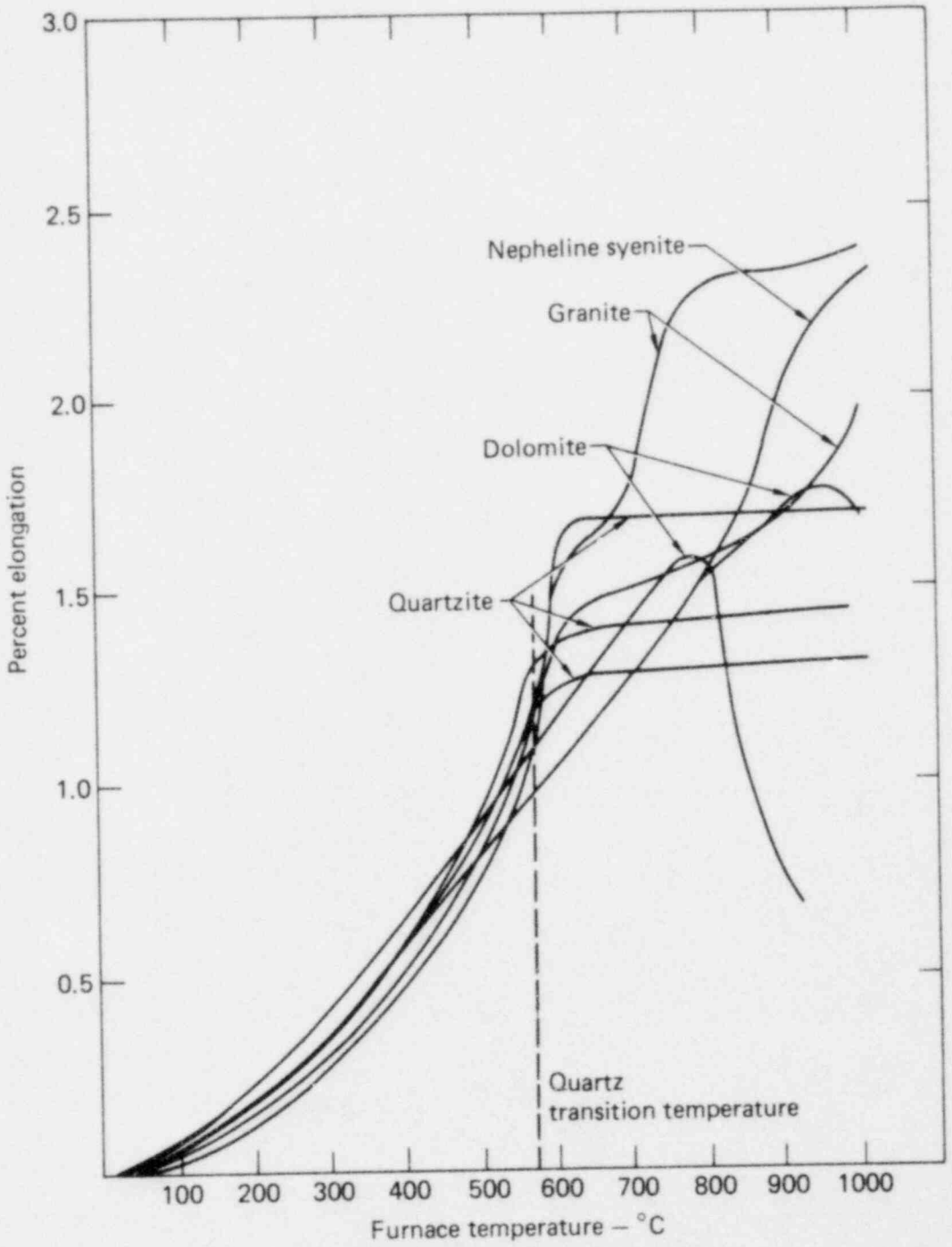

FIG. 3-34. Average linear expansion of samples having excellent and very good spallability (from Clark et al., 1969; Geller et al., 1962).

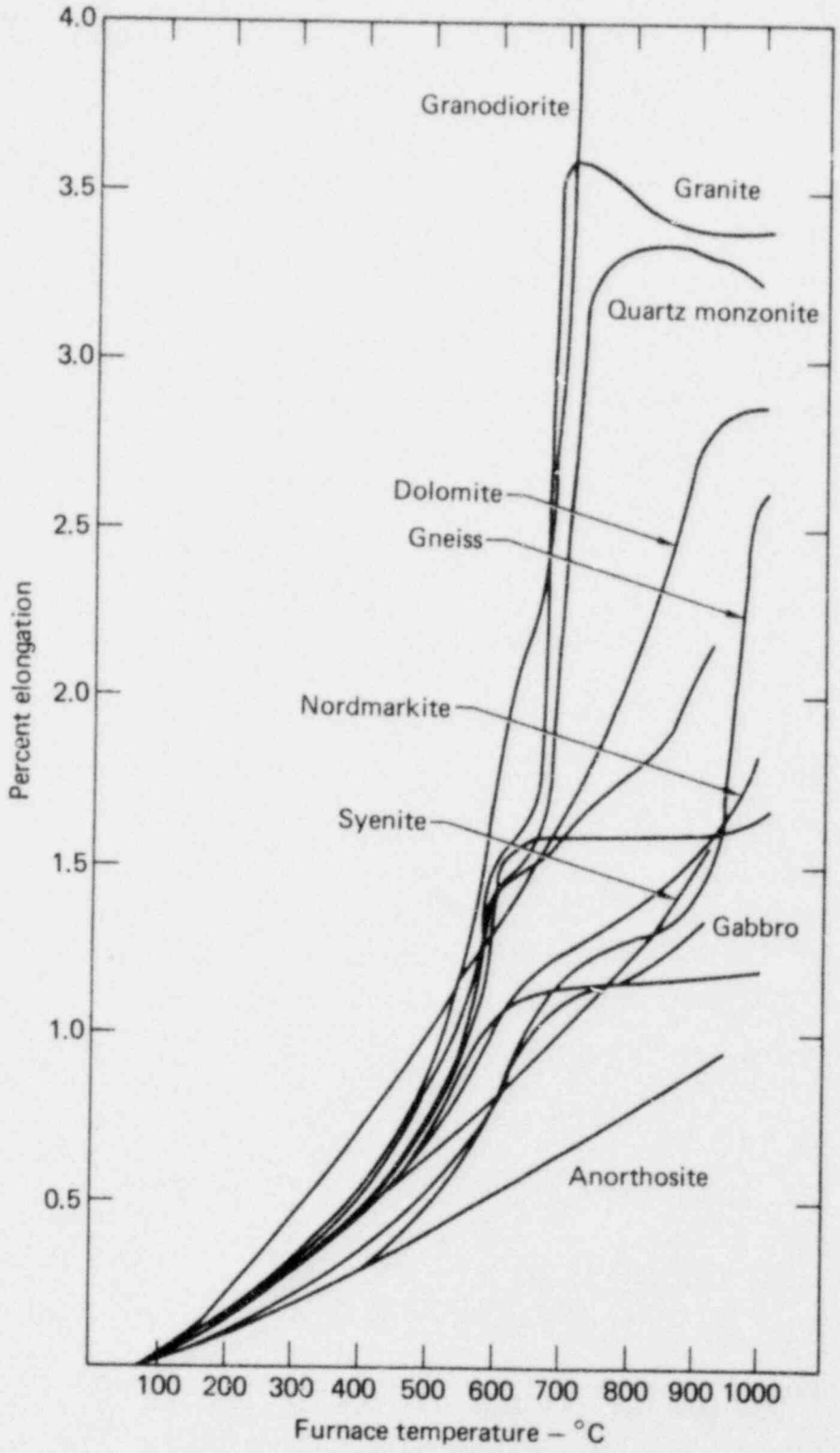

FIG. 3-35. Average linear expansion of samples having good and fair spallability (from Clark et al., 1969; Geller et al., 1962). Unlabeled curves were not identified.

TABLE 3-14. Compression tests on granite under several atmospheric conditions (from Charles, 1959). The machine loading rate was 0.005 in./min.

Prior treatment	Test temperature	Test atmosphere	Average failure stress, MPa
60 hours in saturated steam (240°C, 345 MPa)	25°C	Saturated water vapor	151.7
None	240°C	Dry nitrogen	135.9
None	240°C	Saturated water vapor	41.4
None	25°C	Saturated water vapor	162.1
None	-195°C	Liquid nitrogen	257.9

Other Considerations

To date, most studies have been performed using rock types which are considered to be "homogeneous and isotropic." It is assumed that average properties do not vary markedly from point to point within the rock mass, and that they do not vary substantially with respect to orientation. The second assumption has been borne out by a number of experimental investigations carried out in the laboratory. Table 3-15, for example, shows the results of measurements made on samples taken at various orientations from a block of Stripa granite. Young's modulus, wave velocity, compressive strength, and density are relatively insensitive to orientation. Table 3-16, however, presents the results of another set of experiments that were done on a gneissose granite. These latter results suggest that directional properties must be considered in some rock masses.

Because of the long time frame in which repository behavior must be considered, it is important to evaluate the effect of creep on rock strength and rock behavior. Although considerable information has been collected on the behavior of salt and saltlike materials, relatively little work has been done on the creep relationship for hard rocks, such as granite. Stress-time and strain-time relationships for Westerly Granite are presented in Figs. 3-36 and 3-37. Figure 3-36 indicates that the strength of Westerly Granite decreases as the period of applied stress increases. However, it is not clear

TABLE 3-15. Small-scale anisotropy test results for Stripa granite (from Swan, 1978). A pair of specimens was taken from a block of Stripa granite at each of four orientations in the x-z plane.

Specimen orientation[a]	Density, kg/m^3	Wave velocity, m/s	Young's modulus, GPa	Compressive strength, MPa
0^o	2616.9	5164.2	66.8	227.4
0^o	2616.9	5196.3	63.0	81.2
30^o	2614.4	5268.8	65.8	237.2
30^o	2609.8	5213.0	64.6	227.4
60^o	2613.8	5310.1	64.4	207.6
60^o	2616.3	5312.1	66.6	233.9
90^o	2617.8	5353.5	64.4	181.2
90^o	2619.7	5409.7	67.0	234.8

[a]Angle of specimen in original block, with respect to an arbitrary z-axis.

TABLE 3-16. Summary of anisotropic properties of gneissose granite (from Rodrigues, 1970).

Site	Moduli of elasticity,[a] GPa			Maximum anisotropy (e)	Ultimate strength,[a] MPa			Maximum anisotropy, (e_1)	e/e_1
Alvarenga	76.9	42.9	30.3	2.54	126.8	132.6	99.8	1.33	1.91
(two specimens)	37.8	17.5	24.3	2.16	46.4	84.2	66.7	1.82	1.19
Alto Lindoso	37.4	48.3	30.4	1.59	112.5	108.8	123.6	1.14	1.39
(three specimens)	49.9	36.2	28.5	1.75	125.0	117.7	125.6	1.07	1.64
	26.5	34.2	41.3	1.56	74.6	110.2	99.0	1.48	1.05
Vilarinho	48.1	42.3	38.3	1.25	132.7	123.8	109.8	1.21	1.03
(two specimens)	48.6	34.6	36.3	1.41	134.6	101.5	96.8	1.39	1.01
				Av = 1.75				Av = 1.35	Av = 1.31

[a]Values are given for each of three orthogonal axes.

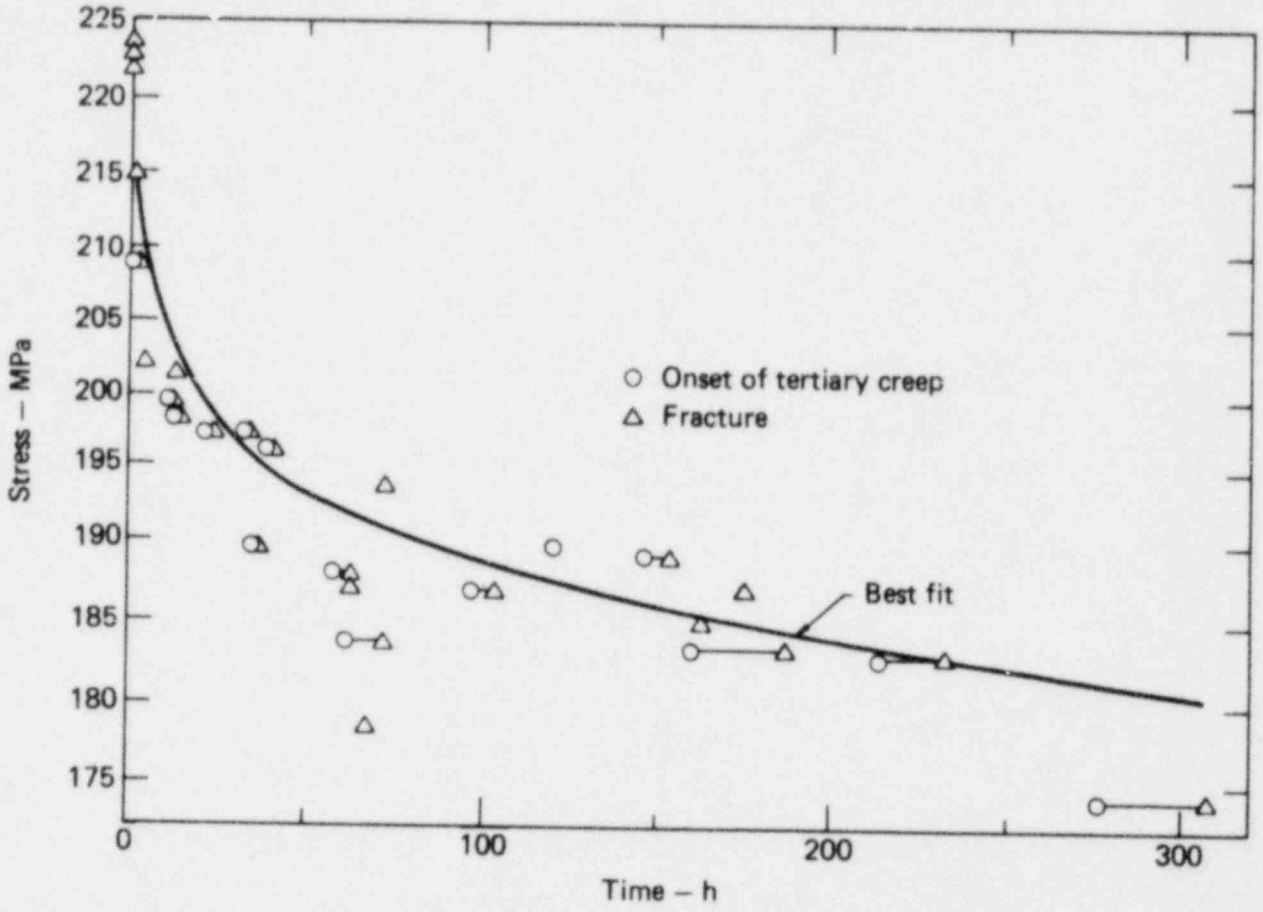

FIG. 3-36. Time rec or failure at various stress levels, for Westerly Granite (from Wawers. 1974).

whether the strength will continue to decrease beyond 250 or 300 hours, or whether it will reach some plateau. This unsettled question is extremely important when evaluating long-term behavior. For granite samples under a constant load of 26,630 psi (Fig. 3-37), the strain increased rather rapidly, then increased at a constant rate, then changed into tertiary creep. The sample finally failed.

Table 3-17 is a summary of creep data collected at room temperature for two granites and one granodiorite. The strain is proportional to the stress raised to an exponent varying between 1 and 3.3.

Although important, the collection of good creep data is extremely difficult, because of the very long time involved and the sophistication of the equipment necessary to provide controlled loading. Curent data are

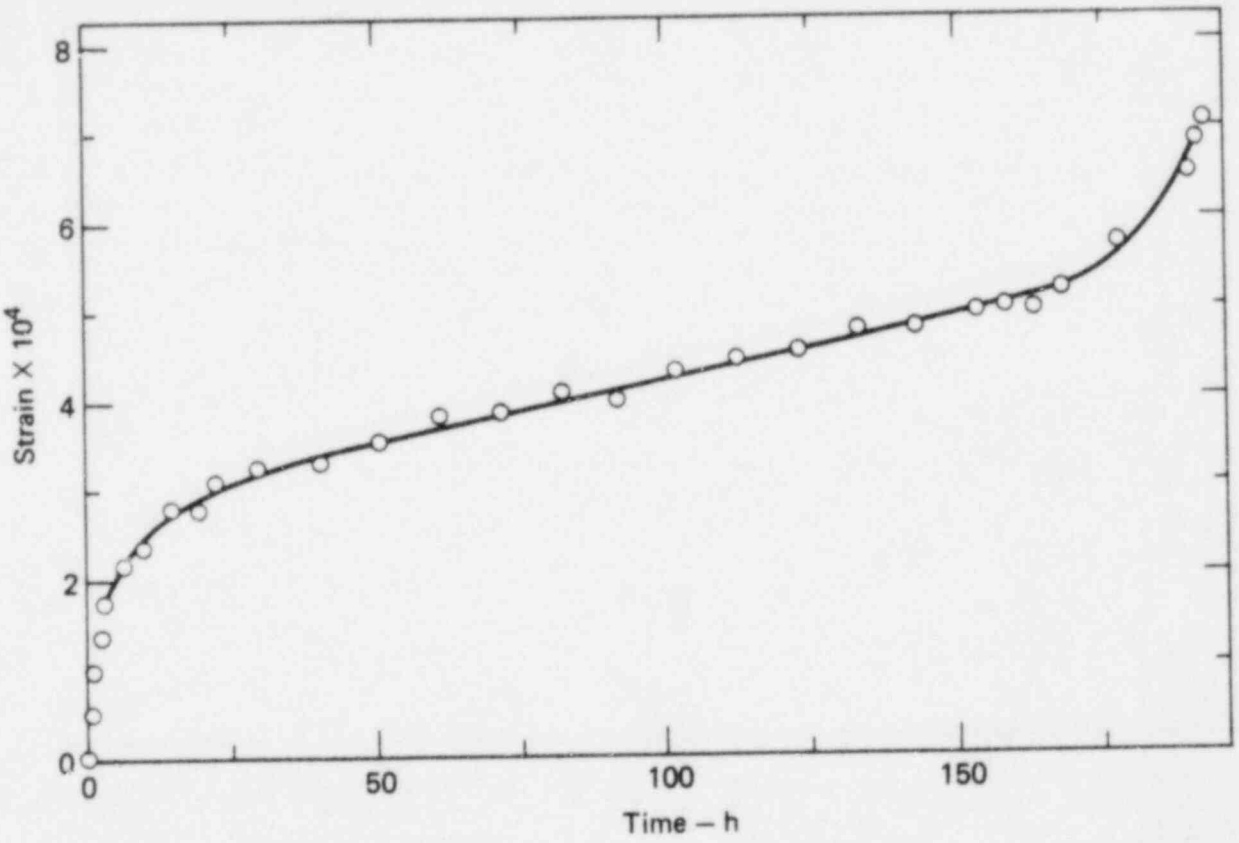

FIG. 3-37. Typical creep curve for water-saturated Westerly Granite (from Wawersik, 1974). The constant applied stress was 26,630 psi.

insufficient to allow creep to be incorporated into predictive models for hard-rock repositories.

Other geomechanical factors should be considered in evaluating repositories in granite. One is the behavior of rock under cyclic loading conditions. The rock mass itself will undergo cyclic heating and cooling, and the effects of this cycling are not necessarily reversible. Very little information exists regarding this phenomenon. Rock materials may also weaken due to radiological or chemical effects.

TABLE 3-17. Values of the exponent n in the relation between strain (ε) and stress (σ): $\varepsilon = A\sigma^n$. The data (compiled by Robertson, 1964) were collected at room temperature. The hydrostatic pressure in each case was zero.

Rock type	Maximum strain, 10^{-3} cm/cm	Maximum stress, MPa	Exponent (n)
Granite	1	355	3.3
Granite	0.08	101	2.1
Granodiorite	0.2	10.1	1.0

Scaling of Laboratory Results

The discussion to this point has focused primarily on intact rock samples. In underground excavations, however, it is not the intact rock that causes problems, but rather the discontinuities, such as jointing, faulting, dikes, etc. There are many ways of trying to incorporate such discontinuities into a design. One method is to model individual features and to describe them in terms of normal and shear joint stiffnesses. Another approach is to treat the entire rock mass as a continuum, but to reduce the modulus, strength, and other properties obtained in the laboratory for intact rock. The most common approach is to take laboratory properties and apply some sort of scaling factor to them to obtain a first estimate of the field properties.

Table 3-18 compares the rock properties for intact granite to those for the rock mass. Only the values for Young's modulus, uniaxial compressive strength, and tensile strength vary; all the other values are assumed to be the same in the two cases. For the rock mass, Young's modulus has been reduced by a factor of three, the compressive strength by about 30%, and the tensile strength from 6.9 to 0 MPa. However, these figures are extremely misleading and should not be used for modeling purposes.

The apparent modulus of a rock mass can be very low under small loads, since it is determined primarily by the closing of joints. Very large deformations are thus possible under rather low stresses. When internal boundaries are present, discontinuities tend to absorb the displacement, and

TABLE 3-18. Rock properties for a generic granite (from ONWI, 1978).

	Intact rock	Rock mass
Index properties:		
Unit weight, kg/m^3	2643.3	2643.3
Natural moisture content, %	--	--
Porosity, %	0.4	0.4
Stress-strain properties:		
Young's modulus, GPa	50.3	17.2
Poisson's ratio	0.18	0.18
Strength properties:		
Strength parameters:		
A	4.5	4.5
k	0.75	0.75
Uniaxial compressive strength, MPa	182.8	131
Tensile strength	6.9	0
Thermal properties:		
Coefficient of linear thermal expansion, 10^{-6} $^oC^{-1}$	31.0	31.0
Heat capacity, J/g-^oC, at:		
0^oC	0.88	0.88
100^oC	0.92	0.92
200^oC	0.96	0.96
300^oC	1.05	1.05
400^oC	1.09	1.09
Thermal conductivity, W/m-^oC, at:		
0^oC	2.86	2.86
50^oC	2.70	2.70
100^oC	2.56	2.56
150^oC	2.44	2.44
200^oC	2.34	2.34
300^oC	2.15	2.15
400^oC	1.99	1.99
Hydrologic properties:		
Horizontal permeability, 10^{-8} m/min	3.05	3.05
Vertical permeability, 10^{-8} m/min	3.05	3.05

Poisson's ratio may actually be close to zero. As a further consequence of this scaling effect, the uniaxial compressive strength of cubes of some materials varies as the inverse of the square root of the length of the side. (For samples of other shapes, the strength is dependent upon the width-to-height ratio.) This leads to the relation

$$\text{strength (large cube)} = \text{scaling factor} \times \text{strength (small cube)},$$

where

$$\text{scaling factor} = \sqrt{\frac{\text{side length (small cube)}}{\text{side length (large cube)}}}$$

The scaling factor for the compressive strength in Table 3-18 is 131/182.8 = 0.72. Typically, the values for the intact rock were determined using samples 5 cm in diameter; therefore, the side length of the "rock-mass sample" (corresponding to a scaling factor of 0.72) is about 10 cm. Consequently, to use the values in Table 3-18 one would have to assume that rock-mass properties are adequately represented by test results from a 10-cm sample. This may or may not be appropriate.

The tensile strength of intact rock, as has been noted earlier, varies from zero to some fraction, generally one-tenth to one-twentieth, of the compressive strength of the rock. If the tensile strength of the rock mass were really zero, it would be extremely difficult to support openings such as those created underground every day in granitic rocks.

An example of variation in strength with sample size has been provided by Pratt et al. (1972), as shown in Fig. 3-38. There appears to be a characteristic length of 0.5 to 1 m, at which strength becomes relatively constant. The variation in strength with sample size, as shown in this figure, suggests that the strength for large samples could be an order of magnitude lower than that for smaller samples. (The 0.5-m characteristic length may not be at all appropriate when large openings are considered, since some other characteristic discontinuity would then be the determining factor for rock-mass strength.)

The modulus would be expected to follow a trend similar to that for compressive strength, since the two properties are closely related.

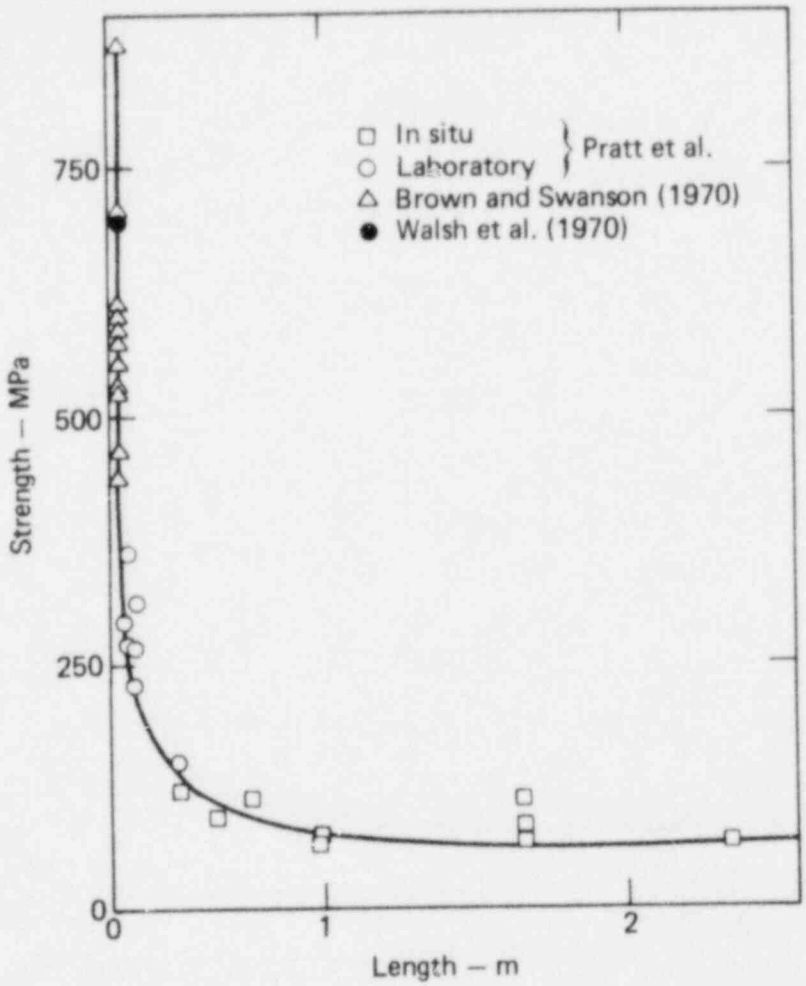

FIG. 3-38. Effect of sample size on the uniaxial compressive strength of quartz diorite (from Pratt et al., 1972).

Figure 3-39 shows the relationship between the in situ modulus and the number of fractures observed in the core. There is a rather strong correlation between the two parameters, with the modulus decreasing as the fracture number increases. Figure 3-40 shows in situ modulus results for Stripa granite. The tests were conducted in 3.8-cm-diameter holes drilled into the rock mass. The volume of rock tested in each case was relatively small, though much greater than the volume that would have been tested had the core alone been examined. Note that the average in situ modulus, even for this relatively small volume, was about one-half the laboratory value.

All of these results emphasize the problem of scaling tests performed on small samples of rock to in situ values. In light of this difficulty, a number

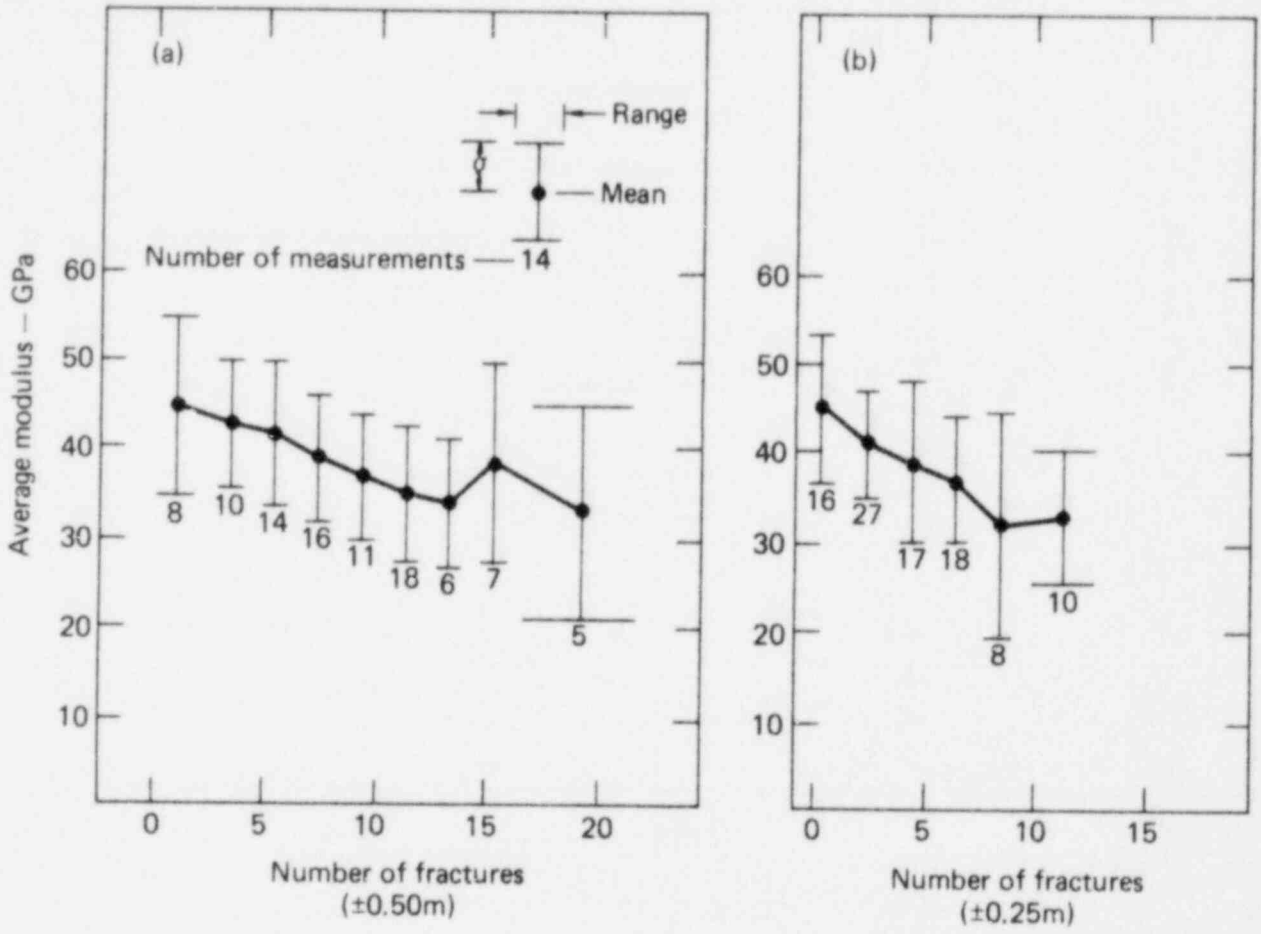

FIG. 3-39. In situ Young's modulus as a function of fracture density, as determined from a visual inspection of the core (from Nelson et al., 1979). In (a), the fractures were counted in a 1-m interval centered on the test point; in (b), the interval was 0.5 m.

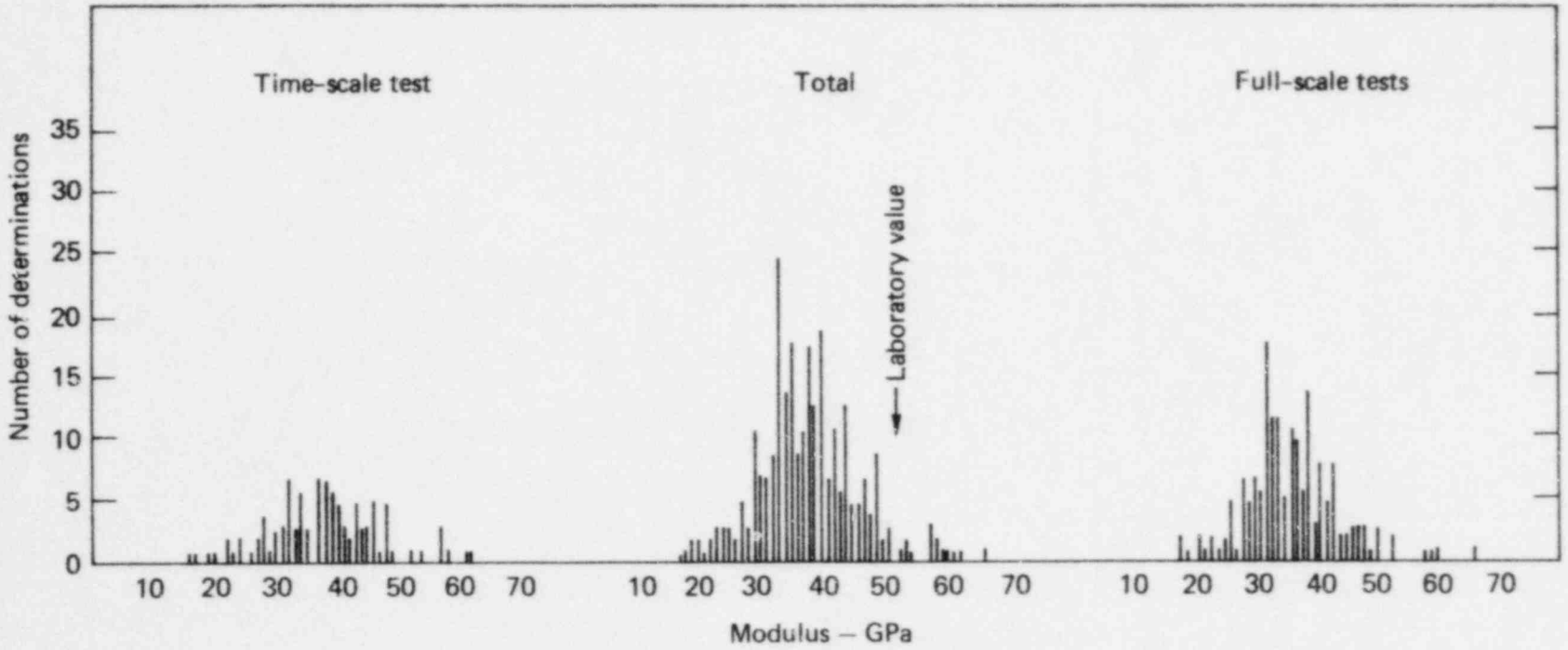

FIG. 3-40. Histograms of CSM-cell determinations of Young's modulus in Stripa granite (from Nelson et al., 1979). Full-scale and time-scale tests reflect two different test series at Stripa.

of in situ experiments are either underway or planned at Stripa. The purpose is to gather thermal and mechanical data appropriate for loading conditions similar to those that would be expected in an actual repository. Models are being prepared for predicting the field behavior. Of crucial importance is how well the input parameters describe the actual field situation.

The initial predictions will be made using laboratory values for thermal conductivities, specific heat, density, thermal diffusivity, coefficient of linear expansion, Poisson's ratio, and Young's modulus (such as those in Table 3-19, which were used at Stripa), or some scaled laboratory values. The problem in the latter case is justifying the scaling values used for the initial approximation. Adjustments can then be made by comparing predicted results with those actually measured. The adjustments can take the form of either revised input parameters or a revised model. The new values (or model) can then be verified by applying them to a new loading situation.

Figures 3-41 through 3-47 compare theoretical predictions based on the properties of small intact samples with preliminary field measurements from the Stripa mine. Predicted temperatures (based on laboratory values for thermal conductivity, density, diffusivity, and specific heat) and actual temperatures agree closely, suggesting that size effects on these thermal parameters may be relatively small. As seen in Figs. 3-45 through 3-47, however, the predicted and actual displacements are quite different, the actual values being considerably less than those projected. These predictions are based upon average laboratory values for Young's modulus and the linear thermal expansion coefficient. The initial portions of the displacement

TABLE 3-19. Laboratory values for properties of Stripa granite.

Thermal conductivity	3.2 W/m-^{o}C
Specific heat	837 J/kg-^{o}C
Density	2600 kg/m^{3}
Thermal diffusivity	1.47×10^{-6} m^{2}/s
Coefficient of linear thermal expansion	11.1×10^{-6} ^{o}C^{-1}
Poisson's ratio	0.23
Young's modulus	51.3 GPa

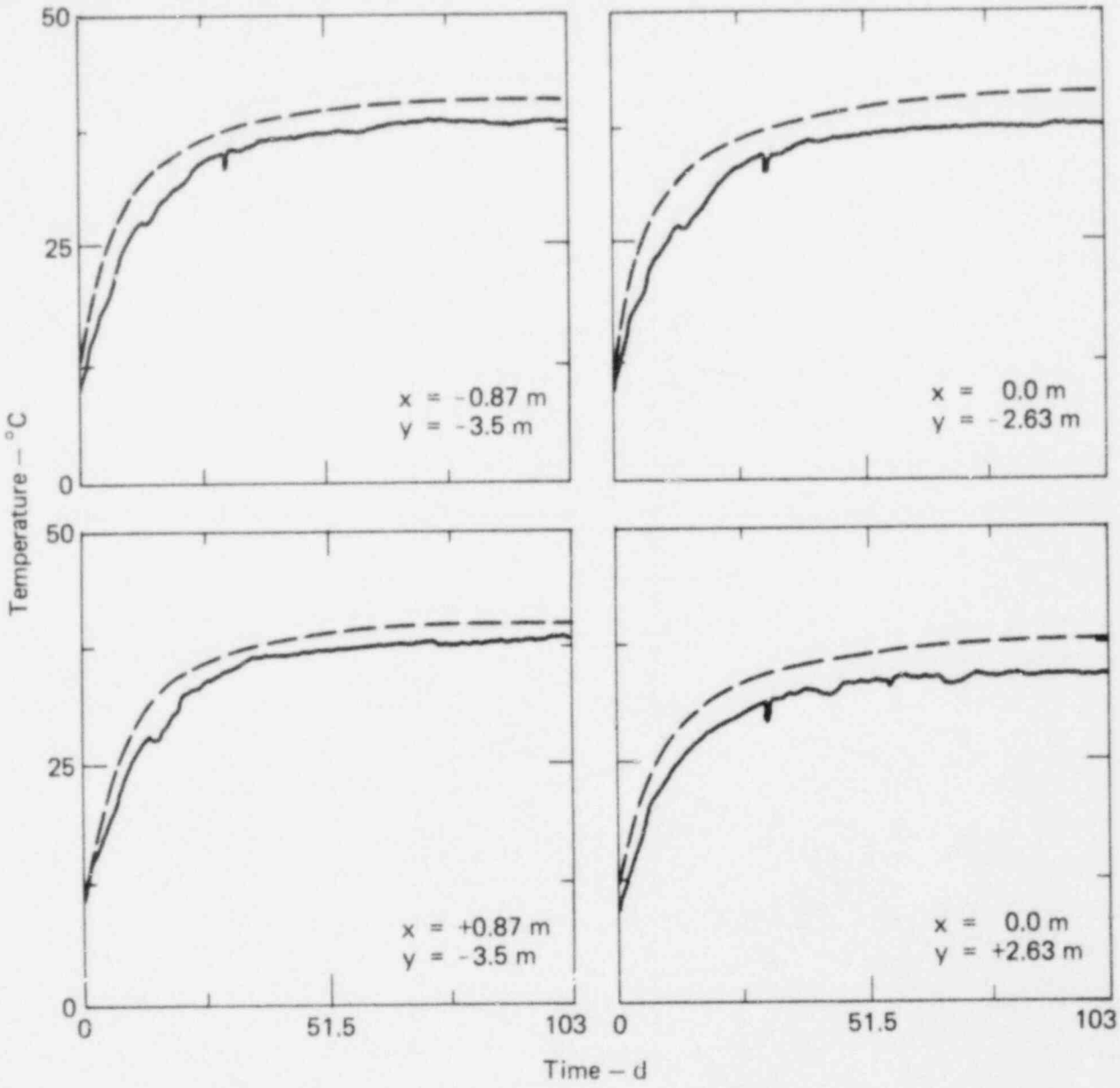

FIG. 3-41. Predicted temperatures (dashed lines) and measured temperatures (solid lines) as functions of time 0.87 m from 1.1-kW heaters in granite (from Cook and Hood, 1978). See Fig. 3-42 for heater positions in the x-y plane.

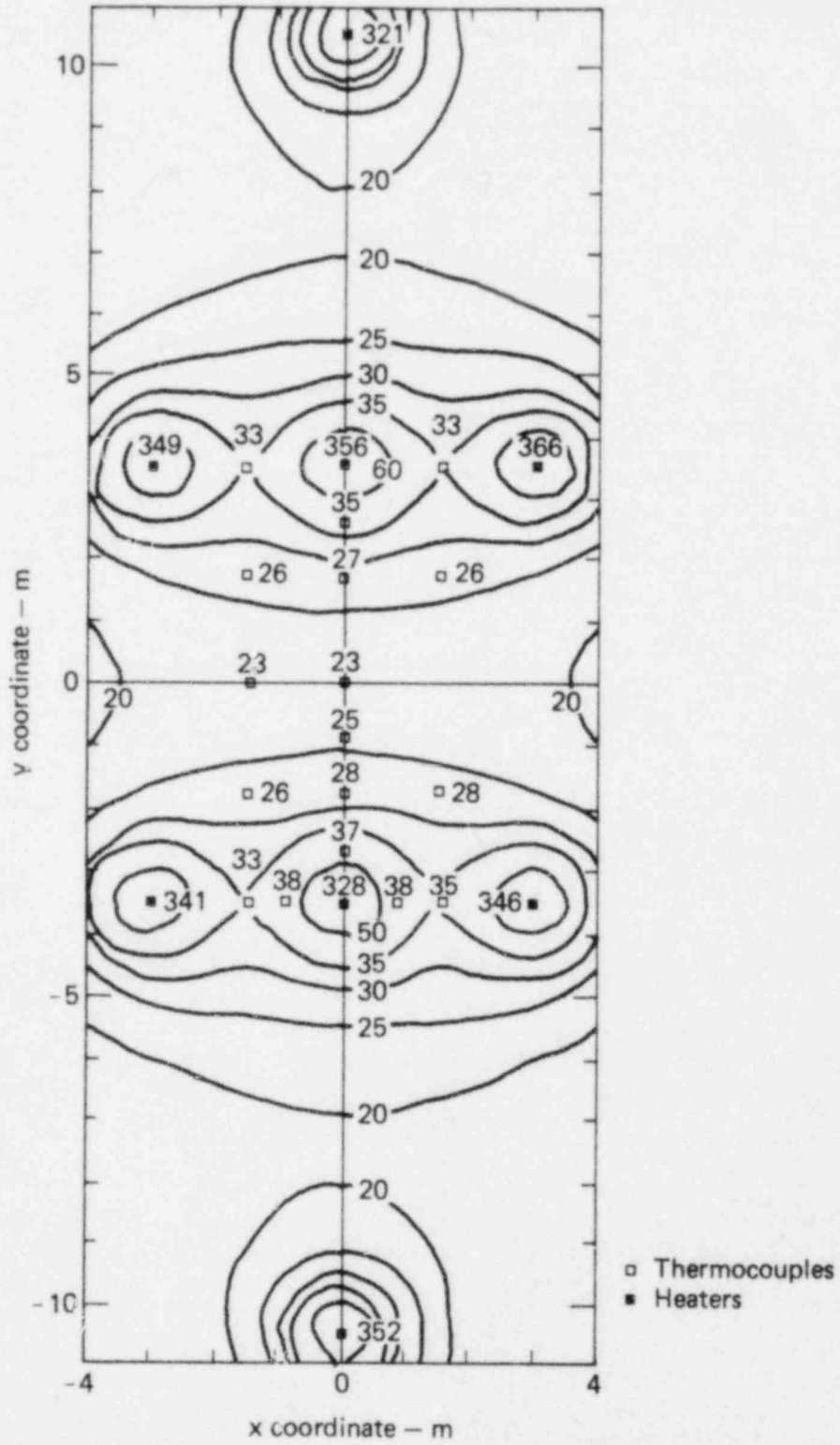

FIG. 3-42. Predicted isotherms and measured temperatures in a horizontal plane through the middle of the Stripa time-scale experiment, after 90 days of heating (from Cook and Hood, 1978). Temperatures at heaters and thermocouples are measured values.

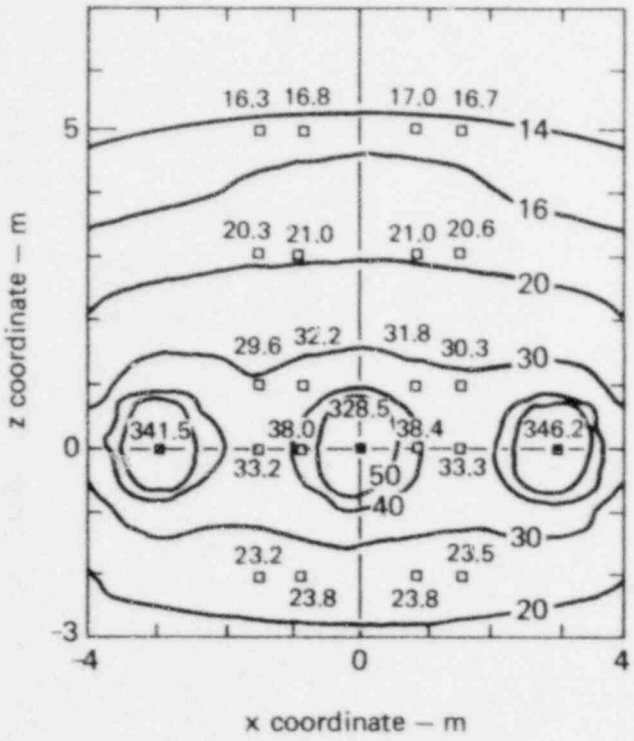

FIG. 3-43. Predicted isotherms and measured temperatures in a vertical plane (y = -3.5 m) containing three of the time-scale heaters at Stripa, after 90 days of heating (from Cook and Hood, 1978).

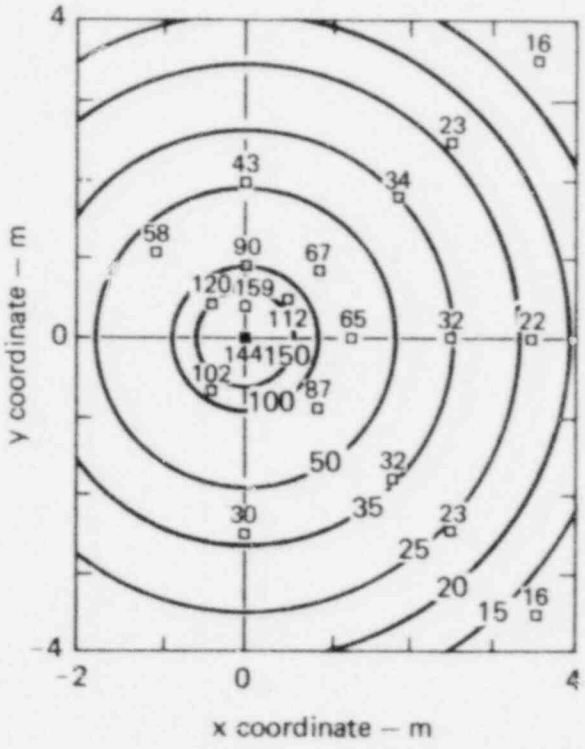

FIG. 3-44. Predicted isotherms and measured temperatures in a horizontal plane through the middle of the 5-kW full-scale heater at Stripa, after 65 days of heating (from Cook and Hood, 1978).

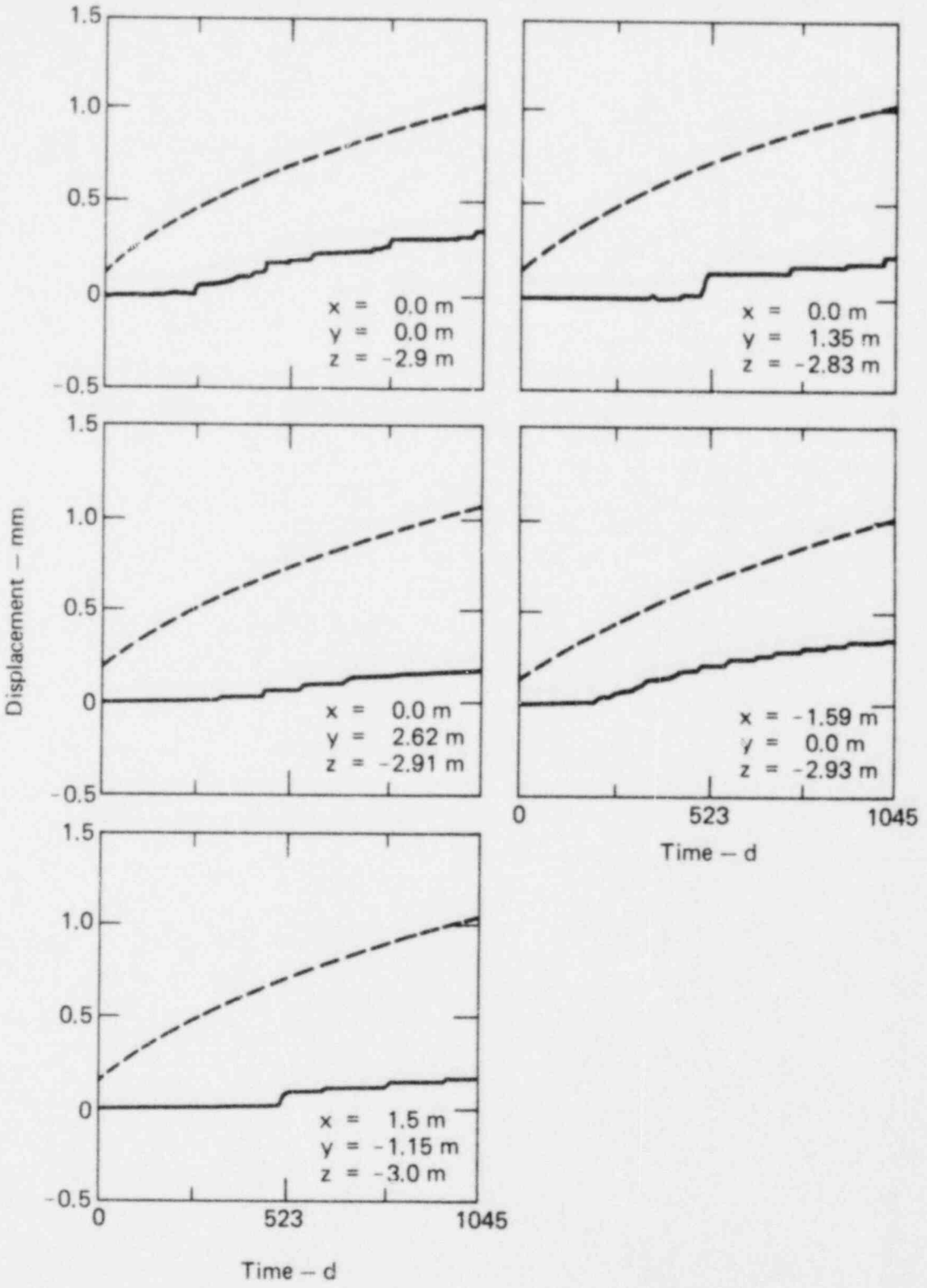

FIG. 3-45. Predicted and measured relative displacements (dashed and solid lines, respectively) at Stripa, plotted as functions of time (from Cook and Hood, 1978).

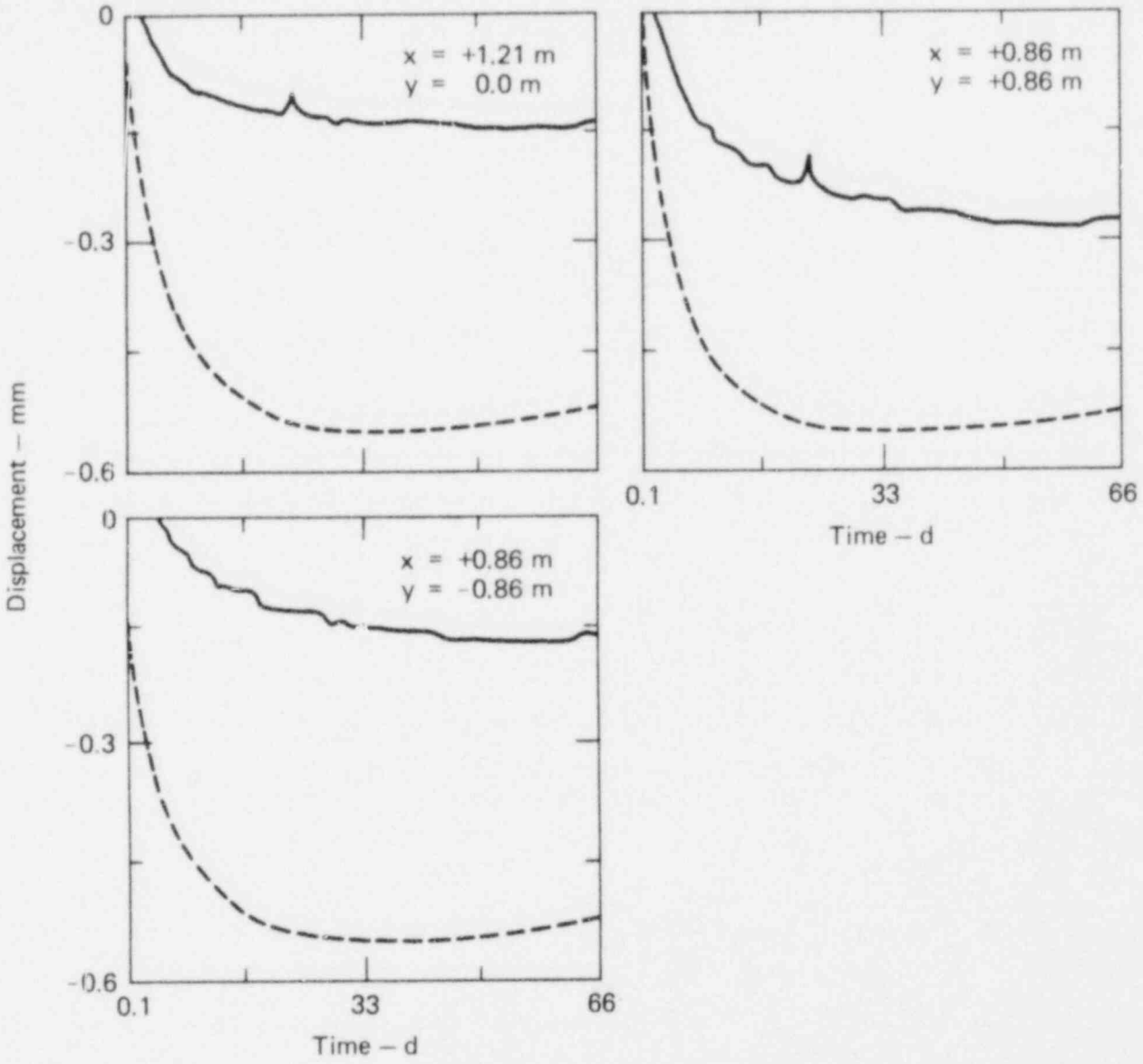

FIG. 3-46. Predicted and measured horizontal displacements of the rock (dashed and solid lines, respectively) in the mid-plane of the 5-kW full-scale heater at Stripa (from Cook and Hood, 1978).

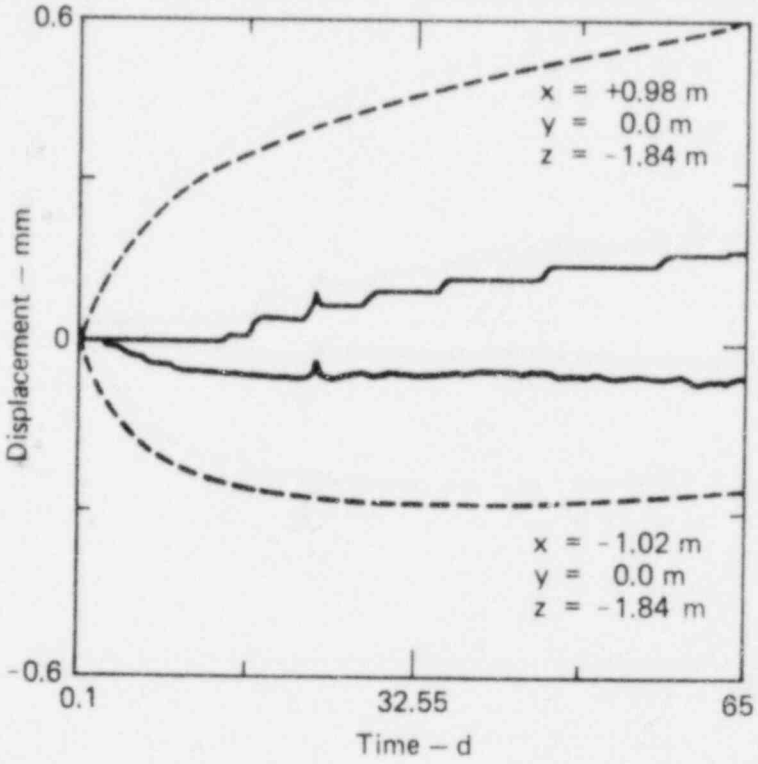

FIG. 3-47. Predicted and measured horizontal displacements (dashed and solid lines, respectively) below the 5-kW full-scale heater at Stripa (from Cook and Hood, 1978).

curves differ the most. The experimental results show essentially no displacement for a considerable period of time. Eventually, the experimental curves follow a slope not unlike that predicted from theory. These observations can be easily explained by the presence of joints or other discontinuities between the measurement points which absorb internally any displacement. They could also be explained by nonlinear modulus-temperature or expansion coefficient-temperature curves. There could, of course, be other reasons for the disparity.

These findings should not be taken as evidence of the failure of theory to adequately predict results. The disparity arises merely from the inability of researchers to insert into models the appropriate rock-mass parameters, whether they be mechanical parameters such as strength and density, thermal parameters, or thermoelastic parameters. The major emphasis in the near future will be on gathering and evaluating data on in situ rock-mass characteristics which are adequate to current models.

Fresh, unweathered granitic rocks have extremely low permeabilities. Groundwater flow occurs almost entirely along fractures. Since porous flow is essentially nonexistent, this chapter deals primarily with fracture flow, including discussions of groundwater flow through single fractures, flow through fracture networks, regional flow systems, hydraulic dispersivity, and the effects of temperature on the hydraulic characteristics of a rock mass. (See Chapter 3, Volume 1, for a discussion of the fundamentals of groundwater flow through porous media.)

Table 3-20 is a compilation of conductivity and porosity data. The conductivity data are from both lab and field measurements. In comparing the conductivities for the various granitic rock types, remember that, while laboratory measurements generally measure the interstitial conductivity, field tests reflect both interstitial and fracture flow characteristics. With fresh, unweathered granite, we can generally assume that the conductivity values measured in the field are predominantly due to fractures. However, if the rock is weathered, we will not be able to determine the relative contributions of fracture and interstitial flow.

Groundwater Flow through Fractured Rock

Although Darcy's law was developed from observations of porous flow, the relationship may be extended to describe fracture flow in an effectively nonpermeable rock mass. This extension of Darcy's law was first proposed in a thesis by Snow (1965), who concluded that laminar flow through fractures is analogous to flow between smooth parallel plates. Based upon this model, he determined that hydraulic conductivity K may be expressed as

$$K = \frac{\rho g (2b)^2}{12\mu} = \frac{g(2b)^2}{12\nu} \quad , \tag{3-1}$$

where

ρ = fluid density,
g = acceleration of gravity,
$2b$ = fracture aperture,
μ = viscosity,
ν = kinematic viscosity.

TABLE 3-20. Hydraulic and thermal measurements for granite.[a] Letters in parentheses specify laboratory (L) or field (F) measurements; where no letter appears, the type of measurement was not specified in the original reference.

Rock type and origin	Porosity, %	Hydraulic conductivity, m/d	Reference
Stripa granite (F)		1.7×10^{-6} to 34×10^{-6}	Lundstrom and Stille, 1978
Metasediments, Straight Creek Tunnel (F)		2.1×10^{-3}	Hurr and Richards, 1974
Granites (L)		7.4×10^{-8} to 3.3×10^{-4}	Brace, 1979
Metamorphics (L)		4.4×10^{-7} to 8.3×10^{-5}	Brace, 1979
White Lake Gneiss (L)		7.5×10^{-10} to 7.5×10^{-9}	Brace, 1979
Fractured metamorphics, Front Range, Colo., (F)		4.1×10^{-3} to 8.3×10^{-3}	Brace, 1979
Crystalline rocks, dam sites in western U.S., (F)		0.4-4.9	Brace, 1979
Laramie Granite (F)		8.3×10^{-4} to 4.2×10^{-3}	Brace, 1979
Crystalline basement rocks, Aiken, S.C. (F)		8.3×10^{-7} to 8.3×10^{-2}	Brace, 1979
Stripa granite (F)		8.3×10^{-7} to 1.7×10^{-5}	Brace, 1979
Granites and gneisses, Sweden (F)		8.3×10^{-7} to 0.4	Brace, 1979
Barre Granite (dense, medium-grained)	0.4	$<9 \times 10^{-3}$	Kulhany, 1975
Silver Plume Granite, Straight Creek Tunnel site, pilot bore, Colo.	1.19(2.5,25)		Hurr and Richards, 1974

continued

[a]Values are presented in the form A(B,C), where A is either the single value reported, the mean, or the range of values (A_1-A_2); B is either the difference between the maximum and minimum reported values or the range of values (B_1-B_2); and C is the number of samples tested. Both B and C or C alone may be absent. NR signifies "not reported."

TABLE 3-20 continued.

Rock type and origin	Porosity, %	Hydraulic conductivity, m/d	Reference
Quartz monzonite, Climax stock, Nevada Test Site	0.7-1.1		Carroll et al., 1966
Monzonite porphyry, Grand Coulee pumping plant, Grant County, Wash.	2.32(2.44,16)		USBR, 1953
Quartz diorite, Garden Valley dam site, Boise, Idaho	2.7 (0.1)		USBR, 1953
Diorite gneiss, Sec. 1, T. 6 S., R. 77 W., Montezuma quad, Colo.	0.49(1.07,10) 0.22(0.10,3)		USBR, 1953
Diorite, no location	1.7(8.1,12)		Judd, 1969
Mineralized diorite, Utah	0.94(1.65,5)		Windes, 1949
Diorite (gneissic-diorite-gabbro), N.Y.	0.8(0.4,2)		Windes, 1949
Pegmatite, Morrow Point Dam, Montrose, Colo.	0.93(NR,4)		Dodd, 1967
St. Cloud gray granodiorite, Precambrian	1.5	$<9 \times 10^{-7}$	--
Granite, Md.	0.08		Windes, 1949
Granite, Nev.	0.09		Windes, 1949
Granite, N.C.	0.07		Windes, 1949
Granite, no location	1.6(11.1,146)	1(1,41)	Judd, 1969
Granite, no location	1.6		Kulhany, 1975
Fremont Canyon Granite (coarse-grained)	0.8		Kulhany, 1975
Mitidieri Quarry porphyritic granite	3.6		Kulhany, 1975
Valinhos Quarry granite	3.2		Kulhany, 1975
Cantareira Quarry granite	2.2		Kulhany, 1975

continued

TABLE 3-20 continued.

Rock type and origin	Porosity, %	Hydraulic conductivity, m/d	Reference
Piccicacco Quarry tourmaline granite	1.2		Kulhany, 1975
Granite (coarse-grained), Polehill power plant, Loveland, Colo.	1.0(1.4,27)		USBR, 1953
Pegmatite granite, Polehill power plant, Loveland, Colo.	1.0		USBR, 1953
Slightly altered granite, Grand Coulee pumping project, Grant County, Wash.	2.61(1.01,18)		USBR, 1953
Granite, Grand Coulee pumping plant, Grant County, Wash.	1.59(1.48,32)		USBR, 1953
Granite, Unaweep granite site, Grand Junction, Colo.	0.6		Blair, 1956
Granite, Vt.	0.9		Windes, 1949
Lac du Bonnet batholith, Manitoba (F)		4.2×10^{-6} to 4	Brace, 1979
Granodiorite, Los Alamos, N.M. (F)		5.8×10^{-6} to 6.6×10^{-2}	Brace, 1979
Crystalline basement, Rocky Mountain Arsenal (F)		4.9×10^{-1} to 6.6×10^{-1}	Brace, 1979
Climax stock, Colo. (F)		2.5×10^{-1} to 7.5×10^{-1}	Brace, 1979

Intrinsic permeability k can then be expressed as

$$k = \frac{(2b)^2}{12} \tag{3-2}$$

Relating this back to Darcy's law (Eq. 3-3, Vol. 1), an equation describing the flow rate q per unit width in a single fracture can be written (Apps et al., 1979):

$$q = \frac{g(2b)^3 \frac{dh}{dl}}{12\nu} \tag{3-3}$$

This relationship, demonstrating discharge to be proportional to the cube of fracture aperture, is known as the cube law. It confirms that only slight changes in aperture size can cause large changes in flow. Correspondingly, average, or effective, velocity may be expressed as

$$v = \frac{\rho g(2b)^2 \frac{dh}{dl}}{12\mu} = K \frac{dh}{dl} \tag{3-4}$$

The area considered in determining velocity of flow , the cross-sectional area of the fracture, and the porosity of the open fracture is unity. Table 3-21 illustrates the hydraulic conductivities and the average velocities that result from Eqs. 3-1 and 3-4, for a range of aperture widths and assuming water at ambient conditions under a hydraulic gradient of 0.001.

As flow velocities increase, roughness of the fractures will cause turbulence and nonuniform flow within the fracture plane. Louis and Maini (1970), Sharp et al. (1972), and Gale (1975) have investigated nonlinear, non-Darcian flow through an "equivalent" aperture--a parallel-plate model having the same hydraulic behavior as the natural fracture.

Gale ran double-set packer tests on single fractures in a borehole. Using a constant head, he was able to measure the rate at which a single fracture would take water. With this information, he used a form of the cube law to calculate the equivalent aperture. A summary of Gale's work, Table 3-22, shows the calculated equivalent apertures to differ from the true

TABLE 3-21. Calculated hydraulic conductivity and effective velocity for water flowing through a single fracture (from Apps et al., 1968).

Aperture (b), μm	Hydraulic conductivity (K), m/s	Effective velocity (v)	
		in m/s	in km/y
0.1	8.2×10^{-9}	8.2×10^{-12}	2.6×10^{-7}
1.0	8.2×10^{-7}	8.2×10^{-10}	2.6×10^{-5}
10.0	8.2×10^{-5}	8.2×10^{-8}	2.6×10^{-3}

TABLE 3-22. Fracture data and equivalent fracture apertures for selected fractures at Sambro, Nova Scotia (from Gale, 1975).

Fracture depth, m	Aperture size,[a] m	Excess hydraulic head, m	Flow rate, 10^{-3} ft^3/s	Calculated equivalent aperture, m
2.85	0.030-0.024	0.14	4.46	0.0011
4.020	0.0030-0.0061	3.8	0.98	0.00021
		5.28	1.12	0.000207
5.063	0.0015	15.7	0.027	0.00004
		22.9	0.45	0.00009
6.117	0.0015-0.0030	1.77	0.67	0.00026
		4.02	1.29	0.00024
		7.59	1.56	0.00021
8.806	0.0015-0.0030	6.05	1.29	0.000207
		12.7	1.87	0.00019
7.315	0.0015	3.097	0.003	0.000034
		7.251	0.005	0.000030
12.50	--	7.102	0.001	0.000046

[a]Estimated from borehole periscope log.

(measured) apertures by at least an order of magnitude, the true apertures being larger. Because roughness of fracture walls and nonuniform flow within the fracture plane are very difficult to evaluate directly, the concept of equivalent apertures is very significant in current approaches to modeling.

Fracture Networks

Many parameters have a bearing on the rate of groundwater flow through a fracture network. Fracture spacing, aperture sizes, orientation, and continuity are among the most significant factors. Also of importance is the roughness of fracture walls, wall coatings, fracture fillings, and the uniformity of the apertures.

Joint and Fracture Systems. Early research in granitic tectonics conducted by Hans Cloos (Kendorski and Mahtab, 1976) identified an orthogonal system of joints characteristic of nearly all granitic plutons:

- Q-fractures or cross-joints result from extensive fracturing parallel to the principal direction of stress in the rock mass.
- S-joints or longitudinal fractures form parallel to the flow lines or crystal orientation and result from failure along the anisotropy resulting from the flow.
- L-joints are flat-lying joints resulting from variations in vertical loading or rebound.

Although later tectonic activity may superimpose additional fracture systems on a granitic mass, nearly all such masses possess the primary set of orthogonal joints identified by Cloos. Price (1966) confirms the basic concepts of Cloos; however, he also concludes that these primary joints have little hydraulic significance. Price proposes that brittle fractures resulting from unloading and uplift are of the most significance to groundwater flow.

Variations in Aperture and Fracture Spacing. Snow (1965, 1968a-c), Lewis and Burgy (1964), Uhl and Sharma (1978), and others concur that the permeability and fracture porosity of crystalline rocks decrease with depth and that the rock type is of less importance in describing these parameters than is fracture geometry. Snow (1968b) found that fracture spacings generally

increase with depth, while fracture openings generally decrease. In studies of crystalline rock at four dam sites in Colorado, he found fracture spacings at the weathered surface to range from 0.15 to 1.2 m, increasing to 1.5 to 4.6 m immediately beneath this surface, and to 5 to 11 m at a depth of 61 m. Effective apertures inferred from packer tests were observed to range from 75 to 400 μm in the upper 9 m of the rock mass, declining to 50 to 100 μm at depths of 15 to 61 m (Fig. 3-48).

Corresponding to the observed changes of fracture spacing and aperture sizes with depth is a decline in both fracture porosity and permeability. Fracture porosity declines from 0.05% near the surface to approximately 0.0005% at 122 m; it is generalized that fracture porosity decreases approximately tenfold per 61 m of depth (Snow, 1968a). Permeability measured at equivalent depths at the four dam sites varied; however, all followed a logarithmically declining trend with depth.

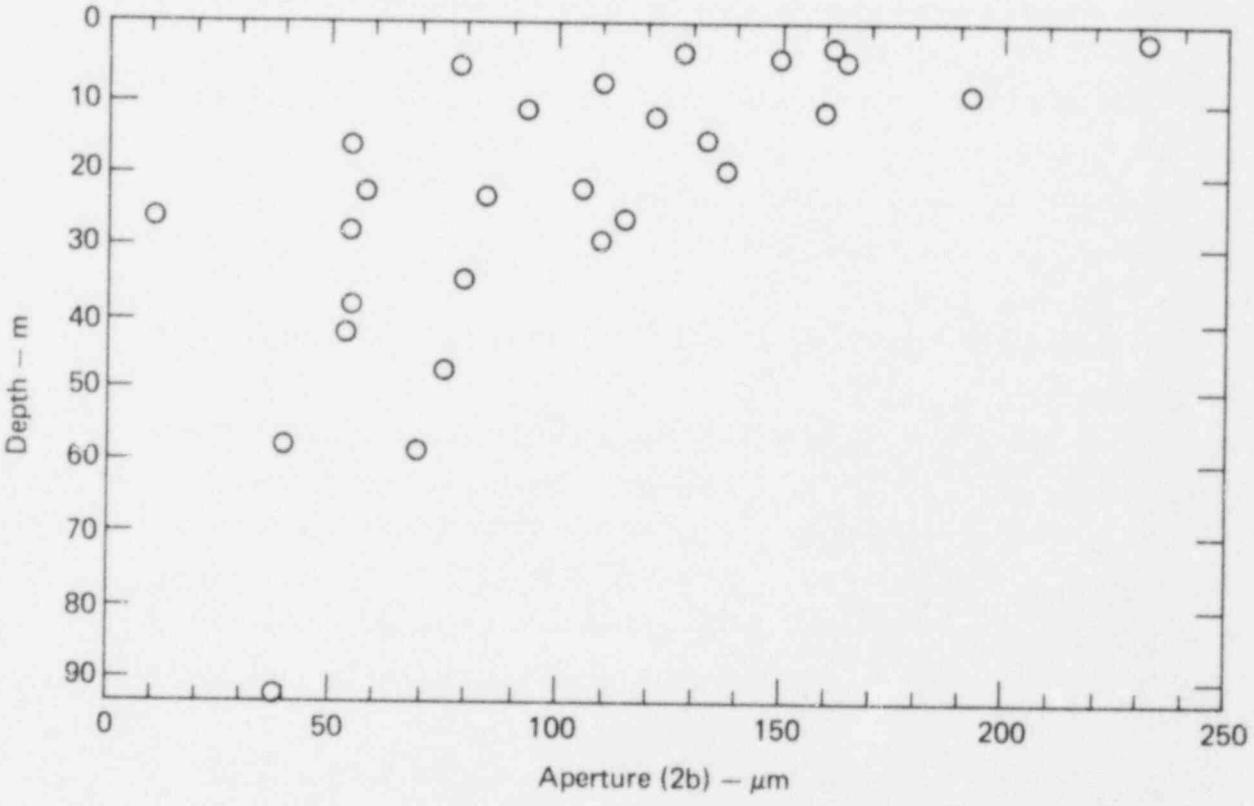

FIG. 3-48. Fracture openings in the gneisses of the Front Range, Colorado, computed from injection tests (from Snow, 1968b).

Based on data from the four dam sites, Snow (1968b) suggested a technique for estimating the permeability of a fractured crystalline rock mass. By plotting the mean permeability of each depth zone against mean depth (Fig. 3-49), and constructing a line through these points by means of a least-squares fit, Snow concluded that permeability varies with depth according to the following equation:

$$\log k = -8.9 - 1.67 \log d \quad , \tag{3-5}$$

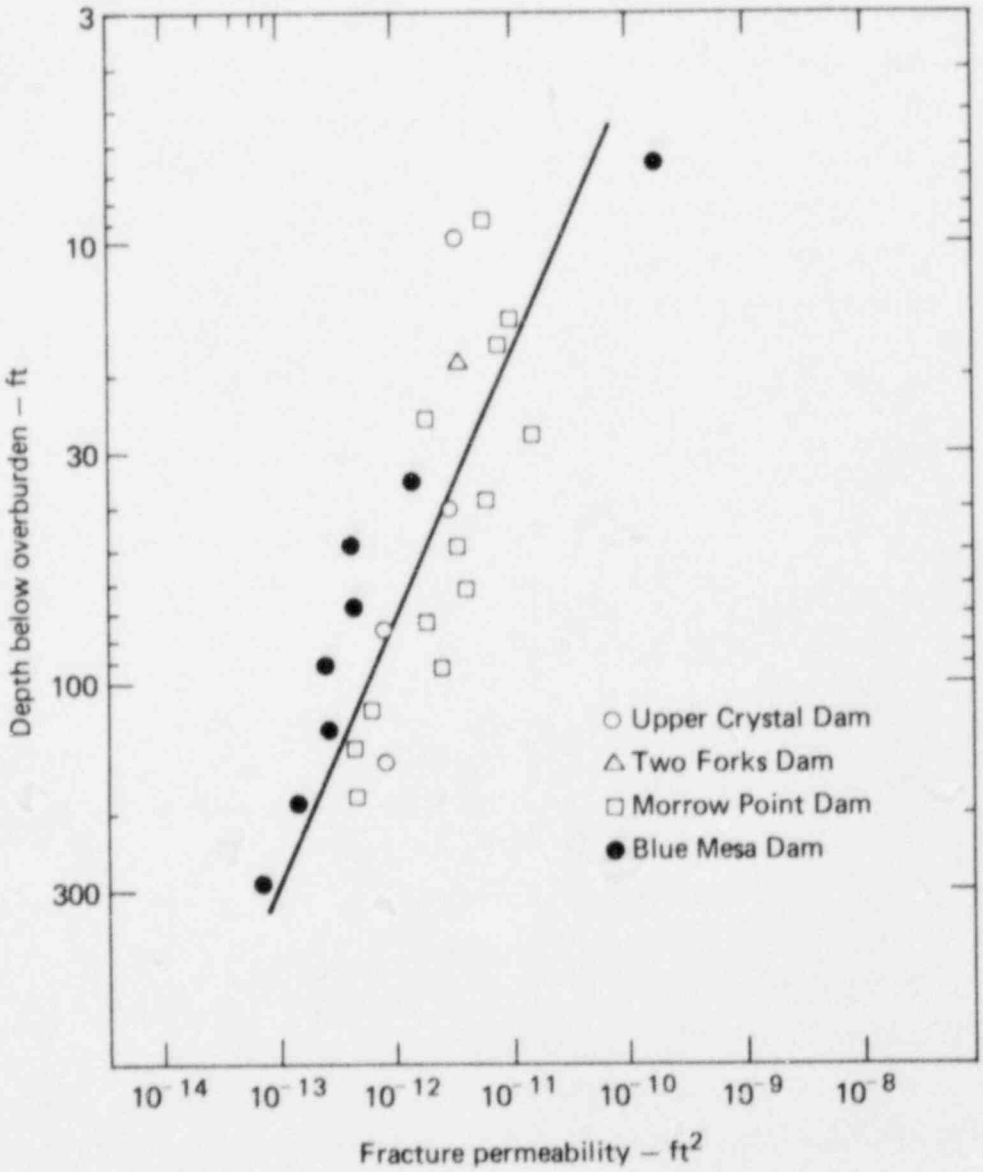

FIG. 3-49. The mean permeability in each depth zone at four dam sites, plotted against the mean depth of the midpoints of the test sections (from Snow, 1968b).

where k is the intrinsic permeability in ft^2, and d is the depth below the surface of the rock mass in feet.

Research conducted in Sweden concluded that permeability declines somewhat more rapidly with depth along an exponential curve (ONWI, 1978, Vol. 21). Laboratory work with fractured granite in artificial stress fields (Pratt et al., 1971) correlates somewhat more closely with the conclusions of Snow; however, this research considered only decreasing fracture density with depth. At depths exceeding 450 m, the validity of either relationship is uncertain. Pratt suggested that, as normal stress increases, fracture permeability asymptotically approaches a value approximately ten times the permeability of the rock matrix.

The fracture porosity of a rock mass with a specific permeability depends on the fracture geometry and the fracture aperture. Snow (1968b) concluded from his work that an orthogonally fractured rock mass at a specific depth with uniform fracture openings has a porosity that is related to fracture spacing by the following relation:

$$\phi = 3(3k/2)^{1/3} (2/\Delta)^{2/3} = 5.45(k/\Delta^2)^{1/3} \qquad (3\text{-}6)$$

where

ϕ = effective porosity,
k = intrinsic permeability in ft^2,
Δ = fracture spacing in feet.

The apparent spacings of individual fractures within each of three assumed orthogonal sets of water-bearing fractures as observed at the Colorado dam sites is summarized in Fig. 3-50. Snow assumed that fracture spacings are normally distributed. More recent work by Priest and Hudson (1976) suggests that spacing is exponentially distributed. However, the effect this might have on calculations of porosity or permeability was not studied.

In recent years, some disagreement has developed among authors as to whether this decreasing permeability is due in greater degree to decreasing aperture size or increasing fracture spacing. Raven and Gale (1976) and Kendorski and Mahtab (1976) found that aperture size decreases with depth

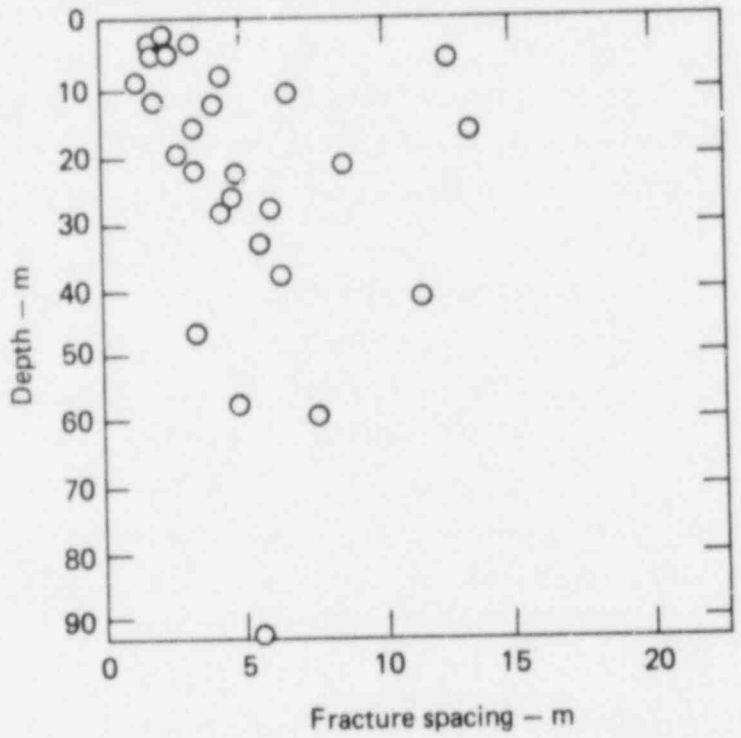

FIG. 3-50. Apparent spacing of fractures in each of three assumed orthogonal sets of water-bearing fractures in gneisses of the Front Range, Colorado, computed from injection tests (from Snow, 1968b).

while fracture geometry remains constant. Conversely, Swedish investigators on the Stripa project concluded that fractures with significant apertures persist to depth, but that fracture spacing increases (ONWI, 1978).

It is generally accepted that stress can have a large effect on the permeability of rock. The decrease in permeability with depth, as demonstrated by Davis and Turk (1964) and by Snow (1968b), is often considered to be stress related. Work by Iwai (1976) on man-made fractures in basalt, granite, and marble generally supports the concept of decreasing aperture. Under normal stresses ranging from 0 to 20 MPa, Iwai found both aperture and hydraulic conductivity to decrease with increased stress. However, hydraulic conductivity asymptotically approached a minimum value. Imperfect matching of opposing surfaces caused apertures to approach a minimum of 15 μm as normal pressures approached 20 MPa.

Recent work by Brace (1979) to some degree contradicts the accepted concept of declining permeability with depth. Brace assembled laboratory and in situ permeability measurements from a number of locations and presented

this data in the form of a histogram (Fig. 3-51). From these data, Brace draws the following conclusions:

- The average intrinsic permeability of the more permeable crystalline rocks is about a thousand times that measured in the laboratory. This variance is due in part to the dependence of permeability values on sample size in laboratory determinations.
- There is a hint of a decrease in permeability with depth, but hardly enough to justify the exponential relationships suggested in the literature.
- At nearly every site, some portion of the rock sampled by the drill holes has a permeability of 1 to 100 mD. This relatively permeable zone may be as deep as 3.3 km.

Given the square relationship between flow velocity and aperture size, it is particularly critical to define, at least on a site-specific basis, the relationship between aperture size and depth.

Orientation and Continuity of Fractures. In many fractured crystalline bodies, the average aperture varies with fracture orientation. Given the cubic relationship between aperture and flow, the orientation of large fractures with respect to the potential gradient thus makes a major difference in groundwater flow velocity and direction. The definition of fracture orientations is critical to the determination of anisotropic permeability.

Fracture mapping in many geologic environments has shown that fractures cannot be assumed to be continuous within their own planes (Apps et al., 1979). Continuity is the most difficult of the fracture parameters to measure in situ. However, defining the continuity of fractures is of prime importance in describing groundwater movement. Long-duration well tests that involve large volumes of rock and single-fracture cross-hole tests are currently most widely used for determining fracture continuity.

Fracture Network Flow

Equations describing flow through a fracture network can be developed from the flow equation for a single fracture:

$$v = K \frac{dh}{dl} \qquad (3\text{-}7)$$

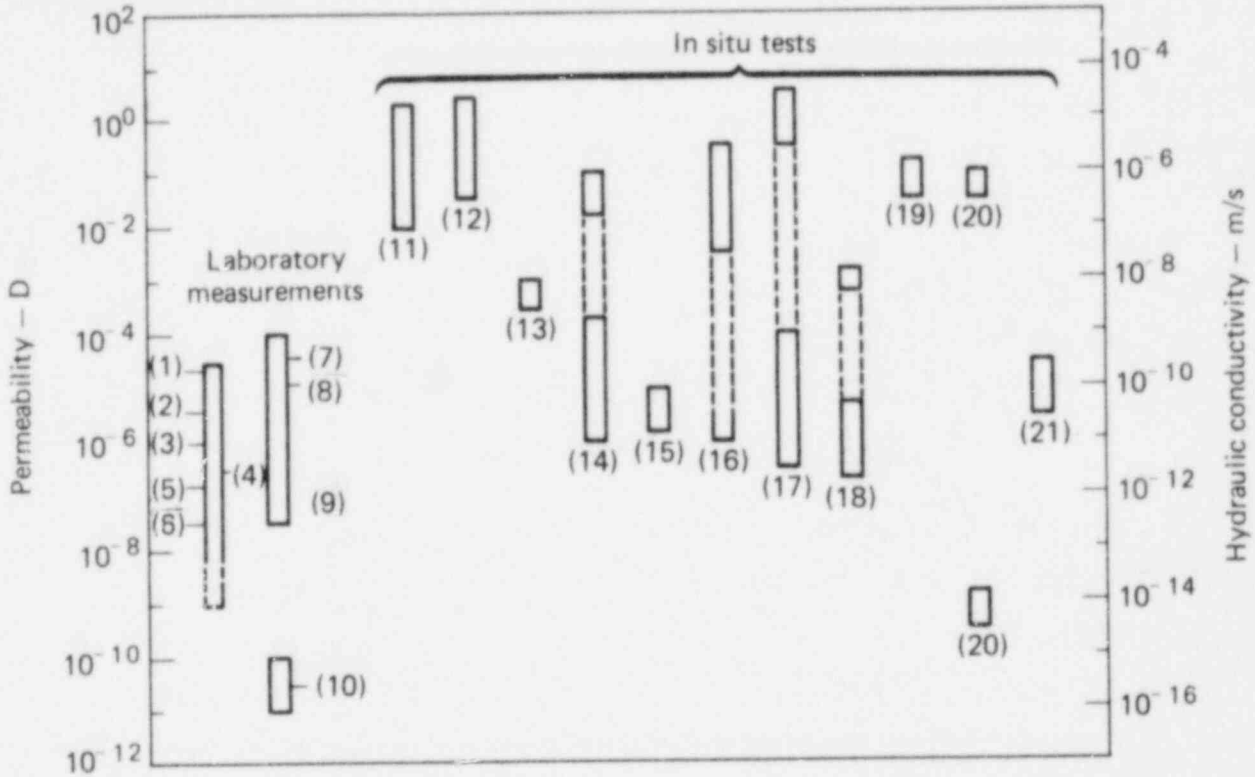

1 Laramie Granite
2 Quincy Granite
3 Westerly Granite
4 Samples from Los Alamos, N.M.
5 Barre Granite
6 Ontario granites
7 Front Range Gneiss
8 Front Range Schist
9 Quartzite
10 White Lake Gneiss
11 Metamorphics–Colorado Front Range (well tests)
12 Crystalline rock at 38 western dam sites
13 Laramie Granite–well test
14 Crystalline basement rock–pump test from Aiken S.C.
15 Stripa granite–pumping tests
16 Granites and gneiss–500 pumping tests, Sweden
17 Lac duBonnet batholith–pumping tests, Pinawa, Manitoba
18 Granodiorite–pumping tests, Los Alamos, N.M.
19 Crystalline basement–injection tests, Rocky Mt. Arsenal, Denver, Colo.
20 Climax granitic stock–pressure decay tests
21 Quartzite

FIG. 3-51. Summary of laboratory and in situ measurements of permeability in crystalline rocks, as compiled by Brace (1979).

For anisotropic conditions in a rock mass, the equation can be rewritten as

$$\{v\} = [K_p]\{i\} \quad , \tag{3-8}$$

where

$\{v\}$ = velocity vector,
$\{i\}$ = potential gradient vector,
$[K_p]$ = a second-order tensor formed from the permeability terms of each fracture set.

The derivation continues (see Apps et al., 1979) by defining the area hydraulic conductivity K_p in terms of the gradient and the flow rate per unit area q_A:

$$q_A = K_p i \quad . \tag{3-9}$$

For a set of fractures with a frequency λ, the single fracture conductivity K can then be related to the area conductivity by

$$K_p = 2b\lambda[K] \quad . \tag{3-10}$$

Assuming a uniform set of fractures oriented in the x-y plane with aperture 2b,

$$[K_p] = 2b\lambda \begin{bmatrix} \frac{g(2b)^2}{12\nu} & 0 & 0 \\ 0 & \frac{g(2b)^2}{12\nu} & 0 \\ 0 & 0 & \frac{g(2b)^2}{12\nu} \end{bmatrix} = \begin{bmatrix} \frac{\lambda g(2b)^3}{2\nu} & 0 & 0 \\ 0 & \frac{\lambda g(2b)^3}{2\nu} & 0 \\ 0 & 0 & \frac{\lambda g(2b)^3}{2\nu} \end{bmatrix} \tag{3-11}$$

The principal permeabilities and their orientations are the eigenvalues and eigenvectors of the conductivity tensor formed from the combination of the tensors for the individual fractures (Apps et al., 1979). A detailed summary of the derivation of conductivity tensors from single-fracture data may be

found in Bianchi and Snow (1969). Although K almost certainly varies with direction in rocks, principal values of the conductivity tensor are rarely given (Brace, 1979). Network flow studies using the conductivity tensor are, to date, principally theoretical and have not been confirmed in the field.

Regional Groundwater Flow

While fluid flow through individual fractures is well understood and flow through fracture networks has been studied theoretically, groundwater flow on a regional scale is only beginning to be investigated.

Fundamental Regional Flow Characteristics. In a granite drainage basin, groundwater movements vary laterally and vertically in the various fracture networks that connect to allow groundwater flow through the region. In general, water will be recharged into the country rock in topographically lower areas. In the recharge area, the direction of water movement is principally downward, the depth of penetration depending upon fracture geometry, continuity, and numerous other geologic parameters. Groundwater flow eventually becomes roughly horizontal until a zone of discharge is reached where the flow lines turn upward. The distance between recharge and discharge points in a granite drainage basin may range from only a few tens of meters to many kilometers.

In many granite drainages, the water table roughly parallels surface topography. Water table configuration, and hence topography, often controls the locations of recharge and discharge zones. As demonstrated on the flow nets of Fig. 3-52, the size of recharge and discharge zones vary depending on their position and the degree of topographic relief in the basin (Apps et al., 1978).

Regional groundwater flow may also be interrupted by geologic anomalies such as faults or shear zones. These features occur on scales from a few meters in length to tens of kilometers. If the fractures associated with these features are open, they may channelize groundwaters and control the movements of both surface waters and groundwaters within a basin. Such features have been observed carrying significant groundwater flows at depths in excess of 3.5 km (Brace, 1979; Robinson, 1978). Often, however, faults and shear zones are filled with rubble which has undergone extensive chemical or

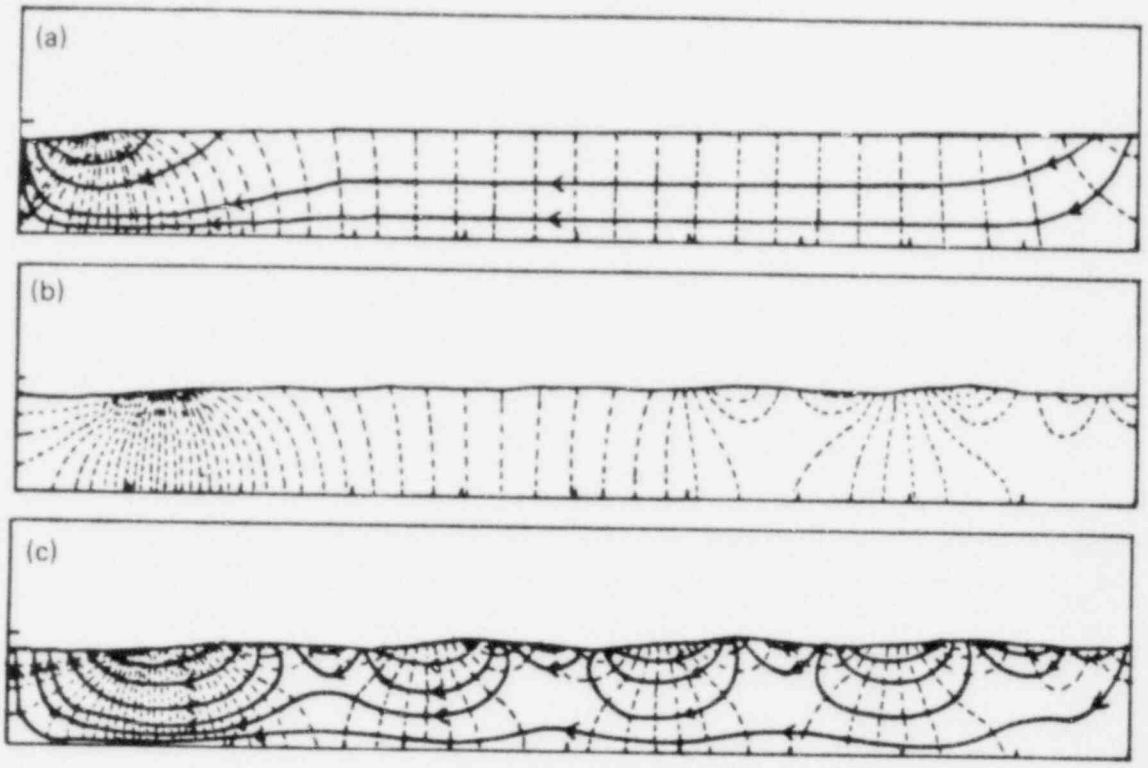

FIG. 3-52. Effect of topographic relief on regional groundwater flow through homogeneous, isotropic media (from Freeze and Witherspoon, 1967). The dashed lines are contours of equal potential. In (b) and (c), one with flow lines, one without, the effect of topographic relief can be seen, in contrast to (a).

mechanical alteration, producing a clay-rich material of very low permeability known as fault gouge. In areas where fractures and voids associated with faults or shear zones are filled with gouge, or with other fines or precipitates, the feature may act as a barrier to groundwater flow.

Layer Models of Regional Systems. Various authors have attempted to identify different horizons in crystalline aquifers to simplify descriptions of groundwater flow. Hurr and Richards (1974) suggested breaking down each aquifer into an active zone and a passive zone. The active zone was defined as that near-surface, weathered zone in which the water table is subject to seasonal fluctuation, and in which significant flows may be observed. The passive zone was defined as an underlying zone of lower permeability in which water may be stored for tens to thousands of years. In research at the Straight Creek Tunnel in Colorado, the depth of the contact between the active

and passive zones was found to fluctuate; however, it was identified as the point at which the seismic velocity increased from 3780 m/s to approximately 5400 m/s.

In modeling studies for the ONWI (1978), three zones of saturation were considered. The upper zone was identified as that of the highest permeability, holding young waters containing both ^{14}C and tritium. The intermediate zone was identified as that bearing water of intermediate age containing ^{14}C, but lacking tritium. The deepest and least permeable zone was identified as containing the oldest water which bears no measurable tritium or ^{14}C.

Either technique for identifying specific horizons in crystalline aquifers can be a simplification of some assistance in modeling. However, the boundaries between aquifer zones are often quite vague and are difficult to define in the field.

Representative Elementary Volume. Regional evaluations of groundwater systems are often done by continuum modeling. This technique requires that representative values be assigned to parameters for a finite volume element. Consequently, some technique must be developed for establishing representative values from field data. Bear (1972) has proposed the concept of the representative elementary volume (REV). As illustrated in Fig. 3-53, the REV (u_o) is that volume for which a small increase in volume will have no significant effect on the value of the parameter measured.

For volumes smaller than the REV, discrete fracture effects will influence the value of the parameter as the test volume is increased by small increments. However, for a volume equivalent to or larger than the REV, we move into the domain of porous media effects (ONWI, 1978). A list and summary of some of the models currently being used for regional flow analyses are presented by ONWI (1978).

Effects of Temperature on Fracture Flow Systems

During the initial stages of repository construction and loading, groundwater movement can be adequately defined by the approach outlined in previous sections. However, as the repository becomes hotter in later stages of its life, the rate and direction of groundwater flow may be altered. Large-scale permeability tests at the Stripa Mine Project (Lundstrom and

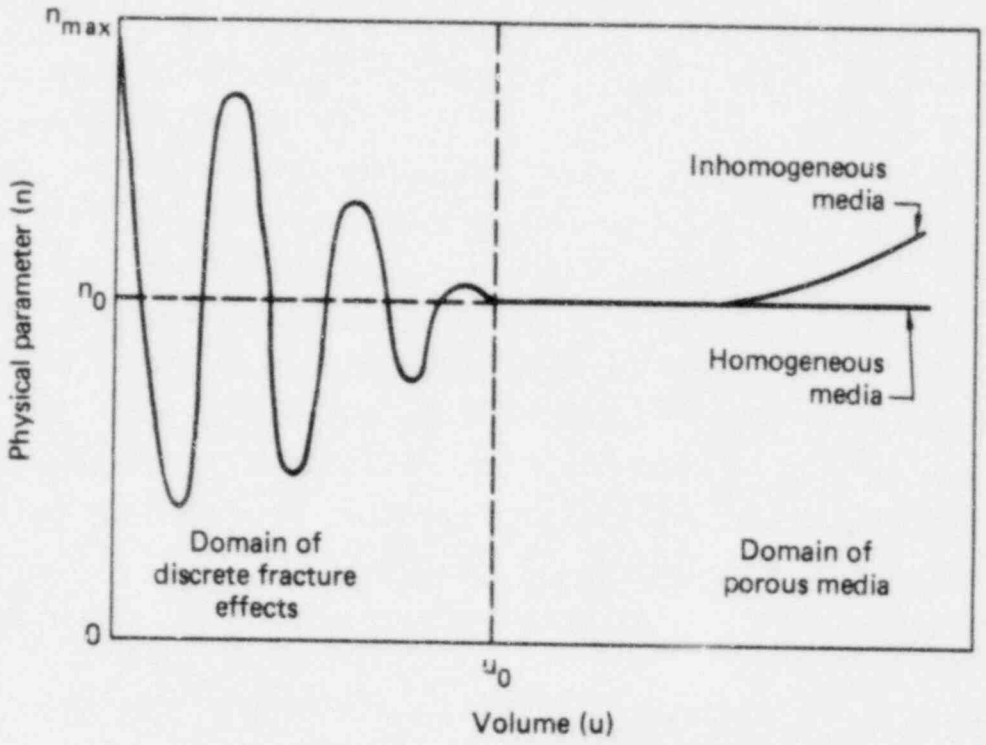

FIG. 3-53. Definition of a representative elementary volume u_0 (from Bear, 1972). For volumes larger than u_0, an accurate value of u can be estimated.

Stille, 1978) confirmed that the permeability of the rock mass decreased by 50% as the temperature increased from 10 to 35°C. This decline in permeability can probably be attributed principally to a decrease in aperture size along fractures--a result of thermal expansion of the rock mass.

Thermal convection may also alter groundwater movements in a crystalline rock mass. In model studies conducted for the ONWI (1978), large convection cells were predicted to develop in the country rock surrounding a repository. However, Apps et al. (1978) suggested that, in fractured rocks of very small aperture, the Rayleigh number is so large that a local heat source is unlikely to cause natural circulatory convection. To establish throughflow due to a buoyancy unbalance requires recharge from a surrounding rock mass that is filled with cold groundwater. If the repository is sited in nearly impermeable rock, the low velocities of the regional system will restrict cold water inflow and control overall fluid movement.

It should be noted that few, if any, large-scale field studies have been undertaken to evaluate the effects of thermal convection in a granite rock mass. Most information now available is purely theoretical or is drawn from modeling studies which incorporate assumed hydraulic and thermal parameters.

REFERENCES: CHAPTER 3

Anderson, A. L., 1948, "Role of the Idaho Batholith during the Laramide Orogeny," Econ. Geol. 43, 84.

_____, 1952, "Multiple Emplacement of the Idaho Batholith," J. Geol. 60, 255.

Apps, J. A., N. G. W. Cook, and P. A. Witherspoon, 1978, An Appraisal of Underground Radioactive Waste Disposal in Argillaceous and Crystalline Rocks: Some Geochemical, Geomechanical, and Hydrogeological Questions, Lawrence Berkeley Laboratory, Berkeley, Calif., LBL-7047.

Apps, J., T. Doe, B. Doty, S. Doty, R. Galbraith, A. Kearns, B. Kohrt, J. Long, A. Monroe, T. N. Narasimhan, P. Nelson, C. R. Wilson, and P. A. Witherspoon, 1979, Geohydrological Studies for Nuclear Waste Isolation at the Hanford Reservation, Volume II: Final Report, Lawrence Berkeley Laboratory, Berkeley, Calif., LBL-8764.

Bateman, P. C., L. D. Clark, N. K. Huber, J. G. Moore, and C. D. Rinehart, 1963, The Sierra Nevada Batholith--A Synthesis of Recent Work across the Central Part, U.S. Geol. Survey Professional Paper 414D.

Bear, J., 1972, Dynamics of Fluids in Porous Media (American Elsevier, New York).

Becraft, G. E., et al., 1962, Geology and Mineral Deposits of the Jefferson City Quadrangle, Jefferson and Lewis and Clark Counties, Montana, U.S. Geol. Survey Professional Paper 428.

Bell, E. A., and M. G. Sherrill, 1974, Water Availability in Central Wisconsin, an Area of Near Surface Crystalline Rock, U.S. Geol. Survey Water Supply Paper 3033.

Biachi, L., and D. T. Snow, 1969, "Permeability of Crystalline Rock Interpreted from Measured Orientations and Apertures of Fractures," Annals of Arid Zones 8, 221.

Blair, B. E., 1955, Physical Properties of Mine Rock, Part III, U.S. Bureau of Mines Report of Investigation 5130.

_____, 1956, Physical Properties of Mine Rock, Part IV, U.S. Bureau of Mines Report of Investigation 5244.

Brace, W. F., 1979, "Permeability of Crystalline and Argillaceous Rocks," submitted to Int. J. Rock Mech. Min. Sci.

Brandon, J. R., 1976, Rock Mechanics Properties of Typical Foundation Rock Types, Engineering and Research Center, Bureau of Reclamation, REC-ERC-74-10.

Brown, W. S., and S. R. Swanson, 1970, Influence of Load Path and State of Stress on Failure Strength and Stress-Strain Properties of Rocks, University of Utah, Mechanical Engineering Dept., UTEC-70-025.

Campbell, C. D., 1940, "Structural Problems of the East Border of the Colville Batholith," abstract in Bull. Geol. Soc. Am. 51, 2019.

Carlsson, H., 1978, Stress Measurements in the Stripa Granite, Lawrence Berkeley Laboratory, Berkeley, Calif., LBL-7078.

Carroll, R. D., J. H. Scott, and D. R. Cunningham, 1966, Elastic Moduli of Granite Rock from In Situ Measurements of Seismic Velocity, U.S. Geol. Survey Professional Paper 550C.

Charles, R. J., 1959, "The Strength of Silicate Glasses and Some Crystalline Oxides," paper given at the Conf. on Fractures, Swampscott, Mass.

Clark, G. B., et al., 1969, Rock Properties Related to Rapid Excavation, final report to the Office of High Speed Ground Transportation (Contract 3-0143).

Cook, N. G. W., and M. Hood, 1978, Full-Scale and Time-Scale Heating Experiments at Stripa: Preliminary Results, Lawrence Berkeley Laboratory, Berkeley, Calif., LBL-7072.

Crowder, D. F., 1959, "Granitization, Migmatization, and Fusion in the Northern Entiat Mountains, Washington," Bull. Geol. Soc. Am. 70(7), 827.

Darton, N. H., 1906, Geology of the Bighorn Mountains, U.S. Geol. Survey Professional Paper 51.

Davis, S. N., and L. J. Turk, 1964, "Optimum Depth of Wells in Crystalline Rocks," Ground Water 2(2), 6.

Deere, D. U., and R. P. Miller, 1966, Engineering Classification and Index Properties for Intact Rock, Air Force Weapons Laboratory, Kirkland AFB, N.M., AFWL-TR-65-116.

Dodd, J., 1967, Morrow Point Dam and Power Plant Foundations Investigations, report on Bureau of Reclamation Colorado River Storage Project, Colorado.

Freeman, D. C., J. A. Sawdye, and F. A. Mumpton, 1963, "Mechanism of Thermal Spalling in Rocks," in Proc. 11th Symposium on Rock Mechanics, Colo. School Mines Quart. 58(4).

Freeze, R. A., and P. A. Witherspoon, 1967, "Theoretical Analysis of Regional Ground Water Flow. 2. Effect of Water-Table Configuration and Subsurface Permeability Variation," Water Resources Res. 3(2), 623.

Gale, J., 1975, A Numerical, Field, and Laboratory Study of Flow in Rocks with

Deformable Fractures, University of California, Berkeley, Ph.D. dissertation.

Griggs, D. T., F. J. Turner, and H. C. Heard, 1960, "Deformation of Rocks at 500° to 800°C," in Griggs and Handin, Rock Deformation, Geol. Soc. Am. Memoir 79.

Hamilton, W., and W. B. Myers, 1974, "Nature of the Boulder Batholith of Montana," Bull. Geol. Soc. Am. 85, 365.

Hanley, E. J., D. P. DeWitt, and R. F. Roy, 1978, "The Thermal Diffusivity of Eight Well-Characterized Rocks for the Temperature Range 300-1000°K," Engin. Geol. 12, 31.

Hasan, S. E., 1978, "Thermophysical Properties of Rocks," in Proc. 19th U.S. Rock Mechanics Symposium.

Hawley, C. C., and R. A. Wobus, 1977, General Geology and Petrology of the Precambrian Crystalline Rocks, Park and Jefferson Counties, Colorado, U.S. Geol. Survey Professional Paper 608B.

Herget, G., A. Pahl, and P. Oliver, "Ground Stresses below 3000 Feet," in Proc. 9th Canadian Rock Mechanics Symposium, Kingston, Ontario, pp. 281-307.

Huang, W. T., 1962, Petrology (McGraw-Hill, New York).

Hurr, R. T., and D. B. Richards, 1974, "Hydrologic Investigations," in C. S. Robinson et al., Engineering Geologic, Geophysical, Hydrologic and Rock Mechanics Investigations of the Straight Creek Tunnel Site and Pilot Bore, Colorado, U.S. Geol. Survey Professional Paper 815, pp. 79-88.

Hutting, M. T., W. A. G. Bennett, V. E. Livingston, Jr., and W. S. Moen, 1961, Geologic Map of Washington, scale 1:500,000.

Iwai, K., 1976, Fundamental Studies of Fluid Flow through a Single Fracture, University of California, Berkeley, Ph.D. dissertation.

Judd, W. R., 1969, Strain Distribution around Underground Openings: Statistical Methods to Compile and Correlate Rocks. Properties and Preliminary Results, Purdue University technical report 2.

Kendorski, F. S., and M. A. Mahtab, 1976, "Fracture Patterns and Anisotropy of San Manuel Quartz Monzonite," Bull. Assoc. Engin. Geol. 13(1).

Krauskopf, K., 1941, "Intrusive Rocks of the Okanogan Valley and the Problem of Their Correlation," J. Geol. 49, 1.

Kulhany, F. H., 1975, "Stress Deformation Properties of Rock and Rock Discontinuities," Engin. Geol. 9, 327.

Kunar, A., 1968, "The Effect of Stress Rate and Temperature on the Strength of Basalt and Granite," Geophys. 33(3), 501.

Larson, E. S., 1948, Batholith and Associated Rocks of Corona, Elainor, and San Luis Rey Quadrangles, Southern California, Geol. Soc. Am. Memoir 29.

Larsen, E. S., and R. G. Schmidt, 1958, A Reconnaissance of the Idaho Batholith and Comparison with the Southern California Batholith, U.S. Geol. Survey Bulletin 1070A.

Lee, C. F., 1978, Design of Hydraulic Tunnels in Rock for Generating Stations, Geotechnical Engineering Dept., Ontario Hydro.

Lehnhoff, T. F., and J. D. Scheller, 1975, "The Influence of Temperature Dependent Properties on Thermal Rock Fragmentation," Int. J. Rock Mech. Min. Sci. 12, 255.

Lewis, D. C., and R. H. Burgy. 1964, "Hydraulic Characteristics of Fractured and Jointed Rock," Ground Water 2(3), 4.

Lindroth, D. P., and W. G. Krawza, 1971, Heat Content and Specific Heat of Six Rock Types at Temperatures to 1000°C," U.S. Bureau of Mines Report of Investigation 7503.

Louis, C., and T. Maini, 1970, "Determination of In Situ Hydraulic Parameters in Jointed Rock," in Proc. 2nd Congress International Society for Rock Mechanics, Belgrade, Vol. 1.

Lundstrom, L., and H. Stille, 1978, Large Scale Permeability Test of the Granite in the Stripa Mine and Thermal Conductivity Test, Lawrence Berkeley Laboratory, Berkeley, Calif.

Maldonado, F., 1977, Summary of the Geological and Physical Properties of the Climax Stock, Nevada Test Site, U.S. Geol. Survey Open File Report 77-356.

Mirkovich, V. V., 1968, "Experimental Study Relating Thermal Conductivity to Thermal Piercing of Rocks," Int. J. Rock Mech. Min. Sci. 5, 205.

Morris, D. A., and A. I. Johnson, 1967, Summary of Hydrologic and Physical Properties of Rock and Soil Materials as Analyzed by the Hydrologic Laboratory of the USGS, U.S. Geol. Survey Water Supply Paper 1839D.

Nelson, P., et al., 1979, Preliminary Report on Geophysical and Mechanical Borehole Measurements at Stripa, Lawrence Berkeley Laboratory, Berkeley, Calif., LBL-8280.

Obert, L., 1963, Shot Hard Hat, Static Stress Determinations, U.S. Dept. of Defense report.

Office of Nuclear Waste Isolation (ONWI), 1978, Technical Support for GEIS:

Radioactive Waste Isolation in Geologic Formations, Oak Ridge, Tenn., Y/OWNI/TM-36.

Osterwald, F. W., 1955, "Petrology of the Precambrian Granitic in the Northern Bighorn, Wyoming," J. Geol. 63, 310.

Pardee, J. T., 1918, Geology and Mineral Deposits of the Colville Indian Reservation, Washington, U.S. Geol. Survey Bulletin 677, pp. 11-34.

Parson, Brinckerhoff, Quade and Douglas, Inc. (PBQ&D), 1976, Thermal Guidelines for a Repository in Bedrock, published by Office of Nuclear Waste Isolation, Oak Ridge, Tenn., Y/OWI/SUB-76/16504.

Pratt, H. R., H. S. Swolfs, W. F. Brace, A. D. Black, and J. W. Handin, 1971, "In Situ and Laboratory Measurements of Velocity and Permeability," Int. J. Rock Mech. Min. Sci.

Pratt, H. R., et al., 1972, "The Effect of Specimen Size on the Mechanical Properties of Unjointed Diorite," Int. J. Rock Mech. Min. Sci. 9, 513.

_____, 1978, Thermal and Mechanical Properties--Stripa, Sweden, Terra Tek, Salt Lake City, Utah.

Price, N., 1966, Fault and Joint Development in Brittle Rock (Pergamon, New York).

Priest and Hudson, 1976, "Discontinuity Spacings in Rock," Int. J. Rock Mech. Min. Sci. 13, 135.

Ramspott, L. D., et al., 1979, Technical Concept for a Test of Geologic Storage of Spent Reactor Fuel in the Climax Granite, Nevada Test Site, Lawrence Livermore Laboratory, Livermore, Calif., UCRL-52796.

Raven, S., and J. Gale, 1976, "Evaluation of Structural and Groundwater Conditions in Underground Mines and Excavations," in Subsurface Containment of Solid Radioactive Wastes, Geol. Survey of Canada Progress Report EMR/GSC-RW.

Richey, J. E., 1963, "Granite," Water Power, June, pp. 237-242.

Robertson, E. C., 1964, "Viscoelasticity of Rocks," in State of Stress in Earth's Crust (Elsevier, New York).

Robinson, C. S., 1978, Hydrology of Fractured Crystalline Rocks, Henderson Mine Colorado, Soc. of Min. Engin. technical paper.

Rodrigues, F. P., 1970, "Anisotropy of Granites," in Proc. 2nd Congress International Society for Rock Mechanics, Belgrade.

Ross, C., 1963, Model Composition of the Idaho Batholith, U.S. Geol. Survey Professional Paper 475C, pp. 80-70.

Sharp, J. C., Y. N. T. Maini, and T. R. Harper, 1972, "Influence of Groundwater on the Stability of Rock Masses," Trans. Sec. A, Inst. Min. Metall. 81(782), A13.

Skinner, B. J., 1966, "Thermal Expansion," in Handbook of Physical Constants, Geol. Soc. Am. Memoir 97.

Snow, D. T., 1965, A Parallel Plate Model of Permeable Fractured Media, University of California, Berkeley, Ph.D. dissertation.

_____, 1968a, "Rock Fracture Spacings, Openings, and Porosities," J. Soil Mech. Foundations Div. ASCE 94(5MI), 73.

_____, 1968b, "Hydraulic Characteristics of Fractured Metamorphic Rocks of the Front Range and Implications to the Rocky Mountain Arsenal Well," Colo. School Mines Quart. 63(1), 167.

_____, 1968c, "Fracture Deformation and Changes of Permeability and Storage upon Changes of Fluid Pressure," Colo. School Mines Quart. 63(1), 201.

Swan, G., The Mechanical Properties of Stripa Granite, Lawrence Berkeley Laboratory, Berkeley, Calif., LBL-7074.

Thirumalai, K., 1970, Rock Fragmentation by Creating a Thermal Inclusion with Dielectric Heating, U.S. Bureau of Mines Report of Investigation 7424.

Travis, R. L., 1955, "Classification of Rocks," Colo. School Mines Quart. 50(1), 98.

Tsui, K. K., 1979, A Study on the Thermomechanical Stability of Rock Caverns, Geotechnical Engineering Dept., Ontario Hydro, report 78239.

Uhl, V. W., Jr., and G. K. Sharma, 1978, "Results of Pumping Tests in Crystalline-Rock Aquifers," Ground Water 16(3).

U.S. Bureau of Reclamation (USBR), 1953, Physical Properties of Some Typical Foundation Rocks, Concrete Laboratory report SP-39.

Van Schmus, W. R., L. G. Medaris, Jr., and P. O. Banks, 1975, "Geology and Age of the Wolf River Batholith, Wisconsin," Bull. Geol. Soc. Am. 86(7), 907.

Walsh, J. B., W. F. Brace, and W. R. Wawersik, 1970, Attenuation of Stress Waves in Cedar City Quartz Diorite, Air Force Weapons Laboratory, Kirkland AFB, N.M., AFWL-TR-70-8.

Waters, A. C., 1938, "Petrology of the Contact Breccias of the Chelan Batholith," Bull. Geol. Soc. Am. 49, 763.

Waters, A. C., and K. B. Krauskopf, 1941, "Protoclastic Border of the Colville Batholith," Bull. Geol. Soc. Am. 52(9), 1355.

Wawersik, W. R., 1974, "Time-Dependent Behavior of Rock in Compression," in Proc. 3rd Congress International Society for Rock Mechanics, Denver, Colo.

Windes, S. L., 1949, Physical Properties of Mine Rock, Part I, U.S. Bureau of Mines Report of Investigation 4459.

_____, 1950, Physical Properties of Mine Rock, Part II, U.S. Bureau of Mines Report of Investigation 4727.

Wingquist, C. F., 1970, Elastic Moduli of Rock at Elevated Temperatures, U.S. Bureau of Mines Report of Investigation 7269.

Wright, F. H., 1967, Shot Pile Driver, In Situ Rock Stress, U.S. Dept. of Defense report.

APPENDIX TO CHAPTER 3: GLOSSARY OF TERMS

Bulk Modulus (Modulus of Compression): The ratio of the change in average stress to the change in unit volume.

Hydraulic Conductivity: For a porous, isotropic medium and a homogeneous fluid, the volume of fluid at the existing kinematic viscosity that will move in unit time under a unit hydraulic gradient through a unit area measured at right angles to the direction of flow.

Hydraulic Gradient: The change in static head per unit distance in a given direction. If not specified, the direction is generally understood to be that of the maximum rate of decrease in head. The gradient of the head is a mathematical term that refers to the vector denoted by Δh or grad h, whose magnitude dh/dl is equal to the maximum rate of change in head, and whose direction is that in which the maximum rate of increase occurs. The hydraulic gradient and the gradient of the head are equal but of opposite sign. Both are dimensionless.

Modulus of Elasticity (Modulus of Deformation): The ratio of normal stress to normal strain for a material under given loading conditions; numerically equal to the slope of the tangent (hence, tangent modulus) or the secant (hence, secant modulus) of a stress-strain curve. The use of the term modulus of elasticity is recommended for materials that deform in accordance with Hooke's Law, the term modulus of deformation for materials that deform otherwise.

Permeability (Intrinsic): A measure of the relative ease with which a porous medium can transmit a liquid under a potential gradient. It is a property of the medium alone, dependent upon the shape and size of the pores, and is independent of the nature of the liquid and of the force field causing movement.

Poisson's Ratio: The ratio of the transverse normal strain to the longitudinal normal strain of a body under uniaxial stress.

Porosity (Effective): The amount of interconnected pore space available for fluid transmission. It is expressed as a percentage of the total volume occupied by the interconnecting interstices. Although effective porosity has

been used to mean about the same thing as specific yield, such use is discouraged.

Shear Failure: Failure resulting from shear stresses.

Specific Heat: Defined as

$$c = \frac{dQ}{dV} ,$$

where dQ is the quantity of heat necessary to raise the temperature of a unit mass of the substance through the small temperature range from V to V + dV. Specific heat depends on both the temperature and the assumed mode of heating. It is expressed in cal/g-^{o}C. The specific heat of water at 15^{o}C is 1 cal/gm-^{o}C. Some authors regard the above definition as that of heat capacity or heat capacity per unit map of the substance, they define the specific heat of a substance as the ratio of its heat capacity per unit map to that of water.

Storage Coefficent: The volume of water an aquifer releases from or takes into storage per unit surface area of the aquifer per unit change in head. In a confined water body, the water derived from storage with decline in head comes from expansion of the water and compression of the aquifer; similarly, water added to storage with a rise in head is accommodated partly by compression of the water and partly by expansion of the aquifer. In an unconfined water body, the amount of water derived from or added to the aquifer by these processes is generally negligible compared to that involved in gravity drainage or filling of pores; hence, in an unconfined water body, the storage coefficient is virtually equal to the specific yield.

Strain: Deformation per unit length. Normal strain is the deformation per unit length in the direction of the deformation. Shear strain is the deformation per unit length at right angles to the deformation or, more commonly, the relative change in the angle defining the sides of an infinitesimal element.

Strength: The maximum stress that a body can withstand without failing by rupture or continuous deformation. Rupture strength or breaking strength refers to the stress at the time of rupture. If, after a certain stress has been reached, a body deforms continuously without any increase in stress, this is also called strength. By common usage, it can be described as the greatest

stress that a substance can withstand in normal short-time experiments, or the highest point on a stress-strain curve.

Stress: The force per unit area, as the area approaches zero, acting within a body. Biaxial Stress: The state of stress where either the intermediate or the minor principal stress equals zero. Effective Stress (effective pressure, intergranular pressure): The average normal force per unit area transmitted from grain to grain in a granular mass. It is the stress that is effective in mobilizing internal friction. Field Stress: The stress existing in a rock mass independent of any man-made works. Residual Stress: Stress that exists in a formation owing to previously applied forces or deformations. Triaxial Stress: A state of stress where the three principal stresses have finite magnitudes, or simply a three-dimensional state of stress. Neutral Stress (pore pressure, pore water pressure): Stress transmitted through the pore water (water filling the voids of the mass). Normal Stress: The stress component normal to a given plane. Principal Stress: Stresses acting normal to three mutually perpendicular planes intersecting at a point in a body on which the shear stresses are zero. Major Principal Stress: The largest principal stress (without regard to sign).

Thermal Conductivity: Defined as

$$K = \frac{Qd}{(V_0 - V_1)St} ,$$

where Q is the quantity of heat which flows in time t through a plate of a substance having a thickness d and cross-sectional area S; and V_0 and V_1 are the temperatures at the upper and lower surfaces of the plate. The conductivity generally depends upon the temperature. For nonhomogeneous solids, the conductivity varies from point to point, as well as in direction at each point.

Thermal Diffusivity: The change of temperature which would be produced in a unit volume of substance by the quantity of heat which flows in unit time through a unit area of a layer of the substance of unit thickness with unit difference of temperature between its faces. It is defined in terms of the thermal conductivity K, density ρ, and specific heat c as

$$k = \frac{K}{\rho c} .$$

Transmissivity: The rate at which water of the prevailing kinematic viscosity is transmitted through a unit width of the aquifer under a unit hydraulic gradient. Though spoken of as a property of the aquifer, it also depends on the saturated thickness of the aquifer (b) and the properties of the contained liquid. It is equal to an integration of the hydraulic conductivities across the saturated part of the aquifer perpendicular to the flow paths.

Uniaxial Stress: A state of stress where the minor and intermediate principal stresses are zero.

LLL:1980/3

NRC FORM 335 (7-77)

U.S. NUCLEAR REGULATORY COMMISSION

BIBLIOGRAPHIC DATA SHEET

1. REPORT NUMBER (Assigned by DDC)
NUREG/CR-0912, Vol. 1
UCRL-52719, Vol. 1

4. TITLE AND SUBTITLE (Add Volume No., if appropriate)
Geoscience Data Base Handbook for Modeling a Nuclear Waste Repository

2. (Leave blank)

3. RECIPIENT'S ACCESSION NO.

7. AUTHOR(S)
Dana Isherwood

5. DATE REPORT COMPLETED
MONTH: December YEAR: 1979

9. PERFORMING ORGANIZATION NAME AND MAILING ADDRESS (Include Zip Code)
Lawrence Livermore Laboratory
7000 East Avenue
Livermore, California 94550

DATE REPORT ISSUED
MONTH: January YEAR: 1981

6. (Leave blank)

8. (Leave blank)

12. SPONSORING ORGANIZATION NAME AND MAILING ADDRESS (Include Zip Code)
Division of Waste Management
Office of Nuclear Material Safety and Safeguards
United States Nuclear Regulatory Commission
Washington, D.C. 20555

10. PROJECT/TASK/WORK UNIT NO.

11. CONTRACT NO.
FIN No. A0277

13. TYPE OF REPORT
Final Report

PERIOD COVERED (Inclusive dates)
August 1978 to December 1979

15. SUPPLEMENTARY NOTES

14. (Leave blank)

16. ABSTRACT (200 words or less)

This handbook contains reference information on parameters that should be considered in analyzing or modeling a proposed nuclear waste repository site for high-level, transuranic & spent-fuel waste. Only those parameters & values that best represent the natural environment are included. Rare extremes are avoided. Where laboratory & field data are inadequate, theoretical treatments & informed engineering judgments are presented.

Volume 1 contains a data base on salt as a repository medium. Chapters on the geology of bedded & dome salt, the geomechanics of salt, hydrology, geochemistry, natural & man-made features, & seismology provide compiled data & related information useful for studying a proposed repository in salt.

Volume 2 is the result of a scoping study for a data base on the geology, geomechanics & hydrology of shale, granite, & basalt as alternative repository media. Except for the geomechanics of shale, most of the sections contain relatively complete compilations of the available data, as well as discussions of the properties that are unique to each rock type.

17. KEY WORDS AND DOCUMENT ANALYSIS

17a. DESCRIPTORS

17b. IDENTIFIERS/OPEN-ENDED TERMS

18. AVAILABILITY STATEMENT
Unlimited

19. SECURITY CLASS (This report)
Unclassified

21. NO. OF PAGES

20. SECURITY CLASS (This page)
Unclassified

22. PRICE
$